EXPERIMENTAL STUDY OF TWO-DIMENSIONAL TURBULENT WALL JET DEVELOPMENT WITH AND WITHOUT LONGITUDINAL FREE STREAM PRESSURE GRADIENT

A THESIS

Presented to

The Faculty of the Graduate Division

by

Douglas Howard Neale

In Partial Fulfillment

of the Requirements for the Degree

Doctor of Philosophy in the School of Aerospace Engineering

Georgia Institute of Technology

June 1971

In presenting the dissertation as a partial fulfillment of the requirements for an advanced degree from the Georgia Institute of Technology, I agree that the Library of the Institute shall make it available for inspection and circulation in accordance with its regulations governing materials of this type. I agree that permission to copy from, or to publish from, this dissertation may be granted by the professor under whose direction it was written, or, in his absence, by the Dean of the Graduate Division when such copying or publication is solely for scholarly purposes and does not involve potential financial gain. It is understood that any copying from, or publication of, this dissertation which involves potential financial gain will not be allowed without written permission.

_____

_____

7/25/68

EXPERIMENTAL STUDY OF

TWO-DIMENSIONAL TURBULENT WALL JET DEVELOPMENT

WITH AND WITHOUT LONGITUDINAL FREE STREAM PRESSURE GRADIENT

Approved:

Chairman

Date approved by Chairman: 6/14/71

ACKNOWLEDGMENTS

I wish to especially thank Professor James E. Hubbartt for his constant support during my graduate work. His willingness to contribute unselfishly to every facet of my work has brought this thesis to its present state.

I also must thank Dr. Howard M. McMahon and Dr. Louis H. Bangert for their guidance in the presentation of this manuscript.

To those who made the test facility a reality, I express my gratitude. Research Engineers John C. Handley, John G. Palfrey and George T. Bird were instrumental in the design of the experimental apparatus while Dewey L. Ransom and Calvin H. Wiser molded our ideas into hardware.

I wish to thank fellow graduate student J. N. Liaw for his most capable assistance in interpreting the experimental data.

My continuing education was made financially possible by a NASA Fellowship and by the U. S. Army Project Themis.

Finally, I must thank my wife, Ingrid, whose confidence in me has never wavered.

TABLE OF CONTENTS

LIST OF TABLES

LIST OF ILLUSTRATIONS

LIST OF SYMBOLS

C_f	friction coefficient $\left(C_f = \tau_w/q\right)$
d	Preston tube diameter
h	jet slot height
q	dynamic pressure
Re	Reynolds number
T	temperature
U	velocity
U_τ	friction velocity
X	cartesian coordinate (streamwise)
Y	cartesian coordinate (normal to wall)
β	ratio of jet momentum excess to initial boundary layer momentum deficit (reference velocity = U_{e_o})
δ	velocity profile thickness parameter
Δ	difference
Δp	difference between Preston tube total pressure and local static pressure

θ	momentum thickness
ν	kinematic viscosity
ρ	gas density
τ_w	local skin friction

Subscripts

o	jet exit plane
1	jet peak (Figure 17, Chapter IV)
2	Half-velocity, jet layer (Figure 17, Chapter IV)
3	minimum velocity (Figure 17, Chapter IV)
4	half-velocity, wake layer (Figure 17, Chapter IV)
e	edge (main stream)
j	jet
S	static
T	total
w	wake

SUMMARY

An experimental study of various wall jet flows was conducted in the Georgia Tech wall jet facility. The major areas of investigation were:

1. The wall jet injected into still air.
2. The wall jet under a constant-pressure main-stream flow.
3. The wall jet subjected to an adverse pressure gradient imposed by a retarded main-stream flow with a substantially thickened initial boundary layer.
4. The wall jet subjected to an adverse pressure gradient imposed by a retarded main-stream flow with a thickened and distorted initial boundary layer.

The investigations proceeded systematically from the simple to the more complex wall jet flows. The studies of wall jets in still air and wall jets in constant-pressure free streams establish the characteristics of simple wall jet flows. With the behavior of these comparatively uncomplicated flows known, more complex wall jets were studied. These adverse pressure-gradient cases provide a study of wall jet flow in which the initial boundary layer momentum deficit is significant in comparison with the jet momentum excess. Evidence of this relatively large initial momentum deficit is present throughout the measured development of these wall jets.

Detailed velocity profile and local skin friction measurements were made. For the case in which no main-stream flow was present, the studies were carried out for a wide range of slot Reynolds numbers. For the wall jets with main-stream flow, selected ratios of free-stream velocity to jet velocity at the jet slot were investigated. In each of the studies measurements were performed at several streamwise distances from the point of jet injection.

The growth of characteristic thickness and decay of jet peak velocity is presented in the text for all wall jet studies. In addition, velocity and temperature profile similarity is described. Skin friction laws are demonstrated for the constant-pressure wall jets and a single "law of the wall" valid for all wall jet studies is set forth. Finally, the skin friction and velocity profile measurements are presented in tabular form for those desiring more detail for construction of analytical models of wall jet flow.

CHAPTER I

INTRODUCTION AND LITERATURE REVIEW

Introduction

The term "wall jet" was first introduced by Glauert [1] to describe the flow of a plane jet which is bounded on one side by a nonporous surface. The earliest analytical and experimental work concentrated on wall jets which were generated by injecting the flow tangent to the surface into quiescent surroundings. However, as practical applications have become clear, "wall jets" have encompassed those cases in which the slot flow is introduced tangent to the surface beneath an external stream flowing in the same direction. In addition, the external stream may have developed a substantial boundary layer on the wall upstream of the slot and may impress pressure gradients in the streamwise direction on the developing wall jet flow downstream of the slot.

Major applications of wall jet flows with an external stream are found in boundary layer control and in film cooling. Efforts to develop high lift devices have revealed the value of introducing additional momentum into the boundary layer on the upper surface of airfoils. The slotted flap illustrates a present application. The added momentum not only results in a delay in separation of the boundary layer in adverse pressure gradient but, if sufficiently large,

also generates increased circulation about the lifting body. Both of these effects can contribute measurably to increased lift for a given angle of attack and free-stream velocity. It is important, then, for design purposes and feasibility studies to establish the effect of the controlling parameters involved in the problem so that prediction of the net increase in lift for a given practical set of operating conditions is possible. Accomplishment of this end requires analytical solutions for the development of two-dimensional wall jets which are introduced into an arbitrary initial boundary layer and which are subjected to practical free-stream pressure gradients.

Analytical solutions have, thus far, proven to be quite involved and dependent on complementary empirical information. Generally, those working on analytical models have divided the flow into regions which resemble previously well understood cases. Although there is a strong interaction among the various regimes of the flow, this approach appears to be valid when the requisite empirical information from actual wall jet flows is incorporated.

Literature Review

As previously indicated, the early experimental work involving incompressible turbulent wall jets was limited to cases in which no free stream and consequently no streamwise pressure gradient was imposed. As the practical uses for the wall jet became more obvious, experimental studies were made in which moving streams and pressure gradients were employed. This survey, in an attempt to collect related systematic experimental studies, will include those works in which the

wall jet is directed tangent to a flat downstream surface. The investigations in which no free stream was used are included along with those in which a free stream existed with and without a streamwise pressure gradient.

Infinite Velocity Ratio Investigations

The earliest published experimental work on the two-dimensional wall jet with no main-stream flow was performed by Förthmann [2] as a supplement to his investigation of the plane free jet and partially expanding jet. Förthmann observed the apparent self-preserving nature of wall jet velocity profiles for short distances downstream of the jet slot. His data also indicated that the boundary layer thickness varies linearly with distance from the slot and that the maximum velocity varies inversely as the one-half power of this distance. Further, he concluded from his data that the velocity in the wall layer (between the wall and the velocity maximum) varies as the one-seventh power of the height from the wall, an observation that is not substantiated by later experiments.

The first effort to concentrate experimentally on the wall jet with no free-stream flow was implemented by Bakke [3] in 1957. The experiments were performed using a radial wall jet. In an attempt to verify the analytical results of Glauert [1], Bakke measured velocity profiles to a distance of 20 slot widths from the point of injection for a Reynolds number based on slot height of approximately 30,000. The data provided a record of jet thickness growth and maximum velocity decay with distance from the slot. Bakke found agreement in his work with the results of Förthmann and Glauert and stated,

"within the experimental range and accuracy the velocity profiles are similar and the rate of change of velocity and width of the jet can be expressed by simple power laws." Bakke's data was not sufficiently extensive to reveal the variation of the growth and decay laws with Reynolds number based on slot height that Glauert had predicted.

In 1958, Sigalla [4,5] performed similar measurements for slot Reynolds numbers from 20,000 to 46,000. He likewise verified Glauert's prediction of profile near-similarity. Sigalla's measured growth of jet thickness and decay of maximum velocity agreed within his experimental accuracy with Glauert's analytical prediction and Bakke's experimental results. As an additional contribution, Sigalla presented skin friction measurements obtained by Preston's method. He concluded from his measurements that it is possible to describe the variation of skin friction by a formula similar to the Blasius formula for turbulent pipe flow. He also noted the presence of a region of flow adjustment extending from the slot to a distance of about 20 slot widths downstream. In this "starting region" the jet and free-stream flow undergo a transition from two distinct flows to a true wall jet form. Sigalla's measurements were carried out to 64 slot widths from the jet slot.

In 1961, Schwartz and Cosart [6] used a hot wire anemometer to determine mean velocity profiles for the wall jet into still air. They employed jet velocities from 27 to 83 ft/sec through a 1 inch high slot and measured profiles to a distance of 66 slot widths downstream. Their work once again verified over-all profile similarity and their data for maximum velocity decay showed good agreement with work previously done by others. Schwartz and Cosart included data for

the wall layer. Contrary to Förthmann's suggestion, their measurements indicated that the wall layer velocity profiles follow something close to a one-fourteenth power law for nearly ninety per cent of the layer. As part of their data evaluation, Schwartz and Cosart presented skin friction values calculated from their mean velocity profile data. Their calculated values of skin friction coefficient differed from those directly measured by Sigalla by a factor of two; however, Schwartz and Cosart admitted that their method is highly sensitive to the choice of certain constants used to match the velocity profile. They also noted that the outer layer appears to appreciably affect the wall layer and they suggested that this casts some doubt on the existence of a "law of the wall" relation for the plane turbulent wall jet. Further, since the method of Preston assumes that a law of the wall exists near the wall for all turbulent flows, they questioned the validity of this method in obtaining skin friction information.

Bradshaw and Gee [7] presented velocity profile measurements in 1960. These agreed generally well with those of Sigalla and Bakke and provided additional detail for the wall layer profiles. Bradshaw and Gee also presented skin friction data obtained with a flattened Preston tube. Their values were typically 6 per cent above those obtained by Sigalla.

In 1963 Meyers, Schauer, and Eustis [8] performed further experiments with a wall jet in still air. Their primary objective was to resolve the large discrepancies in wall shear stress data obtained by the previous researchers. They employed a hot film technique

rather than a Preston tube to make these measurements. Meyers et al. discovered that their results were closest to those of Sigalla and Bradshaw and Gee; however, they were unable to resolve the differences since Sigalla's data was still 15 per cent below their values while the data Bradshaw and Gee was 9 per cent below their work.

Finite Velocity Ratio Investigations

In 1959, George [9] presented the first experimental velocity profile information for a wall jet developing under an external stream. He performed his experiments for initial jet to free-stream velocity ratios, U_j/U_{e_o}, of 1.5, 3, and 6 with no streamwise pressure gradient. George noted that the effect of the initial boundary layer was completely erased for all velocity ratios except 1.5. In this case the momentum defect of the boundary layer was of the same order as the momentum of the jet. George also indicated that he detected some over-all profile similarity for velocity ratios of 3 and 6 but that the form appeared to be rather complex. George performed his measurements for a velocity ratio of 3 with free-stream velocities of 50 and 100 ft/sec to observe the effect of the slot Reynolds number. The free-stream velocity for the velocity ratio of 6 was 50 ft/sec and the jet slot height for all measurements was nominally 0.050 inches.

In addition to their experimental work with the infinite velocity ratio cases, Bradshaw and Gee (1960) [7] published data for a wall jet developing a free stream with no streamwise pressure gradient. The data included velocity profiles for an initial jet to free-stream velocity ratio of about 6 to a distance of 750 slot widths downstream. They concluded from their experiments that the ratio of

initial jet momentum excess to initial boundary layer momentum deficit required for the jet just to absorb the boundary layer before the jet peak disappears is a little less than 5. Bradshaw and Gee also presented "law of the wall" data for the wall layer but their conclusions concerning these results were not definitive. The data for the wall jet in still air and beneath a moving stream was taken with a slot height of 0.018 inches and jet velocity of 650 ft/sec.

Bradshaw and Gee also presented velocity profile data for the wall jet developing over a deflected flap with an external moving stream and, thus, a streamwise pressure gradient. Their measurements were performed for a slot height of 0.040 inches and with a jet velocity of 350 ft/sec. They observed that the flow was extremely complex and that an adequate analytical solution would require the help of considerably more experimental detail before becoming a reality.

In 1961, Seban and Back [10] presented their investigation of a wall jet with a very low free-stream velocity. The velocity ratio at the slot was thus still high and their results were very similar to those previously obtained for wall jets into still air. Their measurements were made to a distance of 250 slot widths and their slot Reynolds numbers were well below 10,000. Seban and Back noted that a starting region of about 18 slot widths was required before apparent profile similarity was achieved. The primary objective of this work and many others, however, was to predict heat transfer coefficients. These investigations are not discussed further in the present survey.

In 1961 Patel and Newman [11] experimentally created the conditions necessary for the wall jet outer profiles (from the jet peak,

δ_1, to the free stream, δ_e) to remain similar. These "self-preserving" profiles were obtained by retarding the free-stream flow such that the ratio of local jet peak velocity to free-stream velocity was constant. They suggested that experimental evidence indicates that similarity exists in the outer layer and may extend to the outer region of the wall layer. It should be noted that evidence of an initial boundary layer did not appear in their data. Patel and Newman also measured wall jet profiles for zero pressure gradient cases. These tests were performed for initial velocity ratios of 3 and 4 to a distance slightly over 100 slot widths downstream of the slot. Patel and Newman found that for the zero pressure gradient cases the outer layer profiles demonstrated near similarity and they stated that this augurs well for outer profile similarity in arbitrary pressure gradients. They finally suggested that further profile detail is needed in the wall layer and that more complete skin friction measurements must be made for all wall jet cases.

In 1962, Eskinazi and Kruka [12] expanded the wall jet studies by investigating a variety of initial velocity ratios from 2 to 18.4 to a distance of 465 slot widths downstream of the slot. For the external stream cases they discovered that a simple similarity rule for the entire profile is not valid too far downstream of the slot. Eskinazi and Kruka verified Glauert's suggestion, however, that the flow could be divided into two regions and that similarity parameters could be found for each region. As expected, they discovered that for very high velocity ratios the flow behaved much like the flow observed by Förthmann and Schwartz and Cosart for a wall jet issuing into still

air. Their experiments revealed that, for distances from 20 to 400 slot widths downstream of the slot, over-all similarity in the decay of the velocity excess and the growth of the characteristic jet width is possible for all ratios of jet to free-stream velocities. The similarity is achieved with a streamwise coordinate transformation based on the changing jet to free-stream relative velocities with distance from the slot. Kruka and Eskinazi performed shear stress measurements with a flattened Preston tube. Their results agreed qualitatively with those done before; but quantitatively their results were considerably different. Their work did, however, substantiate that a Blasius-type skin friction formula such as that suggested by Sigalla is valid.

In 1963, Verhoff [13] presented more profile data to support his own similarity solutions. His data included infinite velocity ratio cases as well as finite velocity ratio cases. He also compared his solutions with experimental data from preceding researchers and obtained excellent agreement over much of the profile for a wide range of velocity ratios and slot widths downstream of the jet slot. Verhoff attempted, however, to fit the complete velocity profile with his similarity solution and he did not meet with complete success in the outer region of the outer layer.

In 1963, Eskinazi and Kruka [14] investigated the zero pressure-gradient cases for a wide range of initial velocity ratios and confirmed the similarity expressions for the wall layer and the outer layer require different velocity and length scales. Based on the results of their investigations, they concurred with the earlier findings of

Bradshaw and Gee that the point of zero turbulent shear stress is not located at the jet peak and that the points of partition of the profile are still open to question. Kruka and Eskinazi also investigated skin friction with a flattened Preston tube. Their data did not agree well with previous results such as those of Bradshaw and Gee.

Erian and Eskinazi [15] extended the work of Kruka and Eskinazi in 1964 to include velocity profile and skin friction measurements for a wall jet in a moving stream with a pressure gradient. The pressure gradient was imposed on the wall jet by a single airfoil section attached to the opposite side of the test section. The tests were performed for one initial velocity ratio and no attempt was made to systematically vary pressure gradient; the results were therefore considerably limited in scope.

Gartshore [16] published data on characteristic profile thickness and maximum velocity decay for both finite and infinite velocity ratio cases in 1964. He investigated a slot Reynolds number of 30,800 to a distance of about 120 slot widths for the infinite velocity ratio case. Initial velocity ratios of approximately 2, 3 and 5 were studied to a distance of about 150 slot widths for the finite velocity ratio cases with no streamwise pressure gradient.

In 1965, Harris [17] provided more data for a wall jet with a free-stream pressure gradient. He imposed a mild adverse pressure gradient for velocity ratios between 3 and 6 to a distance of 700 slot widths downstream. Harris' presentation was limited to thickness and maximum velocity information and no profile detail was given.

In 1968, Kacker and Whitelaw [18] recognized the need for more data in the low velocity ratio range and performed their experiments for velocity ratios of 0.75 to 2.74 to a distance of 150 slot widths downstream. The work was done with no pressure gradient applied to the wall jet. Kacker and Whitelaw noted in their work that the trends observed in previous investigations for skin friction seemed to be consistent; however, they still found sizeable differences in values measured.

In 1969, Gartshore and Newman [19] presented their own data for several wall jet cases as follows:

1. A wall jet into still air.
2. A self-preserving wall jet for nominal velocity ratios of 1.3, 2.0 and 3.0.
3. A non-self-preserving wall jet in adverse pressure gradient for nominal velocity ratios of 2.0 and 4.0.
4. A wall jet in zero pressure gradient for nominal velocity ratios of 2.0, 3.0 and 4.0.

They included over-all growth and decay information for comparison with calculations based on their own analytical model; however, they did not present profile detail or skin friction measurements.

Purpose of the Present Investigation

In summary, there exists a good body of experimental information concerning velocity profiles and wall jet development for the still-air and free-stream cases with no streamwise pressure gradient. Within the accuracy of the instrumentation utilized, the velocity profile

results show a good measure of concurrence. A comparison of skin friction data, however, does not reveal generally acceptable agreement. This discrepancy coupled with a lack of corresponding wall layer profile detail has retarded the study of the relative effects of the outer layer and the wall in the streamwise development of the wall jet flow.

The detailed presentation of a systematic study of wall jets developing under streamwise pressure gradient is not yet available. Of the few studies that have been implemented, most are narrow in scope while the rest are lacking in comprehensive detail.

There are several areas, then, in which further experimental studies are required to understand the various wall jet flows. The purposes of this investigation are to contribute to this understanding in the following ways:

1. To present additional wall layer velocity profiles and skin friction detail to help resolve the uncertainty now apparent for the infinite velocity ratio case and for the finite velocity ratio case with no streamwise pressure gradient.
2. To contribute a comprehensive systematic study of wall jets displaying significant residual evidence of an initial boundary layer and developing under adverse free-stream pressure gradient. This study must provide sufficient mean velocity profile and skin friction detail for evaluation of empirical information for use in analytical models.

The work described in "1" should establish confidence in the present experimental method when the results are compared with previously accepted data for the cases in which good agreement has already been achieved. Of particular emphasis in "2" are the cases in which the jet does not overpower the initial free-stream boundary layer. In these instances the effect of the boundary layer persists throughout the decay of the jet peak. Such cases are of primary interest since air supplies for auxiliary functions in aircraft are at a premium and minimum effective slot blowing is desirable.

CHAPTER II

THE WALL JET EXPERIMENTAL APPARATUS

Test Bed Detail

The wall jet data presented in this work was obtained in the testing components shown in Figure 1. The main-stream flow is brought through a contraction in the vertical dimension into the boundary layer development section. This section is 8 inches high, 30 inches wide and 18 inches long (internal dimensions). As the name suggests, the boundary layer development section is included for controlling the development of the main-stream floor boundary layer beneath which the jet will be injected. Three primary means of controlling boundary layer development are incorporated into this component. First, a roughening agent may be attached to the floor for thickening the layer. Second, also for the purpose of thickening, a base region of adjustable height is available by raising or lowering the contraction fairing on the floor at the entrance to the section. Third, desired contraction-expansion contours may be attached to the roof of the section to achieve adverse longitudinal pressure gradients to simultaneously thicken the floor boundary layer and decay its profile. Details of this section are given in Appendix A.

The wall jet flow is generated by introducing a two-dimensional jet tangent to the test section floor immediately downstream of the boundary layer development section through a continuous slot (i.e.,

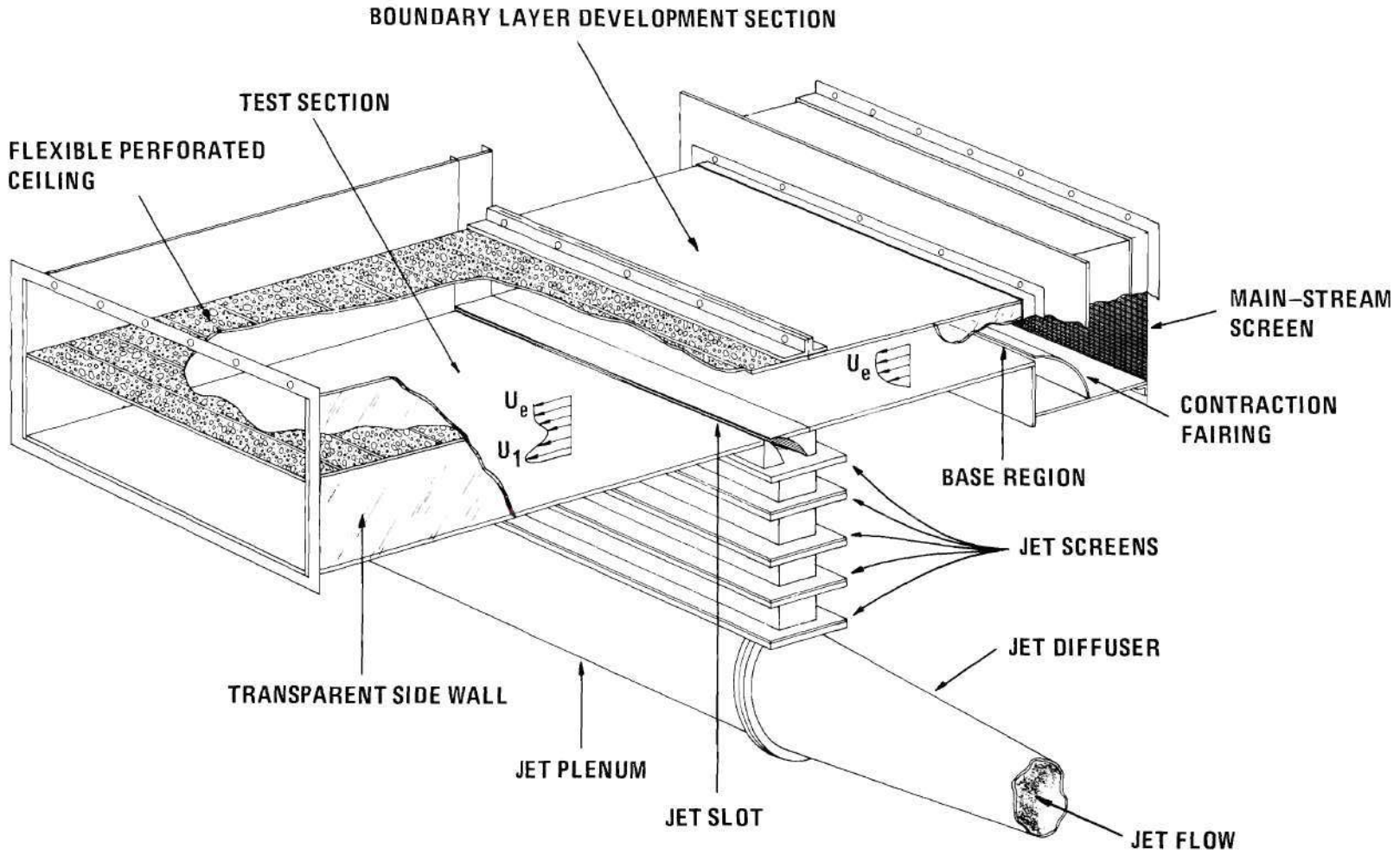

Figure 1. Experiment Test Bed.

without spacers) running the full width of the test section. Jet nozzle details are given in Appendix B, Figure B-1.

The test section has been constructed with clear plexiglas side walls to facilitate observation of visual flow studies and probe locations. Static pressure taps are located along the centerline of the precision flat ground aluminum plate floor and are also located offset 7.5 inches to the right and left of the centerline. The floor is 30 inches wide and 36 inches long. In the test section the developing wall jet flow may be subject to longitudinal pressure gradients. These pressure gradients are created by the controlled bleed of main-stream air through a perforated sheet metal ceiling. This ceiling is matched at its leading edge to the ceiling of the boundary layer development section and may be deformed along its length to achieve additional pressure variations beyond those provided by main-stream bleed alone. The pressure potential is generated by a valve attached immediately downstream of the test section. The test section is described in more detail in Appendix C.

Figure 2 shows the view from the test section exit plane looking upstream. The test section floor appears in the lower foreground followed by the jet slot, the boundary layer development section floor with roughening agent and, finally, the base region. At the top of the figure, the perforated ceiling is in the foreground followed by an expansion contour ceiling in the boundary layer development section. The plexiglas side walls are evident in both sections.

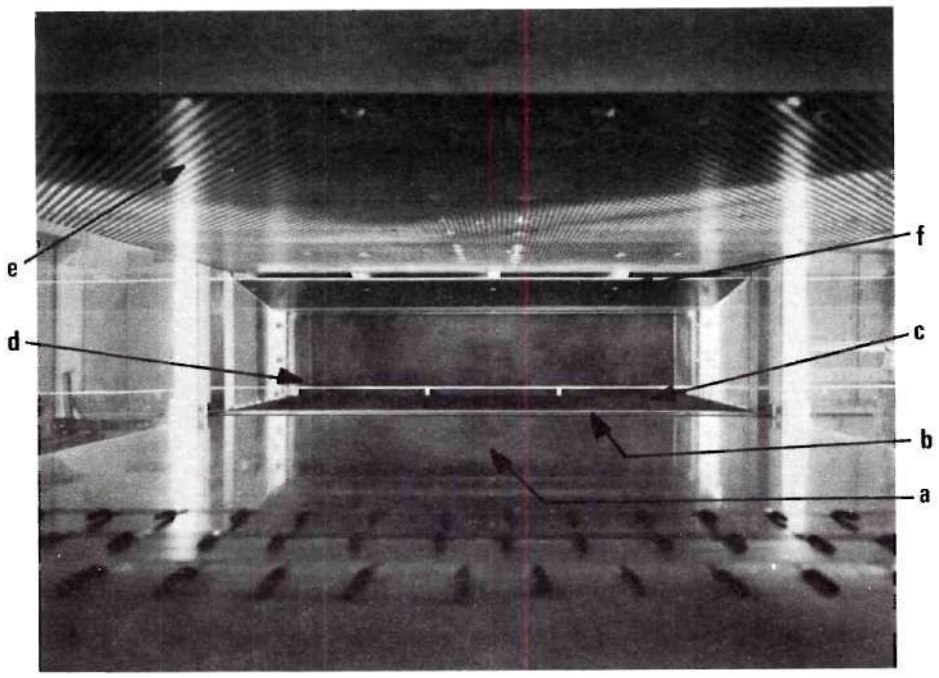

a. Test Section Floor
b. Jet Slot
c. Boundary Layer Development Section Floor
d. Base Region
e. Test Section Ceiling
f. Boundary Layer Development Section Expansion Ceiling

Figure 2. Internal View of Testing Sections

General Rig Description

An over-all test facility diagram is shown in Figure 3. The main-stream flow is provided by a centrifugal blower driven by a constant speed motor. This fan generates test section free-stream velocities of approximately 120 ft/sec. Complete specifications for this blower are given in Appendix D.

The main-stream air from the blower is dumped into a plenum through a closed-end perforated baffle tube as shown in Appendix D, Figure D-3. The plenum is lined with fiberglas acoustic padding for noise abatement in the main-stream flow. From the plenum the flow is re-accelerated through a bellmouth to a circular duct. The main-stream is then brought through a combination transition duct and diffuser to attain a rectangular cross section. At the exit of this transition the flow is passed through three separate screens to insure uniform flow distribution and to reduce large-scale free-stream turbulence. This component is detailed in Appendix E. The main-stream air is then passed into the boundary layer development section as described previously.

The jet air is supplied by a five stage constant speed centrifugal compressor capable of providing discharge flows up to 1300 SCFM at 7.4 PSIG. This capacity translates into ratios of jet to free-stream velocity at the jet slot ranging from 0 to 7 with a nominal free-stream velocity of 120 ft/sec for the slot heights of .155 and .056 inches used in the present series of experiments. The jet compressor discharge flow is taken through circular ducting to a tee. One leg of the tee is provided with a dump valve operated pneumatically from the control

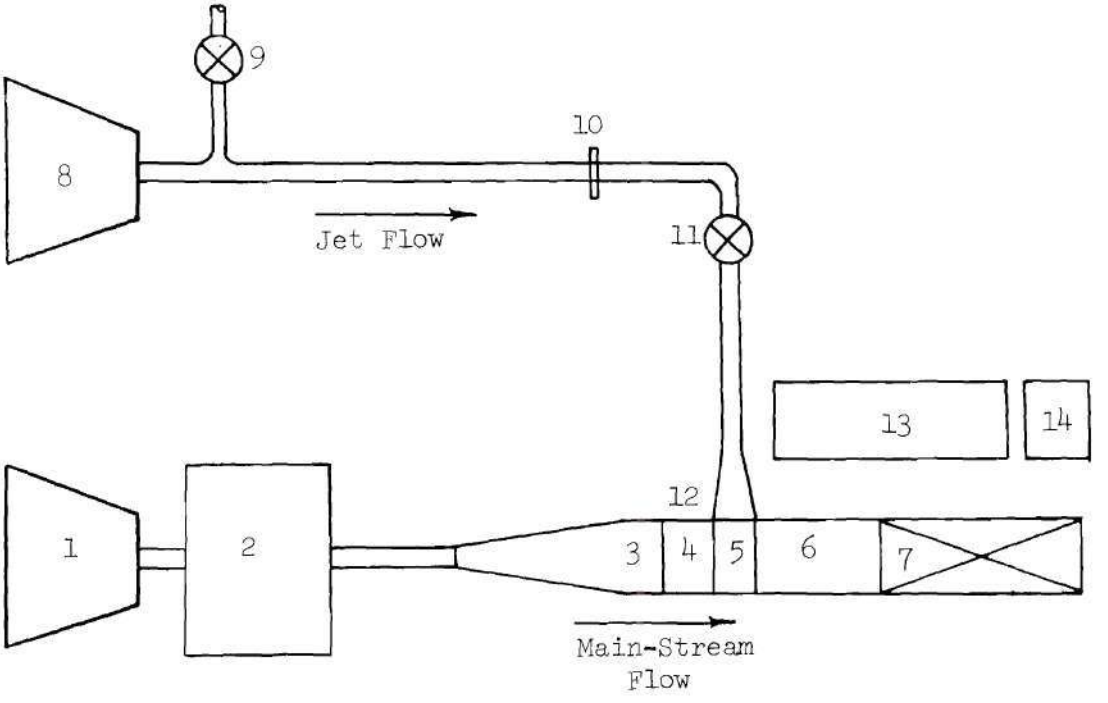

1. Main-stream Blower
2. Main-stream Plenum and Baffle
3. Main-stream Transition and Diffuser Combination
4. Boundary Layer Development Section
5. Jet Slot Section
6. Wall Jet Test Section
7. Main-stream Control Valve
8. Jet Compressor
9. Dump Valve
10. Orifice Meter
11. Jet Control Valve
12. Conical Jet Diffuser
13. Air Supply Control Panel
14. Instrumentation Panel

Figure 3. Apparatus Floor Plan

panel. This valve allows for the controlled discharge of excess compressor flow for low speed operation of the wall jet. The second leg of the tee carries the actual jet air flow and is configured as an orifice run downstream of the tee. An orifice plate for mass flow measurement is located at the end of the run with the necessary static pressure taps placed upstream and downstream of the plate. In addition, a thermocouple probe is located upstream of the orifice to measure the mean flow total temperature. Further details concerning the jet compressor, dump valve and orifice meter are included in Appendix F.

A hand-operated diaphragm-type control valve is located between the orifice and the jet plenum chamber. A 70 inch long, 5 degree conical diffuser just downstream of the jet control valve expands the flow from the standard 6 inch circular duct to the 12 inch diameter jet plenum (Figures 1 and 4). The jet plenum is located directly below the jet slot section. In the plenum the jet air is turned 90 degrees and is carried out through a rectangular aperture in the top. The flow is then passed through four equally spaced screens and is accelerated and turned parallel to the test section floor by the jet nozzle. More information about the jet plenum, screens and jet nozzle assembly is presented in Appendix C.

The main-stream and jet flow exit from the test section into the main-stream valve. This valve has a variable entrance height adapter for matching the perforated ceiling exit height. The valve flap is hinged to this adapter and is manipulated by a lead screw

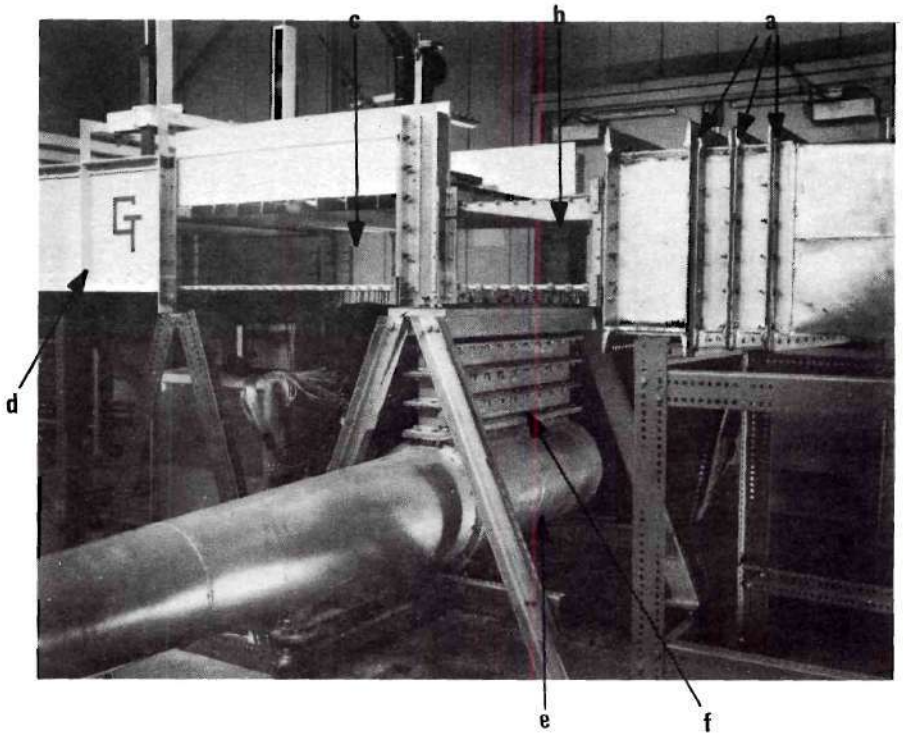

a. Main-Stream Screen Support Flanges
b. Boundary Layer Development Section with Expansion Profile Ceiling
c. Test Section with Non-Deformed Perforated Ceiling
d. Main-Stream Control Valve
e. Jet Plenum Chamber
f. Jet Screen Section

Figure 4. Wall Jet Test Components

mechanism at the downstream end for control of the valve exhaust area. The valve is shown in Figures 4 and 5. The wall jet system is closed in the sense that the laboratory is used as a plenum from which the compressors draw and into which the exhaust flow is discharged.

Description of Data Acquisition Components

The experimental data collected for this work was obtained by employing the test probes shown in Figure 6. Flow velocities were determined with the flattened-tip total head probe, (b), in conjunction with either floor static pressure taps or the static pressure probe, (a). Skin friction measurements were performed by using one or both of the circular Preston tubes shown, (c) and (d). The fluid total temperatures were measured with the copper-constantan thermocouple probe, (e). The probes are presented in greater detail in Appendix H.

For data acquisition the probes were mounted in the actuator shown in Figure 7. This lead screw mechanism is graduated in 0.001 inch increments. The actuator can simultaneously traverse three probes each spaced 1-5/16 inches apart in the carriage.

Total and static pressures were measured independently with two Barocel Electronic Manometer units manufactured by Datametrics Corp., Waltham, Massachusetts. A 10 mm Hg maximum Δp transducer was employed for sensing static pressures while a 1000 mm Hg transducer was used for measuring total pressures. Both transducers are shown in Figure 8. Each transducer output was passed through a separate signal conditioner and read on a separate digital voltmeter in which a 10 volt reading corresponded to the respective maximum transducer capacity. Each

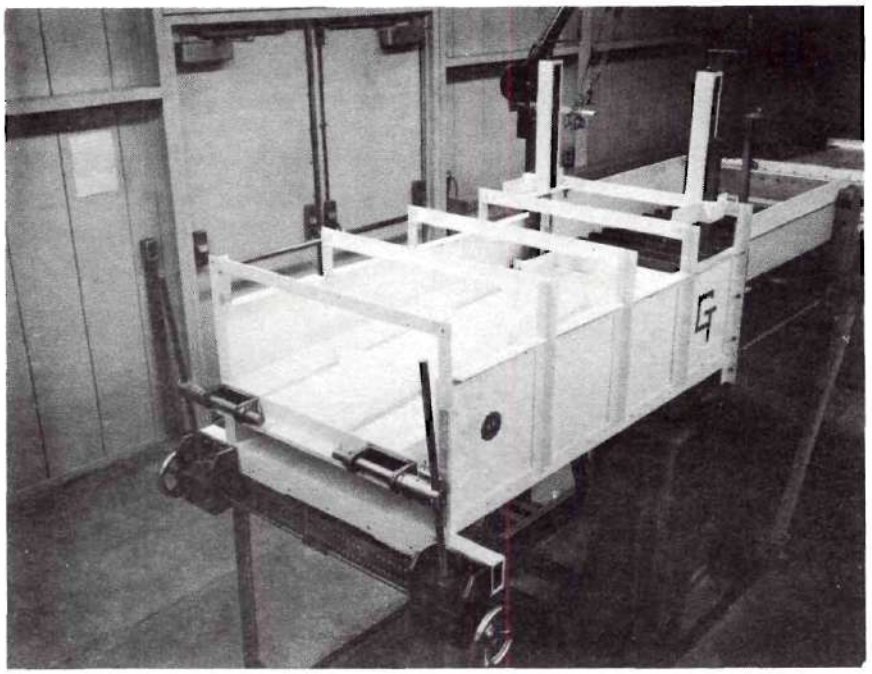

Figure 5. Main-stream Control Valve

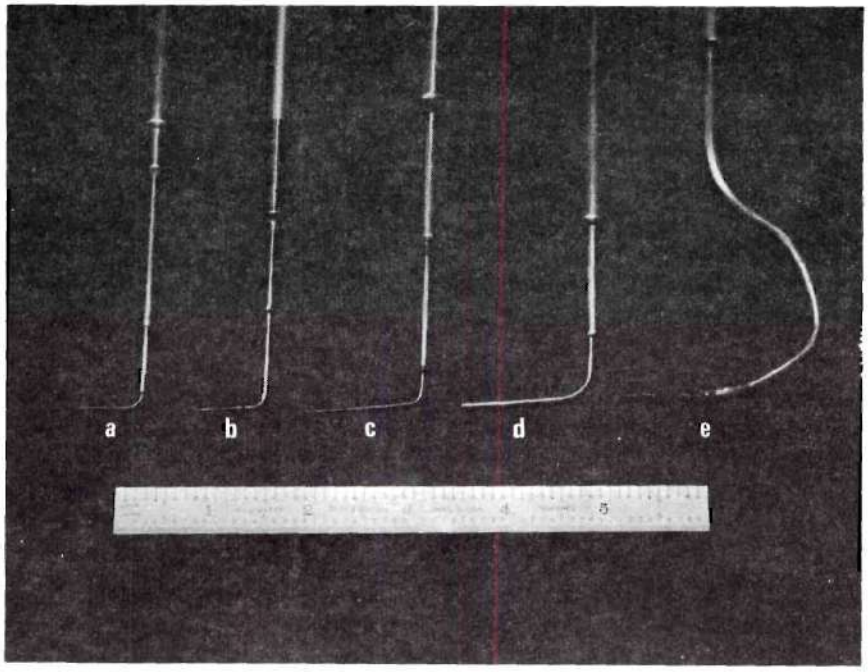

a. Static Pressure
b. Total Pressure
c. Preston (.014 Outside Diameter)
d. Preston (.0625 Outside Diameter)
e. Thermocouple

Figure 6. Test Probes

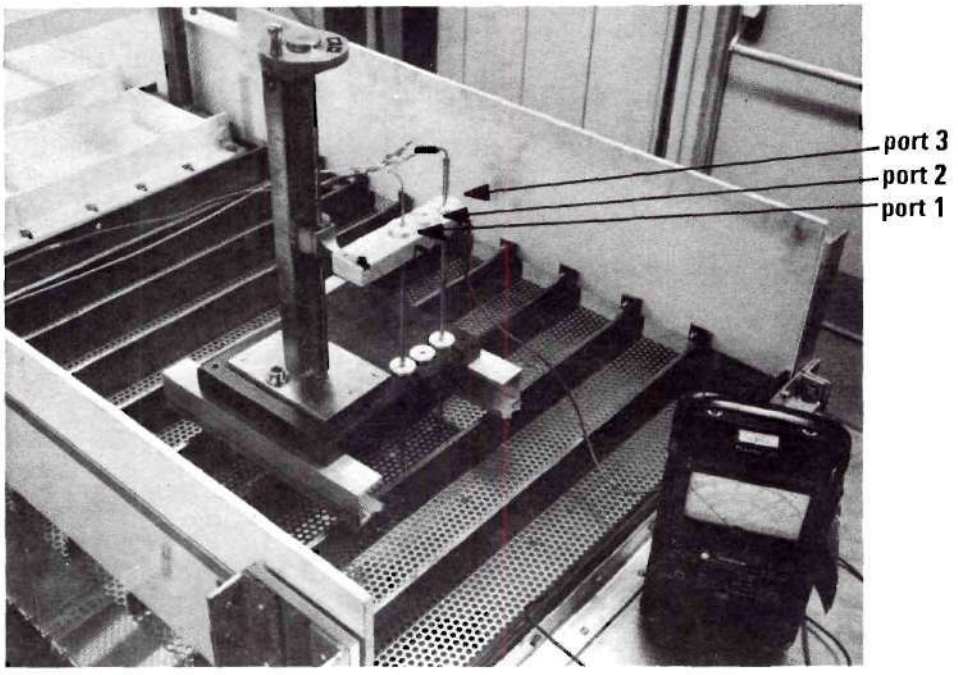

Figure 7. Probe Actuator

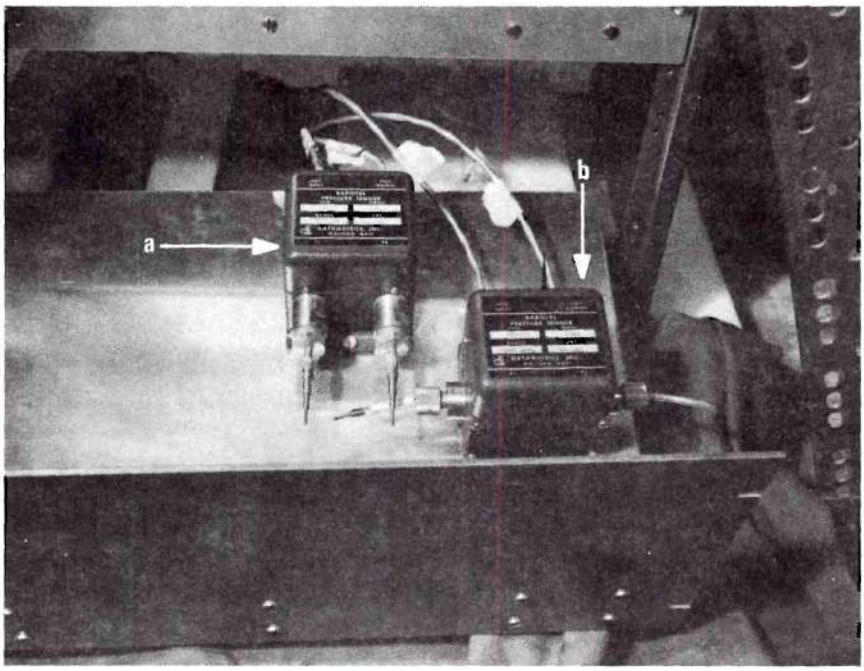

a. 10 mm Hg Maximum Δp
b. 1000 mm Hg Maximum Δp

Figure 8. Barocel Pressure Transducers

signal conditioner was equipped with a range selector switch to amplify the transducer output. This feature allowed small pressures (pressure differences) to be accurately read with the voltmeters. Both voltmeters were provided with variable capacitance dampers for averaging flow pressure fluctuations.

Three 48 channel Scanivalve components were incorporated in the system for rapid sampling of the static pressure and total pressure ports. Two Scanivalve units were used to sample the numerous static pressure ports while the remaining unit was used to select total pressures. A wafer switch was included in each line to allow for rapid verification of zero points during data acquisition. The pressure sensing sequence is shown schematically in Figure 9. The transducers, wafer switches, and Scanivalves are mounted directly under the test section and are shown in Figure 10.

An X-Y plotter was provided as an option for automatic recording of the static pressure profile along the test section.

All rig and flow temperatures were displayed in degrees Fahrenheit on a Honeywell multichannel strip chart recorder mounted on the air-supply control panel. This recorder is calibrated for copper-constantan thermocouples and contains a cold junction temperature correction circuit.

Ambient temperature was read by a mercury thermometer of laboratory quality. A calibrated bourdon-tube barometer was employed to display the local atmospheric pressure. Both instruments are located on the air-supply control panel and adjacent to the test section.

The air-supply control panel and the instrumentation panel are shown in Figures 11 and 12.

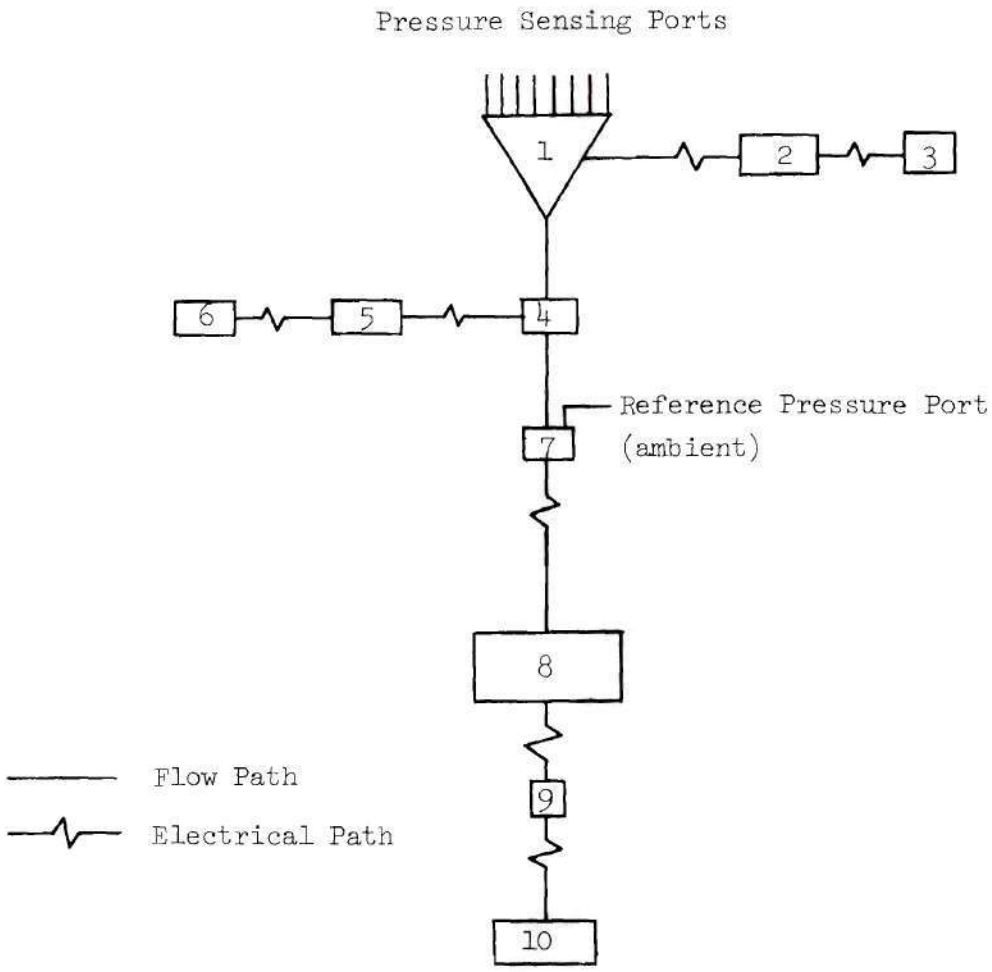

1. Scanivalve Unit
2. Solenoid Driver
3. Station Indicator (1-48)
4. Wafer Switch
5. Solenoid Driver
6. Position Indicator ("Read" of "Zero)
7. Pressure Transducer
8. Signal Conditioner
9. Variable Damper
10. Digital Voltmeter

Figure 9. Pressure Sensing Sequence

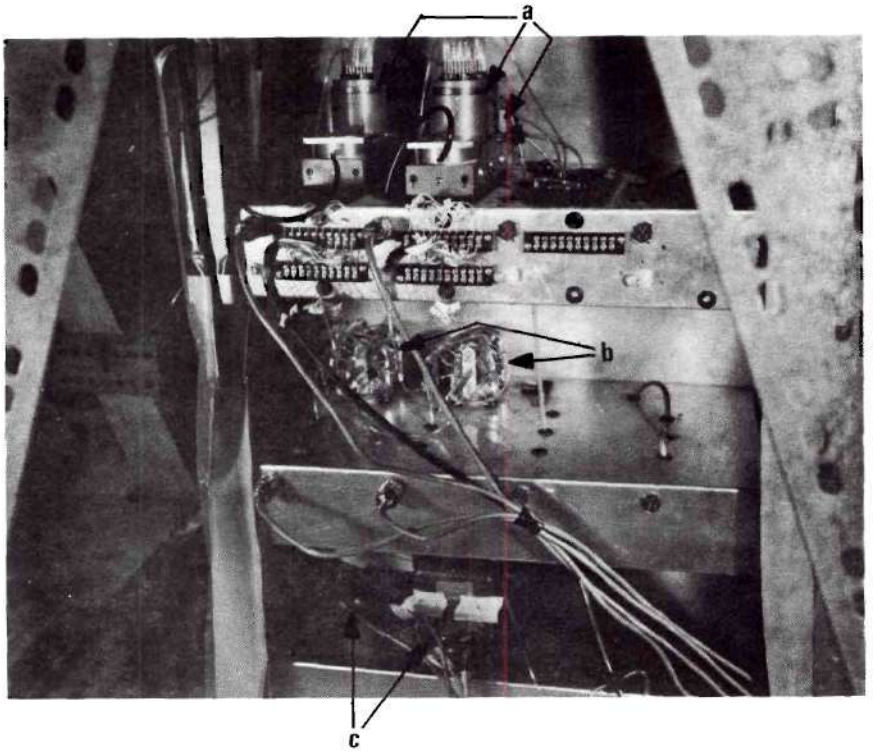

a. Scanivalves
b. Wafer Switches
c. Pressure Transducers

Figure 10. Pressure Sensing Components

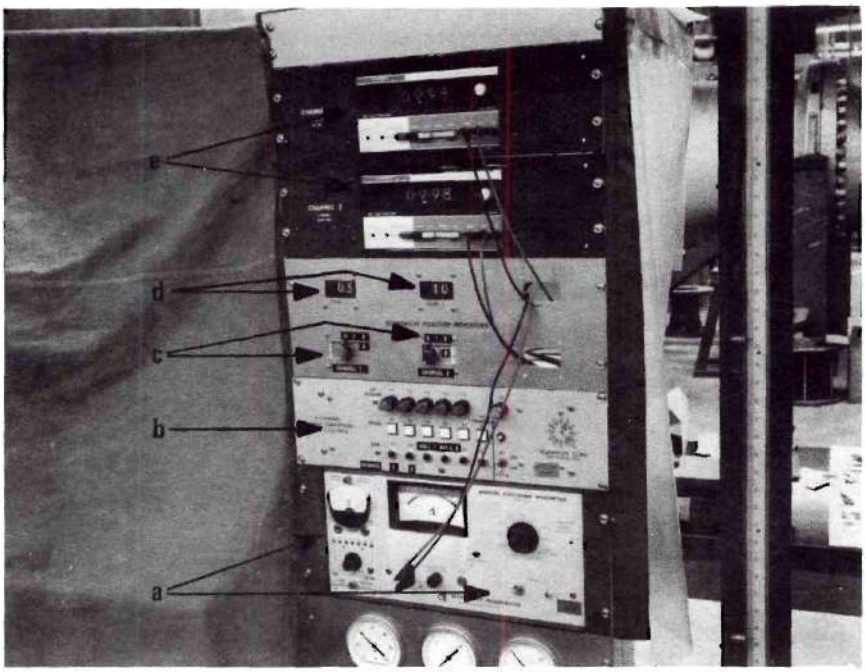

a. Barocel Signal Conditioners
b. Scanivalve Control Panel
c. Variable Capacitance Damping Circuits
d. Scanivalve Station Display
e. Digital Voltmeter

Figure 11. Instrumentation Panel

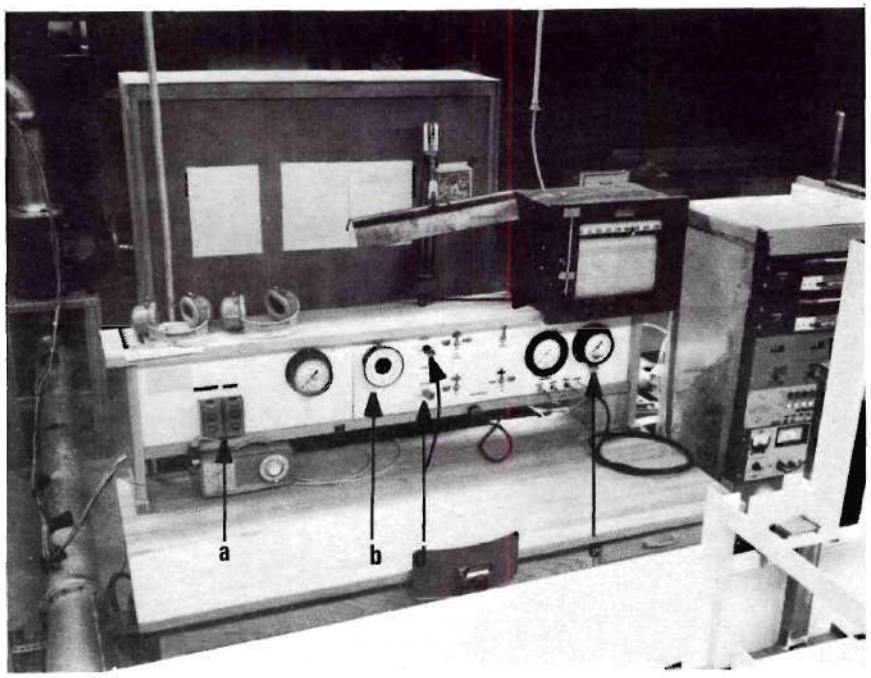

a. Main-stream and Jet Compressor Power Switches
b. Bourdon Tube Barometer
c. Jet Compressor Exhaust Pressure Gage
d. Dump Valve Control Switches
e. Honeywell Multichannel Temperature Recorder

Figure 12. Air-Supply Control Panel

CHAPTER III

EXPERIMENTAL PROCEDURE

Evaluation of Equipment

Temperature Measurement Instrumentation

A laboratory quality mercury thermometer graduated in 1 degree Fahrenheit increments was employed as a standard against which the thermocouple probes used for flow temperature measurement were compared. The thermometer and probes were placed in a water bath which was heated incrementally through a range of temperatures comparable with those encountered under actual test conditions. The thermometer was read directly and the thermocouple output was read through the Honeywell recorder. The two types of instruments differed by no more than 1 degree Fahrenheit throughout the range of temperatures investigated.

Pressure Measurement Instrumentation

Bourdon Tube Barometer. The barometer used for recording ambient pressure at the wall jet apparatus site was calibrated against a precision Mercury-column barometer accurate to ± 0.001 inch of Mercury. In addition, the local U. S. Weather Bureau station was contacted several times for daily pressure readings to check the instruments in hand. In order to establish a significant range of pressures, these comparisons were continued over a period of several weeks. The bourdon-tube barometer required an initial adjustment;

however, once this adjustment was accomplished all readings agreed within 0.01 inch of Mercury over the entire range of barometric pressures recorded.

Pressure Acquisition System. The two independent pressure sensing systems each composed of a Scanivalve unit, wafer switch, pressure transducer, signal conditioner and digital voltmeter were compared before and after each major segment of research. To effect this comparison, both systems were set to monitor a single pressurized plenum chamber. The test consisted of relieving the plenum pressure in steps and recording the digital voltmeter output of each system at every plateau. Both systems used ambient pressure as a reference. Initially the 10 mm and 1000 mm transducers used in the present investigation were compared in this manner. Since this comparison was limited to the range of the smaller capacity transducer, an auxiliary 1000 mm head was substituted for the 10 mm head. The comparison test was then repeated.

Comparison of the 10 mm and 1000 mm transducer systems revealed typically no disagreement over the 10 mm range within the three significant figure accuracy of the digital voltmeters. The maximum difference ever observed was less than 0.2 per cent of the reading. The systems exhibited a typical disagreement of less than 0.5 per cent of the reading when the two 1000 mm heads were compared. The maximum disagreement in the systems over the 1000 mm range was less than 1.0 per cent of the reading. It was noted that the auxiliary transducer consistently registered the lower pressure reading. This situation remained true even in the 0 mm to 10 mm range over which excellent

agreement had previously been verified for the original transducers.

As a further check on the accuracy claimed in the manufacturer's specifications, individual Barocel transducers were calibrated at Georgia Tech and the results were reported by D. K. Mosher [20]. A 10 mm and a 1000 mm transducer were compared over their ranges with a dead weight tester, an accepted laboratory calibration standard, and were found to substantiate the manufacturer's stated accuracy of from 0.1 to 0.25 per cent of the reading. Further, Utterback and Griffith [21] investigated pressure measurement standards and found that the variable capacitance transducer is highly reliable and precise.

It should be remembered that, since the flow under consideration is this study was very nearly incompressible, percentage velocity errors vary approximately as the square root of the corresponding dynamic pressure error. For errors of the small magnitude discussed in the present text, the resulting velocity error is roughly one-half of the dynamic pressure error.

Both of the pressure measurement systems were checked for leakage. All of the ports of each system were individually pressurized to nearly the maximum capacity of their respective transducers and were sealed at that pressure. The pressure decay due to leakage was monitored on the digital voltmeters and was found in every case to be less than 0.2 per cent of the reading per minute. Since the response time of the system was of the order of five seconds, the leakage effect was insignificant.

Probes. As a check of probe geometry effect on total pressure readings, three different total pressure probes were compared. The first

probe, used to obtain the velocity profile data in the present work, consisted of a flattened-tip tube canted downwards at a 6 degree angle to the flow (Appendix H, Figure H-1). The second probe was a flattened-tip tube facing directly into the flow. The third probe was a circular-tip tube facing directly into the flow. The probe tips are detailed in Figure 13. Each probe was used to obtain the same velocity profile at two different lengths from the slot. As shown with typical profiles in Figures 14a and 14b, the data obtained with the three probes probes reveal little measurable evidence of probe geometry effect.

A calibration was performed in turbulent pipe flow for Preston-type probes of 0.0625 and 0.028 inch diameters respectively. The calibration was carried out in a 3 inch diameter seamless aluminum pipe and flow was generated by drawing ambient laboratory air through the pipe into a large vacuum chamber. The entrance of the pipe was fitted with a bellmouth and honeycomb material to insure smooth ingestion of air. The flow was then carried through 18 feet of straight, jointless pipe before reaching the calibration test section. Figure 15 shows a comparison of the present calibration data with Patel's [22] equation based on the results of his Preston tube experiments. The close agreement demonstrated in this figure served as the justification for using Patel's equation in evaluating skin friction from the measurements made in the present work.

For most cases in this investigation, skin friction measurements were performed with a 0.014 inch diameter probe. This probe was checked against the 0.028 inch diameter and the 0.0625 inch diameter probes at several initial velocity ratios, U_j/U_{e_o}, and lengths from the

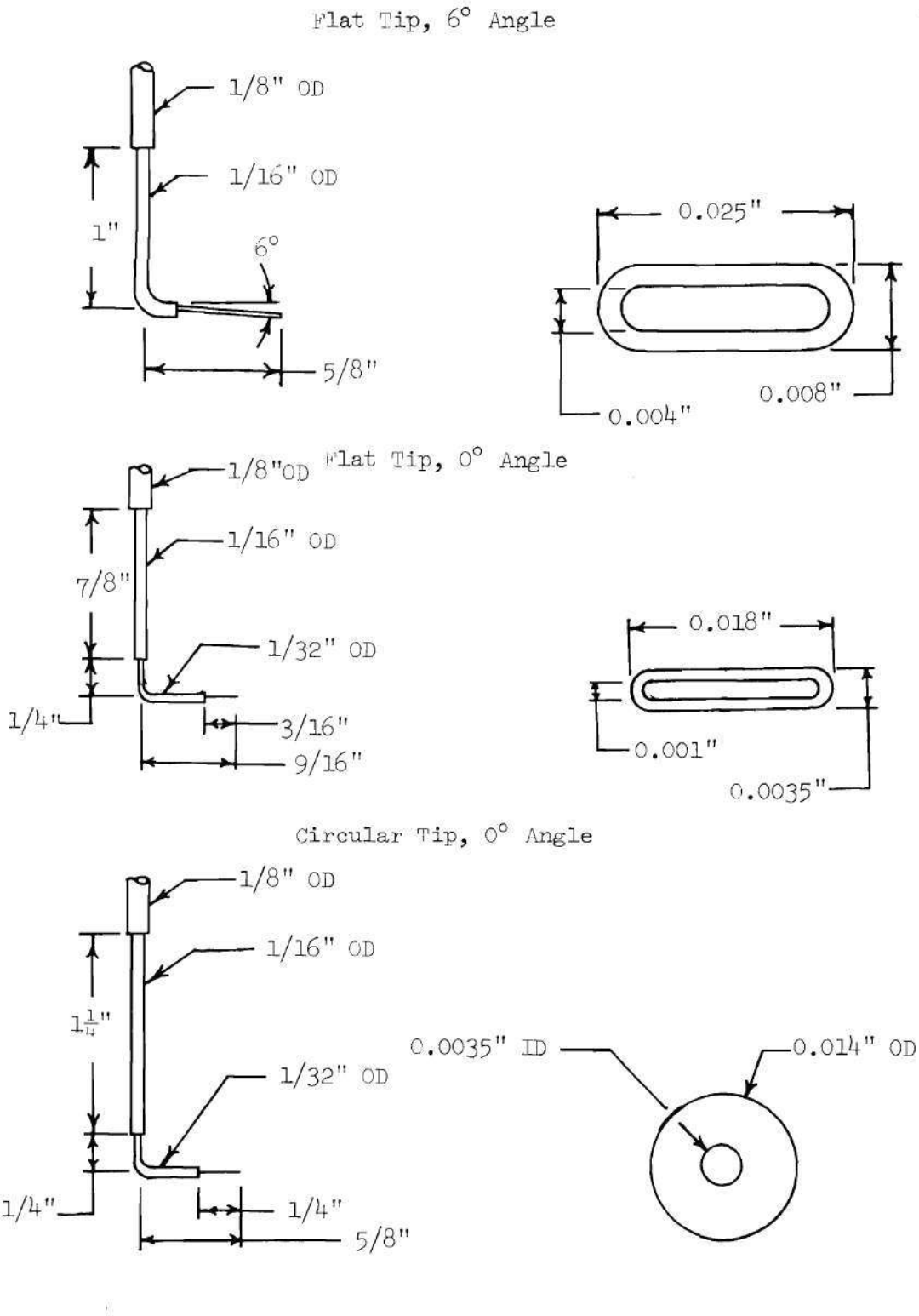

Figure 13. Total Pressure Probe Tip Detail

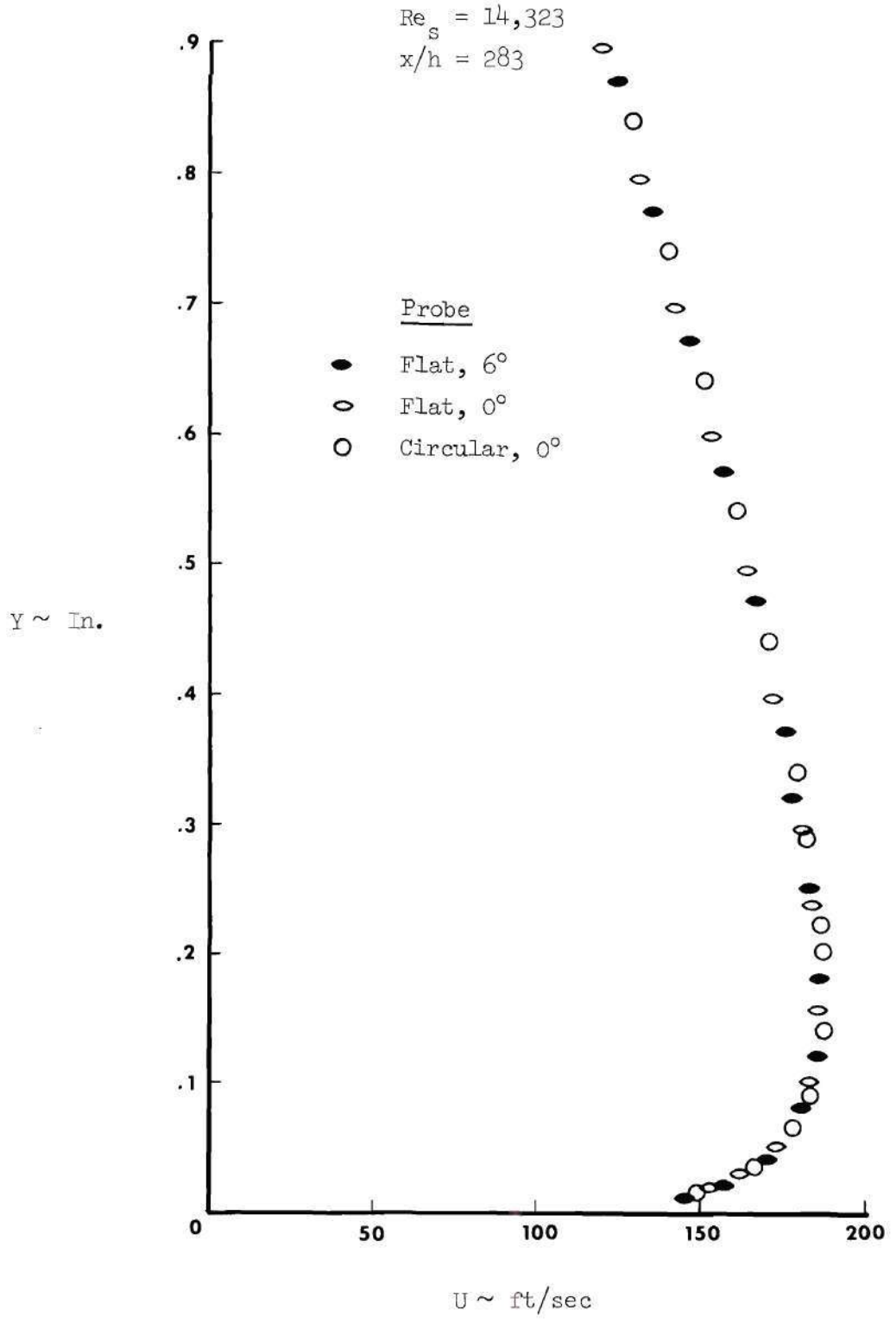

Figure 14a. Probe Comparison

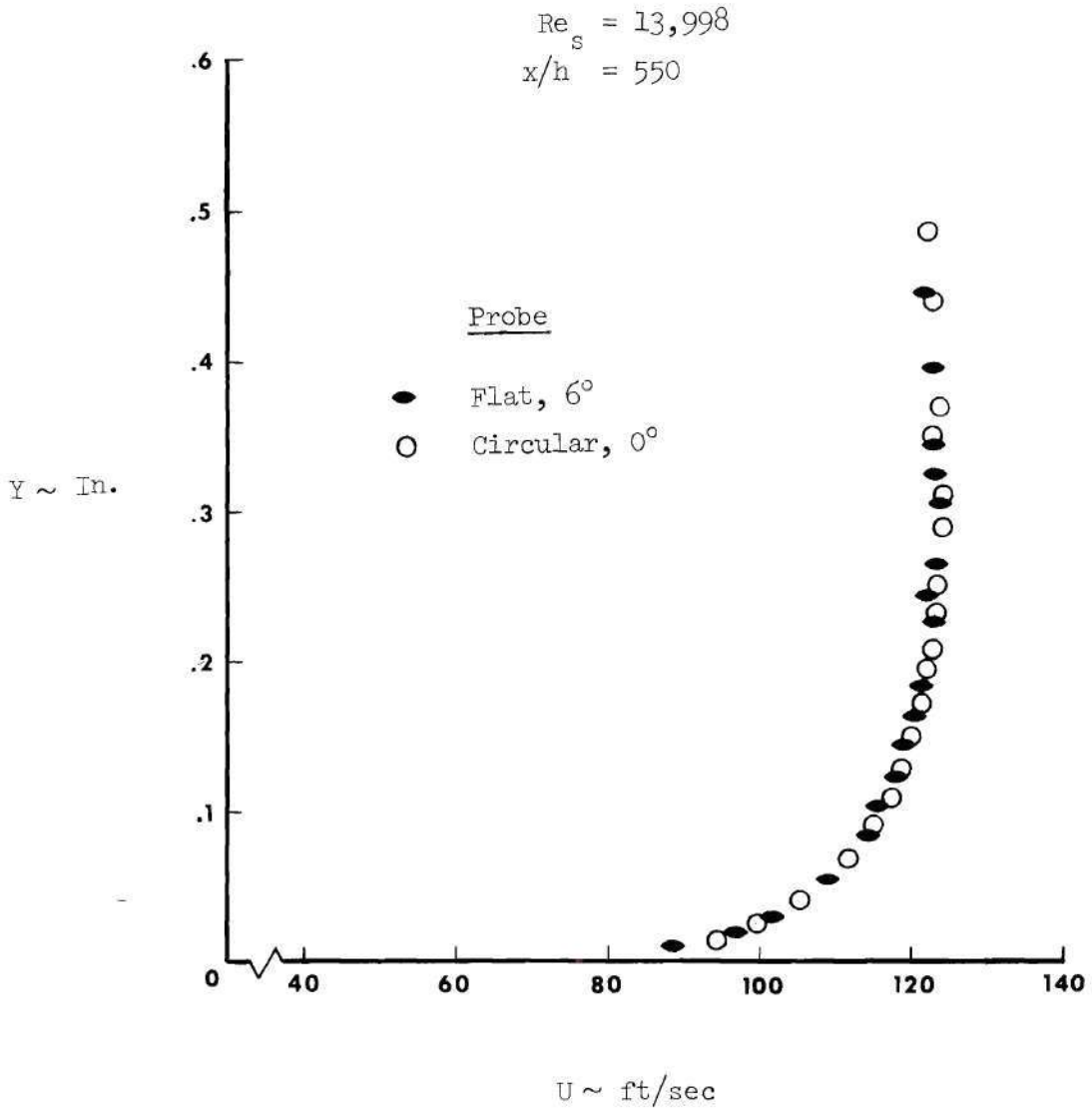

Figure 14b. Probe Comparison

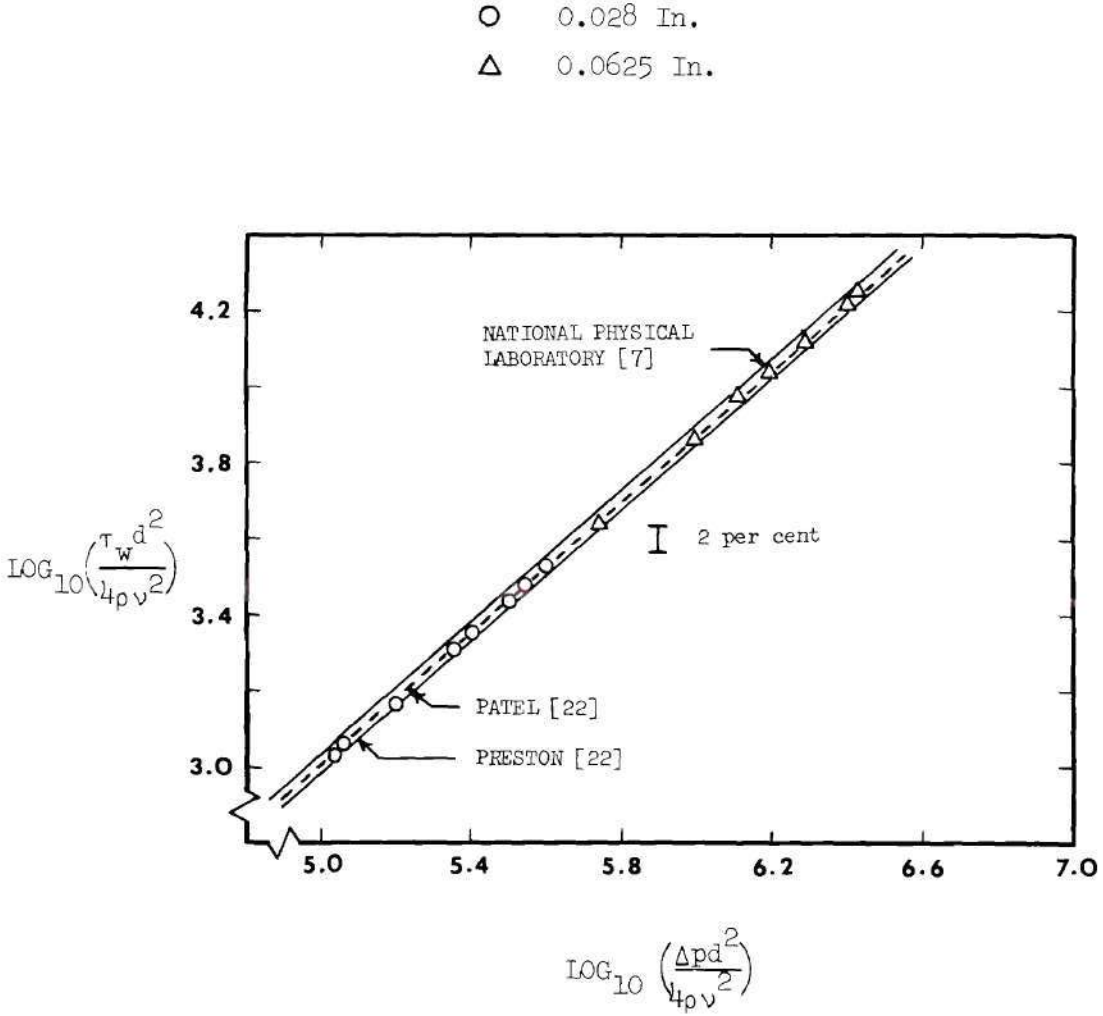

Figure 15. Preston Tube Calibration

slot. The skin friction measurements were found to be in excellent agreement at all locations in which a significant difference between surface static pressure and Preston-tube measured total pressure existed. One such case is shown in Figure 16. Agreement was not good, however, for very thick wall layers. In these cases the small probe was well within the laminar sublayer and was not able to discern a total pressure much different from the local wall static pressure. Typically, in these instances, a 1 to 2 per cent change in total pressure reading resulted in a 20 to 30 per cent change in pressure difference. In actual testing these cases were easily recognized and the 0.0625 inch diameter Preston tube was employed to complete the skin friction measurement.

The static pressure probe was constructed so that velocity profile and skin friction measurements would not be limited to the near-vicinity of floor static pressure taps. The probe was evaluated by comparing its readings with those of various floor taps over a range of pressures encountered in typical test conditions. The results agreed within 1.0 per cent of the reading for the entire range of pressures with the probe registering consistently lower values. This difference in reading corresponds, for the very worst case, to less than 2.2 per cent of the local free-stream dynamic pressure. It was further determined that yaw angles of ± 3 degrees resulted in no change of the measured pressures.

Since the total pressure probe and thermocouple probe were employed simultaneously to obtain velocity profiles, it was necessary

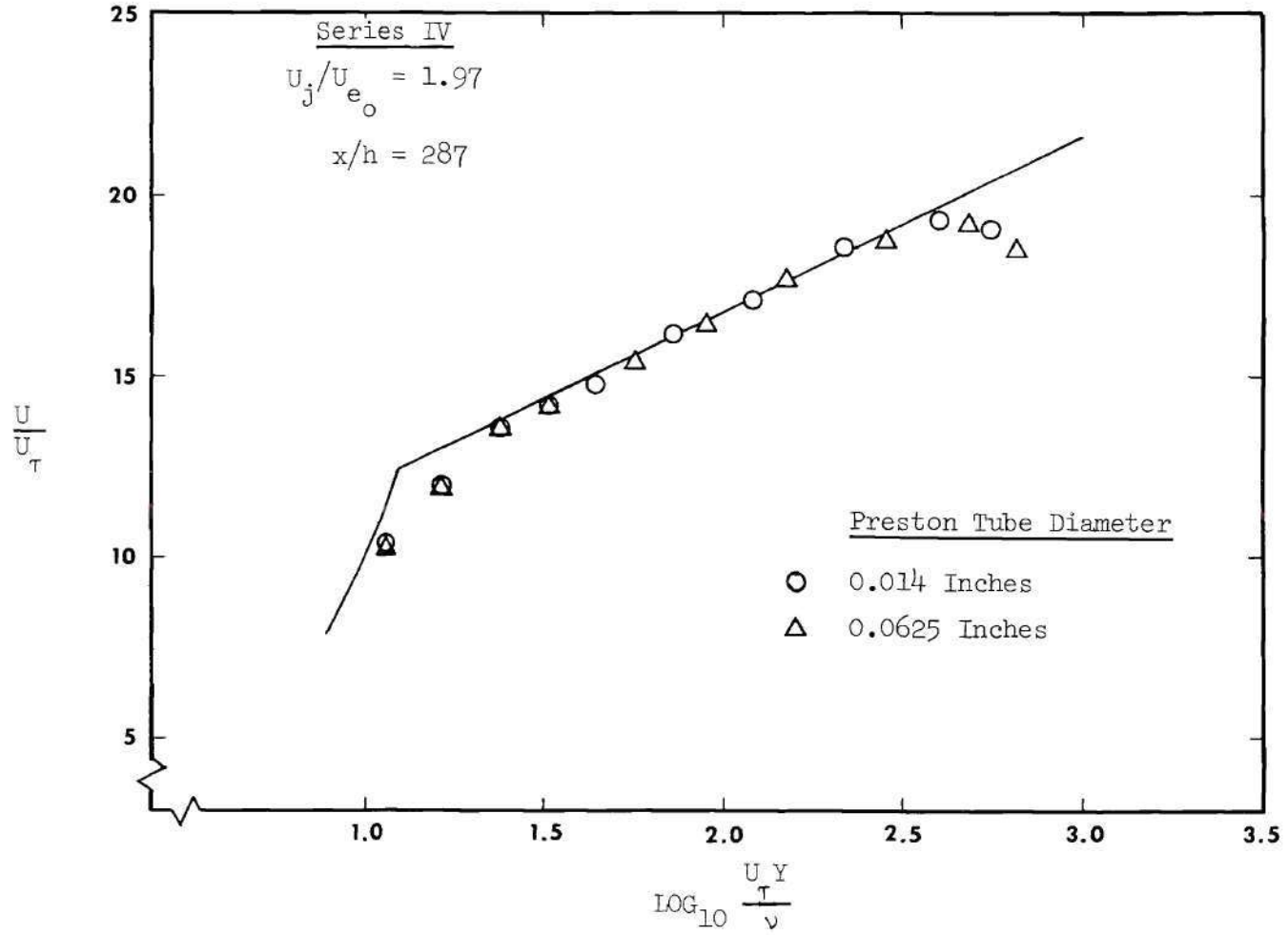

Figure 16. Preston Tube Comparison

to investigate probe interaction effects. The total pressure and temperature probes were fixed in ports 1 and 3 respectively of the probe actuator carriage and both were lowered into the main-stream flow. The thermocouple probe was then released from its fixture and was independently raised and lowered relative to the total pressure probe. The total pressure reading was monitored and, within the accuracy of the instrumentation, no pressure effects from the thermocouple probe presence could be detected.

Probe Actuator. The actuator lead screw was evaluated for accuracy over 7 inches of its travel and all subsequent measurements were made within this span. A steel dowel was mounted in port 3 and the actuator was placed on a precision flat reference surface. A zero point was noted on the lead screw position indicator and the dowel was raised with the actuator crank to match the 1.000 inch travel of a standard height gage. The indicated dowel travel was then recorded and compared to the actual 1.000 inch travel. Combinations of precision gage blocks were employed with the height gage to complete the 7 inch span. In all cases the indicated travel at port 3 agreed within 0.5 per cent of the actual travel. The same test was completed at port 1 over a 4 inch span and the indicated travel was within 0.2 per cent of the actual travel.

Evaluation of Flow

The difficulty in developing uniform slot flow has been emphasized by several authors [7] and [14]. Maintenance of a consistent slot is deemed of major importance. The two slot heights used

for the present investigation were measured with feeler gages over the 30 inch length of the slot. The centerline height of the large slot was 0.155 inches. The slot height decreased on each side of the centerline but remained within 2.0 per cent of the centerline value at least 7 inches to either side. The small slot was 0.056 inches high at the centerline with a variation in height of less than ± 1.7 per cent for at least 9 inches to either side. The slot heights are tabulated in detail in Table 1. Special care was taken in the design of the jet nozzle to insure that no measurable deflection of the knife edge would occur even during maximum jet velocity operation.

Wall jet profiles in still air were then measured and compared at several spanwise positions to evaluate flow two-dimensionality. These spanwise comparisons were made at two streamwise distances from the slot. Similar profile comparisons were also effected for the wall jet under an external stream. These studies were performed after each major alteration in the apparatus geometry. The results of these two-dimensionality investigations proved to be excellent and are presented in Chapter IV in context with the test conditions for which they were performed. Also evident in context are results demonstrating the repeatability of velocity profile and skin friction measurements.

Surveys of the test section floor static pressure were taken for every investigation in which a streamwise pressure gradient was applied to the wall jet flow. A small spanwise static pressure gradient existed in all cases. At any given streamwise location, static pressure was highest on the left side (looking upstream) of the test section and decreased linearly from left to right. The worst spanwise gradient

Table 1. Slot Height Distribution

Distance from Right Side (looking upstream) ~ In.		Nominal Slot Height	
		0.155 In.	0.056 In.
Right	0	-	-
	1	0.134	0.049
	2	0.137	0.052
	3	0.140	0.055
	4	0.145	0.056
	5	0.147	0.057
	6	0.151	0.057
	7	0.152	0.057
	8	0.152	0.056
	9	0.153	0.056
	10	0.153	0.056
	11	0.154	0.056
	12	0.155	0.056
	13	0.155	0.056
	14	0.155	0.056
Centerline	15	0.155	0.056
	16	0.155	0.056
	17	0.155	0.056
	18	0.154	0.056
	19	0.153	0.056
	20	0.153	0.055
	21	0.153	0.055
	22	0.153	0.055
	23	0.153	0.055
	24	0.152	0.055
	25	0.152	0.054
	26	0.151	0.054
	27	0.151	0.054
	28	0.149	0.054
	29	0.148	0.053
Left	30	-	-

occurred about 13 inches downstream of the jet slot. At that location static pressures measured 7.5 inches to either side of the centerline revealed typical differences of ± 1.8 per cent of the mean centerline reading. This difference represented only about 0.7 per cent of the local free-stream dynamic head, however, and was not considered significant. The static pressure distribution became progressively less pronounced downstream of this point of worst distortion.

The jet plenum pressure was easily set and maintained for periods exceeding five hours of continuous testing. The plenum pressure showed no fluctuations within the accuracy of the instrumentation. Total pressure probes inserted through each wall of the jet slot section just ahead of the jet nozzle contraction revealed identical total pressures at each end of the plenum. In addition, a total pressure survey was taken at the jet exit for the entire 30 inch length of the slot. This survey showed that no large scale total pressure gradient existed along the slot and that the jet dynamic pressure variations were no greater than ± 1.0 per cent of the mean value.

Data Acquisition and Reduction

Test Procedure

Apparatus Set-Up. Prior to the initiation of a test run, a calculation was performed to estimate the jet plenum pressure setting required to achieve a desired initial velocity ratio. The Honeywell recorder was turned on and set to monitor the jet plenum temperature. Calibration and zero point checks were then completed on both digital voltmeters. Each Barocel signal conditioner was adjusted in accordance

with the manufacturer's operation manual. The two Barocel transducers were then zeroed with both ports of each referenced to the local atmospheric pressure. The proper Scanivalve unit was stepped to the correct station to monitor the jet plenum chamber pressure with the 1000 mm transducer and the wafer switch was changed from the "zero" position to the "read" position. The jet compressor was started, brought to the pre-calculated plenum pressure setting and allowed to warm up for at least 45 minutes. The main-stream blower was started about 30 minutes after the initiation of the jet flow and was allowed to warm up. During this warm-up period, for the pressure gradient cases, the mainstream valve exhaust area was adjusted until flow separation on the surfaces was located just inside the valve. After warm-up, the total pressure and total temperature probes were lowered into the main-stream flow at a prescribed location just upstream of the jet slot. The main-stream total pressure and total temperature were read through the proper channels of the Scanivalve and Honeywell units respectively. In addition, the free-stream static pressure was recorded by inserting the static pressure probe at the same streamwise location. These measurements combined with the known temperature and pressure in the jet plenum allowed a calculation of the actual initial velocity ratio. A refinement in the jet plenum pressure setting was then made, if necessary, to achieve the desired velocity ratio. The apparatus was allowed to settle to the new jet plenum condition for about ten minutes before the velocity ratio was checked again. In most instances the desired operation point was reached to sufficient accuracy

after one cycle described above.

Data Collection. The main-stream floor boundary layer just upstream of the jet slot was recorded for each set of data measured. A set of data usually encompassed three velocity profiles each taken at different distances from the jet slot, the corresponding skin friction measurements for those profiles and a static pressure survey taken from the 36 centerline static taps and the 12 static taps on either side of the centerline.

To obtain a velocity profile, the total pressure and total temperature probes were fixed respectively in ports 1 and 3 of the probe actuator carriage. The total pressure probe was set lower than the temperature probe such that it would contact the floor first as the carriage was lowered. A Simpson meter was grounded to the test section floor and the positive lead was attached to the top of the total pressure probe. The carriage was lowered until the Simpson meter signalled that the pressure probe had solidly contacted the floor. The crank was carefully turned in the opposite direction to take up the 0.006 inch backlash in the lead screw. The carriage was then drawn upward in 0.001 inch increments until the meter indicated that the probe contact with the floor was tenuous. The "zero" point was noted on the actuator scales. This identical exercise was repeated at least twice more to verify the original zero position within 0.001 inch. With the total pressure probe at the zero location, the positive Simpson meter lead was connected to one lead of the temperature probe. The temperature probe was freed in its holder and was lowered manually until solid contact with the floor was indicated. The probe was then

raised slowly until the meter indicated that contact was about to be lost. The probe was fixed in the actuator carriage in this position. The Simpson meter was again connected to the total pressure probe and the zero point was re-checked to insure that the actuator had not been moved. Both probes were properly aligned with the flow during these manipulations by comparison with scribed lines on the test section floor.

It should be noted that the clear test section side walls were quite helpful in providing visual contact with all probe manipulations. A cathetometer was used initially to check the method of locating the floor with the Simpson meter and total pressure probe. The cathetometer was also used to verify that the total pressure probe did not deflect under aerodynamic forces. The check was made by observing the probe and its image in close proximity with the floor as near-maximum jet flows were started and stopped.

The jet plenum pressure and temperature were checked and recorded on the data sheet along with the zero point of the probes. The ambient pressure and temperature were read and recorded and the Barocel transducers were checked to verify that their zeros had not changed. The velocity profile was then measured by recording the total temperature, total pressure and carriage position in increments ranging from 0.003 inch to 0.200 inch depending on the local rate of change of velocity with height. Each profile consisted of roughly 35 points. Care was taken to check jet plenum conditions and transducer zeros at least once during the recording of each profile. When the main-stream flow was reached, the jet plenum temperature and pressure were again

recorded along with the ambient temperature and pressure. The probe were lowered to the surface and the zero point was verified with the Simpson meter. The temperature and total pressure probes were then removed from the carriage and replaced with the static pressure probe. This probe was lowered to the floor and the static pressure was read and recorded at the exact streamwise and spanwise location at which the velocity profile had been measured.

After the velocity profile measurements were completed, the skin friction measurements were performed with a Preston tube positioned on the floor at those locations at which velocity profiles and wall static pressures were measured. The total pressure reading of the Preston tube was recorded at each location.

The test section floor static pressure survey was recorded as the final segment of the test run. This survey was accomplished by monitoring the test section centerline and off-centerline static pressure taps.

The test was concluded by verifying the jet plenum pressure and temperature, ambient pressure and temperature and the transducer zero points.

Data Reduction. The pressure data and temperature data were transferred from the test data sheets to punched computer cards conforming to the input format of the data reduction program described in detail in Appendix I. This program provides the option of computing any one or all of the following major segments:

1. Initial jet and main-stream velocities.
2. Initial main-stream boundary layer profile and momentum thickness.
3. Wall jet velocity profiles.
4. Local skin friction values.
5. "law of the wall" data.
6. Test section floor static pressure profiles.

CHAPTER IV

EXPERIMENTAL RESULTS

Areas of Investigation

Four separate series of wall jet studies were made in the present work in order to secure experimental results that provide an insight into the mechanisms of various wall flows. Each succeeding series was designed to build upon the previous, simpler case by introducing progressively more complex flow. Figure 17 presents nomenclature for the most complicated wall jet profile form; however, where applicable, the specific terminology is the same for all simpler profiles.

Series I involved the study of the "pure" wall jet in which no free-stream flow is present. The profile form and a composite of typical streamwise development is shown in Figure 18.

A main-stream flow was provided above the jet for the work in Series II. For this case the main stream developed a boundary layer on the floor upstream of the point of jet injection, however, this boundary layer was quickly consumed by the relatively strong jet flow. Typical streamwise development of this flow is shown in Figure 19.

In Series III, the main-stream floor boundary layer was considerably thickened with a rear-facing step and with a roughened surface prior to jet introduction. Downstream of the jet slot an adverse streamwise

pressure gradient was applied to the developing wall jet flow. The combined effect of the thickened main-stream boundary layer and the test section pressure gradient can be seen in Figure 20 in which a valley persists in the velocity profile far downstream of the jet slot.

The main-stream boundary layer was further thickened for the Series IV tests by imposing an adverse pressure gradient on the main-stream flow upstream of the jet slot. This pressure gradient also resulted in distortion of the initial boundary layer profile. The jet was then introduced and the entire developing wall flow was subjected to an additional adverse main-stream pressure gradient. Figure 21 typically demonstrates the severe influence of the initial boundary layer throughout the wall jet development for Series IV.

Actual test conditions for these four series are detailed in the following paragraphs.

Series I

For this case in which there is no main-stream flow, the variable of importance is the Reynolds number based on jet slot conditions. A wide range of this parameter was achieved for the present study through variation of the jet velocity and slot height. Experimental results were obtained for slot heights of 0.056 inches and 0.155 inches and for slot Reynolds numbers from 5,800 to 49,600. The perforated test section ceiling and the main-stream valve were removed for these investigations. Table 2 identifies the detailed information that is available for this series in tabular form in Appendix J.

Series II

The magnitude of the ratio of jet velocity to main-stream velocity at the jet slot, U_j/U_{e_o}, and the momentum deficit of the main-stream floor boundary layer at the jet slot are the important parameters for this series. Values of U_j/U_{e_o} between 1.5 and 6.0 were studied. No effort was made to modify the initial main-stream floor boundary layer for any of these cases. The contraction fairings upstream of the boundary layer development section were set to match the floor and ceiling of the section. The internal height and width of the boundary layer development section were held constant and no roughening agent was applied to the floor. The jet slot was set at a height of 0.155 inches and the perforated ceiling of the test section and main-stream valve were removed for these studies. A summary of the data secured in this work is given in Table 3 and the data is tabulated in detail in Appendix K.

Series III

For these investigations the momentum deficit and thickness of the initial floor boundary layer were significantly increased. To accomplish this, the floor contraction fairing was raised at the entrance to the boundary layer development section creating a step or base region 0.625 inches high. To further thicken the boundary layer, a medium grit sandpaper sheet was affixed to the floor of the boundary layer development section. The jet slot height was fixed at a value of 0.056 inches and values of U_j/U_{e_o} of approximately 1.5, 2.0 and 3.0 were studied. Pressure gradients were applied by reducing the main-stream valve exhaust area to bleed main-stream flow out through the

perforated test section ceiling. The operating condition was set by adjusting the valve such that separation of the wall jet flow occurred just downstream of the test section. Separation was determined by observation of yarn tufts attached to the surfaces of the main-stream control valve and the last five inches of the test section. The available experimental data for this series is summarized in Table 4 and is tabulated in detail in Appendix L.

Series IV

An expansion contour was attached to the ceiling of the boundary layer development section as shown in Appendix A, Figure A-1, so that the main-stream floor boundary layer was subjected to an adverse stream-wise pressure gradient before it reached the test section. As a result, the initial boundary layer under which the jet was injected was further thickened and its profile was distorted. The base region, boundary layer development section floor roughness and jet slot height were maintained as in Series III. As before, the main-stream valve exhaust area was reduced until separation of the wall jet occurred on the floor just downstream of the test section. Nominal initial velocity ratios, U_j/U_{e_o}, of 1.0, 2.0 and 3.0 were investigated. A summary of available data is given in Table 5. The data is tabulated in detail in Appendix M.

Flow Evaluation

A careful evaluation of flow characteristics prior to each series of tests was considered imperative to establish confidence in the subsequent measurements. These investigations were especially important since physical alterations in the apparatus were required

to achieve the wide range of variables and conditions that were studied. The evaluations are presented in the following paragraphs:

Series I

For the 0.155 inch slot, velocity profiles were measured at the centerline and approximately 4 inches to each side of the centerline at x/h = 11, 69 and 198 for Re_s = 49,600 (nominal) and at x/h = 17.5, 69 and 198 for Re_s = 33,500 (nominal). The data revealed little scatter so that differences in the profiles could be directly attributed to flow non-uniformities associated with the slot and with the entrainment of ambient air. For both Reynolds numbers, the greatest profile disagreement occurred nearest the slot. For x/h = 17.5 in the case of Re_s = 33,500, the right and left profiles (looking upstream) showed excellent agreement throughout. Both revealed jet peak velocities, U_1, that were approximately 2.1 per cent above the peak velocity of the centerline profile. Aside from the lower velocity measured in the immediate vicinity of δ_1, the centerline profile agreed very closely with the two side profiles. For example, there typically was no velocity difference among the three profiles in the region of δ_2. The measurements at x/h = 17.5 are shown in Figure 22a. At x/h = 69, the velocity difference at δ_1 was slightly less than 2.1 per cent of the centerline value and at x/h = 198 there was no measurable difference in velocities at δ_1 among the three profiles. As with the closest profiles, there was no difference in velocity in the region of δ_2 at either x/h = 69 or x/h = 198. The velocity profile comparisons at x/h = 69 and x/h = 198 are shown in Figures 22b and 22c respectively.

For Re_s = 49,600, the results were similar to those for Re_s = 33,500 but with slightly smaller differences noted at comparable locations. The centerline peak velocity was still the lowest. At x/h = 69 the right and left peak velocities were only 1.9 per cent above the centerline value. As for the previous case, this difference disappeared completely by x/h = 198 and the profile velocities showed excellent over-all agreement. From the results of these studies it was concluded that the wall jet flow for the 0.155 inch slot was acceptably two-dimensional for the full length of the test section over at least the center portion in which all subsequent profiles were measured.

A velocity profile comparison was also completed for the 0.056 inch slot at 193 slot heights from the slot for Re_s = 5,800. Profiles were measured at 3 inches to the right and left of the centerline as well as directly on the centerline. The center and right profiles agreed very closely; however, the left profile had a jet peak velocity 1.6 per cent greater than centerline value. With the exception of the disagreement in the peak velocity, all three profiles were nearly identical over the entire height. On the basis of these results and those of the previous examination which covered the entire streamwise range, it was concluded that the flow from the 0.056 inch slot was acceptably two-dimensional.

Since the 0.056 inch slot was used almost entirely in conjunction with the studies of main-stream flows with streamwise pressure gradients, its performance was further investigated for just such flow. These studies will be reported presently and will serve as additional

verification of the assumption of two-dimensionality made above.

All subsequent measurements for Series I were performed within the path for which two-dimensionality had been checked.

Series II

A dynamic pressure survey of the main-stream flow was taken at the exit of the boundary layer development section. This survey showed that the dynamic pressure varied by less than ± 2.0 per cent from the mean for the entire flow outside of the wall boundary layers. The corresponding velocity variations were less than ± 1.0 per cent. However, the spanwise velocity differences that could generate three dimensional flow effects were, on the average, a maximum of about 0.25 per cent of the mean. The results of the study are shown in Figure 23.

The main-stream boundary layer just upstream of the jet slot was measured at 3 spanwise locations about the centerline to check for uniformity. The width of the span covered was approximately 7 inches. The centerline boundary layer profile consistently demonstrated the lowest velocities, but the maximum disagreement among the profiles at any height was less than 1.4 per cent above the centerline value. In addition, a two-dimensionality study was performed at distances of 10, 65 and 195 slot heights from the jet slot for a nominal initial velocity ratio of 4.5. These measurements were made at the same spanwise locations as were used for the initial boundary layer study. The three profiles exhibited velocity agreement within 0.5 per cent at each of the streamwise locations investigated. A typical comparison is given in Figure 24. All subsequent skin friction and velocity profile measurements for Series II were taken in the path for which two-

dimensionality had been confirmed by these studies.

It was noted that the results of the two-dimensionality study with free stream reflected much smaller velocity differences about the jet peak than did the study for the jet flow alone. In the pure jet study for the 0.155 inch slot, the plenum pressure was monitored with a Mercury column micro-manometer. It was discovered that this instrument did not have the desired sensitivity and that small plenum pressure changes from the mean could go undetected. The situation was remedied for all later measurements by monitoring the plenum pressure with the 1000 mm Barocel transducer. The pressure was thus read more accurately and was adjusted quickly to compensate for any drift.

Series III

Since the geometry in the boundary layer development section was changed considerably for these cases, a thorough two-dimensionality study was performed before test measurements were attempted. Four separate studies were completed, two with no pressure gradient in the test section and two with a streamwise pressure gradient strong enough to cause separation of the wall jet near the exit of the test section. The adverse gradient and zero pressure gradient tests each consisted of one test with a main stream only and one test with a wall jet in which $U_j/U_{e_o} = 2$ (nominal). In all four studies velocity profile measurements were made at three spanwise locations at approximately 125 and 554 slot heights from the jet slot. The spanwise measurements were made at the test section centerline and at 7 inches to either side of the centerline. The results showed that the worst comparison among the profiles occurred at $x/h = 554$ for the main-stream flow only with pressure gradient. The

right and left profiles (looking upstream) demonstrated maximum velocity differences of about ± 4.0 per cent from the centerline value. These somewhat high values can be attributed to the flow unsteadiness and low velocity associated with nearly separated flow. At x/h = 125, the maximum velocity difference among the profiles at a given height was only about ± 1.5 per cent from the centerline velocity. The jet and main-stream flow combination demonstrated the worst agreement under pressure gradient at x/h = 125. At this station the maximum disagreement was detected at the jet peak velocity. The centerline and left profiles demonstrated nearly identical results at the jet peak while the right profile showed a peak velocity about 3.6 per cent above the centerline value. This maximum difference diminished to 1.5 per cent at x/h = 554. The worst cases just described are shown in Figures 25 and 26. The figures show that the flow is acceptably two-dimensional especially when the total span of 14 inches is considered.

Series IV

The effect of the expansion contour in the boundary layer development section on the main-stream flow was investigated. Velocity profiles through the floor boundary layer were obtained at x/h = 554 with a main-stream flow only and no pressure gradient. The measurements were taken at the centerline and 7 inches to the right and left of the centerline. All three profiles agreed within 1.0 per cent throughout and the results are given in Figure 27.

Velocity profiles were also taken at x/h = 125 for an initial nominal velocity ratio of 2.0 and a severe adverse streamwise test section pressure gradient. These measurements again show a slightly

higher jet peak velocity at the right profile with nearly identical results for the centerline and left profiles. The jet peak velocity on the right was about 2.5 per cent above the values for the center and left profiles. The left profile revealed a less pronounced valley and generally higher velocities from the valley to the free-stream velocity. Figure 28 shows, however, that the profiles are acceptably two-dimensional when the total span of 14 inches is considered.

Wall Jet Experimental Results

The following paragraphs present typical results compiled from the present wall jet experimental investigation. These results not only demonstrate over-all flow development characteristics such as thickness growth and velocity decay but also reveal velocity and temperature profile similarities, skin friction and friction coefficient laws and a "law of the wall" for wall jet flow. Further, the presentation gives evidence of the scope of wall jet flow conditions that have been studied.

Initial Boundary Layer

A representative initial boundary layer profile for each of the major segments of the present research is plotted in Figure 29 for comparison. The respective nominal momentum thickness for each profile is included in the figure. The turbulent boundary layer profile of Series II resulted from natural growth along the floor of the boundary layer development section. The flatness apparent in the Series III profile is a lingering effect of the base region presence at the entrance of the boundary layer development section. The Series IV profile shows

the combined effect of the base region and the adverse pressure gradient to which it has been subjected. As an indication of the strength of the pressure rise and the resulting profile distortion, the wake region of this last profile was evaluated from the similarity form suggested by Coles [23]:

$$\frac{U}{U_\tau} = \underbrace{\frac{2.303}{k} \text{LOG}_{10} \left(\frac{U_\tau Y}{\nu}\right) + C}_{\text{Law of the Wall}} + \underbrace{\frac{2\Pi}{k} \sin^2 \left(\frac{\pi}{2} \frac{Y}{\delta_e}\right)}_{\text{Law of the Wake}} \qquad (1)$$

where $k = 0.41$, $C = 5.0$ and $U_\tau = \sqrt{\tau_w/\rho}$. The constant, Π, is a measure of the wake profile deviation from the linear "law of the wall." Re-arranging (1), the wake deviation may be expressed as,

$$\frac{\Delta U}{U_\tau} = \frac{2\Pi}{k} \sin^2 \left(\frac{\pi}{2} \frac{Y}{\delta_e}\right) \qquad (2)$$

$\Delta U/U_\tau$ was determined for the present data by matching the "law of the wall" portion of Coles' expression at $\text{LOG}_{10} \frac{U_\tau Y}{\nu} = 2.5$. Figure 30 presents the match achieved between the present data and Equation (2) for $\Pi = 3.27$. It is apparent in this figure that a classical wake profile has been achieved. Coles also provided a compilation of data for turbulent boundary layers in adverse pressure gradients in [23]. Included in this compilation is a record of the increasing value of Π for boundary layer profiles as separation is approached. The boundary layer data of Ludwieg and Tillman is presented by Coles as an example of a severe adverse pressure gradient case. It was determined that the present value of $\Pi = 3.27$ represents a profile comparable to that

given by Ludwieg and Tillman when the pressure rise was 95 per cent of the total pressure measured at separation.

Figure 31 shows the ratio of jet momentum excess to boundary layer momentum deficit (both referenced to the local free-stream velocity) at the jet slot as a function of initial velocity ratio, U_j/U_{e_o}, for Series II, III, and IV. It is apparent from these results that the initial boundary layer will exert an important influence in the development of Series III and Series IV wall jet profiles since this ratio is about one or less for these studies.

Wall Jet Growth

Figure 32 presents the influence of slot Reynolds number on the growth of the half-velocity height, δ_2, for the infinite velocity ratio cases (Series I). The theoretical result predicted by Harris [17] is shown along with experimental data from the present study and from Verhoff [13] and Gartshore [16]. Harris' analysis typifies theoretical predictions of slot Reynolds number effect while the data of Verhoff and Gartshore represent reliable experimental results. The present data reflects the predicted slot Reynolds number trend and confirms the near-linear growth rate shown by others.

The effect of initial velocity ratio on δ_2 growth is given in Figure 33. Since the main-stream flow rate was not easily altered, the free-stream to jet velocity ratio at the jet slot was changed by varying the jet flow rate. The growth curves, then, reflect the combined effect of slot Reynolds number and velocity ratio change. The influence of Reynolds number in this plot is indicated by a review

of Figure 32. An increase of the slot Reynolds number for any given initial velocity ratio would decrease the slope of the growth curve and conversely.

Figures 34a and 34b show representative growth from Series III and IV for a nominal initial velocity ratio of 2. Evidence of the adverse pressure gradient can be seen in growth non-linearity, especially in the outer layer parameters. The greater magnitude of growth for Series IV is a reflection of the thickness and distortion of the initial boundary layer for that series. In addition, the adverse test section pressure gradients in Series IV were somewhat more severe than those for Series III and this difference is revealed in the higher rates of growth shown in Series IV. A comparison of typical free-stream velocities for the two series will be shown presently.

The growth data was further examined for clues regarding possible similarity parameters for velocity profile representation. No single length scale was found to yield similarity for the entire wall jet profile. This result was expected since at least two individual length scales, jet slot height and main-stream boundary layer thickness, are initially involved. Velocity profile similarity was achieved by dividing the profile into segments and by defining an individual velocity and length scale for each segment. The results of this approach will be shown under the "Velocity Profile" discussion in the "Wall Jet Profile Similarity" section of this text.

Wall Jet Decay

The effect of slot Reynolds number on the decay of jet peak velocity for Series I is demonstrated in Figure 35. The data is shown

to be consistent in trend with theoretical predictions and in close agreement with the results of comparable measurements of others.

The combined influence of slot Reynolds number and initial velocity ratio is given for Series II in Figure 36. As with the growth curves, the effect of changing slot Reynolds number for a given initial velocity ratio can be perceived from the infinite velocity ratio studies (Figure 35). Reynolds number effect is emphasized for Series II in Figure 37 by plotting jet peak velocity decay referenced to the main-stream velocity.

Representative free-stream velocity retardation and jet peak velocity decay results for series III and IV are given in Figures 38a and 38b for nominal initial velocity ratios of 2 and 3. The figures show that at the furthest downstream measurement location the local free-stream velocity has been retarded to about 60 per cent of its value at the jet slot. Figures 38a and 38b also reveal that the free-stream velocity gradient is more severe close to the jet slot for the Series IV cases than for the Series III work.

The local ratio of minimum velocity to free-stream velocity, U_3/U_e, is presented in Figure 39 for nominal initial velocity ratios of 2.0 and 3.0 for series III and IV. Nearly constant ratios of U_3/U_e have been achieved in the wake layer (δ_3 to δ_e) over a distance of several hundred slot widths. Furthermore, this has been accomplished with significant velocity defects in the wake region. For example, as shown in Figure 39, values of U_3/U_e of approximately 0.55 have been maintained in Series IV.

Figure 40 shows jet layer (δ_1 to δ_3) results from Series III and IV for nominal velocity ratios of 2.0 and 3.0. The Series IV data for $U_j/U_{e_o} = 3.0$ shows that a near-self-preserving condition is present from about 200 to 300 slot widths. The remaining sets of data demonstrate self-preserving conditions for considerably longer distances. The velocity deficit in the wake is also emphasized in this figure. Ratios of U_1/U_3 between 1.2 and 2.8 are obtained over the region for which the velocity ratio, U_1/U_3, is maintained nearly constant.

Figure 41 presents the local ratios of jet peak velocity to free-stream velocity, U_1/U_e, for the cases just described. In these cases significant velocity valleys have been maintained. The figure shows that for $U_j/U_{e_o} = 2$ in Series III and IV the jet peak velocity has dropped well below the local free-stream velocity.

In order to achieve the jet flow rate capability of the present apparatus, it was necessary to generate jet compressor exhaust pressures of about 5 PSIG. This compression resulted in initial jet temperatures which are 50 to 100 degrees Fahrenheit above the main-stream flow temperature. The decay of the jet peak temperature with distance from the slot is given in Figures 42, 43, and 44. Figures 45, 46, 47 and 48 combine the jet peak velocity decay and the jet peak temperature decay. The non-similarity that exists in the velocity-temperature decay is quite evident for all four cases. Abramovich [24] presented individual analytical expressions for the jet peak velocity and temperature decays for a plane, two-dimensional free jet using Taylor's vorticity-transfer theory of turbulence. These expressions can be combined to predict that the ratio of velocity decay to temperature

decay has a constant value of about 1.15. This slope has been reproduced in each of the figures for comparison with the present experimental results. The data shows marked non-linearity as the point of jet peak disappearance is approached; however, at least in the central range, the decay appears to be linear and at a rate close to the theoretical prediction for a pure two-dimensional turbulent free jet. This behavior is especially evident in the Series I data which most closely approximates a free jet issuing into still air.

Wall Jet Profile Similarity

Temperature Profile. Figures 49, 50, 51 and 52 show the non-dimensional temperature profile through the wall jet for each of the major areas of investigation. A review of the tabulated data reveals that for these experiments the total temperature remains essentially constant from the wall to the jet peak velocity. Near the jet peak the temperature begins to decay linearly with height until it reaches T_e. The expression,

$$\frac{T - T_e}{T_1 - T_e} = - 0.588 \frac{Y}{\delta_2} + 1.12 \qquad (3)$$

is a good representation of this decay for all four sets of measurements. T_e should be replaced by T_3 in this expression for Series III and IV measurements.

As previously stated, in the present measurements the initial difference in temperature between the jet and main-stream flows was always between 50 and 100 degrees Fahrenheit. This difference diminished to only about 10 degrees at the measurement stations furthest

downstream. The scatter evident in Figures 49, 50, 51 and 52 can be appreciated when it is considered that a 1.0 degree error in temperature measurement could result in a 5 to 10 per cent error in the abscissa. A 1.0 degree error, however, is insignificant in calculation of flow properties.

It should be expected that the higher jet temperatures and the resulting lower momentum associated with a given slot height and jet velocity for the present work might be seen in differences in wall jet properties when compared to previous work performed with both flows at the same temperature. The temperature differences between the main-stream and jet flows encountered in the present study reflect in density differences at the slot that are about 15 per cent of the main-stream air density. While these differences may become evident in detailed calculations such as those involving integration through the velocity profile, the wall jet growth and decay previously described show no measurable influence of the temperature differences.

Velocity Profile. Figure 53 presents non-dimensional velocity profile data from Series I. Included in the figure is Verhoff's analytical representation of the infinite velocity ratio profile. Verhoff has matched this functional form with his own data as well as with the data of Förthmann [2], Meyers et al., [8], George [9] and Patel [25] for a wide range of slot Reynolds numbers. The present data tends to fall slightly below Verhoff's curve in the region just above the jet peak. This tendency is also noted in the experimental results of the other authors just mentioned. In addition, his formula gives somewhat lower velocities below the jet peak. Verhoff's

expression nevertheless gives a good representation of the data over much of the profile. Figures 55, 56 and 57 show non-dimensional velocity profile results for the jet layer from Series II, III and IV respectively. The similarity parameter, δ_j, used to obtain these plots is defined in Figure 54. Included in each of the figures are two theoretical velocity profile representations. The hyperbolic tangent function is a solution for the two-dimensional free jet with constant eddy viscosity. The exponential function emerges as the constant eddy viscosity solution for a two-dimensional wake with small differences between the free-stream velocity and the minimum velocity in the profile. Both representations are matched to the data at the half-velocity height. Plotted in this manner, neither analytical form gives acceptable agreement in the outer portion of the profile. The hyperbolic tangent function, however, provides an excellent fit to the data for the region from the half-velocity height, δ_2, to the jet peak, δ_1.

It is apparent from Figures 55, 56 and 57 that the similarity form valid in the jet layer does not extend into the wall layer. In Figure 58, typical valley region velocity profile data (in the vicinity of δ_3) is plotted also non-dimensionalized for the jet layer. This data reveals, further, that the jet layer similarity does not extend into the wake layer.

Similarity profiles for the wake layer are shown in Figures 59 and 60 for Series III and IV. The similarity parameter, δ_w, is defined

in Figure 54. The exponential representation plotted in both figures shows excellent agreement with the data from δ_3 to δ_4 ; however, the agreement is not as good as the free-stream velocity is approached. This difference may result from the choice of the half-velocity height as the matching point or it may be a reflection of intermittency errors in the outer profile measurements.

Wall Jet Skin Friction

Friction Coefficient. Figure 61 reveals the slot Reynolds number effect on friction coefficient for the infinite velocity ratio measurements (Series I). The coefficient is plotted in conjunction with a local Reynolds number based on properties at the jet peak in Figure 62. Typical experimental results from Sigalla are included along with a line representing the data Bradshaw and Gee [7]. In the range, $3.8 \leq LOG_{10} Re_{\delta_1} \leq 4.4$ the expression,

$$C_f = 0.0297 \left(Re_{\delta_1} \right)^{-0.182} \tag{4}$$

is a good representation of the friction coefficient for the present data. Although Equation (4) gives values of friction coefficient that are numerically close to those of Sigalla, Figure 62 reveals that this formula exhibits a slope that agrees with the data of Bradshaw and Gee. The present data falls about 5 per cent below the friction coefficient measurements of Bradshaw and Gee.

Friction coefficients measured in Series II are given in Figure

63. For reference, Equation (4) ($U_j/U_{e_o} \sim \infty$) is reproduced along with a friction law obtained from Coles' compilation of Wieghardt's constant-pressure boundary layer data.

The Series II skin friction results were further investigated to determine if a set of unique friction laws based on local velocity ratio, U_1/U_e, exists. One might predict that initially the near-wall portion of the jet flow would resemble a boundary layer in some "starting region" for which the influence of the outer layer has not yet penetrated through the jet. Once a true wall jet flow has been established, however, it may be reasonable to expect the existence of friction laws keyed to local velocity ratio values. Figure 64a shows the data presented in Figure 63 with each point accompanied by its local value of U_1/U_e. Figure 64b hypothesizes a set of friction laws for constant values of U_1/U_e as determined by this author through interpolation of the data in Figure 64a. The laws presented were not deduced with a rigorous curve-fitting routine.

Figure 64b shows that the friction law for the infinite velocity ratio case provides a reasonably good approximation for all instances in which the local velocity ratio is greater than 2. Below this value, the succeeding laws drop at an increasing rate toward the constant-pressure boundary layer law. A review of Figure 64a reveals that the first (lowest Re_{δ_1}) two or three points for each initial velocity ratio, U_j/U_{e_o}, are not consistent with the friction laws shown in Figure 64b. These points tend to fall closer to the boundary layer friction law than would be predicted by the laws based on local velocity ratio. This behavior is to be expected since these points lie closest to the jet

slot and are, thus, in the transition flow between the constant-pressure boundary layer and the true wall jet flow regimes.

Figures 65 and 66 present typical skin friction data obtained under adverse pressure gradient in Series III and IV for a nominal initial velocity ratio, U_j/U_{e_o}, of 2. Each data point is accompanied by the local value of U_1/U_3. The linear friction coefficient decay demonstrated by the zero pressure gradient cases is no longer evident.

Law of the Wall. Figure 67 presents typical near-wall profile data plotted in conjunction with the local skin friction for the infinite velocity ratio cases. The influence of the outer layer can be clearly seen as the Series I data drops below the linear growth of the turbulent boundary layer at the high end of the curve. The lowest data point shown for each Re_s was obtained with the total pressure probe touching the floor and, therefore, cannot be considered reliable.

Figures 68 and 69 show inner profile data for several finite velocity ratios (Series II) at two distances from the jet slot. The influence of slot Reynolds number is revealed by the degree to which the data drops from semi-logarithmic linear growth as the jet peak is approached. The wall layer results presented in these figures are typical of the available data for Series II. Once again, the lowest points must be considered suspect.

The effect of the adverse pressure gradient applied in Series III and IV is evident in Figures 70, 71 and 72. The data presented is taken from Series III but it is representative of all data measured under adverse pressure gradient. The profiles nearest the slot show that the wall layer has not been significantly affected by the pressure rise.

Further downstream, however, the velocity profiles exhibit the distortion that penetrates progressively deeper as the ratio of the pressure gradient to the dynamic head increases with distance from the slot.

The near-wall profile data for all four series of measurements reveals that a linear profile law does exist over a short distance and that this law may be represented by,

$$\frac{U}{U_\tau} = 4.825 \ \text{LOG}_{10} \frac{U_\tau Y}{\nu} + 7.175 \qquad (5)$$

This expression exhibits a lower slope and yields higher values of U/U_τ than Coles' "law of the wall" formula, (1), especially in approximately the lower 15 per cent of the profile. Coles observed this same behavior for the near-wall data in many of the flows he reviewed but he chose to eliminate these points in his curve-fitting procedure. He concentrated instead on the "central" portion of the profile to obtain his formula. Coles suggests that a possible explanation for the difference in his formula and the near-wall data may be found in the higher turbulence levels in this region and to wall-probe interference effects.

If the near-wall data is ignored for the present study, it is apparent that the results in the central portion (say, in the neighborhood of $\text{LOG}_{10} \frac{U_\tau Y}{\nu} = 2.3$) may be represented by a linear expression that is parallel to Cole's formula and approximately 2 per cent higher at $\text{LOG}_{10} \frac{U_\tau Y}{\nu} = 2.3$. In terms of skin friction, Coles' formula yields values of τ_w correspondingly 5 per cent higher than the present

measurements.

Bradshaw and Gee [7] performed a Preston tube calibration in a wall jet in still air on a flat plate. Their subsequent skin friction measurements were shown in Figure 63. As previously discussed, the friction law determined from the present data is parallel with the law of Bradshaw and Gee, but the values of C_f are about 5 per cent below their values. Consequently, it is suggested that the use of Patel's [22] Preston tube calibration formulas leads to values of τ_w that are about 5 per cent too low, at least for the case of the wall jet in still air in which the outer layer influence on the wall layer is most significant. As the wall jet flow approaches true boundary layer behavior ($U_1/U_e \rightarrow 1.0$) it is expected that these errors would diminish and that Patel's calibration formulas would yield correct values of τ_w.

In view of the number of corrections that may be incorporated, this author feels that the most straightforward approach for the present work is to record the experimental data directly as measured. The reader may then exercise the option of applying the data as presented or of selecting whatever corrections he deems necessary for his particular use.

Table 2. Series I Data Index
(Appendix J)

Re_s	h ~ In	x/h	Measurements* Velocity Profile	Measurements* Skin Friction	Summary Index
5,809	0.056	193	x		177
10,916	0.056	283	x		177
13,998	0.056	550	x	x	177
14,323	0.056	283	x	x	177
16,083	0.056	550	x	x	177
19,561	0.155	43		x	181
		69	x	x	181
		89		x	181
		101		x	181
		121		x	181
		140		x	181
		166		x	181
		179		x	181
		198	x	x	181
31,128	0.155	43		x	183
		69	x	x	183
		101		x	183
		140		x	183
		160		x	183
		198	x	x	183
31,451	0.155	43		x	185
		69		x	185
		101		x	185
		134		x	185
		166		x	185
		198		x	185
33,540	0.155	17.5	x		186
		69	x		186
		198	x		186
44,050	0.155	43		x	192
		69		x	192
		101		x	192
		140		x	192
		166		x	192
		198		x	192
49,616	0.155	11	x		186
		69	x		186
		198	x		186

* "x" Denotes Measurements Taken

Table 3. Series II Data Index
(Appendix K)

U_j/U_{e_o}	h ~ In	x/h	Measurements* Velocity Profile	Measurements* Skin Friction	Summary Index
0	0.155	0	x		194
1.49	0.155	30		x	195
		43		x	195
		56		x	195
		69		x	195
		89		x	195
		101		x	195
		101	x		196
		121		x	195
		140		x	195
		198		x	195
		198	x		196
1.74	0.155	30		x	198
		43		x	198
		56		x	198
		69		x	198
		89		x	198
		101		x	198
		121		x	198
		140		x	198
		166		x	198
		198		x	198
2.00	0.155	13	x		202
2.00		26	x		202
1.99		37		x	199
2.00		39	x		202
2.00		52	x		202
2.00		65	x		202
1.99		69		x	199
2.00		97	x		202
1.99		101		x	199
2.00		101	x		200
2.00		129	x		202
1.99		134		x	199
2.00		161	x		202
1.99		166		x	199
2.00		194	x		202
1.99		198		x	199
2.00		198	x		200

Table 3. (continued)

U_j/U_{e_o}	h ~ In	x/h	Measurements* Velocity Profile	Measurements* Skin Friction	Summary Index
2.96	0.155	13	x		208
		26	x		208
		39	x		208
		52	x		208
		65	x		208
		97	x		208
		129	x		208
		161	x		208
		194	x		208
3.93	0.155	13	x		215
3.93		26	x		215
3.92		37		x	214
3.93		39	x		215
3.93		52	x		215
3.93		65	x		215
3.92		69		x	214
3.93		97	x		215
3.92		101		x	214
3.93		129	x		215
3.92		134		x	214
3.93		161	x		215
3.92		166		x	214
3.93		194	x		215
3.92		198		x	214
5.78	0.155	13	x		222
5.78		26	x		222
5.70		37		x	221
5.78		39	x		222
5.78		52	x		222
5.78		65	x		222
5.70		69		x	221
5.78		97	x		222
5.70		101		x	221
5.78		129	x		222
5.70		134		x	221
5.78		161	x		222
5.70		166		x	221
5.78		194	x		222
5.70		198		x	221

* "x" Denotes Measurements Taken

Table 4. Series III Data Index
(Appendix L)

U_j/U_{e_o}	h ~ In	x/h	Measurements*		Summary Index
			Velocity Profile	Skin Friction	
0	0.056	0	x		229
0	0.056	125	x	x	230
0	0.056	554	x	x	230
0	0.056	125	x	x	230
		197	x	x	230
		286	x	x	230
		357	x	x	230
		462	x	x	230
		554	x	x	230
1.52	0.056	125	x	x	235
		197	x	x	235
		286	x	x	235
1.51	0.056	357	x	x	235
		462	x	x	235
		554	x	x	235
2.07	0.056	125	x	x	239
		197	x	x	239
		286	x	x	239
		357	x	x	239
		462	x	x	239
		554	x	x	239
2.92	0.056	125	x	x	243
		197	x	x	243
		357	x	x	243
		462	x	x	243
		554	x	x	243

* "x" Denotes Measurements Taken

Table 5. Series IV Data Index
(Appendix M)

U_j/U_{e_o}	h ~ In	x/h	Measurements*		Summary Index
			Velocity Profile	Skin Friction	
0	0.056	0	x		248
1.05	0.056	125	x	x	249
		196	x	x	249
		287	x	x	249
		357	x	x	249
		463	x	x	249
1.97	0.056	125	x	x	253
		196	x	x	253
		287	x	x	253
1.96		357	x	x	253
		463	x	x	253
2.00	0.056	56	x	x	257
		92	x	x	257
1.99		125	x	x	257
2.00		161	x	x	257
		196	x	x	257
2.99	0.056	125	x	x	261
		196	x	x	261
		287	x	x	261
2.98		357	x	x	261

* "x" Denotes Measurements Taken

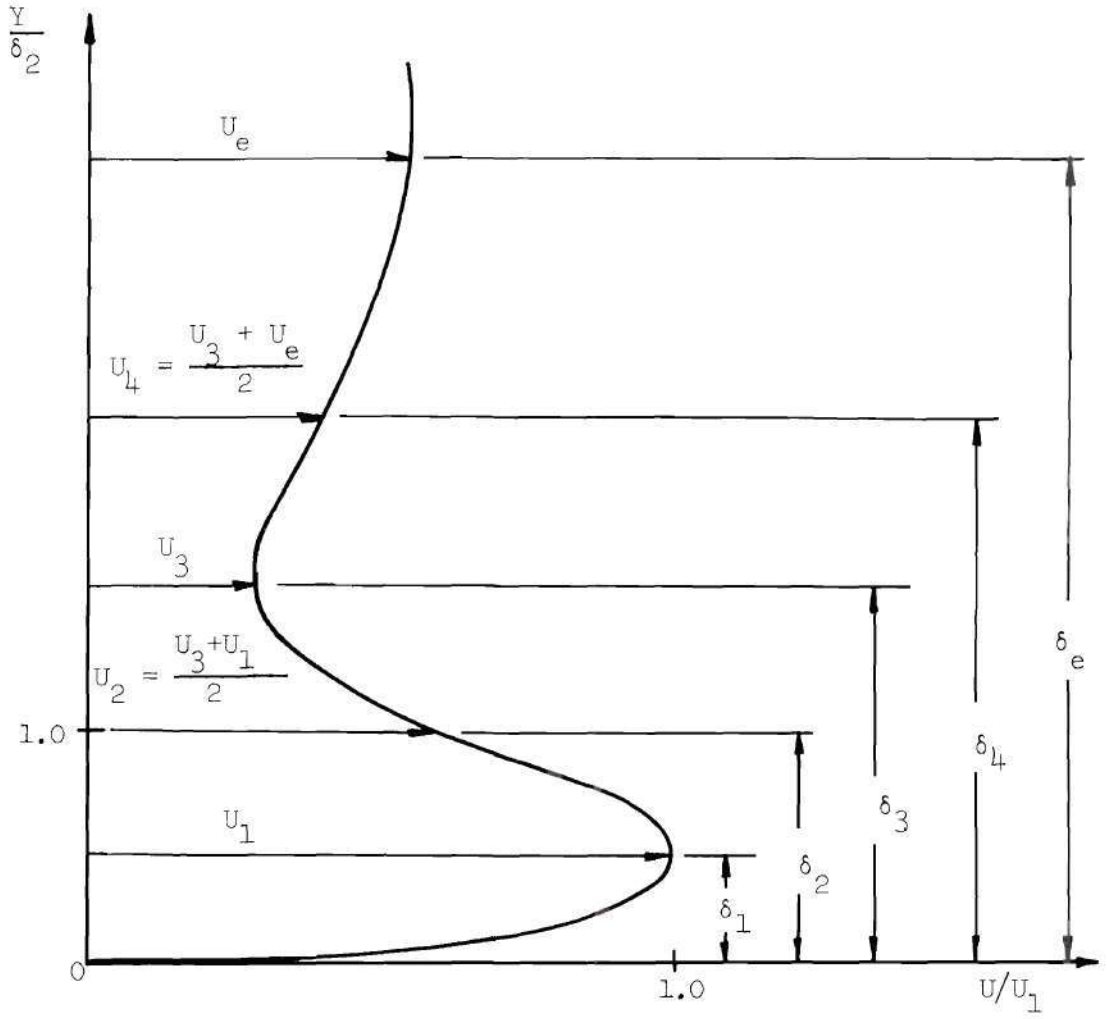

0 To δ_1 ~ "Wall Layer"
δ_1 To δ_3 ~ "Jet Layer"
δ_3 To δ_e ~ "Wake Layer"

Figure 17. Wall Jet Velocity Profile Nomenclature

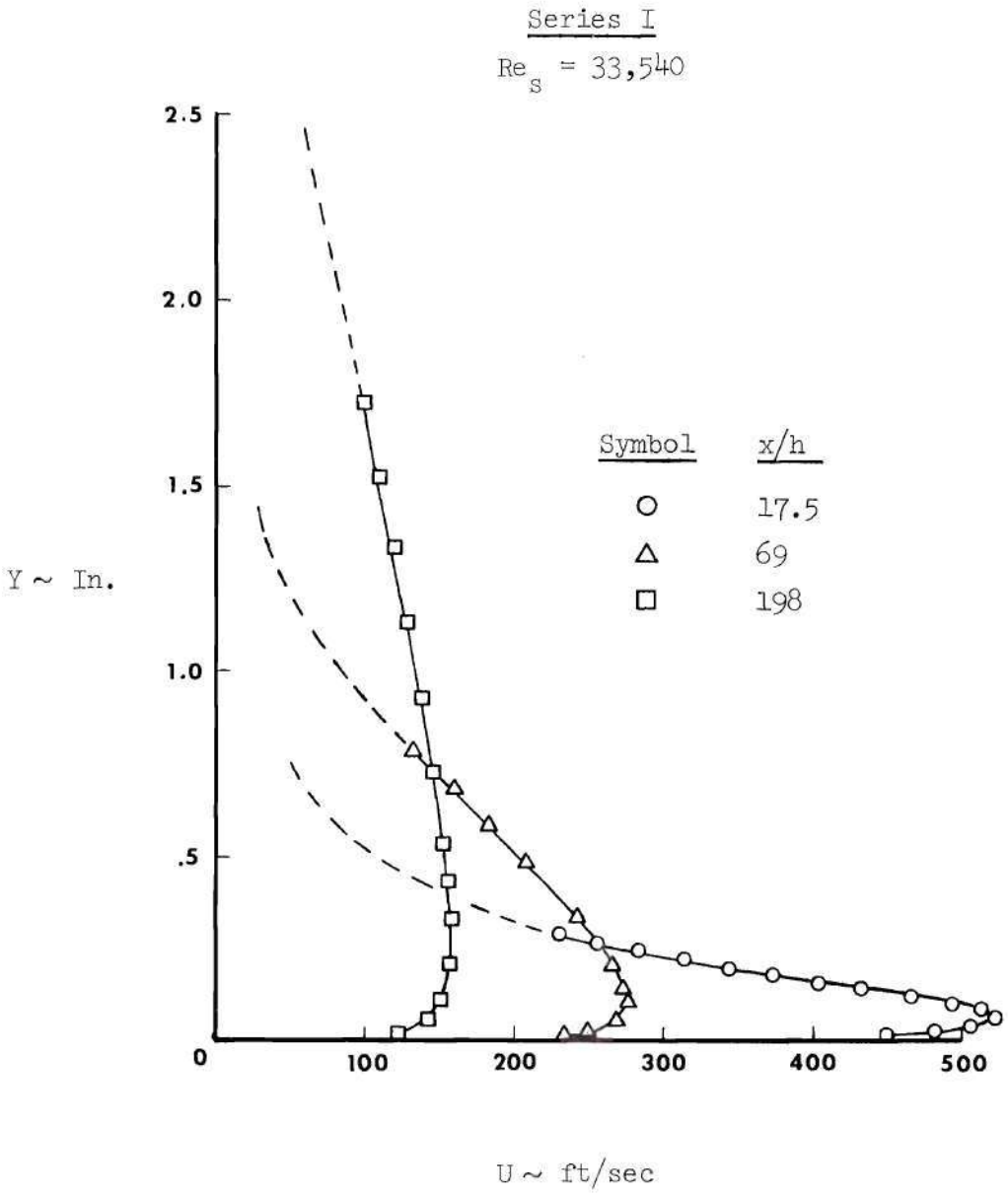

Figure 18. Composite Wall Jet Development

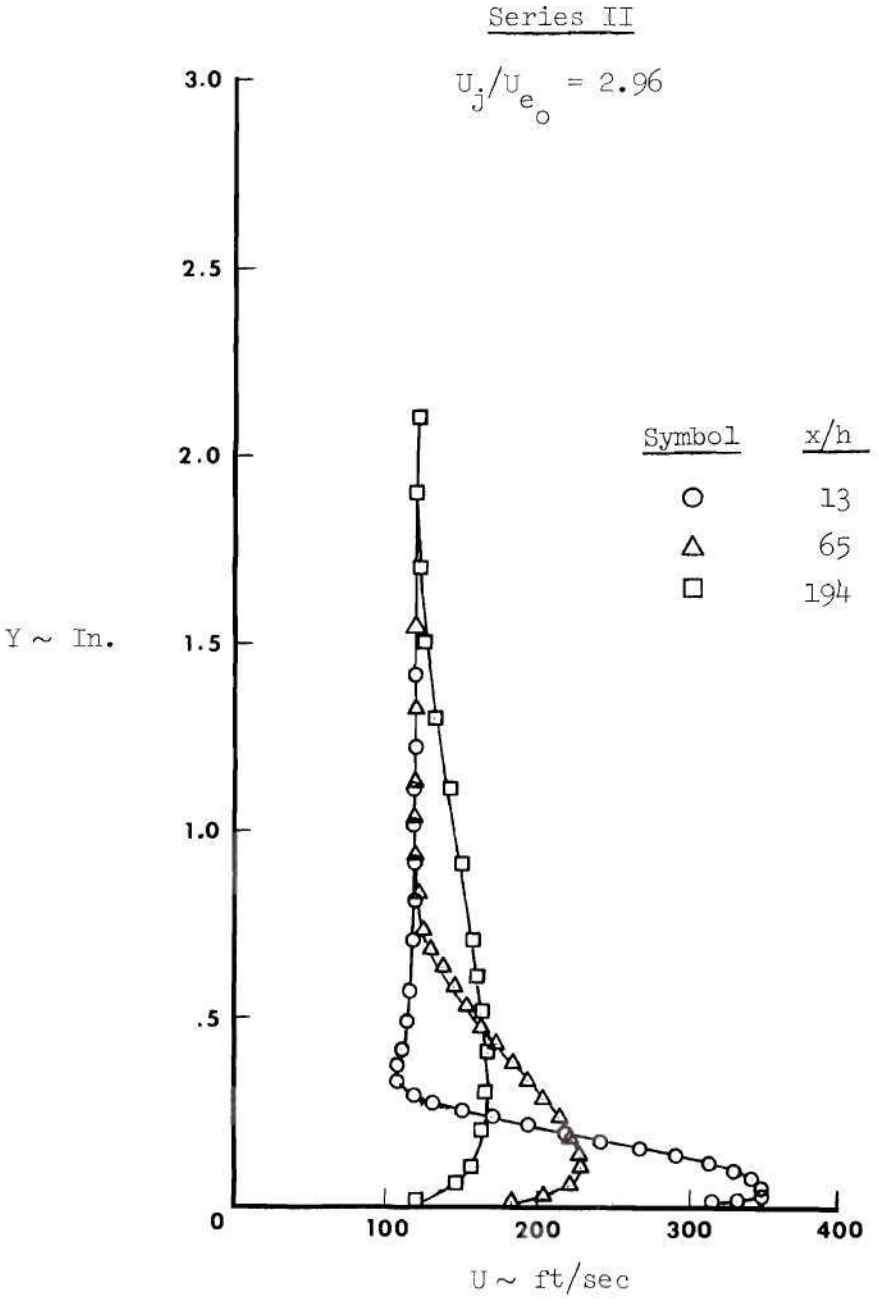

Figure 19. Composite Wall Jet Development

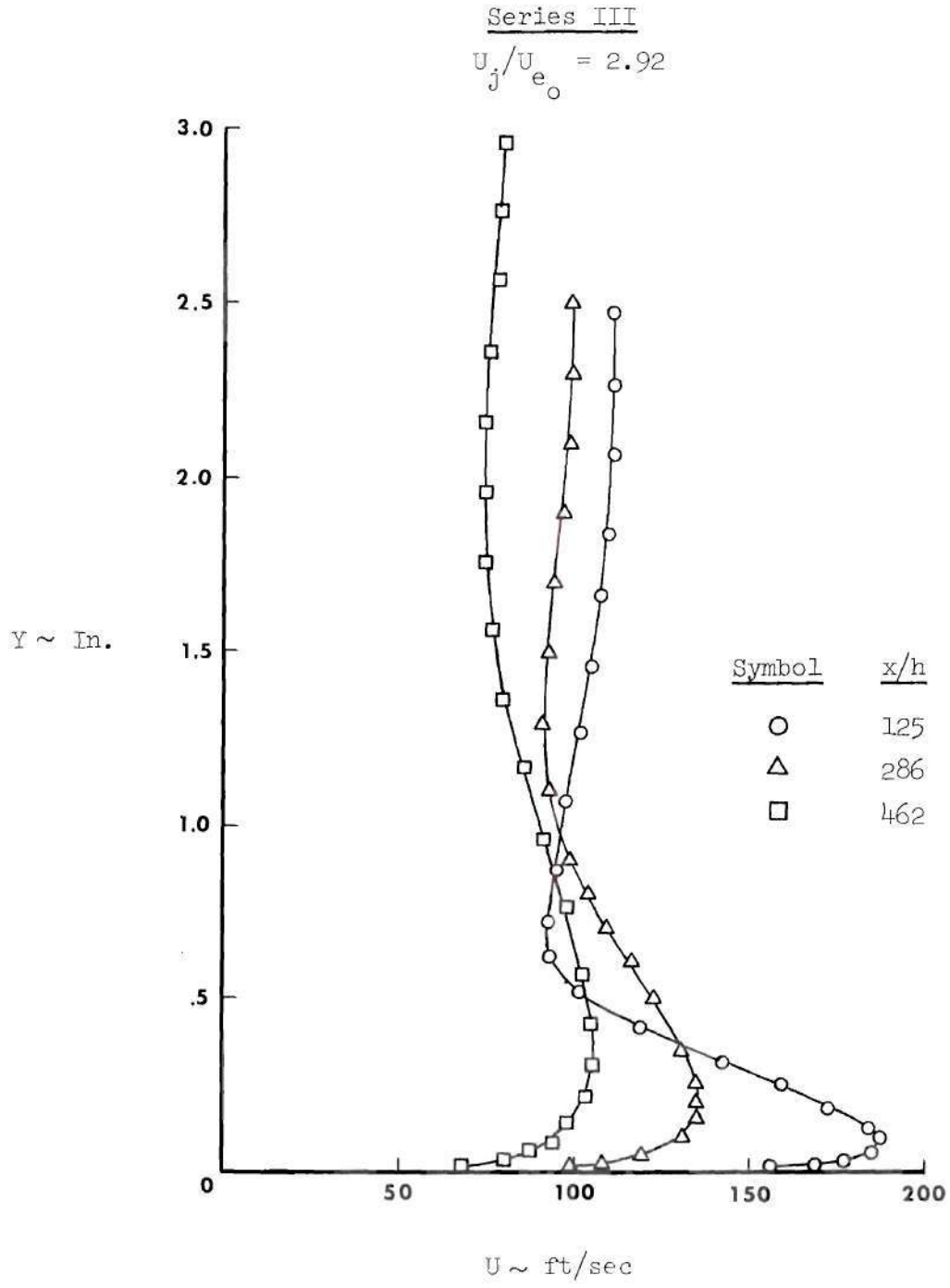

Figure 20. Composite Wall Jet Development

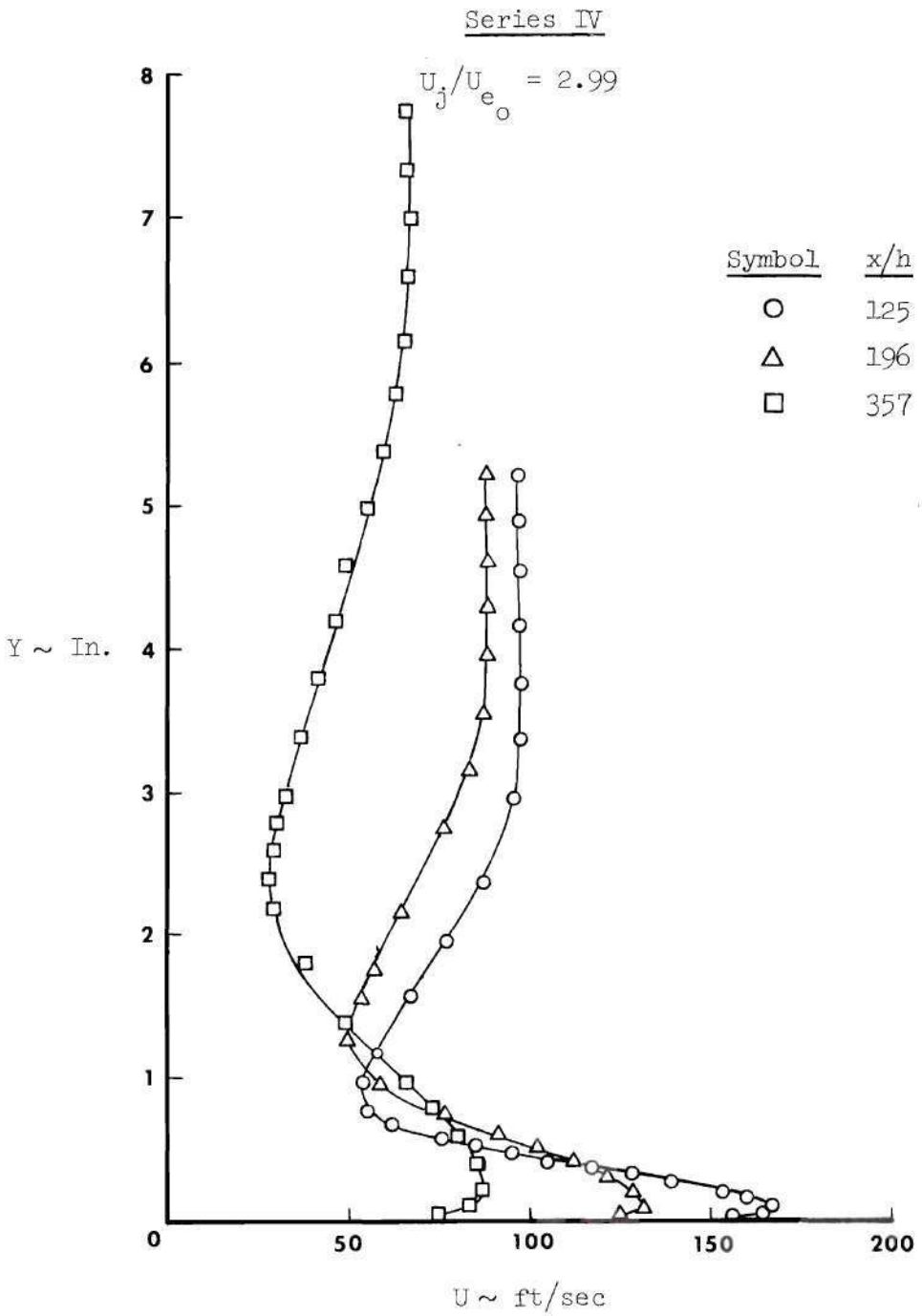

Figure 21. Composite Wall Jet Development

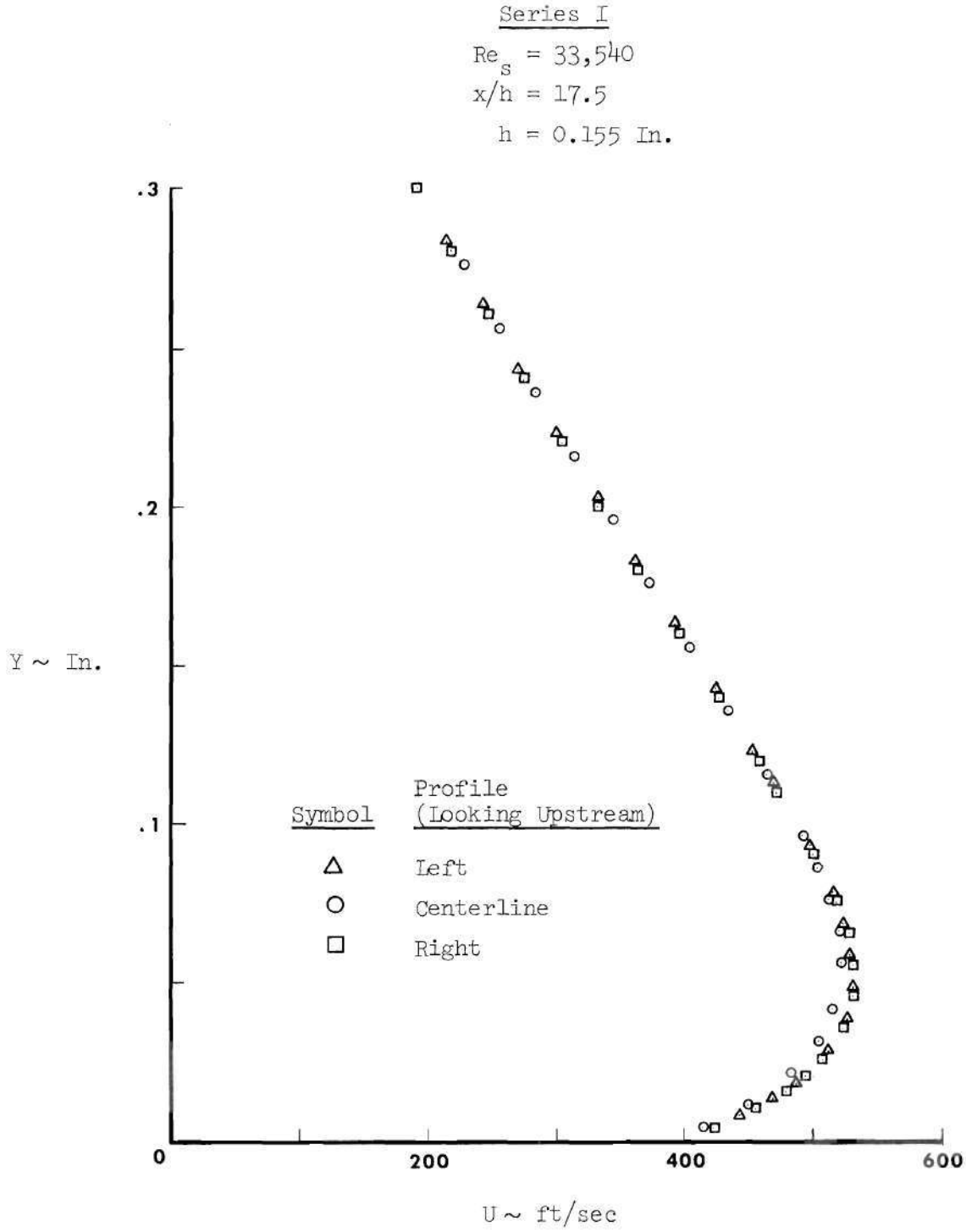

Figure 22a. Flow Evaluation

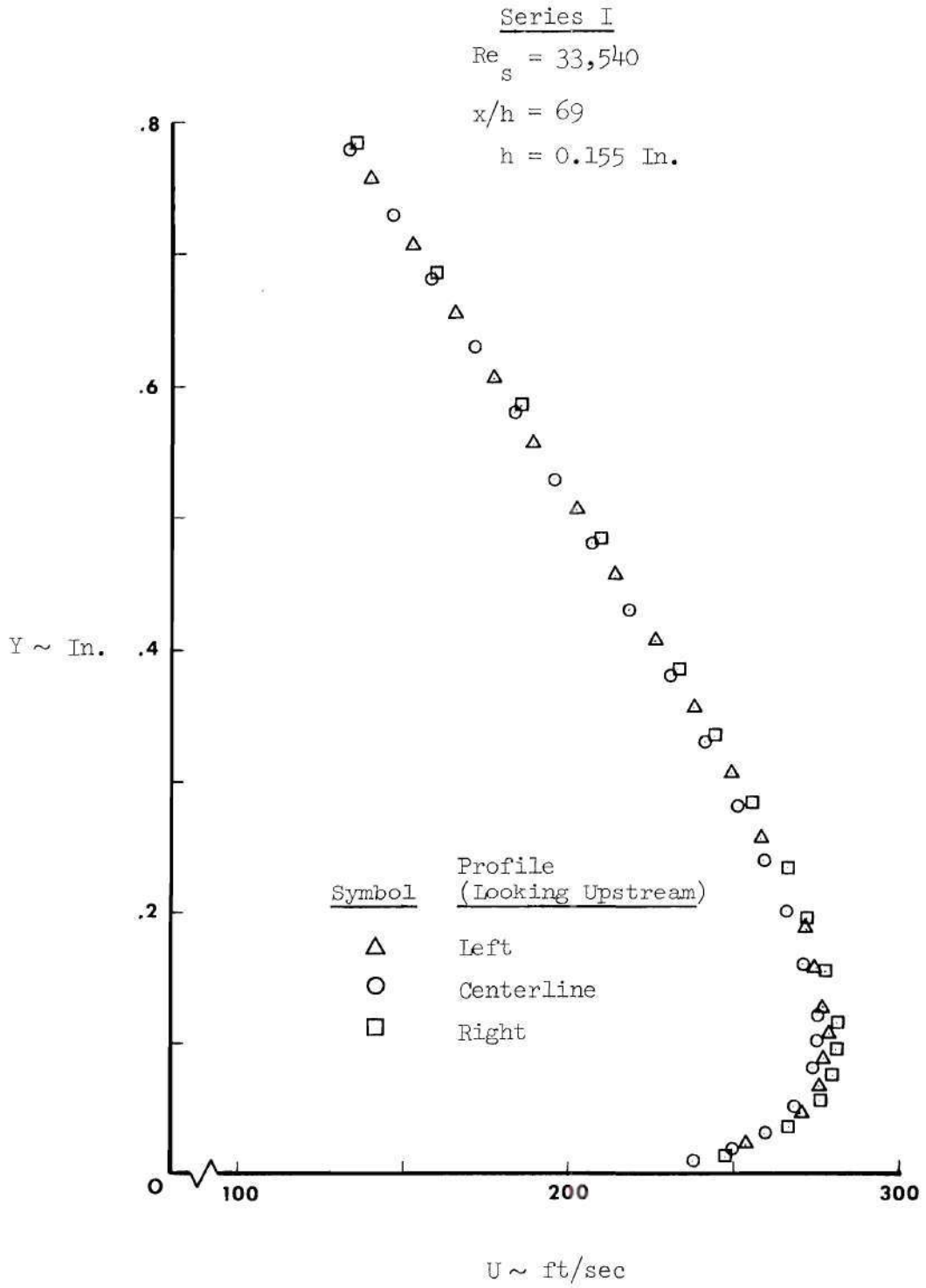

Figure 22b. Flow Evaluation

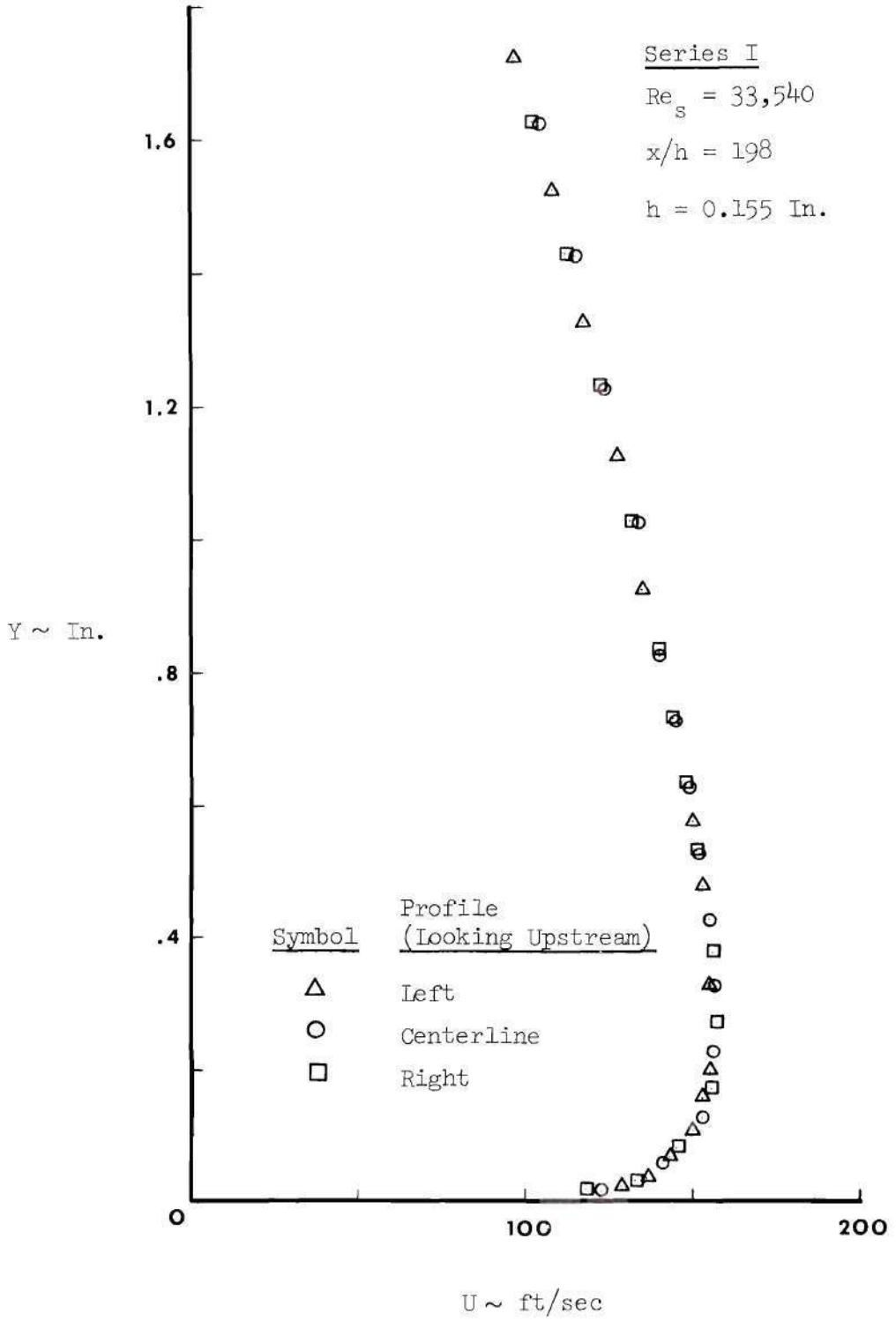

Figure 22c. Flow Evaluation

NOTES

1. Numbers represent percentage deviation from mean dynamic pressure.

2. View looking upstream at exit plane of boundary layer development section.

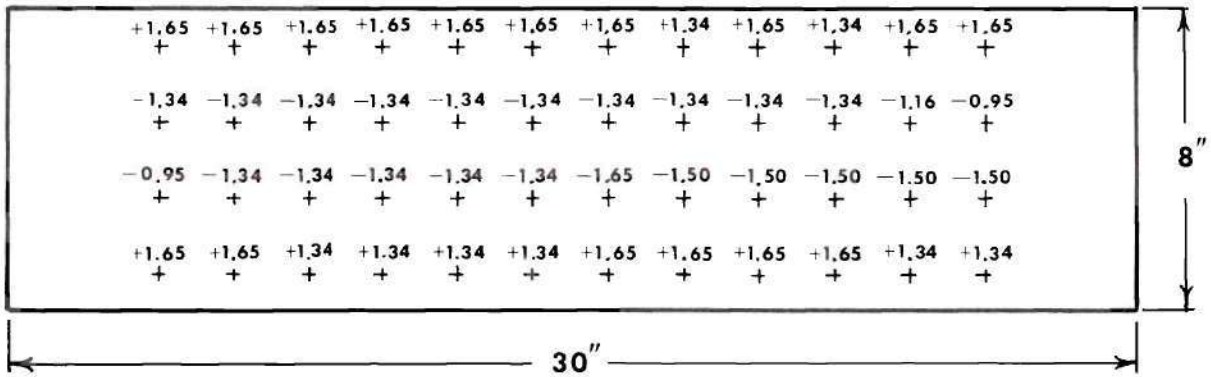

Figure 23. Main-Stream Dynamic Pressure Survey

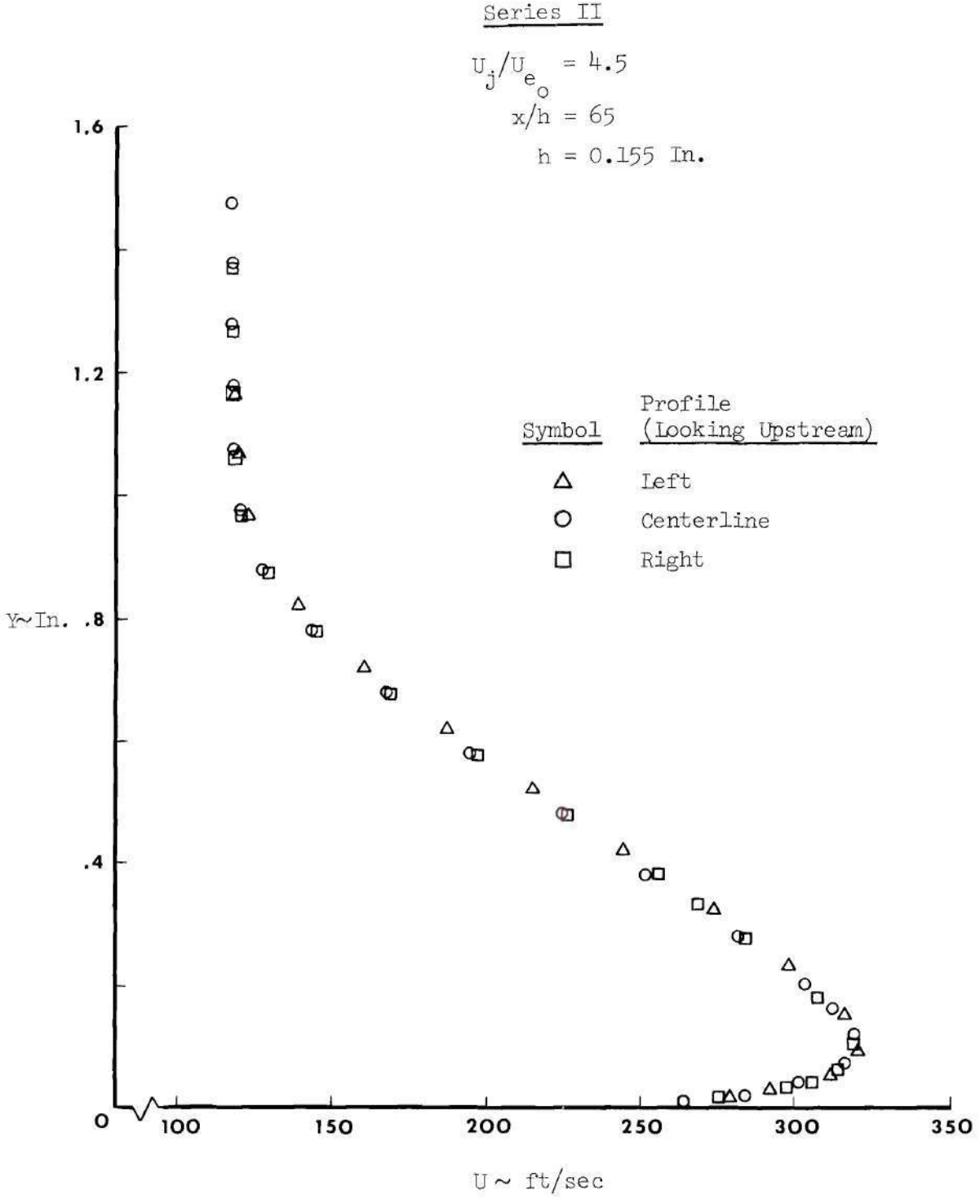

Figure 24. Flow Evaluation

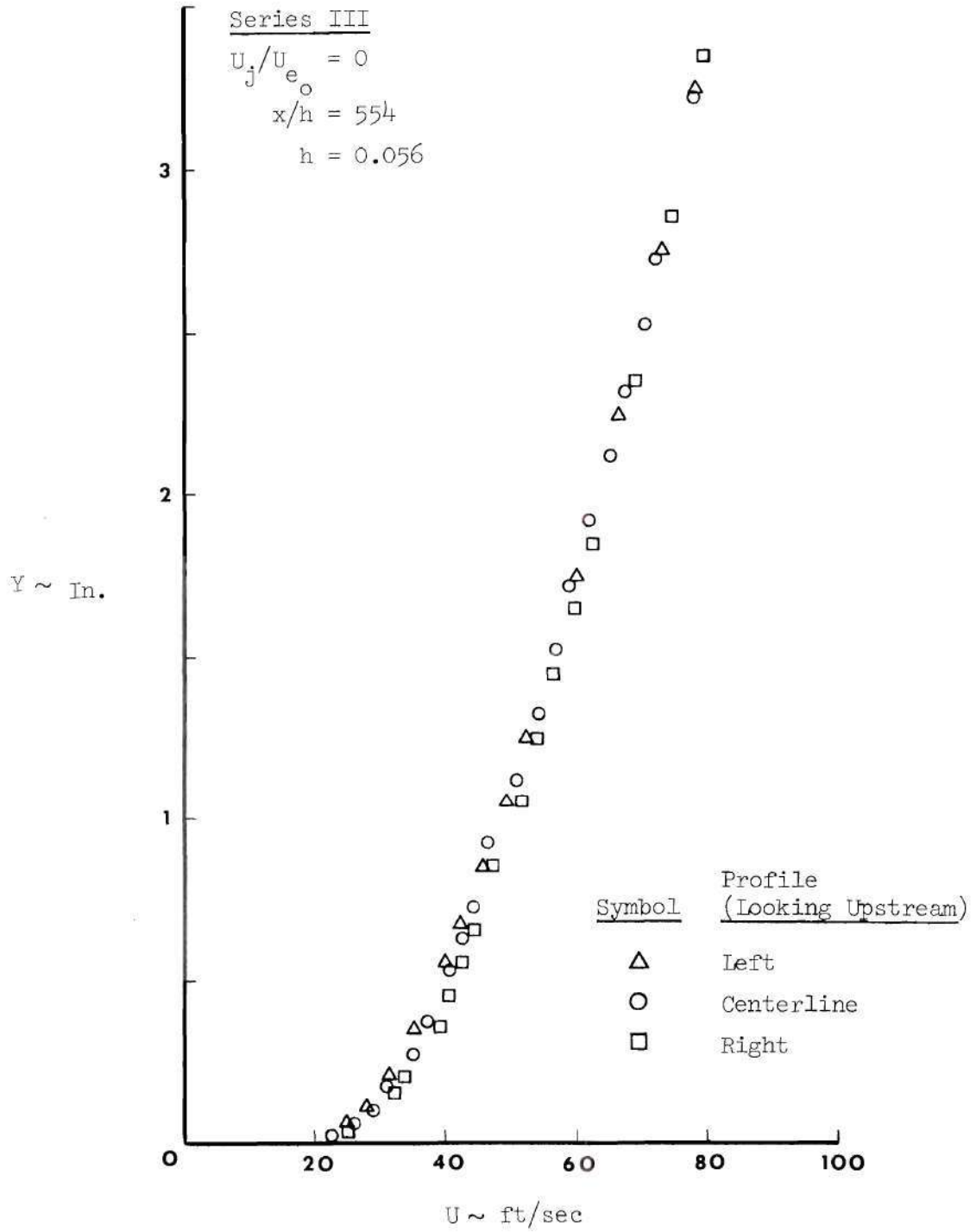

Figure 25. Flow Evaluation

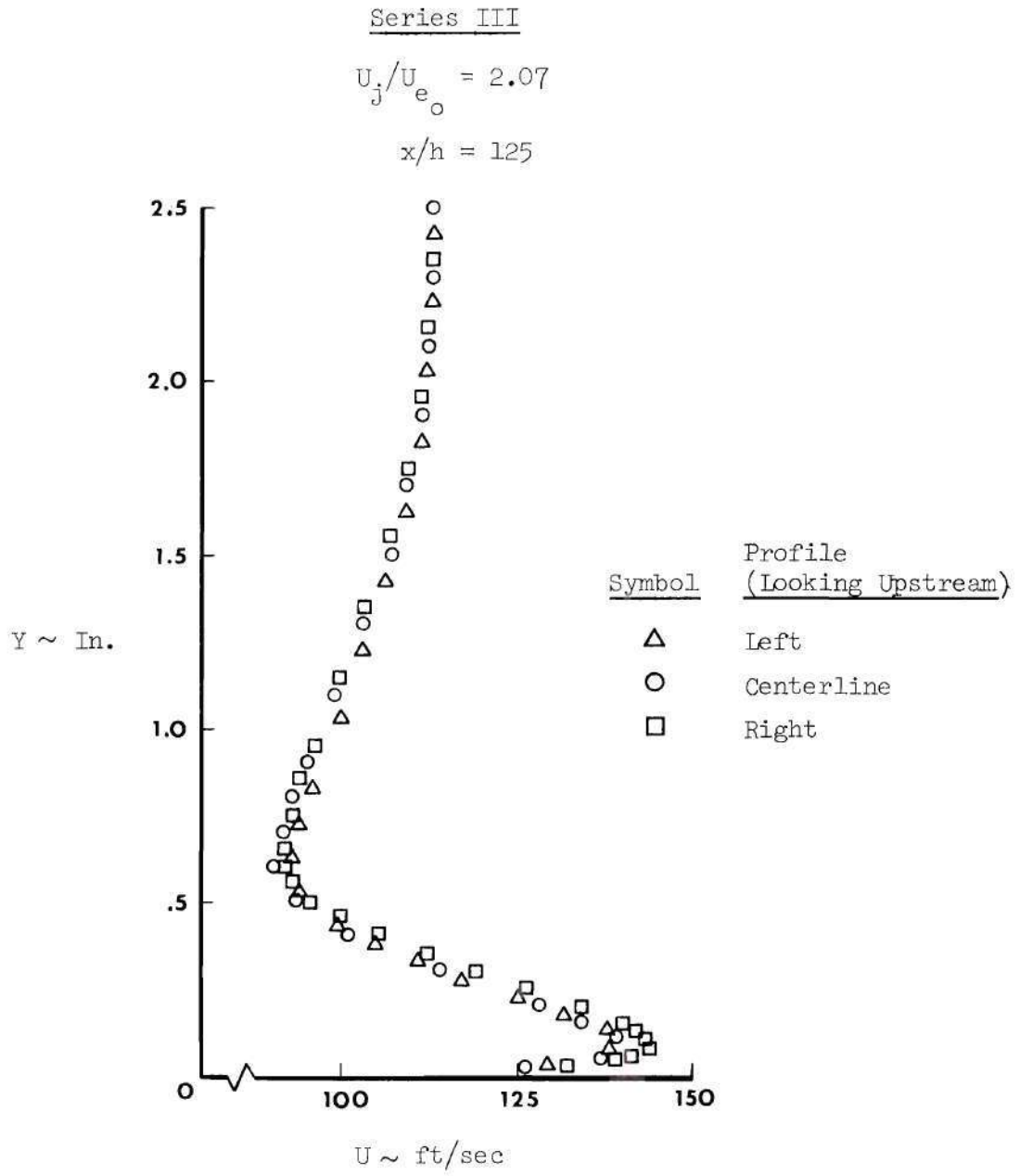

Figure 26. Flow Evaluation

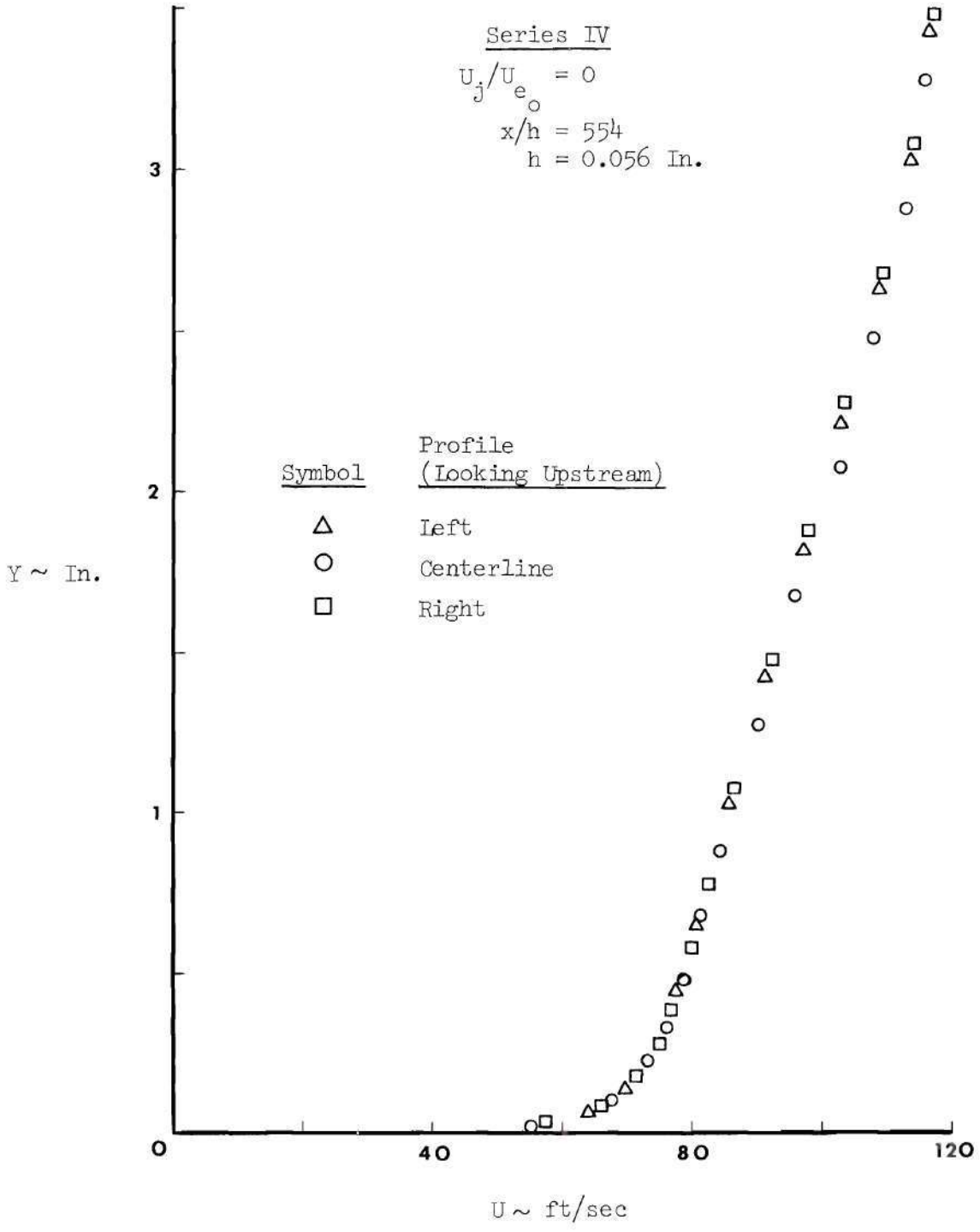

Figure 27. Flow Evaluation

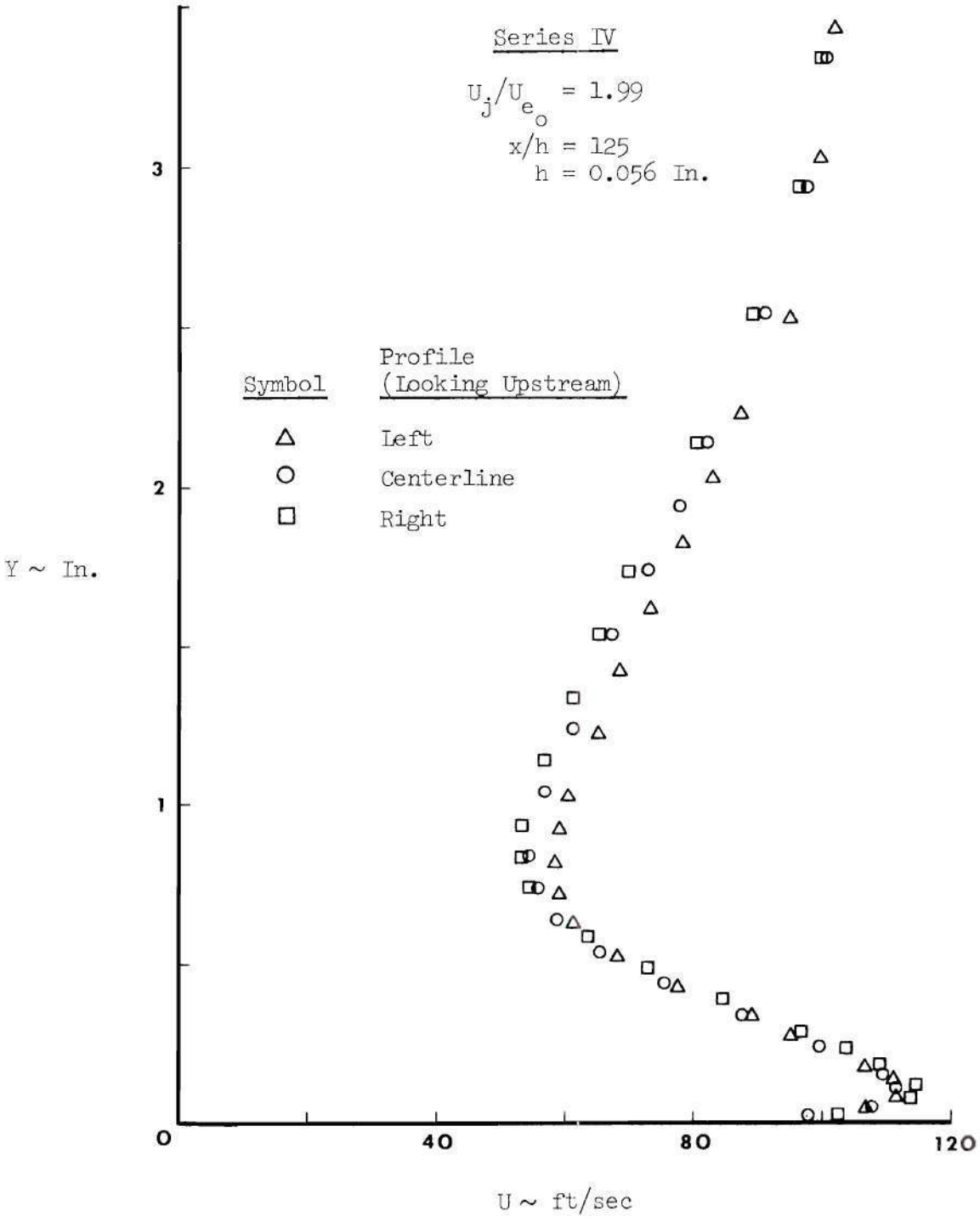

Figure 28. Flow Evaluation

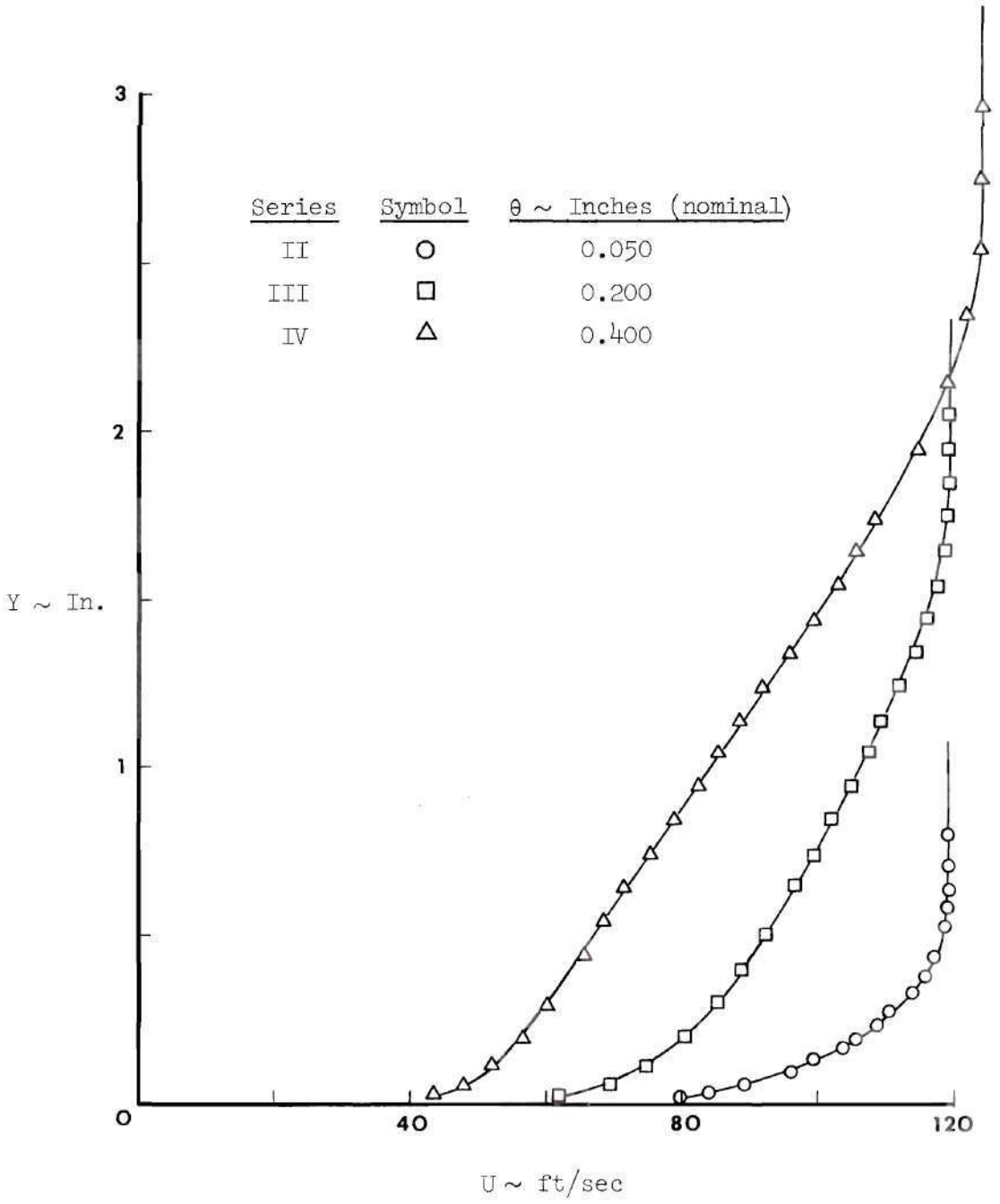

Figure 29. Typical Initial Boundary Layer Profiles

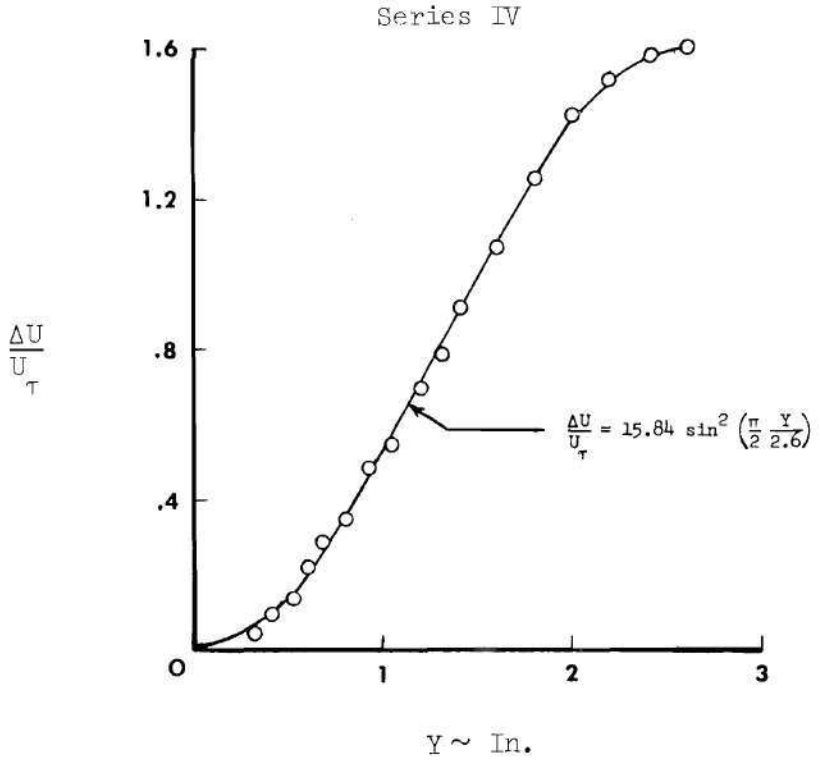

Figure 30. Initial Boundary Layer Wake Region

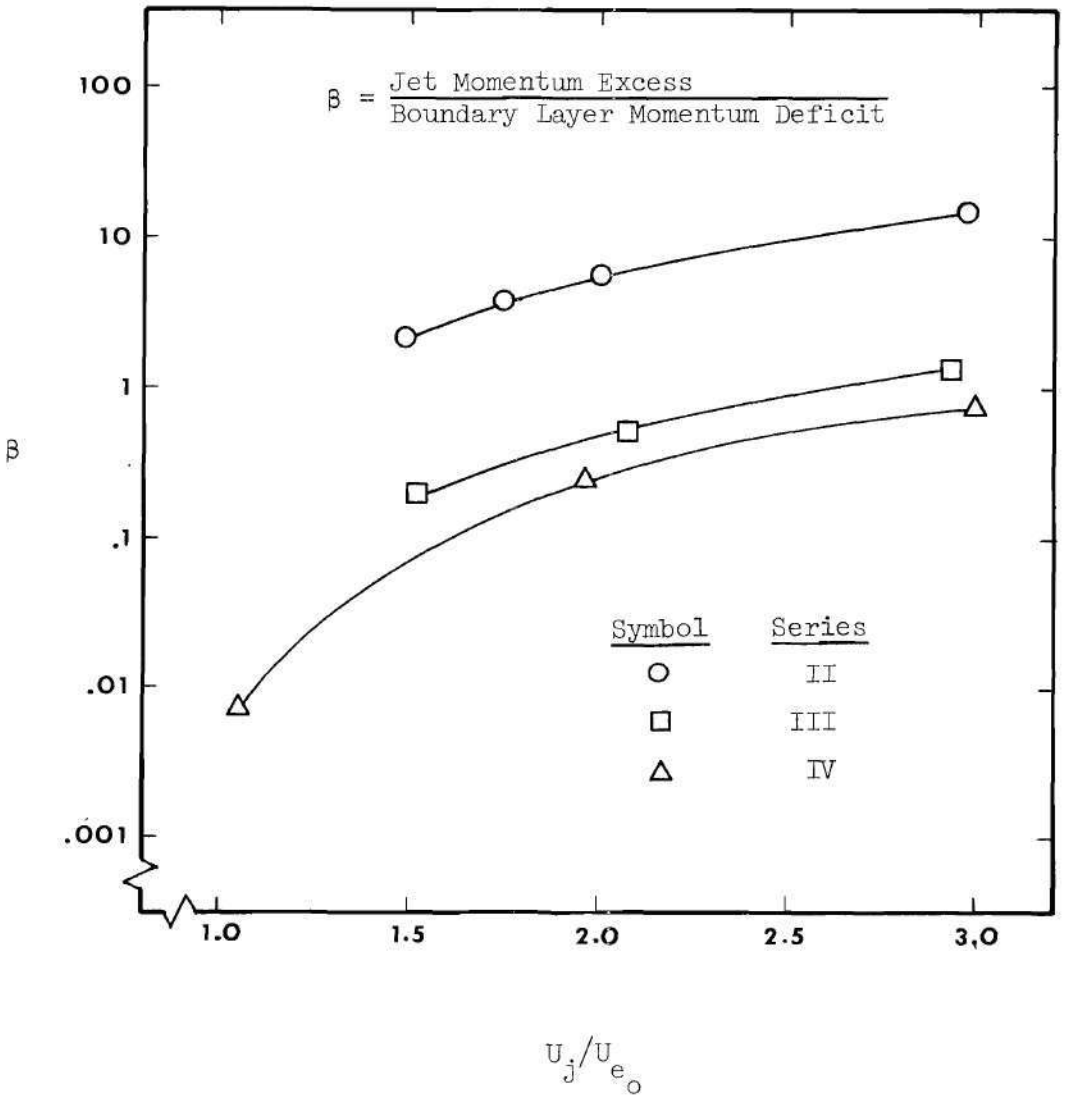

Figure 31. Momentum Excess Ratio at Jet Slot

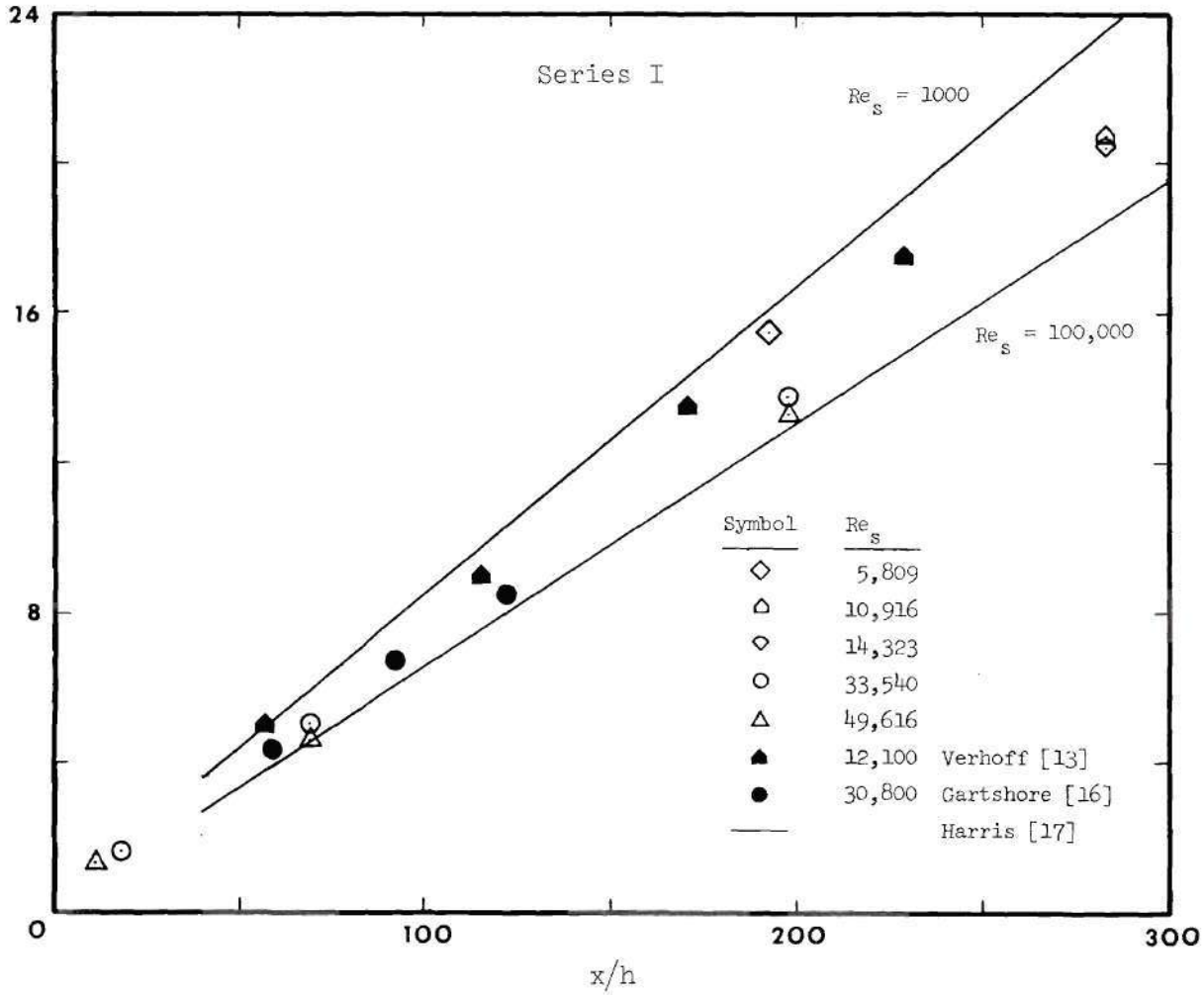

Figure 32. Wall Jet Growth

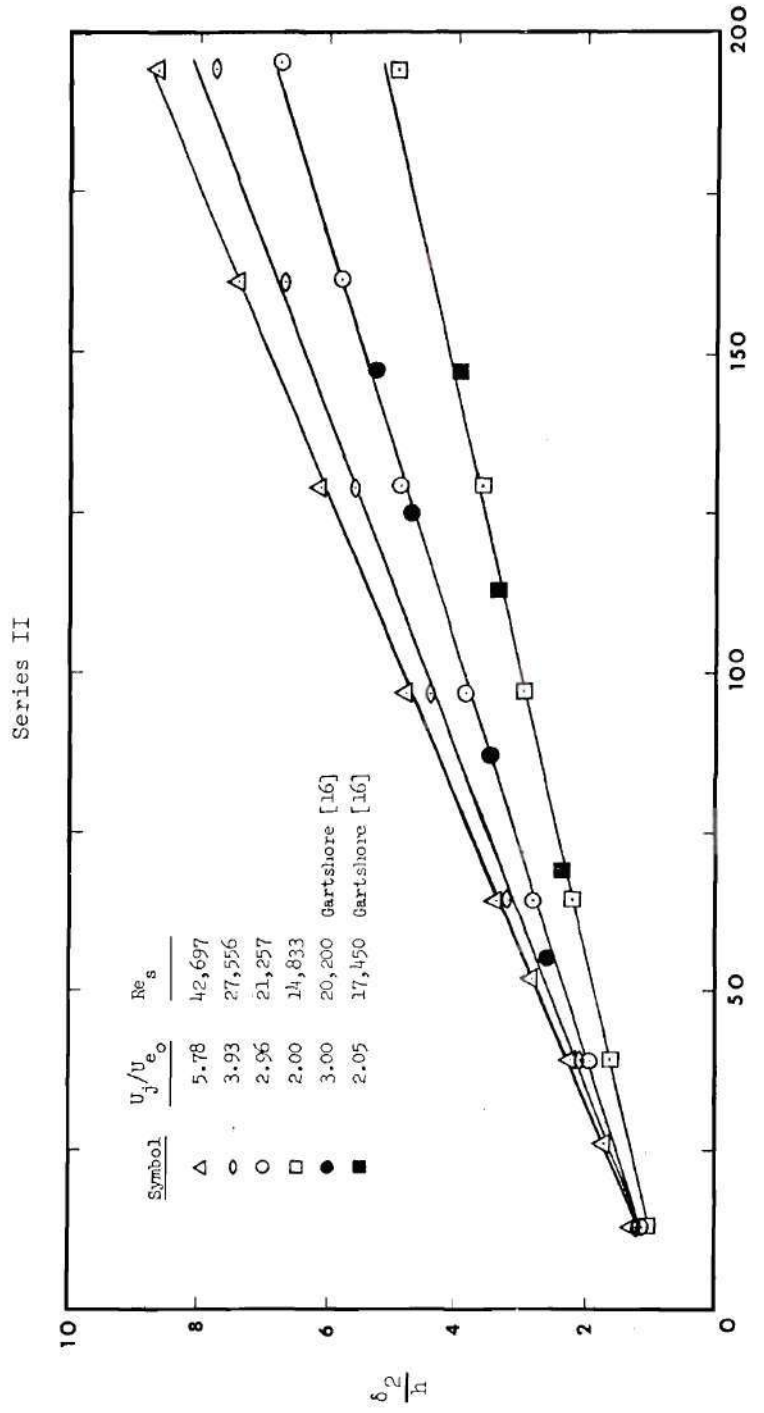

Figure 33. Wall Jet Growth

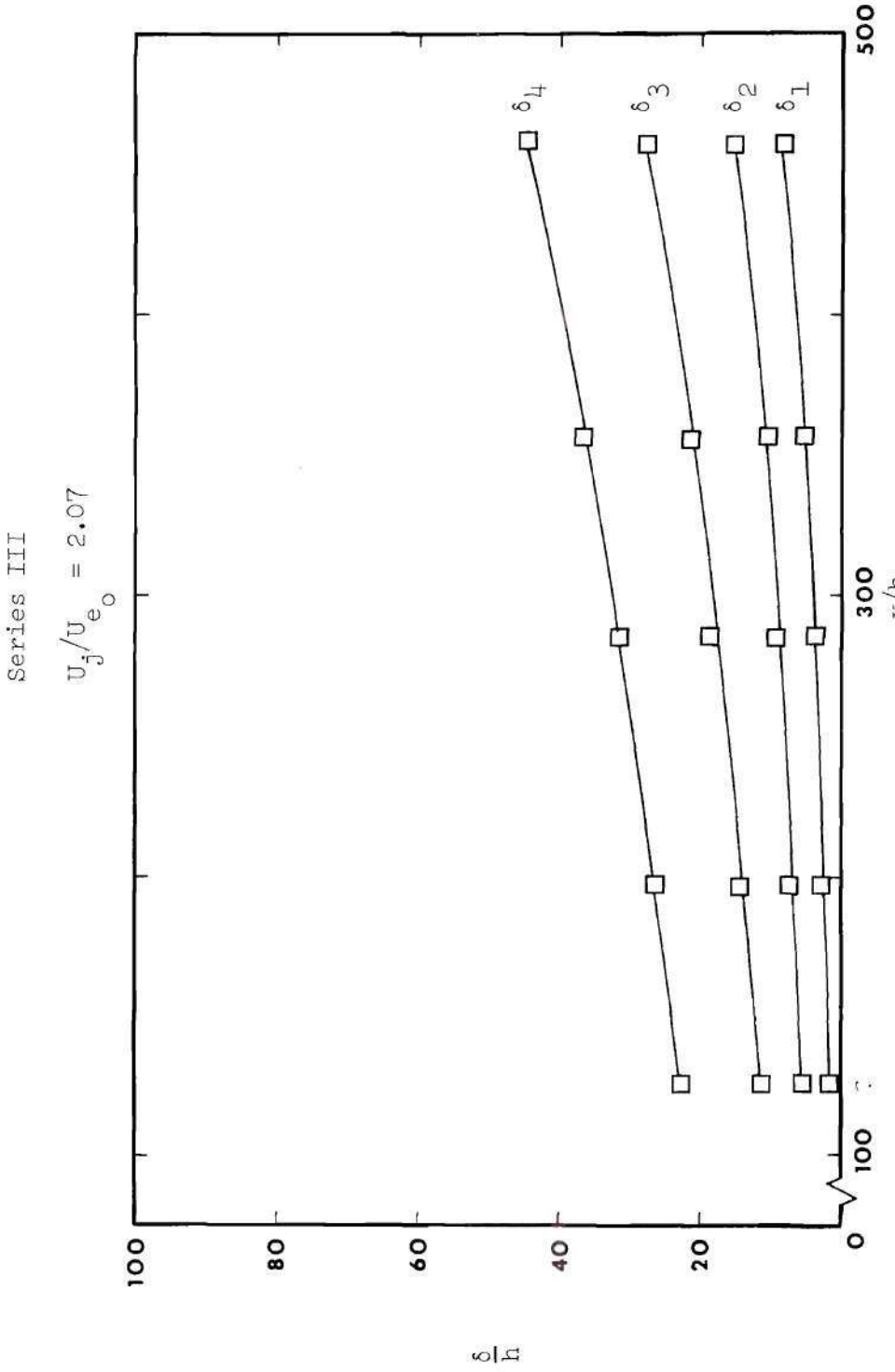

Figure 34a. Wall Jet Growth

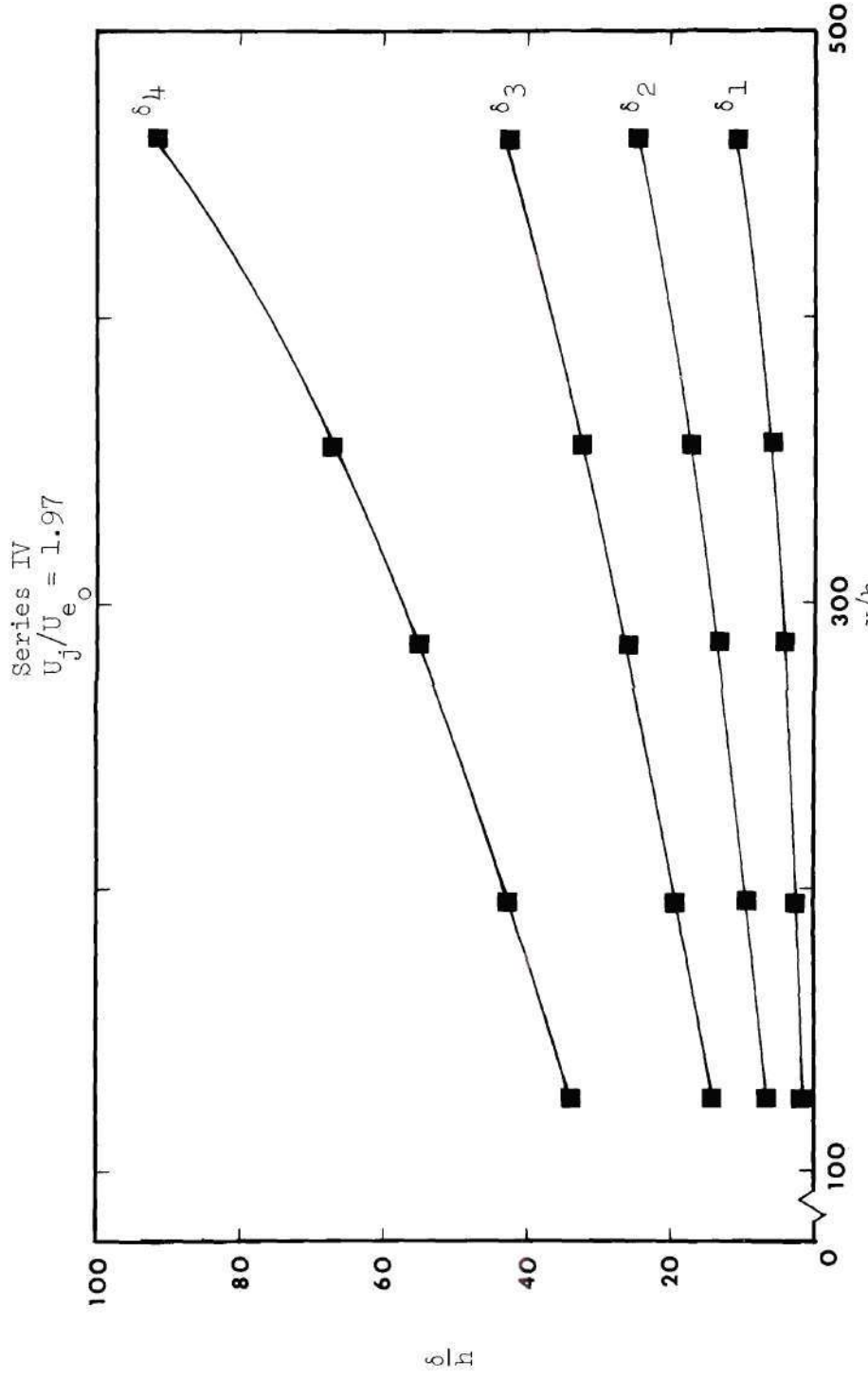

Figure 34b. Wall Jet Growth

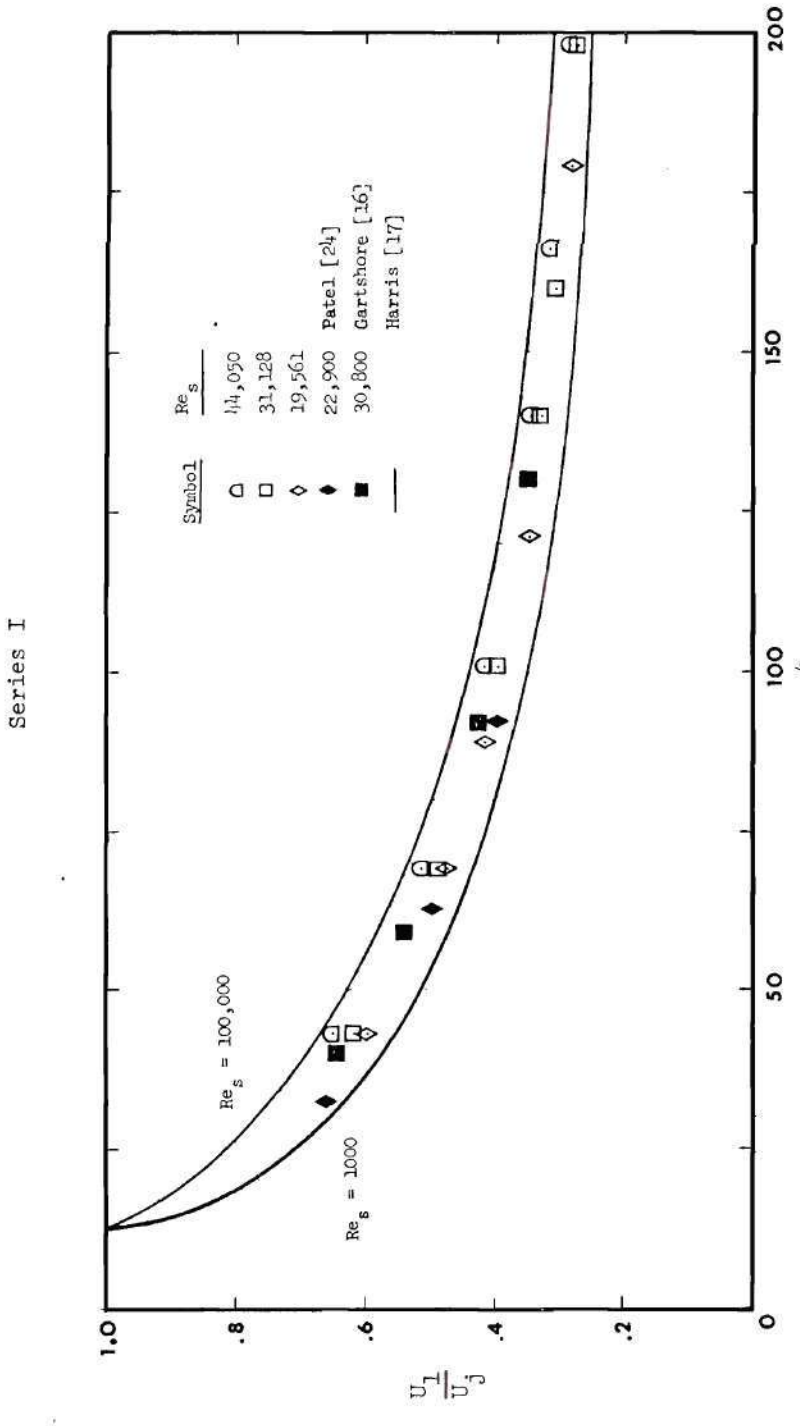

Figure 35. Wall Jet Velocity Decay

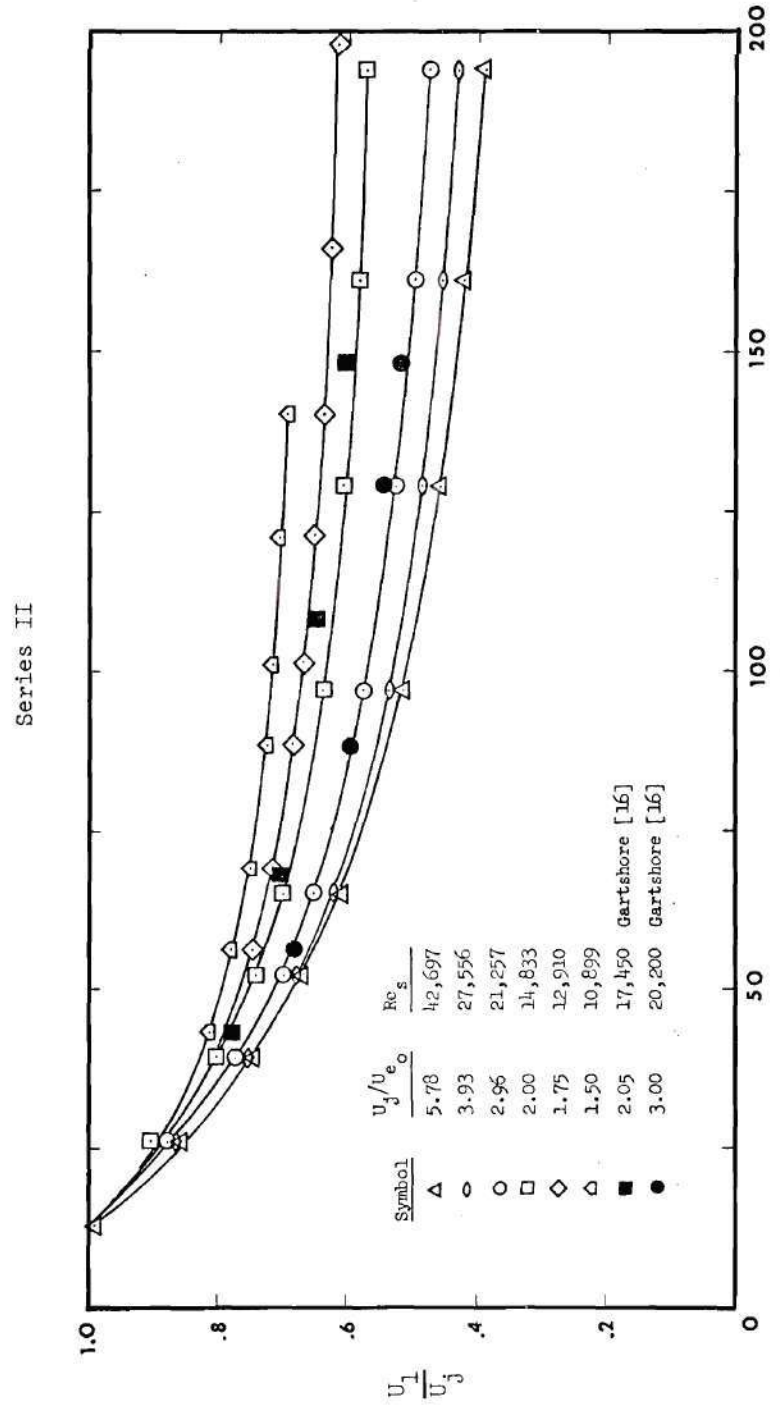

Figure 36. Wall Jet Velocity Decay

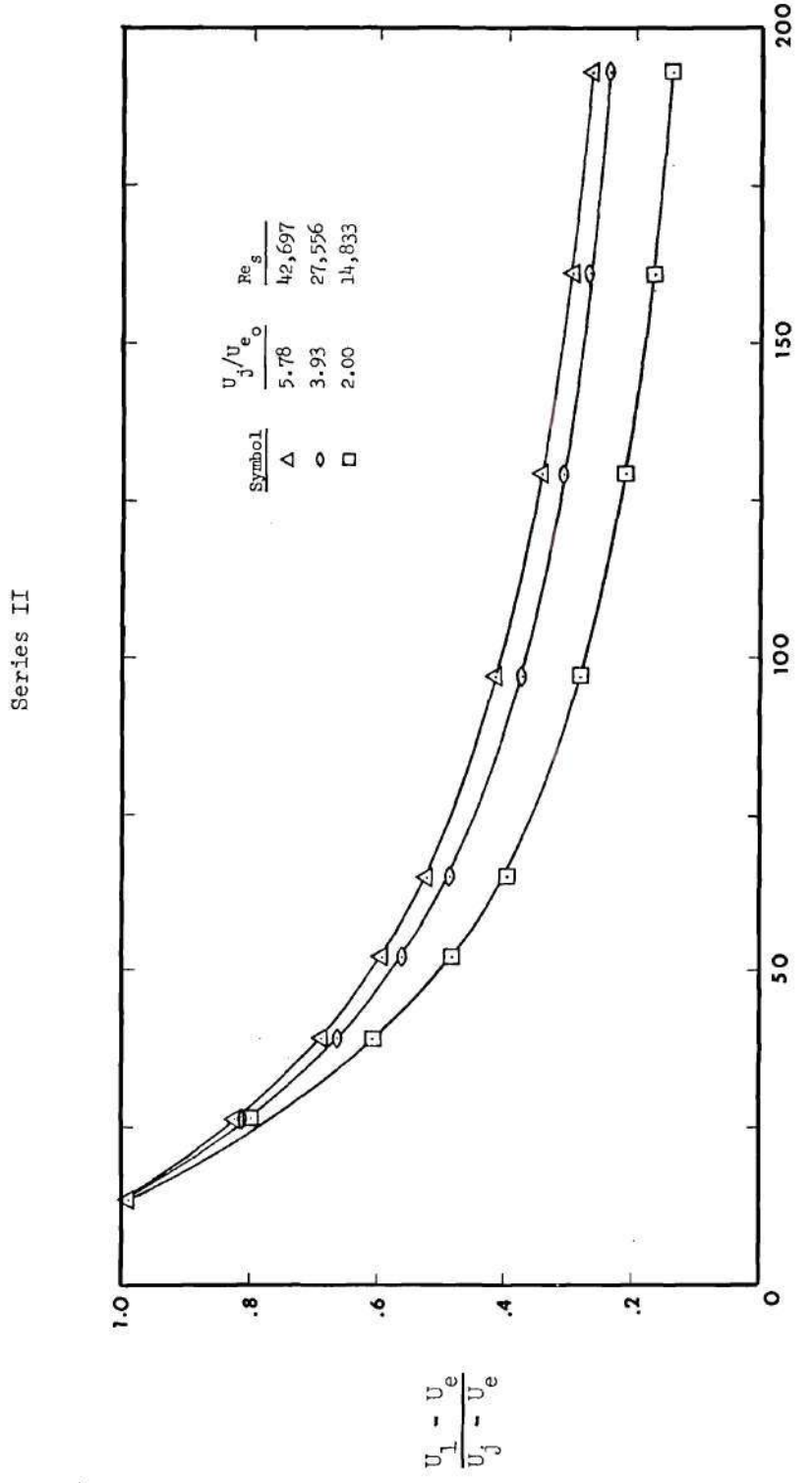

Figure 37. Wall Jet Velocity Decay

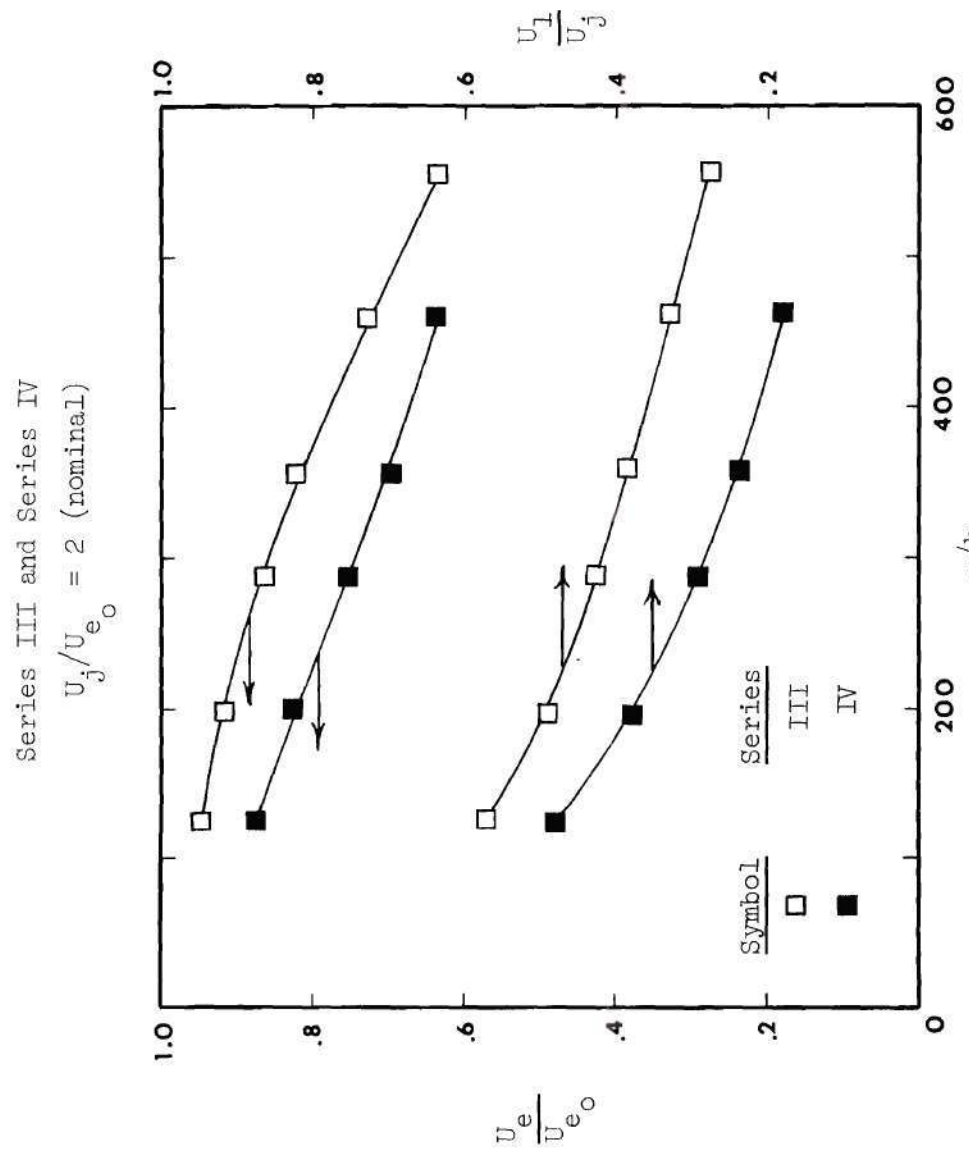

Figure 38a. Wall Jet Velocity Decay

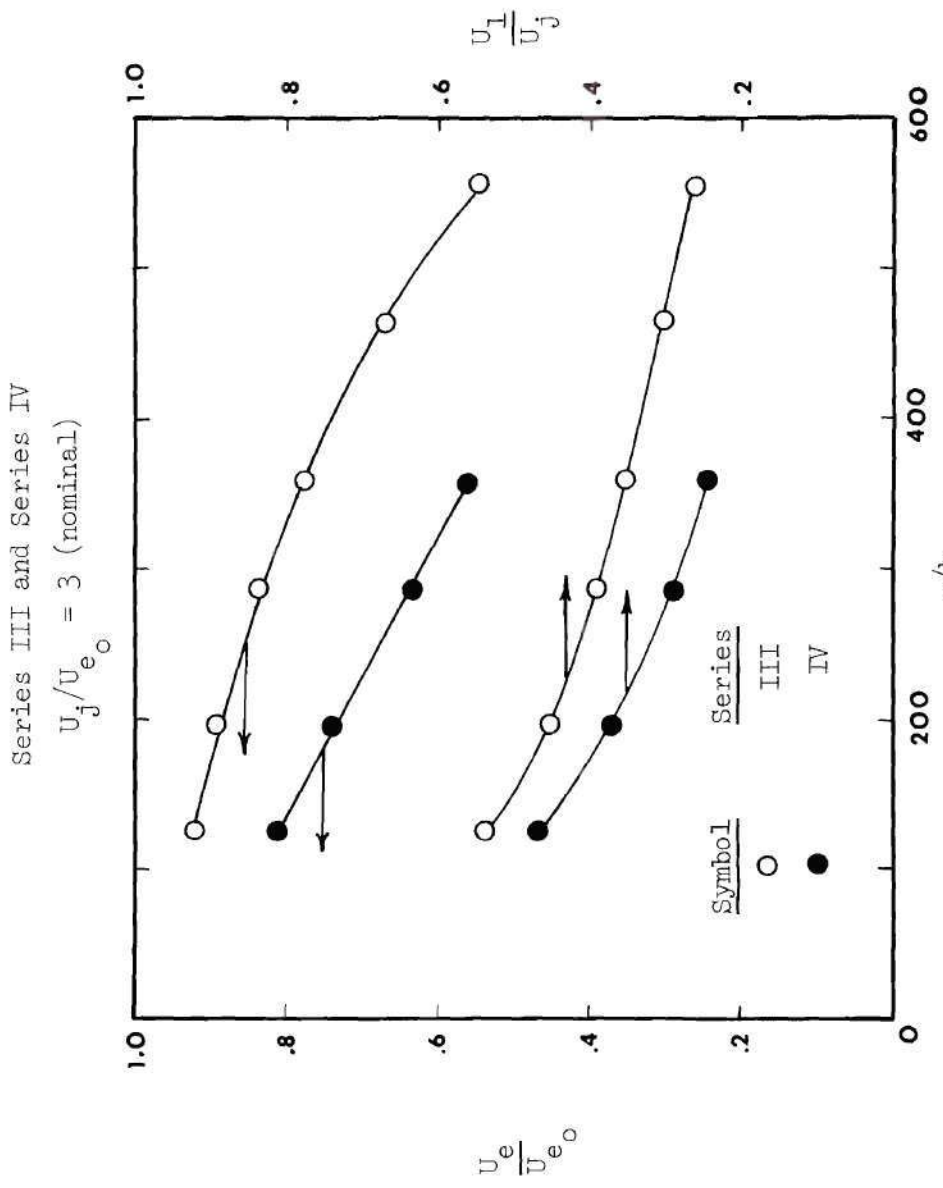

Figure 38b. Wall Jet Velocity Decay

Series III and Series IV

Symbol	Series	U_j/U_{e_o} (nominal)
□	III	2
○	III	3
■	IV	2
●	IV	3

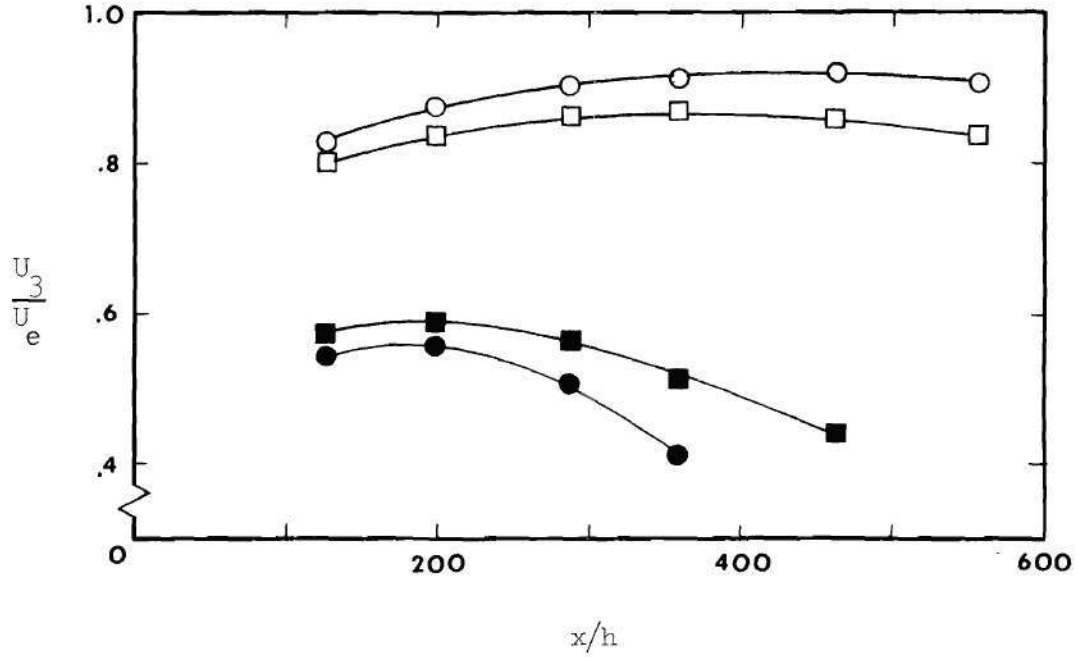

Figure 39. Wall Jet Velocity Decay

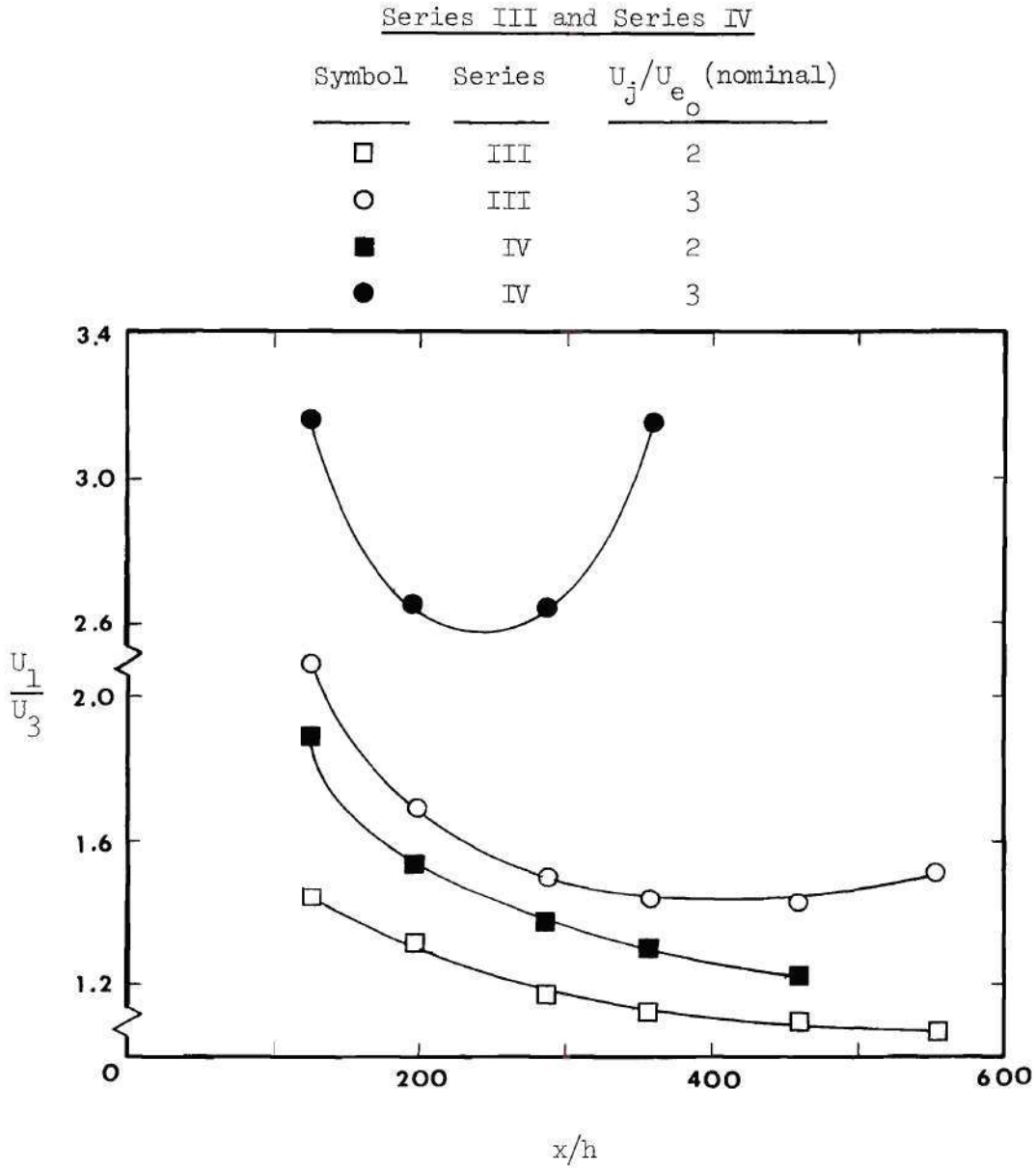

Figure 40. Wall Jet Velocity Decay

Series III and Series IV

Symbol	Series	U_j/U_{e_o} (nominal)
□	III	2
○	III	3
■	IV	2
●	IV	3

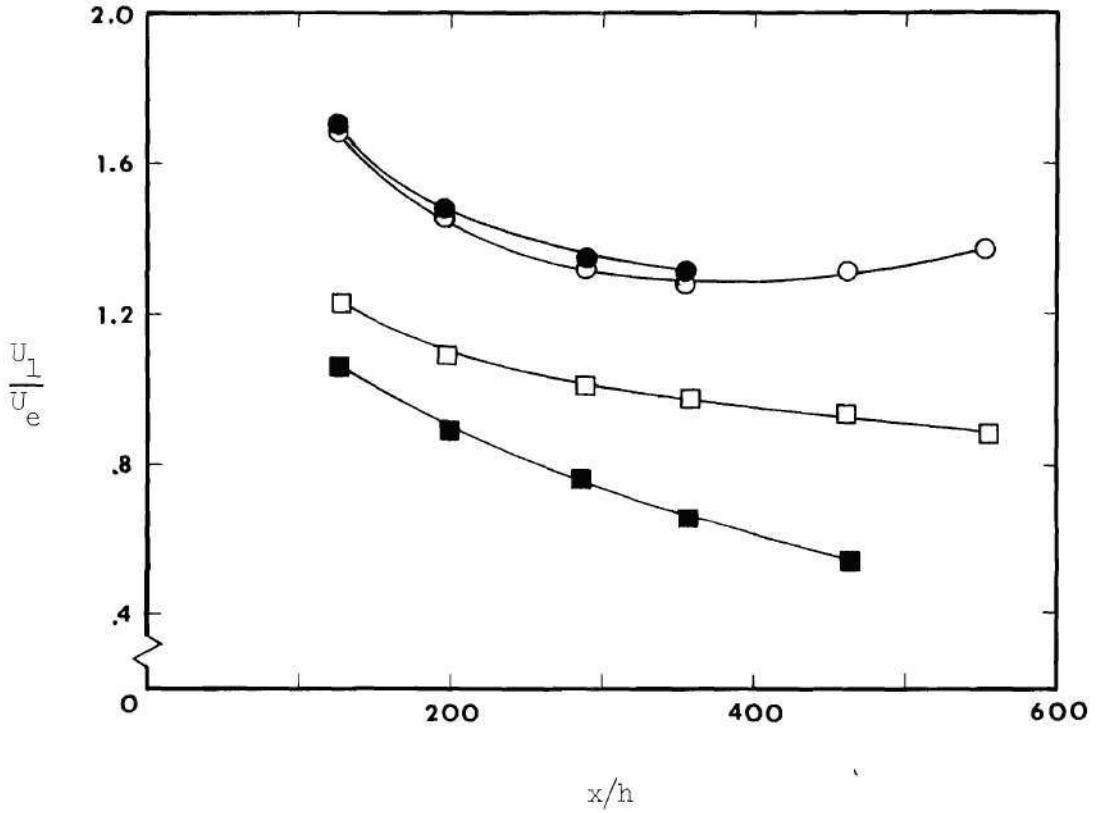

Figure 41. Wall Jet Velocity Decay

Series I

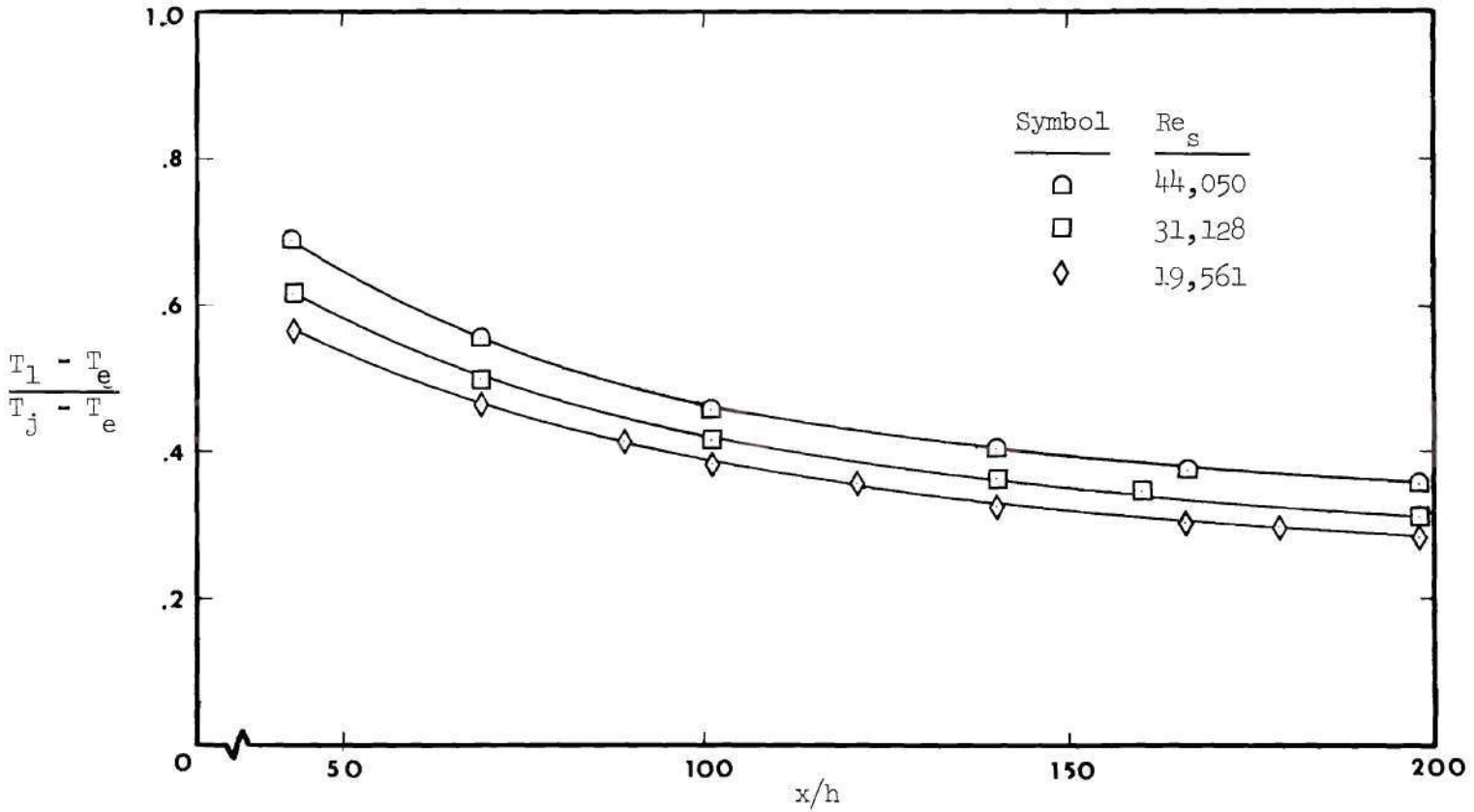

Figure 42. Wall Jet Temperature Decay

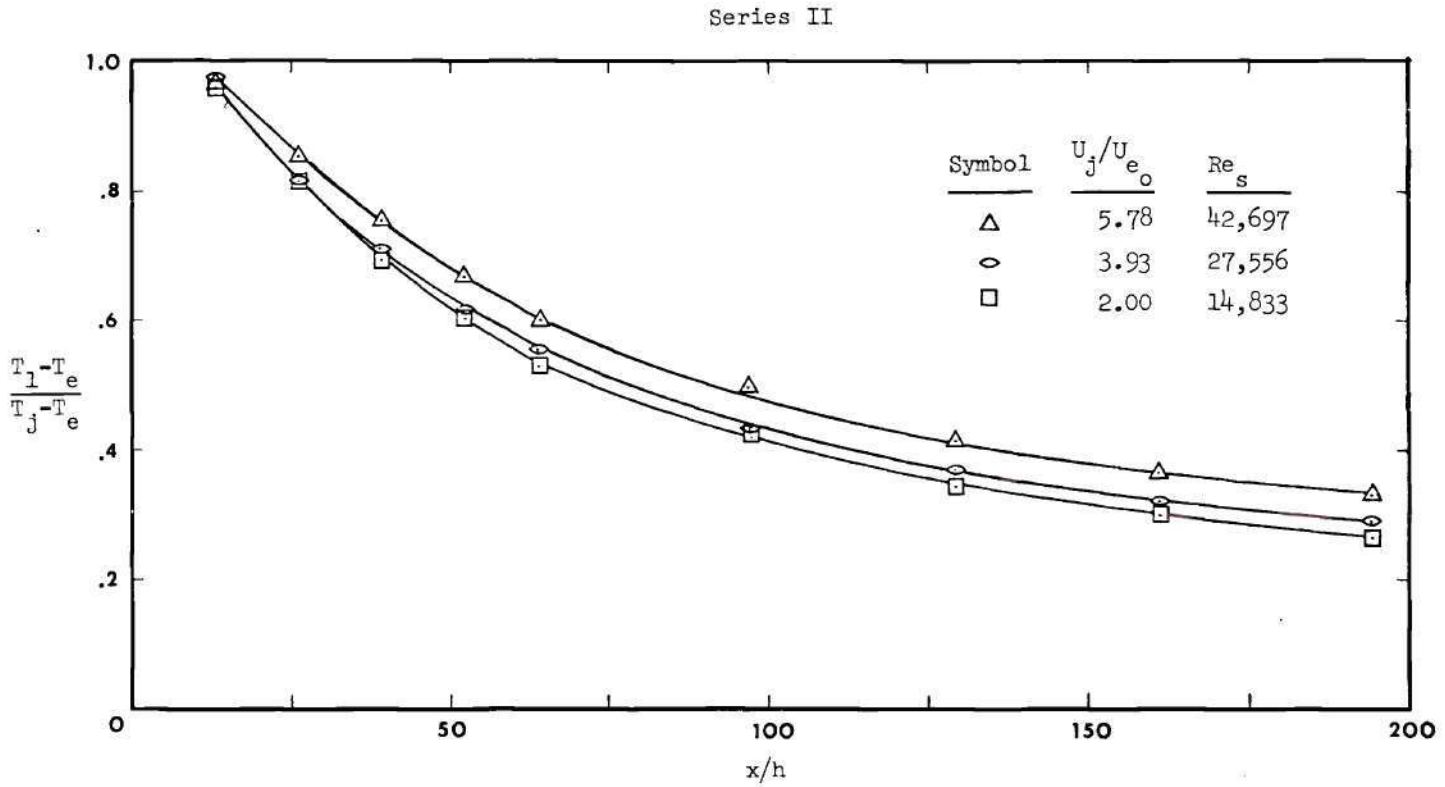

Figure 43. Wall Jet Temperature Decay

Series III

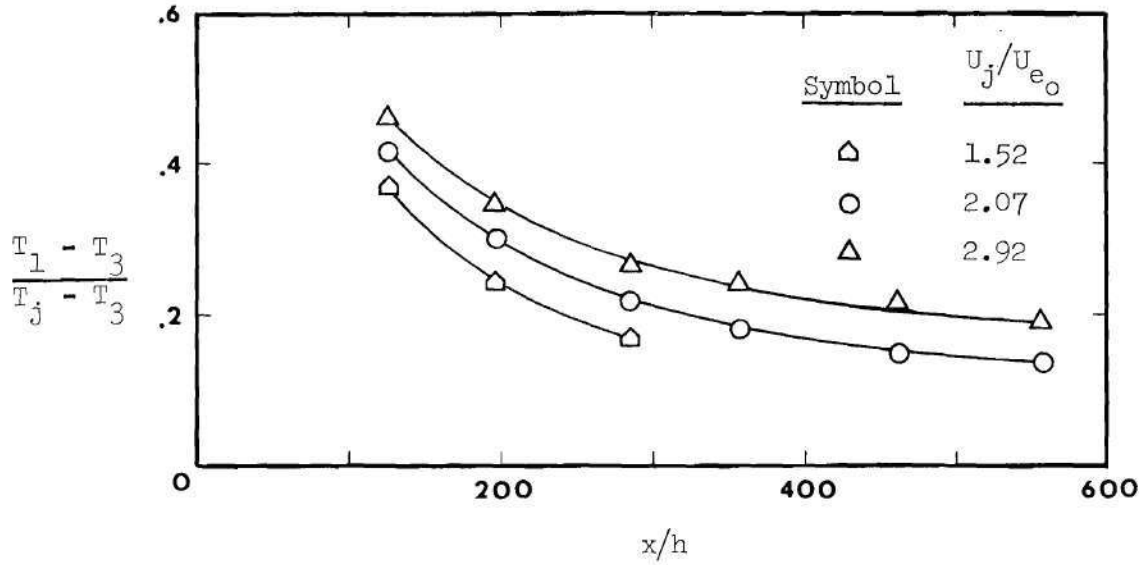

Series IV

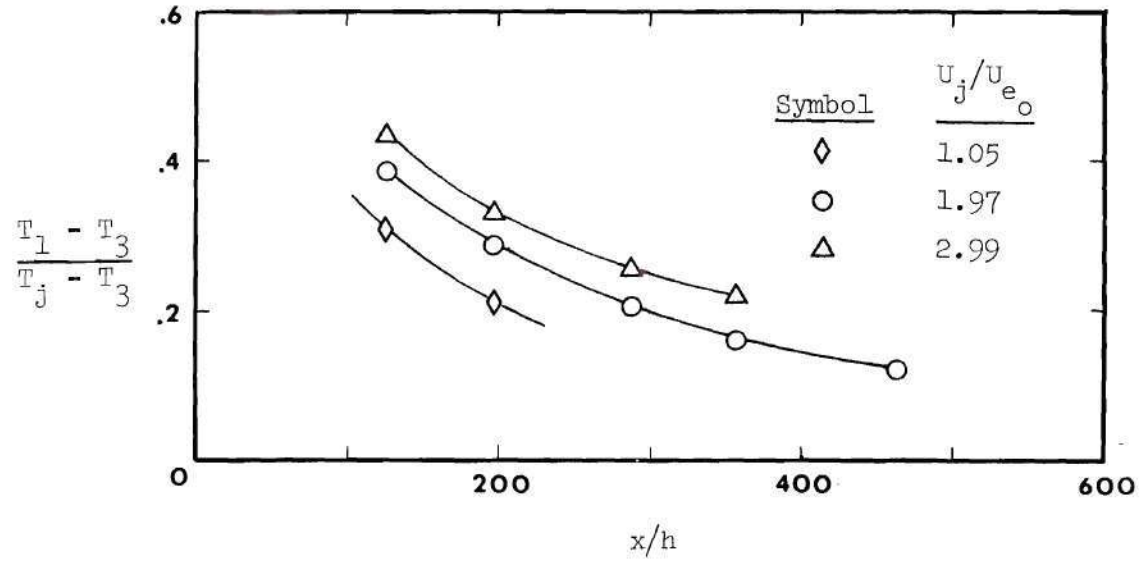

Figure 44. Wall Jet Temperature Decay

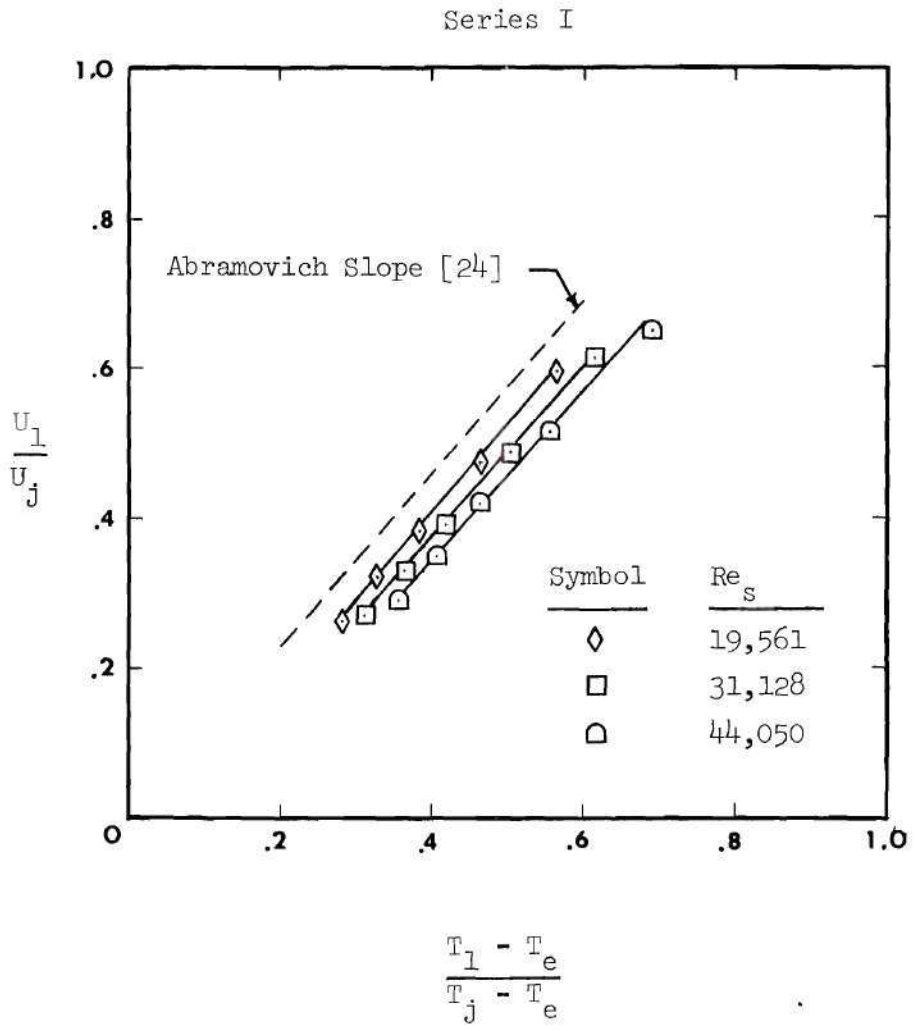

Figure 45. Wall Jet Velocity-Temperature Decay

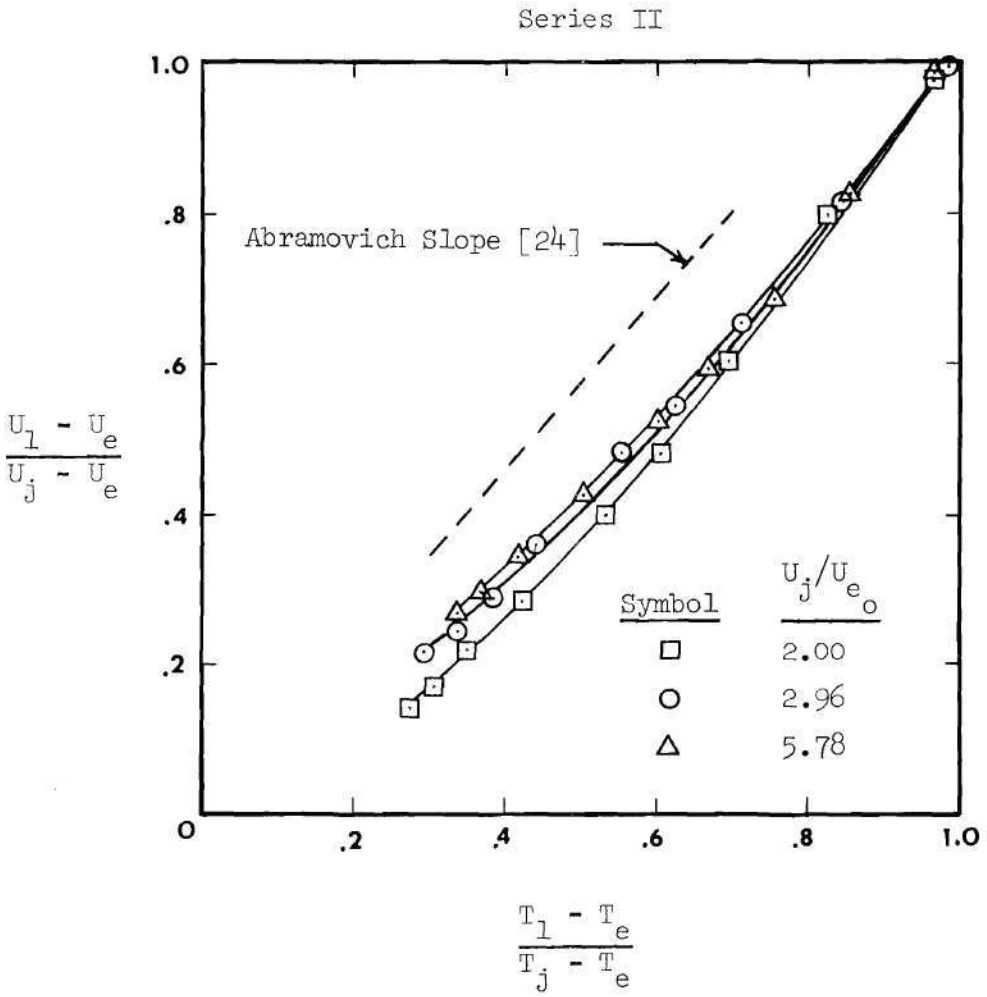

Figure 46. Wall Jet Velocity-Temperature Decay

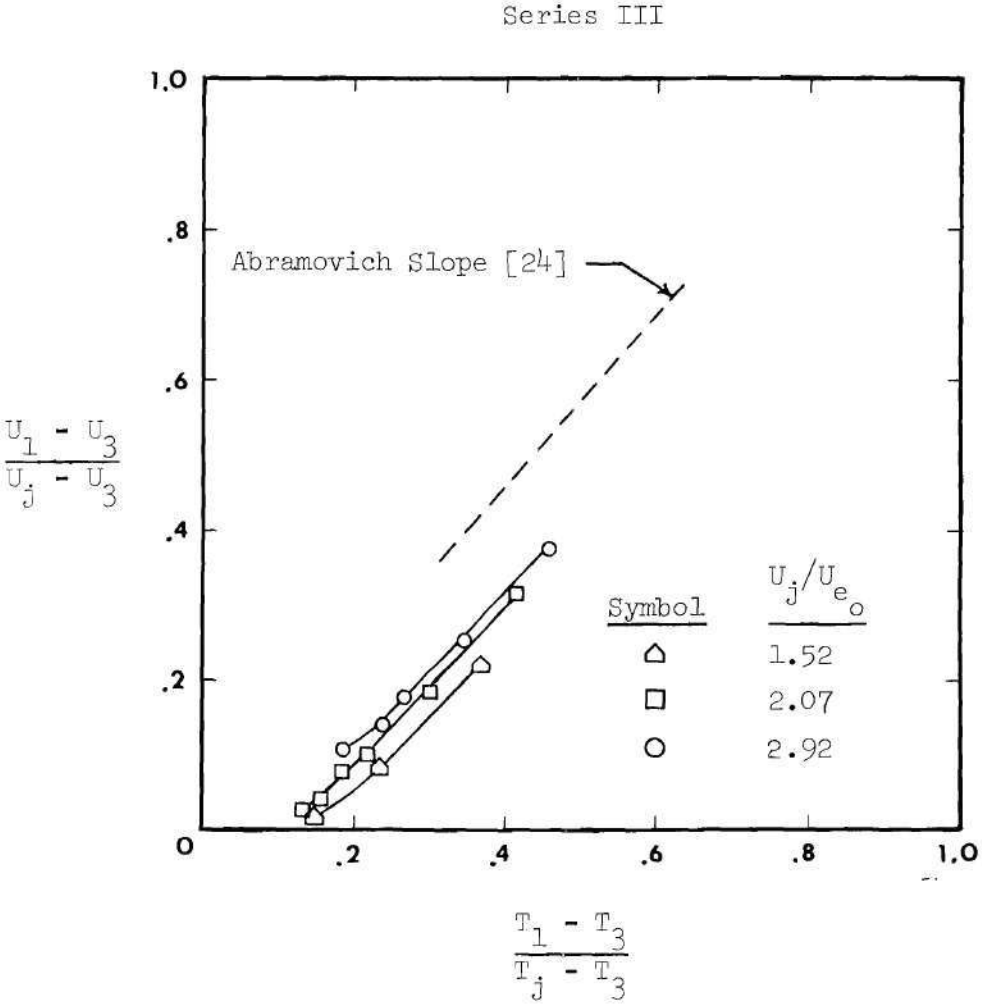

Figure 47. Wall Jet Velocity-Temperature Decay

Series IV

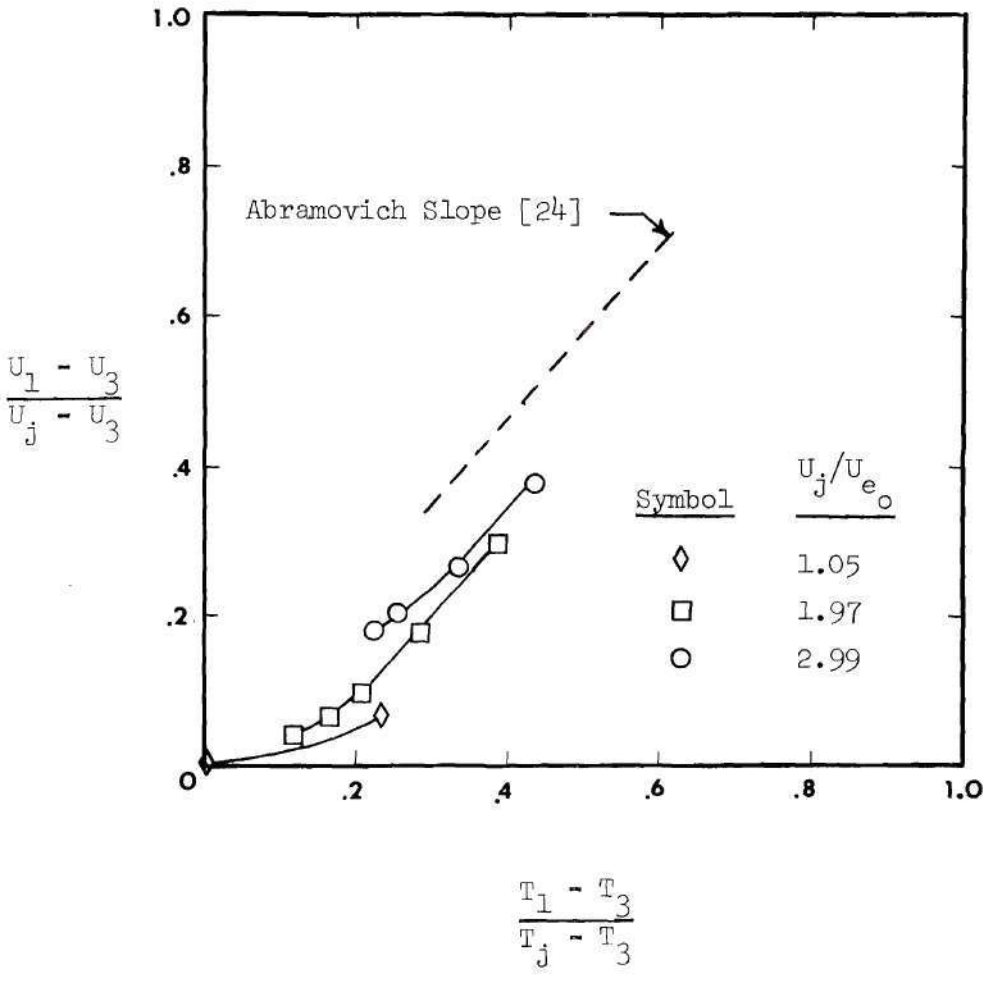

Figure 48. Wall Jet Velocity-Temperature Decay

Series I

Symbol	Re_s	x/h
◇	5,809	193
△	10,916	283
◇	14,323	283
○	33,540	69
●	33,540	198
△	49,616	69
▲	49,616	198

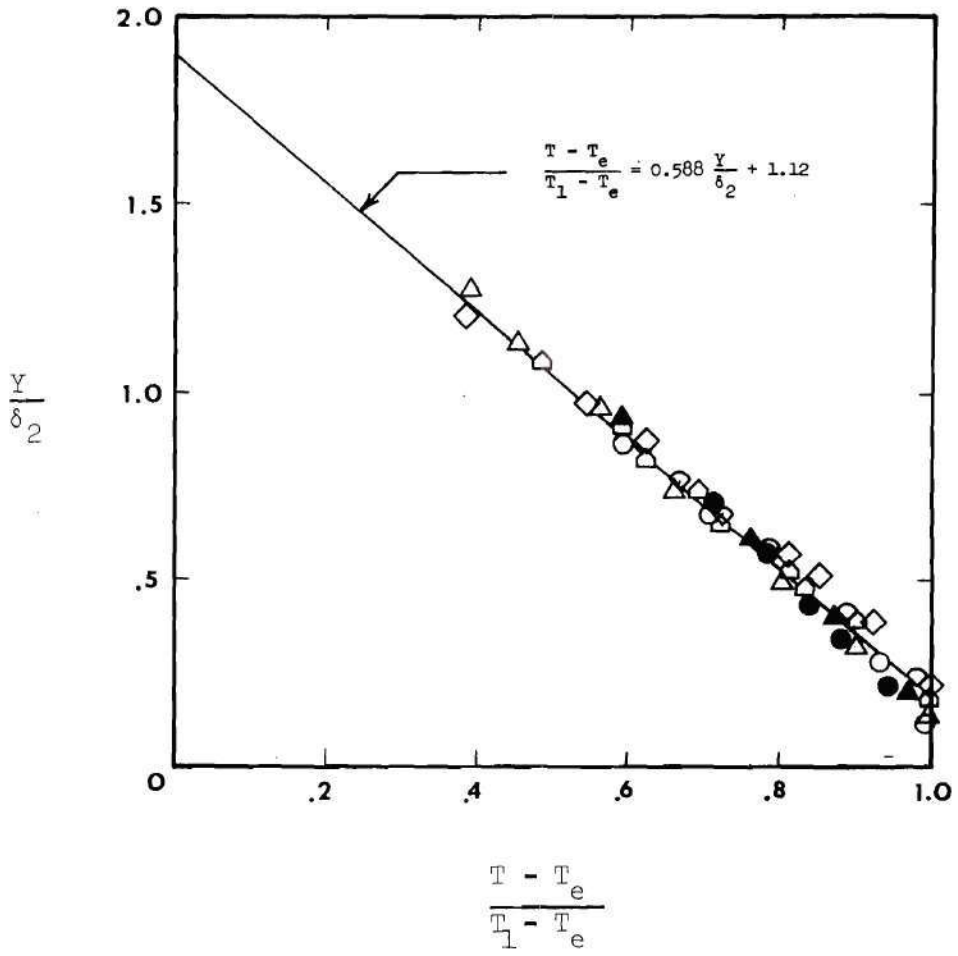

Figure 49. Wall Jet Temperature Profile

Series II

Symbol	U_j/U_{e_o}	x/h
□	2.00	39
■	2.00	194
○	3.93	39
●	3.93	194
△	5.78	39
▲	5.78	194

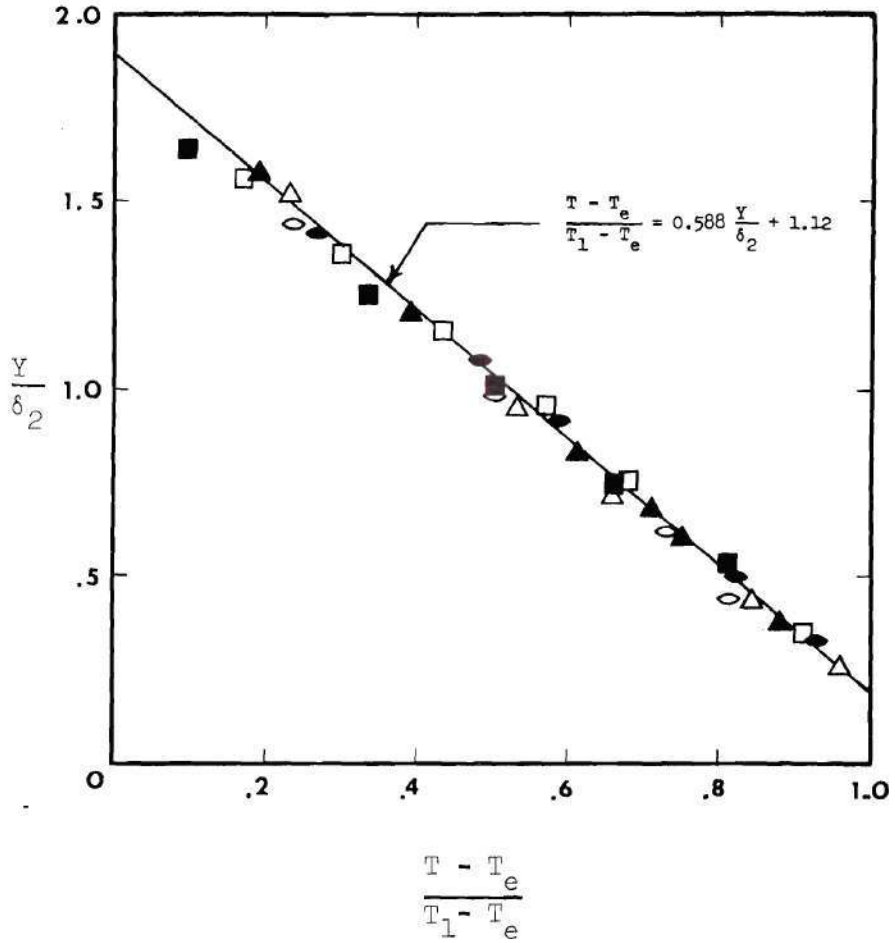

Figure 50. Wall Jet Temperature Profile

Series III

Symbol	U_j/U_{e_o}	x/h
△	1.52	125
□	2.07	125
■	2.07	462
○	2.92	125
●	2.92	462

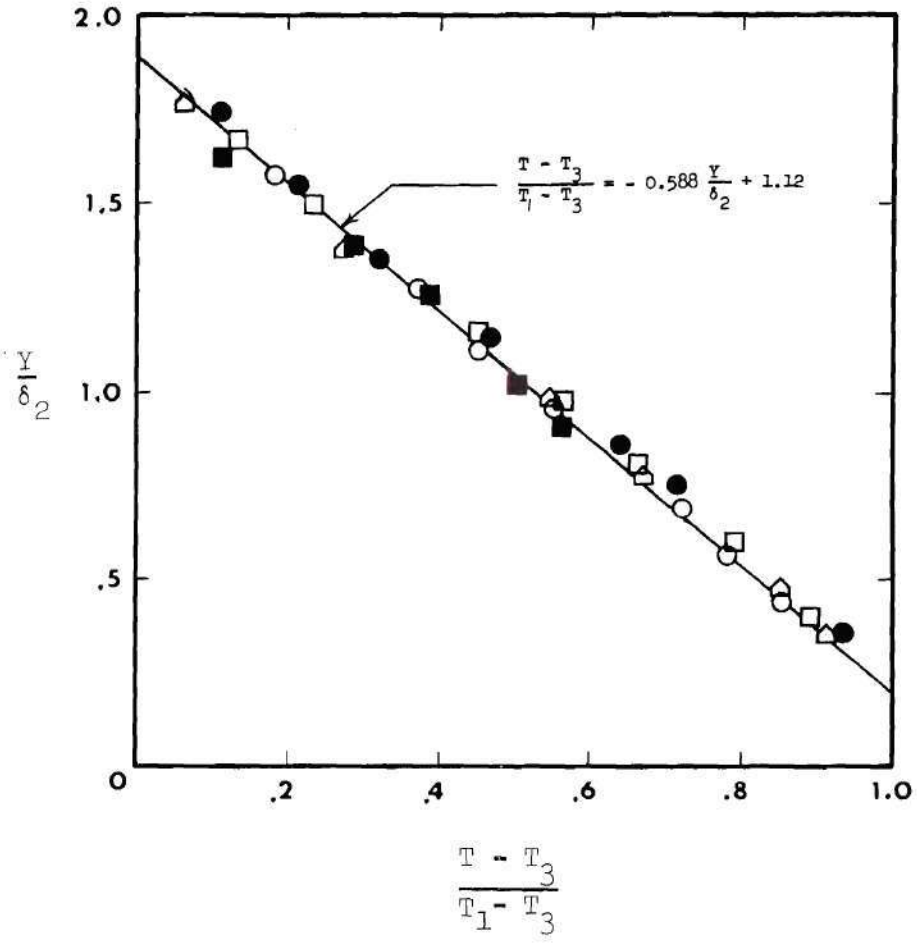

Figure 51. . Wall Jet Temperature Profile

Series IV

Symbol	U_j/U_{e_o}	x/h
◊	1.05	125
◻	2.00	56
□	1.97	125
■	1.97	357
○	2.99	125
●	2.99	357

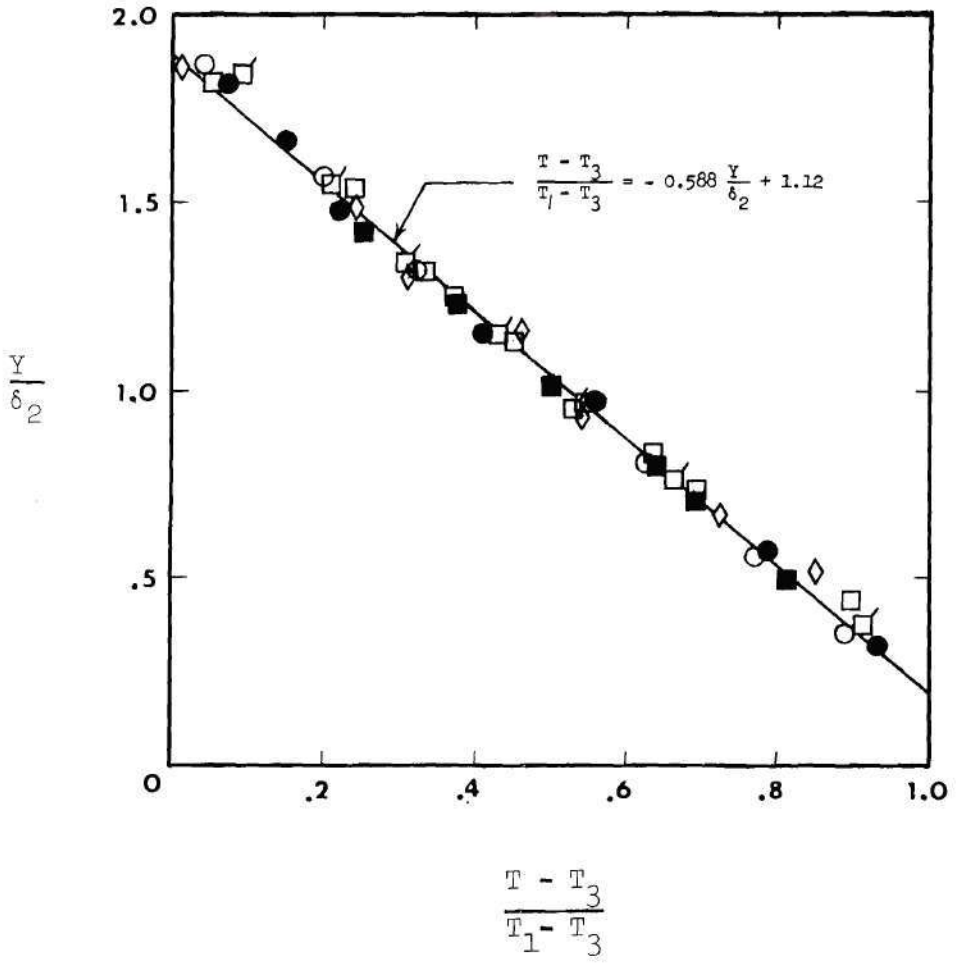

Figure 52. Wall Jet Temperature Profile

Series I

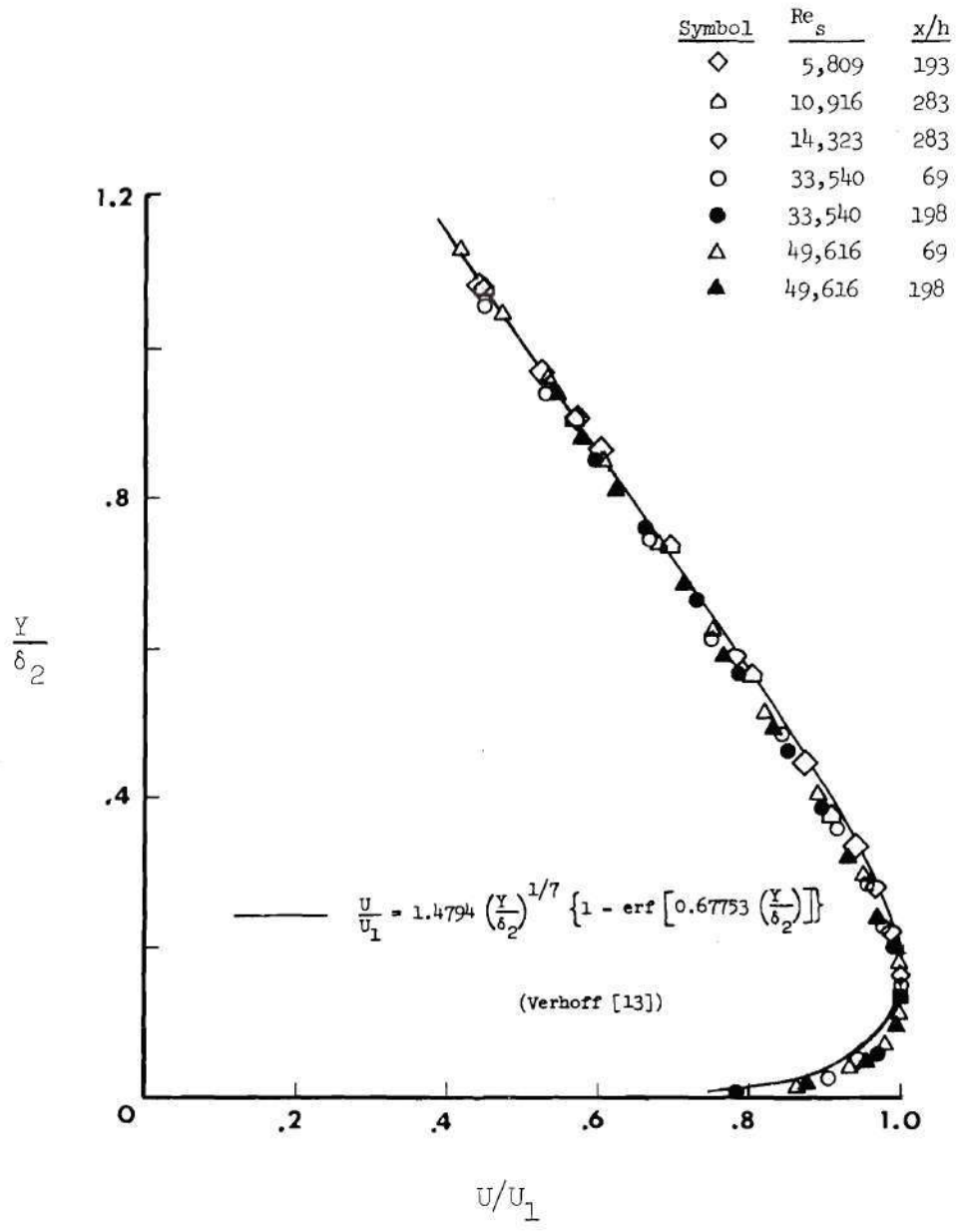

Figure 53. Wall Jet Velocity Profile

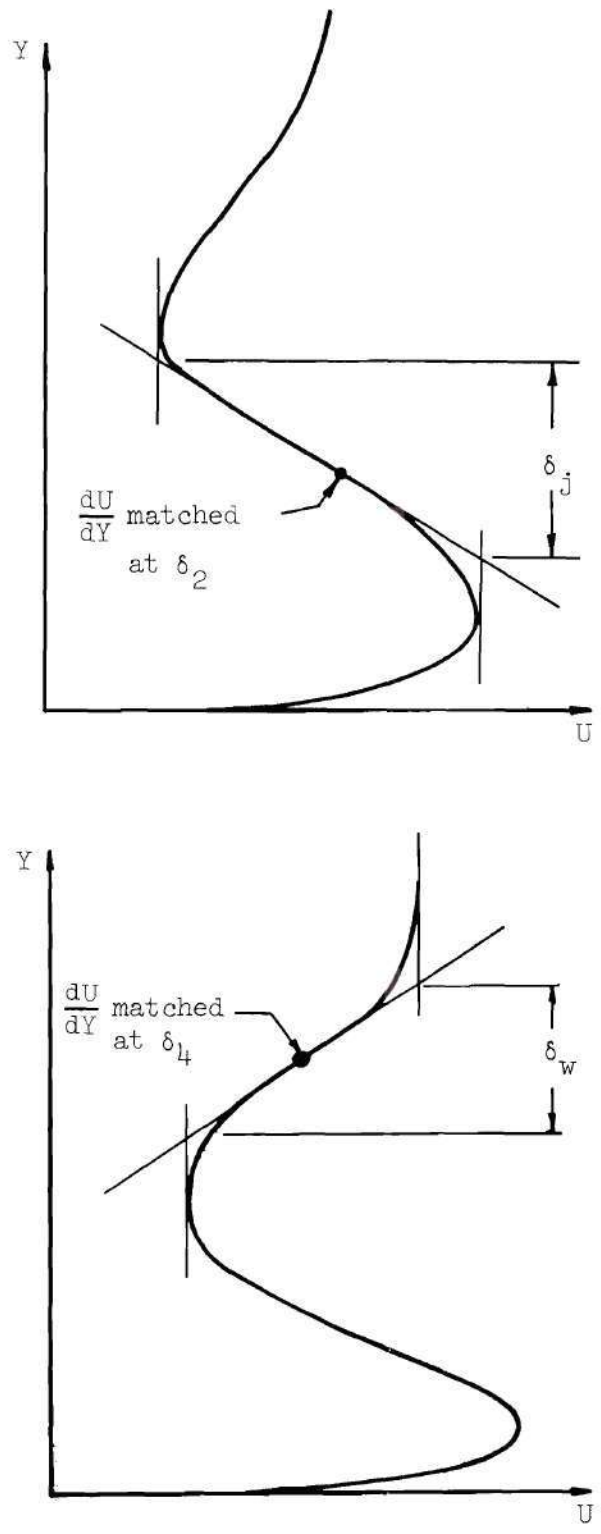

Figure 54. Profile Similarity Parameter

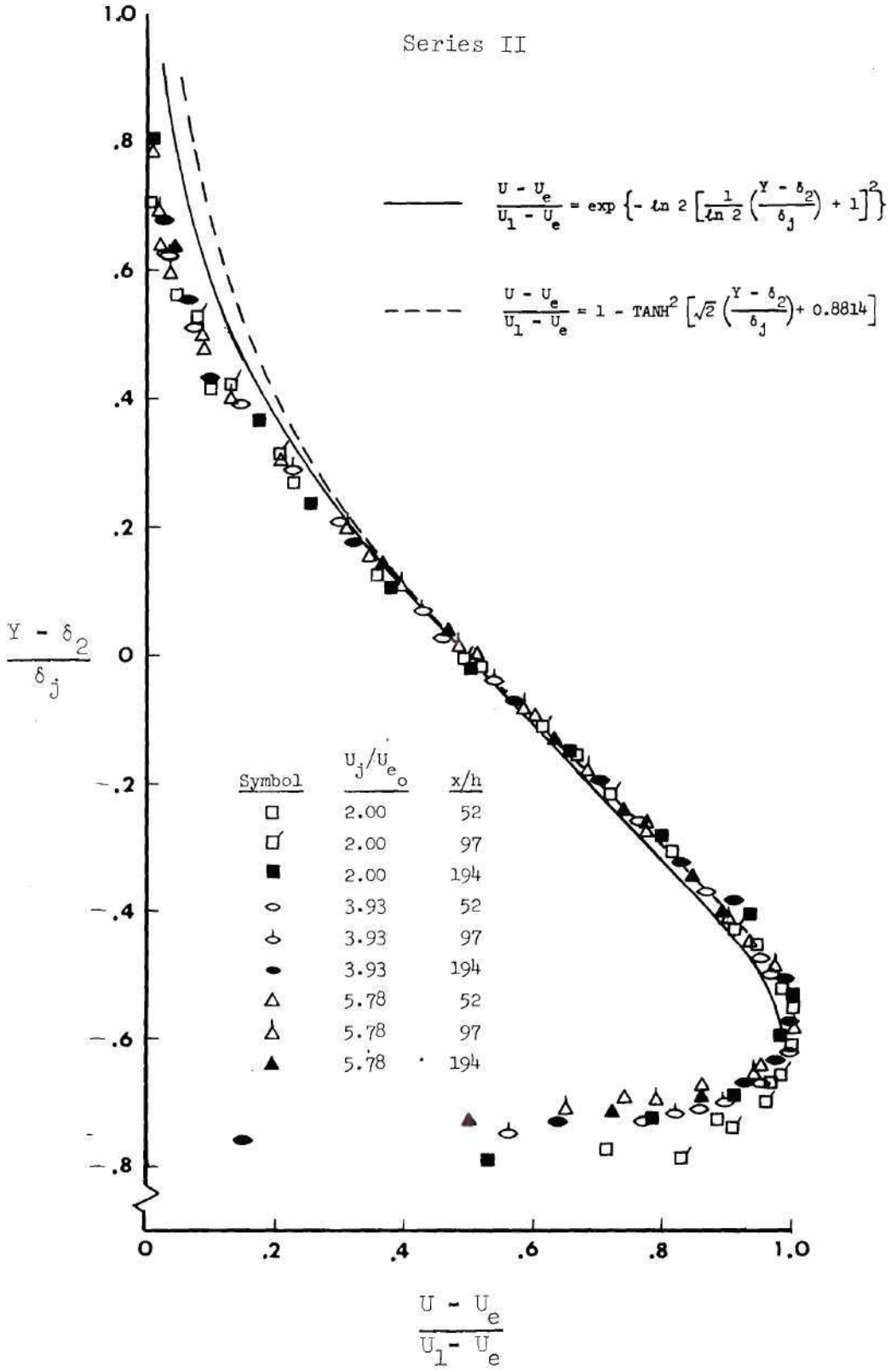

Figure 55. Wall Jet Velocity Profile

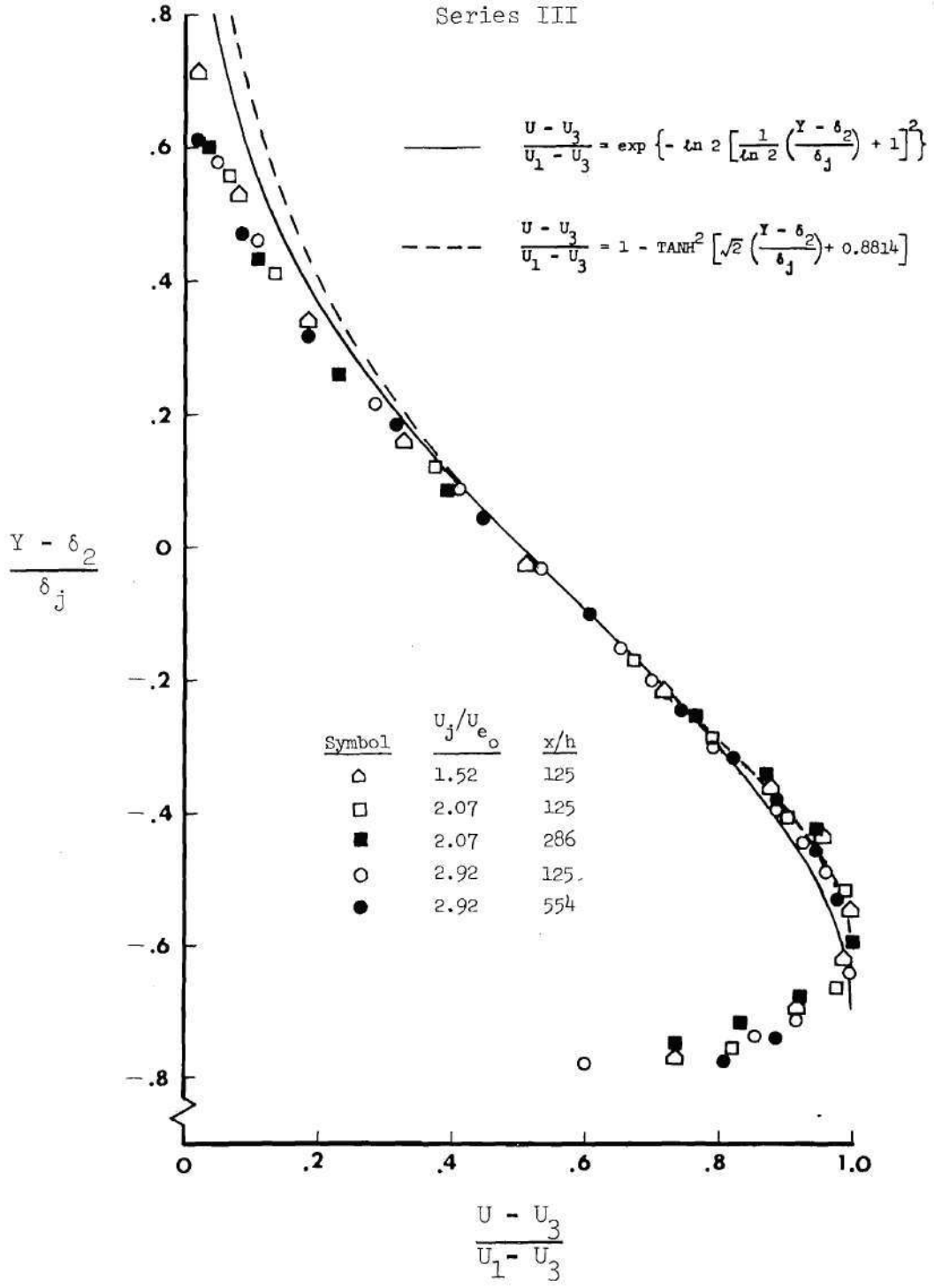

Figure 56. Wall Jet Velocity Profile

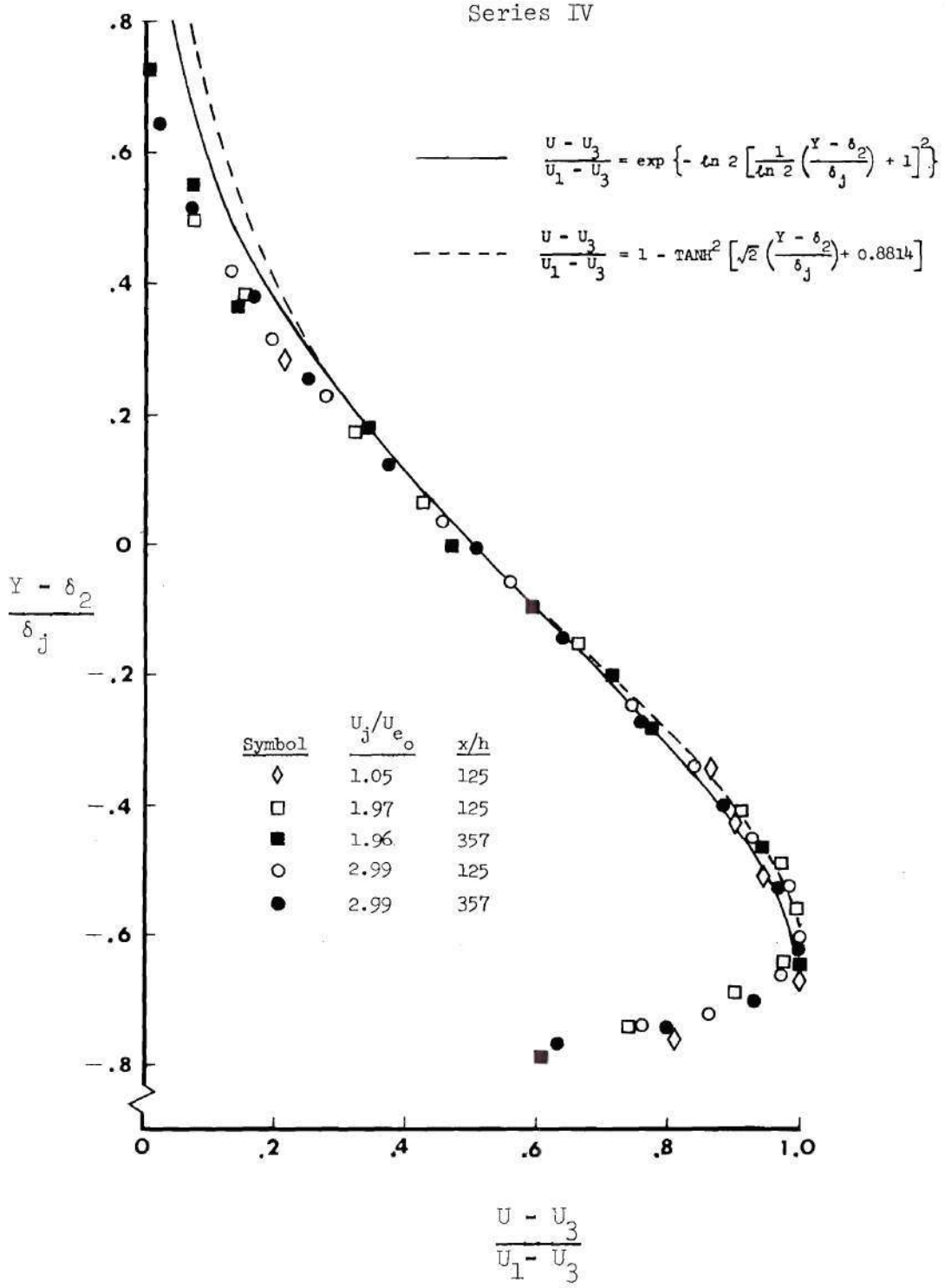

Figure 57. Wall Jet Velocity Profile

Series IV

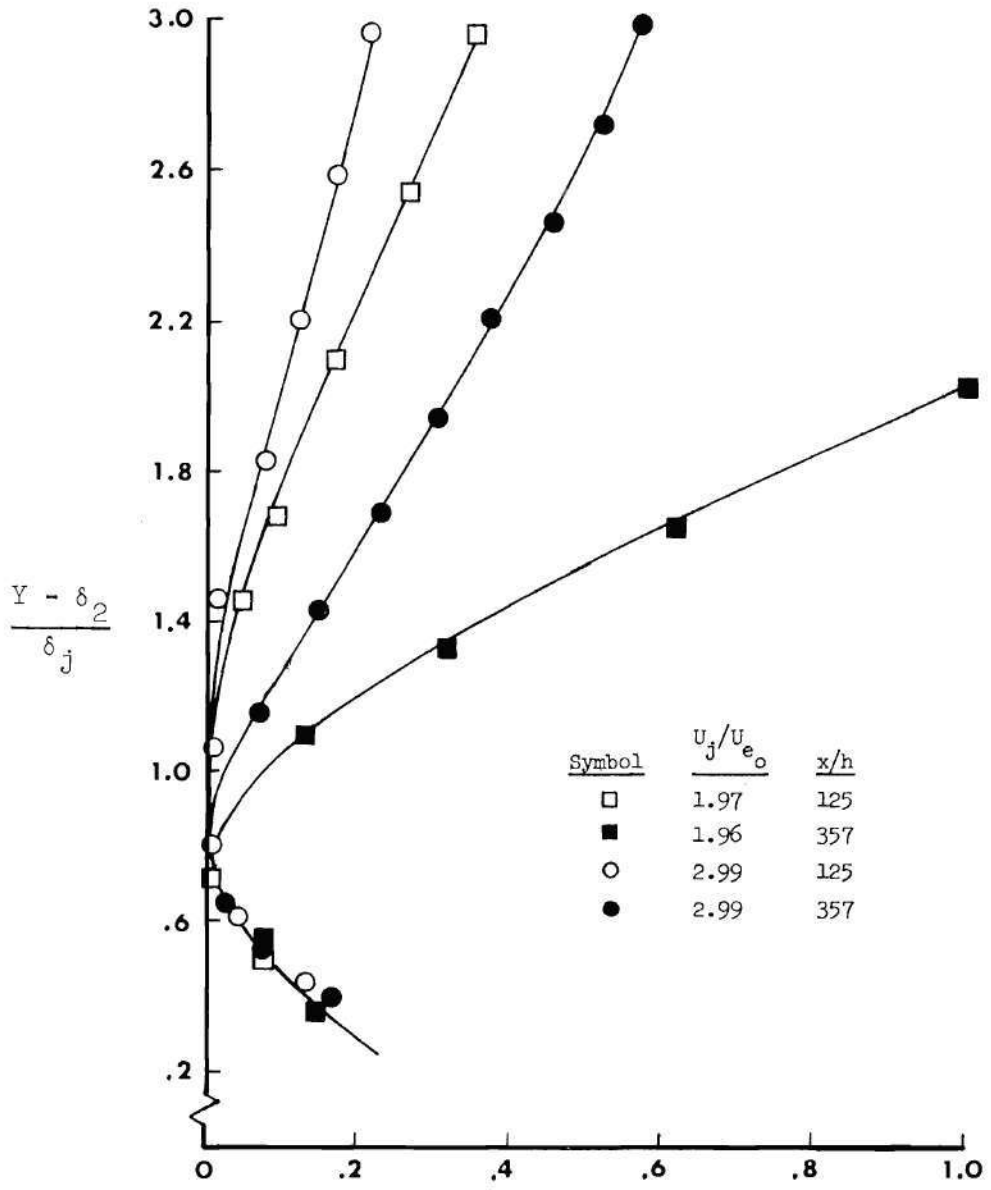

Figure 58. Wall Jet Velocity Profile

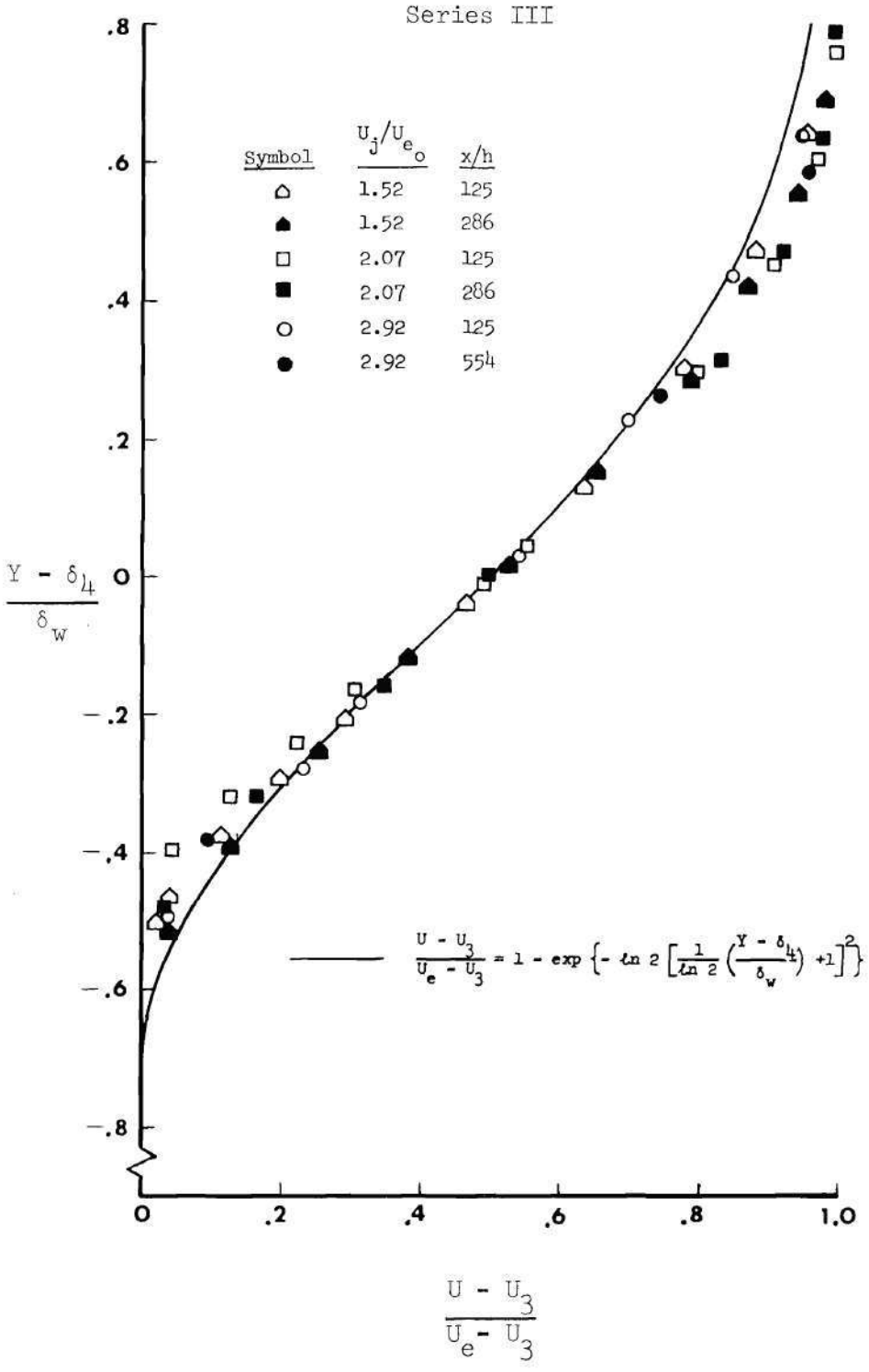

Figure 59. Wall Jet Velocity Profile

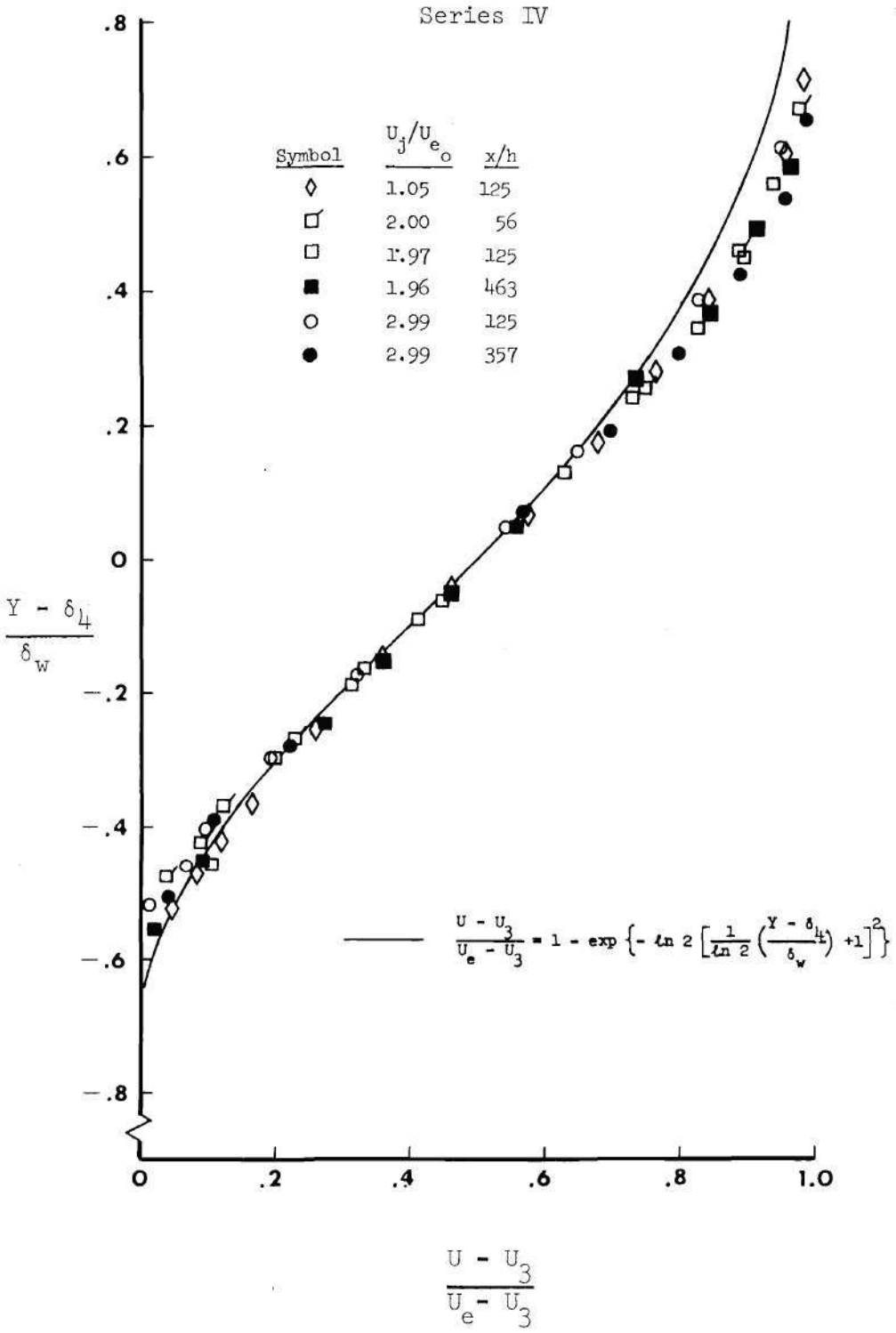

Figure 60. Wall Jet Velocity Profile

Series I

Symbol	Re_s	Symbol	Re_s
⬡	13,998	□	31,128
◇	14,323	▷	31,451
△	16,083	∩	44,050
◊	19,561		

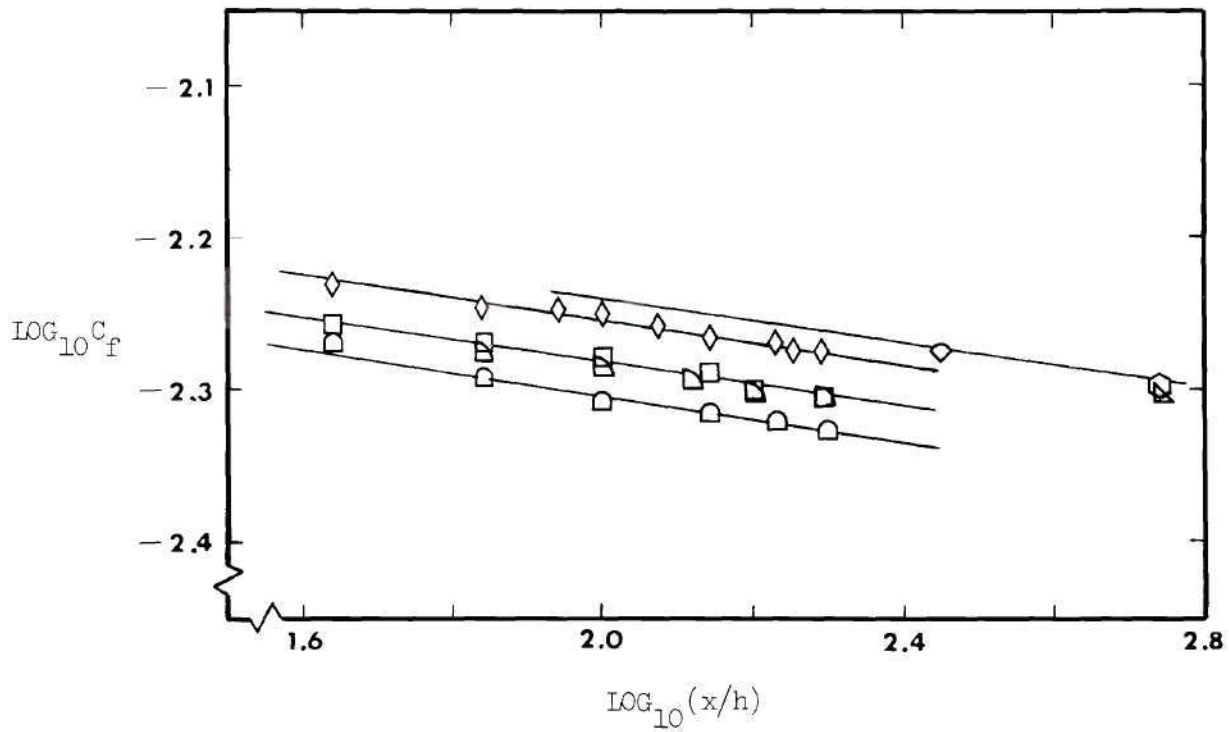

Figure 61. Wall Jet Friction Coefficient

Series I

Symbol	Re_s	Symbol	Re_s
⬡	13,998	□	31,128
◇	14,323	▷	31,451
◺	16,083	⌓	44,050
◊	19,561		

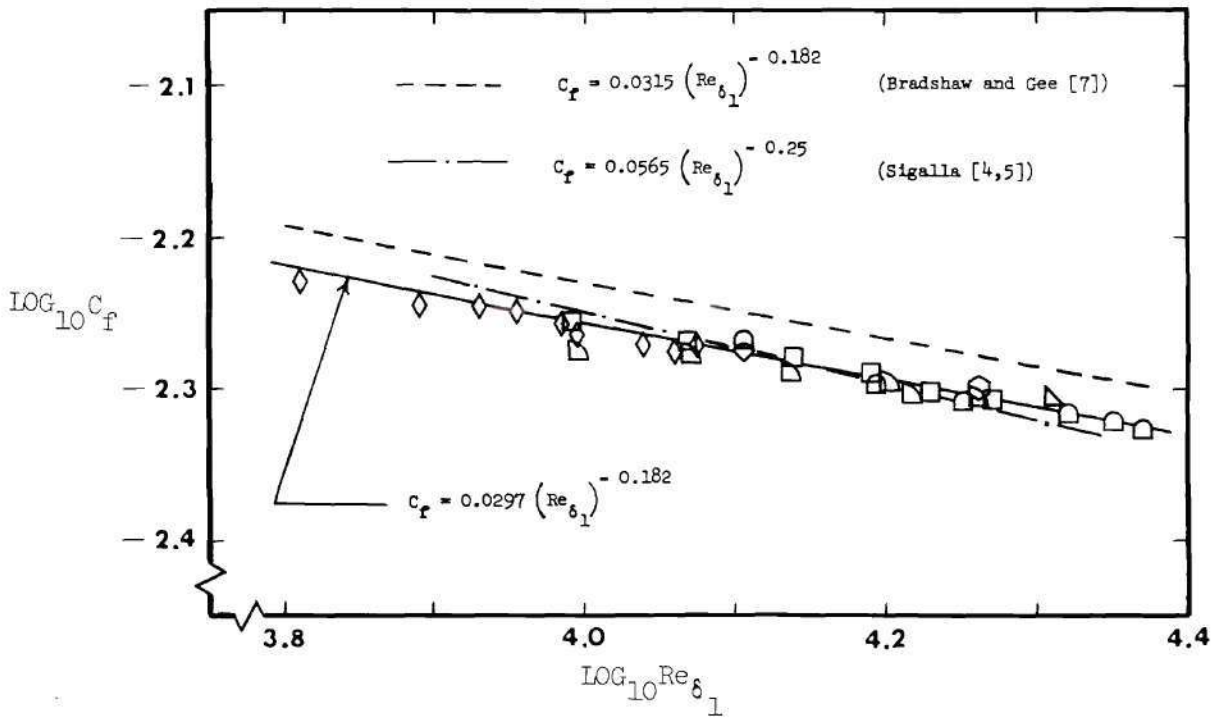

Figure 62. Wall Jet Skin Friction

Series II

Symbol	U_j/U_{e_o}	Symbol	U_j/U_{e_o}
△	5.78	◇	1.74
○	3.93		
□	1.99	⌂	1.49

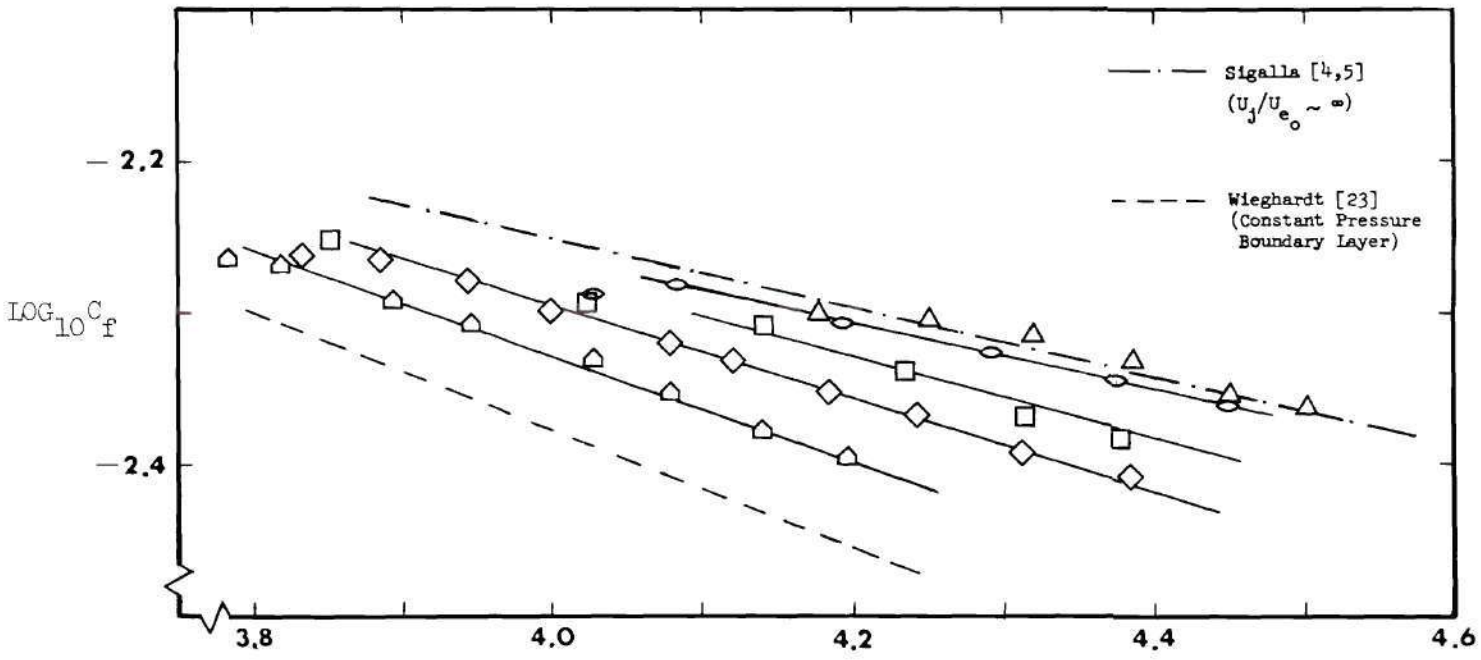

Figure 63. Wall Jet Skin Friction

Series II

Symbol	U_j/U_{e_o}	Symbol	U_j/U_{e_o}
△	5.78	◇	1.74
⬭	3.93		
□	1.99	⌂	1.49

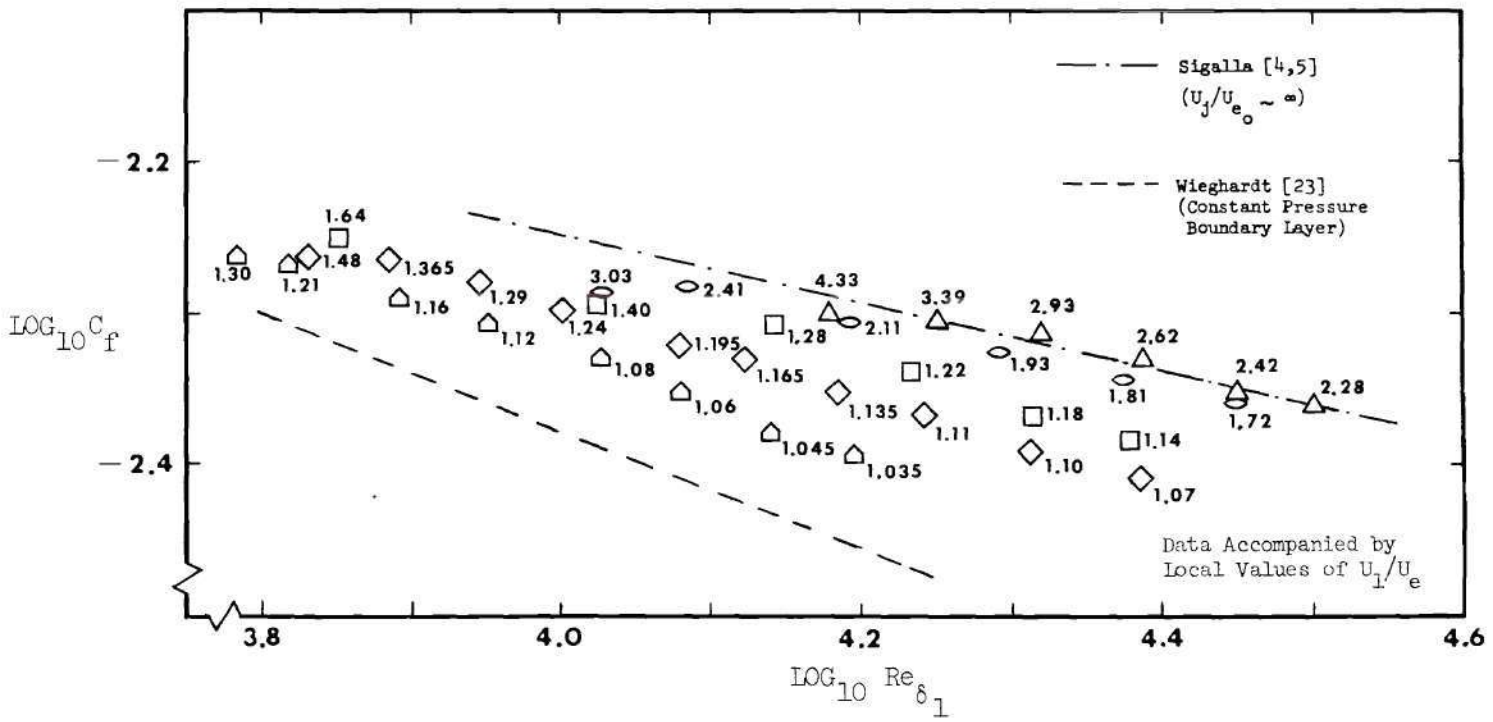

Figure 64a. Wall Jet Skin Friction

Series II

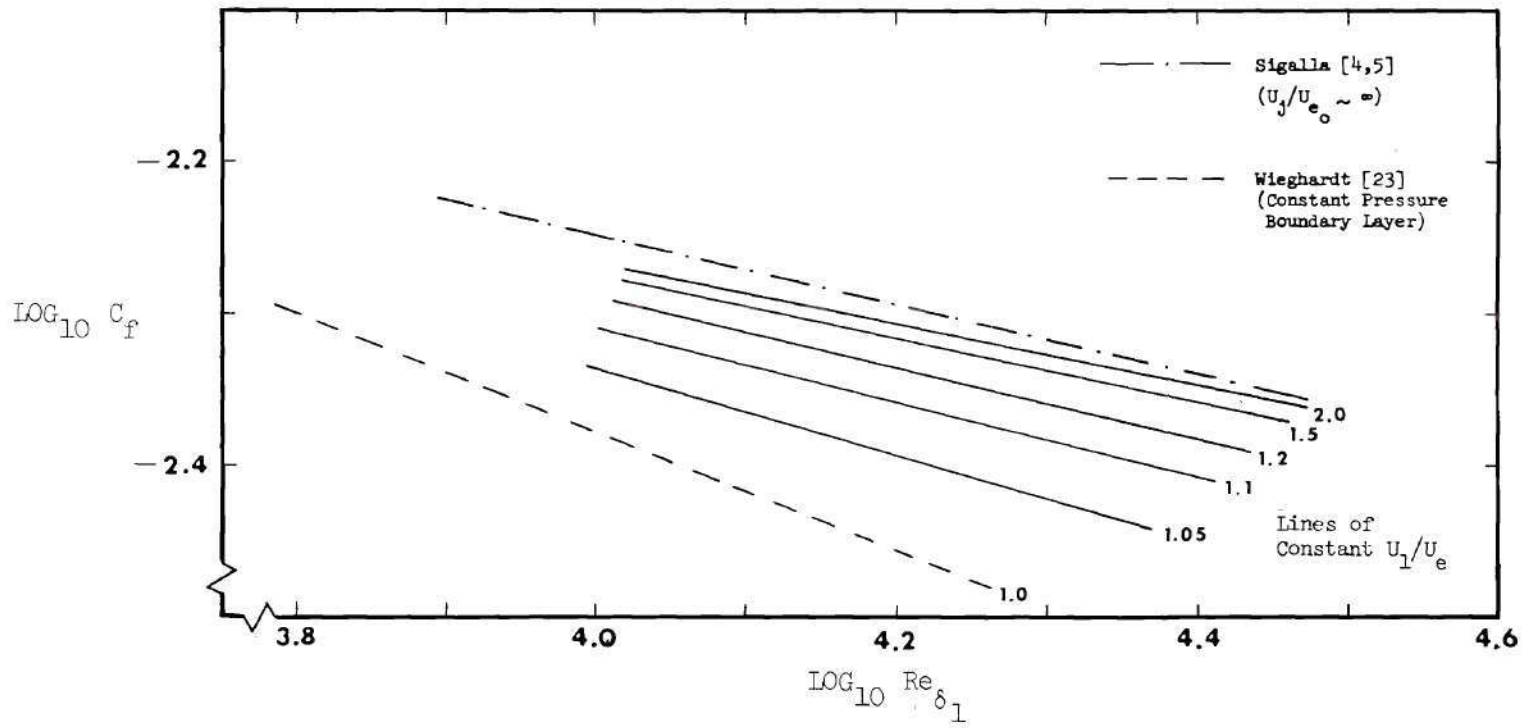

Figure 64b. Wall Jet Skin Friction

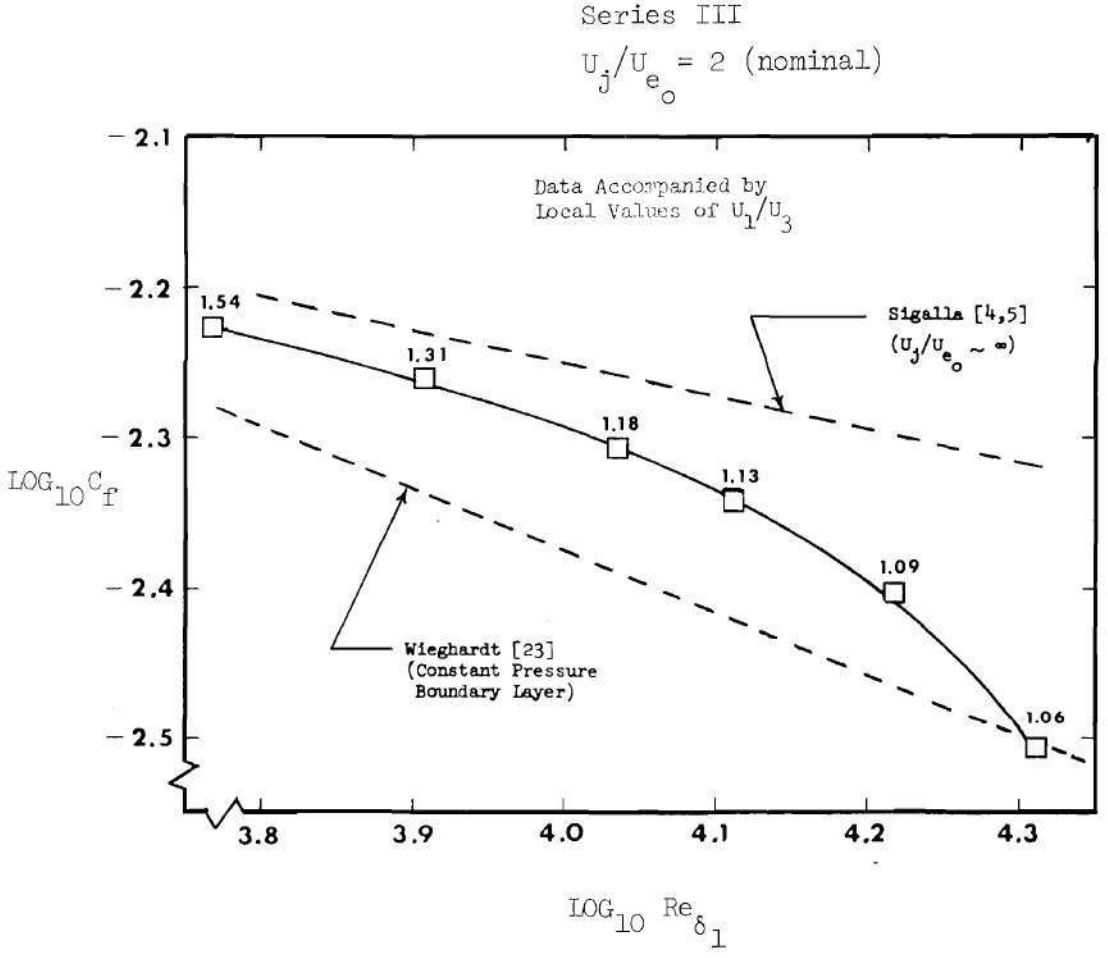

Figure 65. Wall Jet Skin Friction

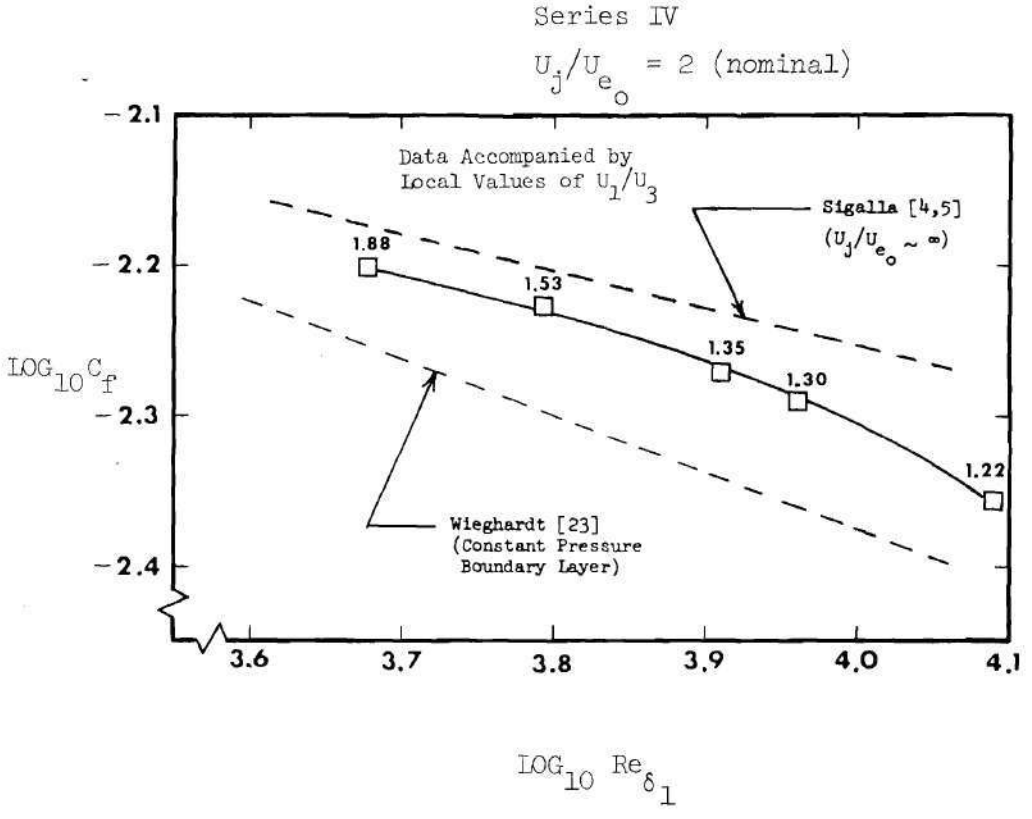

Figure 66. Wall Jet Skin Friction

Series I

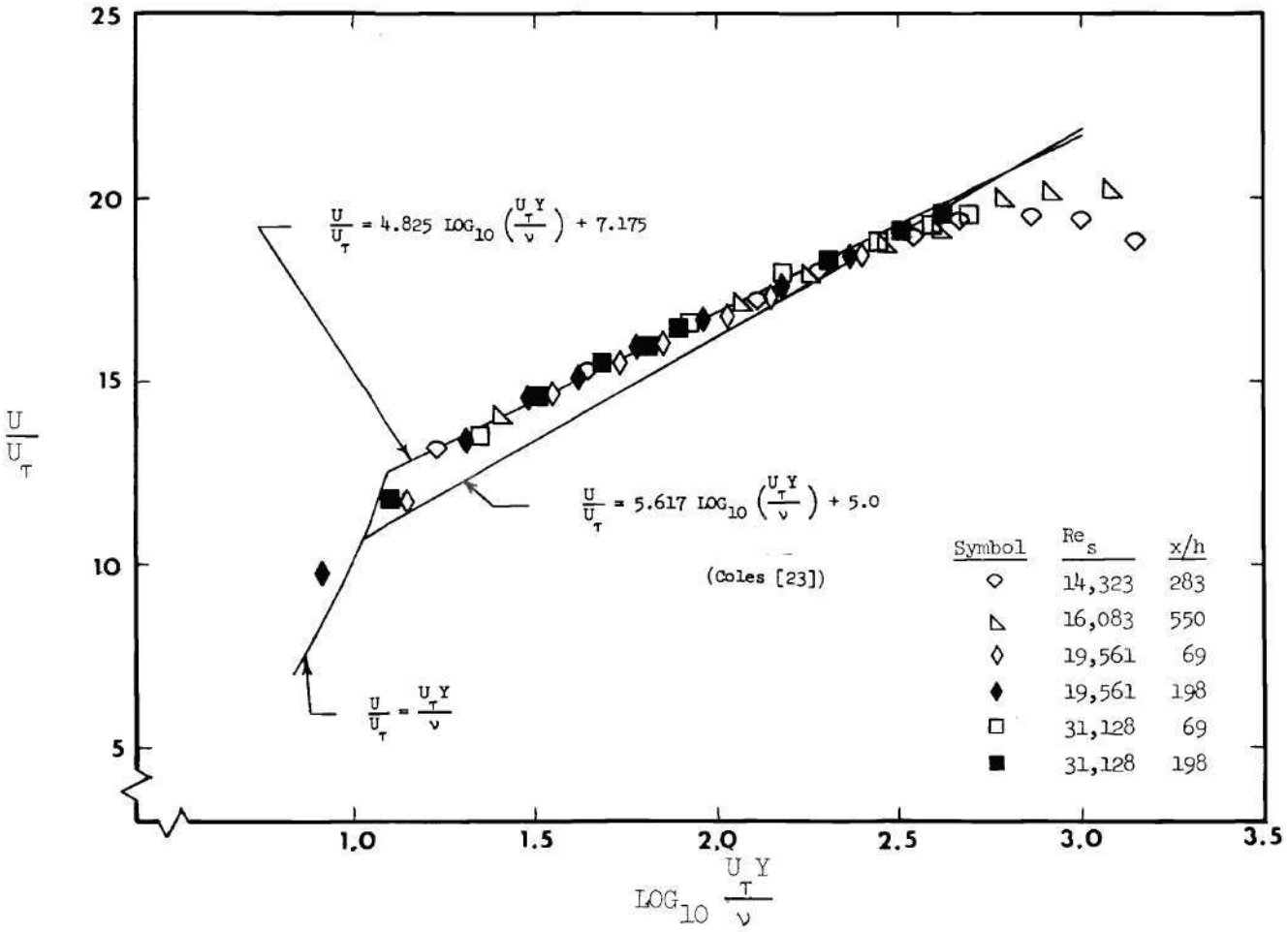

Figure 67. Law of the Wall

Series II

x/h = 97

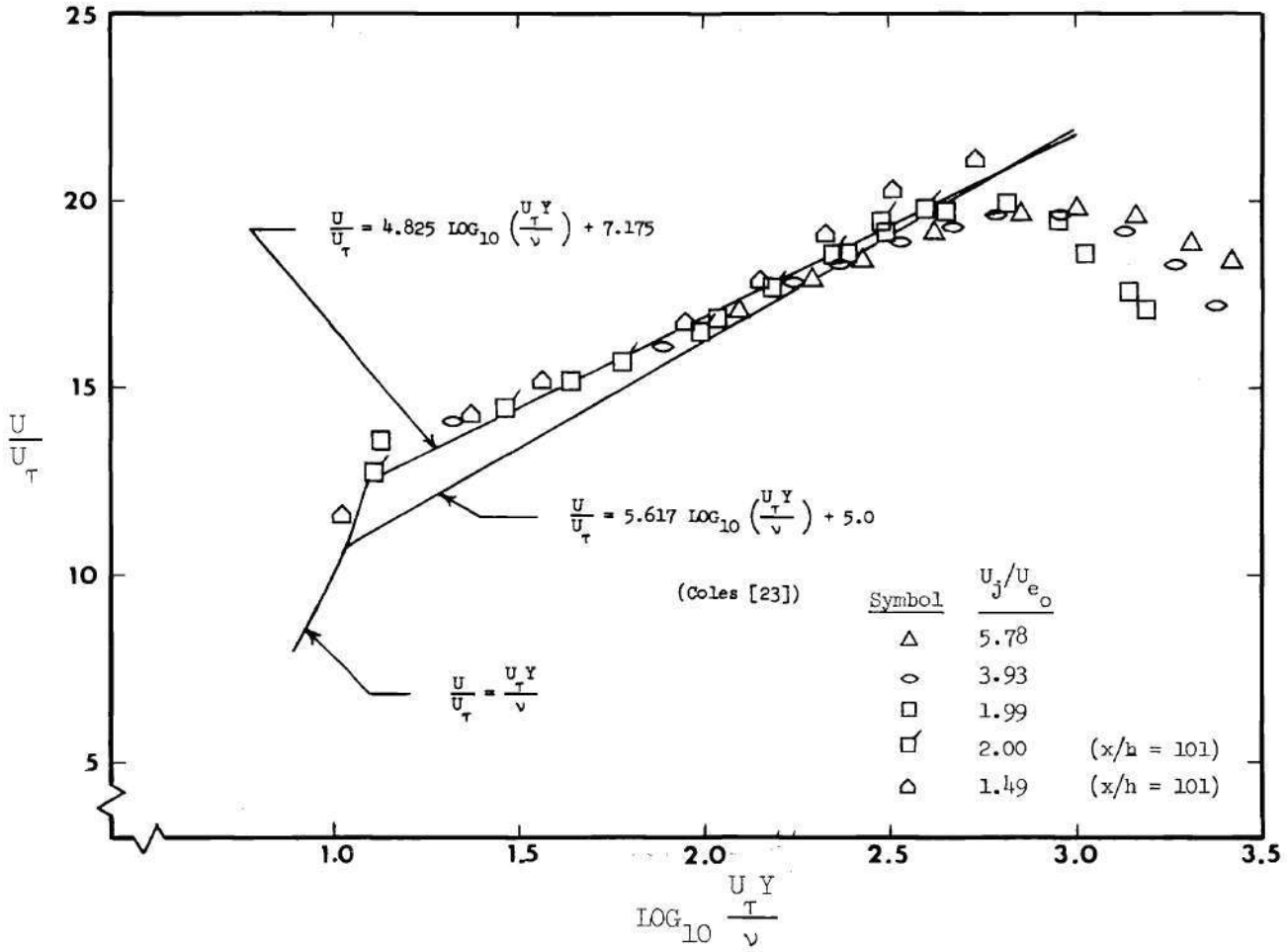

Figure 68. Law of the Wall

Series II
x/h = 194

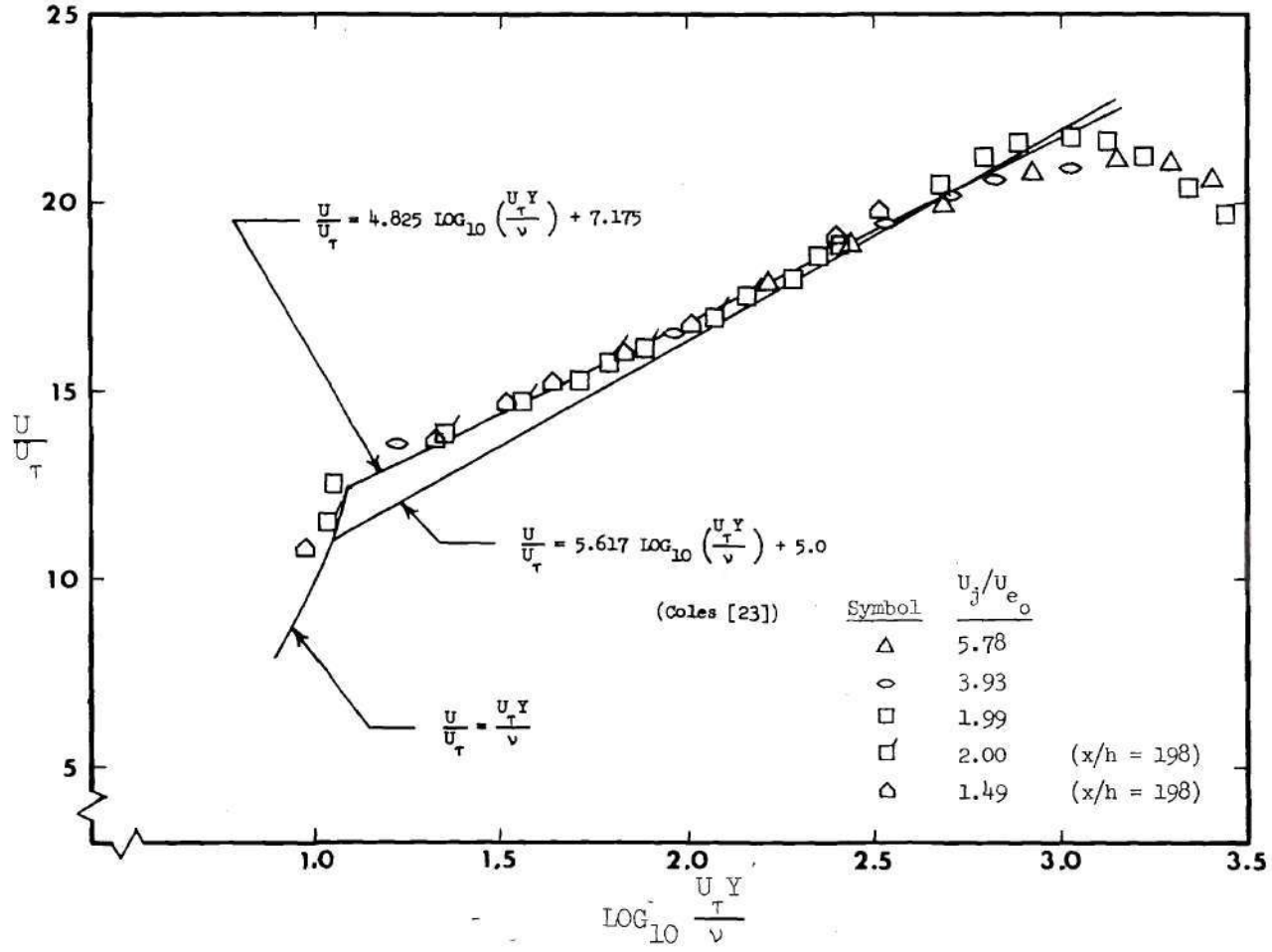

Figure 69. Law of the Wall

Series III

U_j/U_{e_o} = 1.5 (nominal)

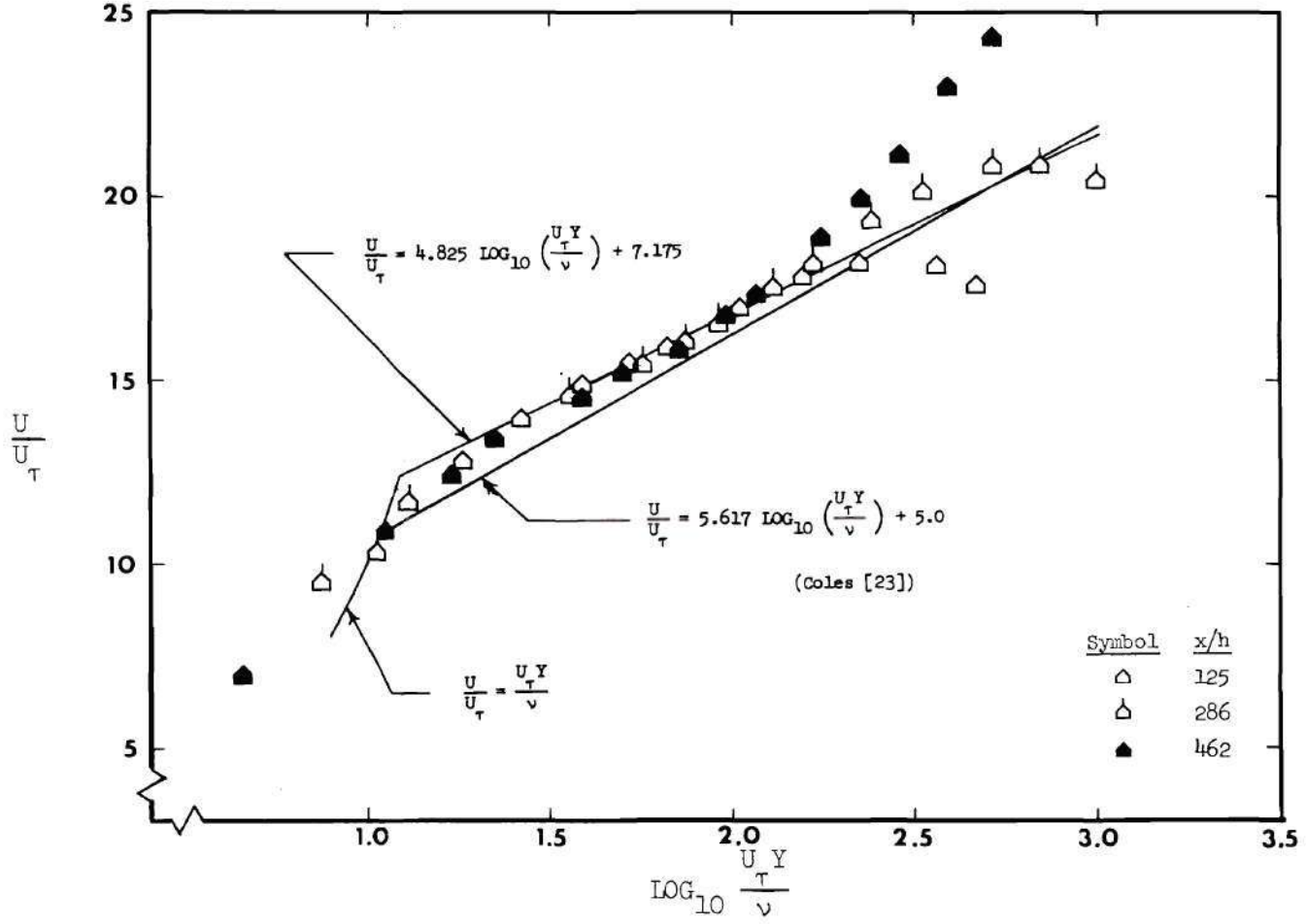

Figure 70. Law of the Wall

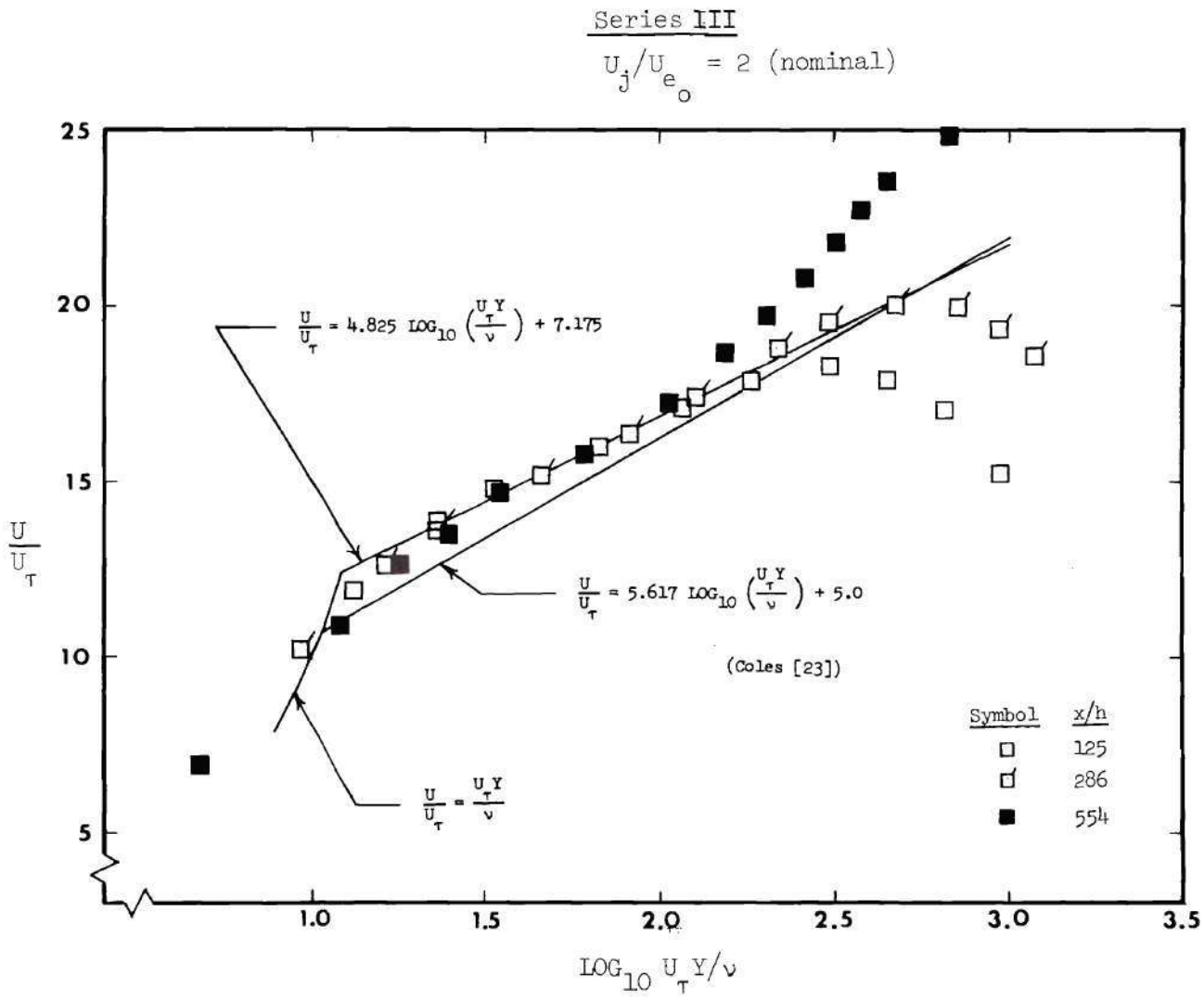

Figure 71. Law of the Wall

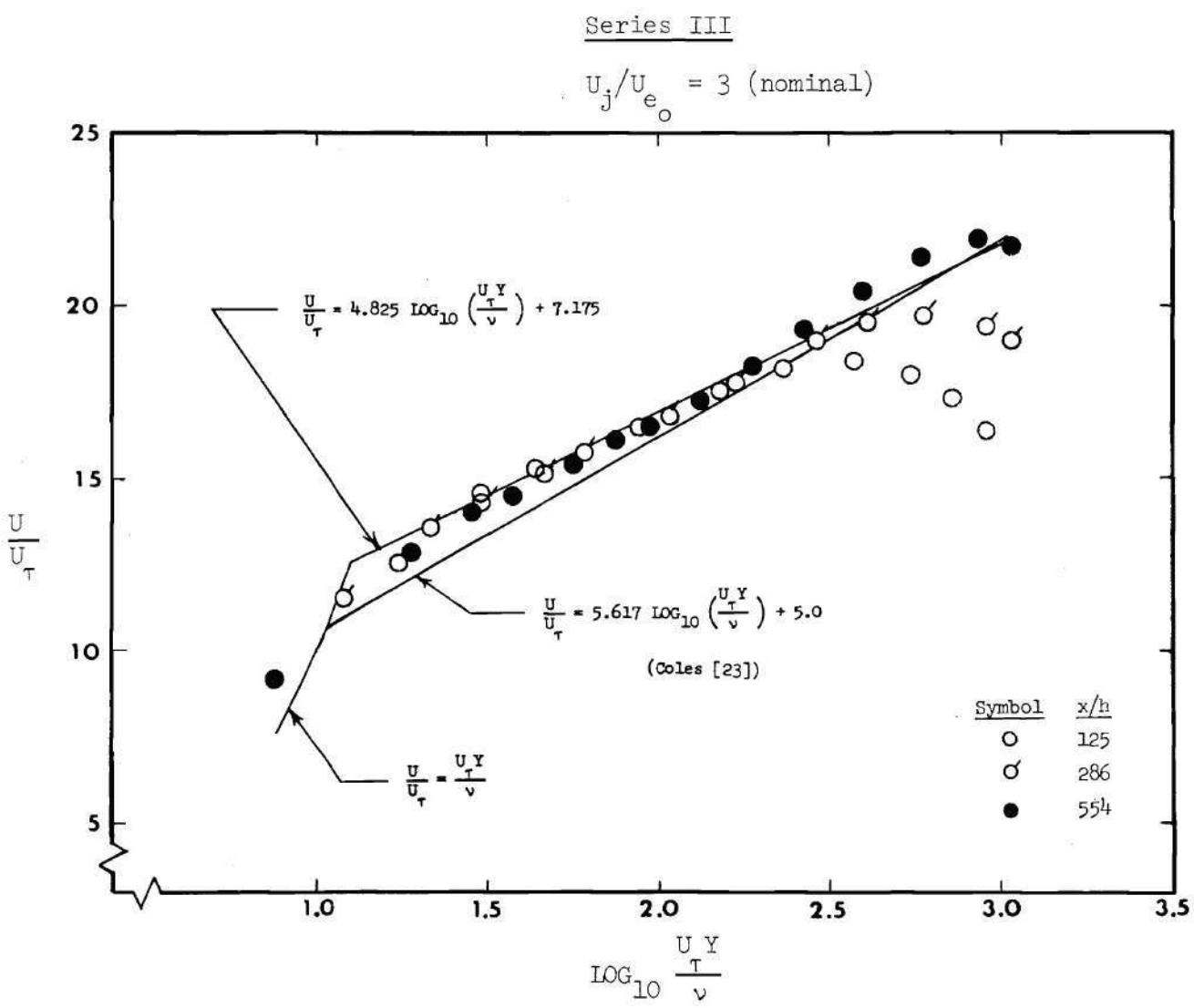

Figure 72. Law of the Wall

CHAPTER V

CONCLUSIONS

The present results show excellent agreement with the experimental findings of previous investigators for both the wall jet in still air and the wall jet with a constant-velocity main-stream flow. The measured growth of the half-velocity height and the decay of the jet peak velocity with distance from the jet slot agree qualitatively with theoretical predictions and quantitatively with comparable measurements of others.

Velocity profile similarity is demonstrated for all four series of wall jet test results. The wall jet in still air and the wall jet with moving stream both exhibit profile similarity from the jet peak, δ_1, to the outer edge, δ_e. The results of the velocity profile measurements for the adverse streamwise pressure gradient cases in which a substantial initial boundary layer is present reveal that similarity exists separately in the two outer layers (i.e., from δ_1 to δ_3, and from δ_3 to δ_e). The profile similarity persists beyond the location at which the jet peak velocity becomes lower than the local free-stream velocity. In fact, similarity is maintained to the point at which evidence of the jet peak disappears.

The near-wall profiles demonstrate similarity in the form of a single "law of the wall" for all measurements. The outer portion of the wall layer, however, does not conform to a simple expression of

similarity. This outer region is influenced by the presence of local pressure gradients, by the local jet to free-stream velocity ratio and by the velocity deficit in the valley above it.

Jet flow temperatures for the present experiments were commonly 50 to 100 degrees Fahrenheit higher than the main-stream flow temperature. This temperature difference reflected in jet densities that were about 15 per cent below the main-stream air density. The reduced densities result in lower jet momentum values for the present cases than would be demonstrated by jets at the same temperature as the main stream with identical slot heights and velocities. The smaller momentum values probably cannot be ignored in analytical computations of wall jet development; however, no discernable alteration in the wall jet growth or decay processes is evident in the experimental data when the present work is compared with the results of others.

Similarity is present in all measurements of the total temperature decay through the wall jet in the direction normal to the wall. For the present experiments, the fluid temperature remains nearly constant from the wall to the jet peak region. Starting near the jet peak, the temperature decays linearly with height to the main-stream (edge) temperature.

A comparison of the velocity and temperature at the jet peak at various distances from the point of jet injection reveals that the streamwise decays are not similar in the sense that the Reynolds analogy holds. In addition, the relation between temperature and velocity decay at the jet peak is altered by changing the slot Reynolds number. The temperature-velocity decay nevertheless approximates a

theoretical prediction for turbulent free jet flow (using Taylor's vorticity-transfer theory of turbulence) through much of the decay process.

The friction data measured with a Preston tube for the wall jet in still air agrees closely with the data presented by Sigalla [4,5]. Skin friction laws are also demonstrated for the present cases with no main-stream pressure gradient. The results indicate that these laws are based on a correlation between skin friction and local velocity ratio, U_1/U_e. The friction coefficients for all values of U_1/U_e above 2.0 are closely approximated by the friction law for a wall jet in still air. However, after the local velocity ratio becomes less than 2.0, the friction coefficients drop rapidly toward the constant-pressure boundary layer friction law. The correlation between skin friction and local velocity ratio is not generally valid for the wall jet flows under adverse pressure gradient.

As indicated previously, the near-wall velocity profile data in combination with the local skin friction measurement reveals that a "law of the wall" exists over a portion of the wall layer. The diverse wall jet conditions that were studied consistently yield the same law. Further, the measurements are identical to those obtained with a Preston tube in turbulent pipe flow by Patel [22]. Coles [23], however, obtained a slightly different law by compiling turbulent boundary layer data from several sources. The law of the wall results differ among authors primarily in the value of skin friction that is employed. If Coles' law of the wall expression is assumed to be correct, it appears that Patel's Preston tube calibration for

determining skin friction may yield values of τ_w that are about 5 per cent too low for wall jets in still air.

The measurements for the present work are recorded without using the corrections that are available for turbulence and probe interference effects. A comparison of three total pressure probes with quite different tip sizes and shapes revealed that the probe interference correction is insignificant. It is hoped that presenting the data in its basic form will avoid confusion in its interpretation.

APPENDIX A

BOUNDARY LAYER DEVELOPMENT SECTION

The boundary layer development section is shown in Figure A-1. The floor and ceiling are 3/8 inch flat aluminum plate. The side walls are 3/8 inch clear plexiglas sheet. The expansion contour ceiling shown in the figure consists of .090 inch aluminum sheet covering five 3/4 inch spars equally spaced over the 30 inch spanwise dimension. The contraction profiles are quarter sections of standard 8 inch aluminum pipe. The floor is roughened by fastening 24 grit (medium) sandpaper sheet to the floor.

SIDE VIEW

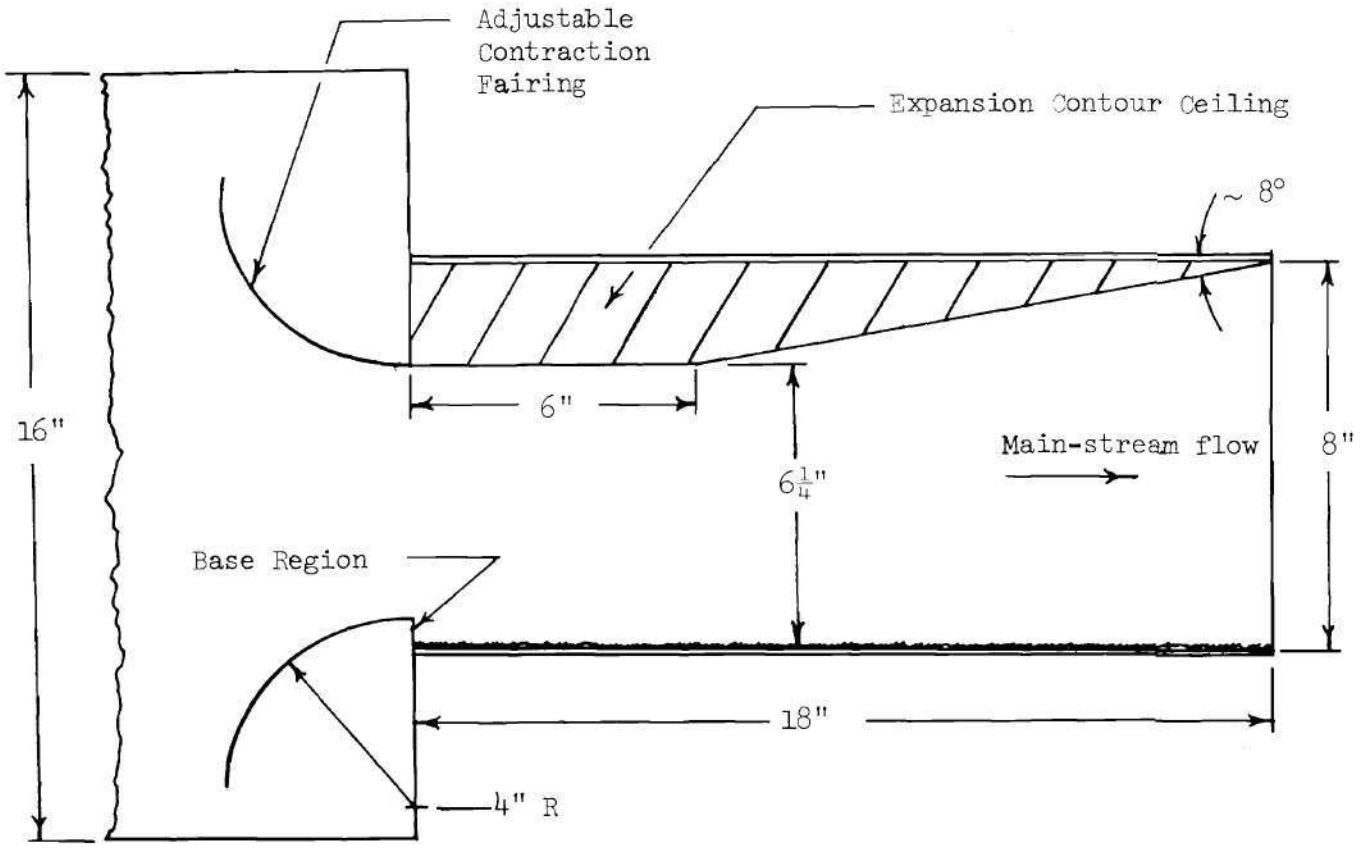

Figure A-1. Boundary Layer Development Section

APPENDIX B

JET NOZZLE

Notes

1. Slot height = spacer height + .030"
2. Inner contour is faired to smooth curve
3. 5° knife edge
4. Drawing not to scale
5. Nominal dimensions given

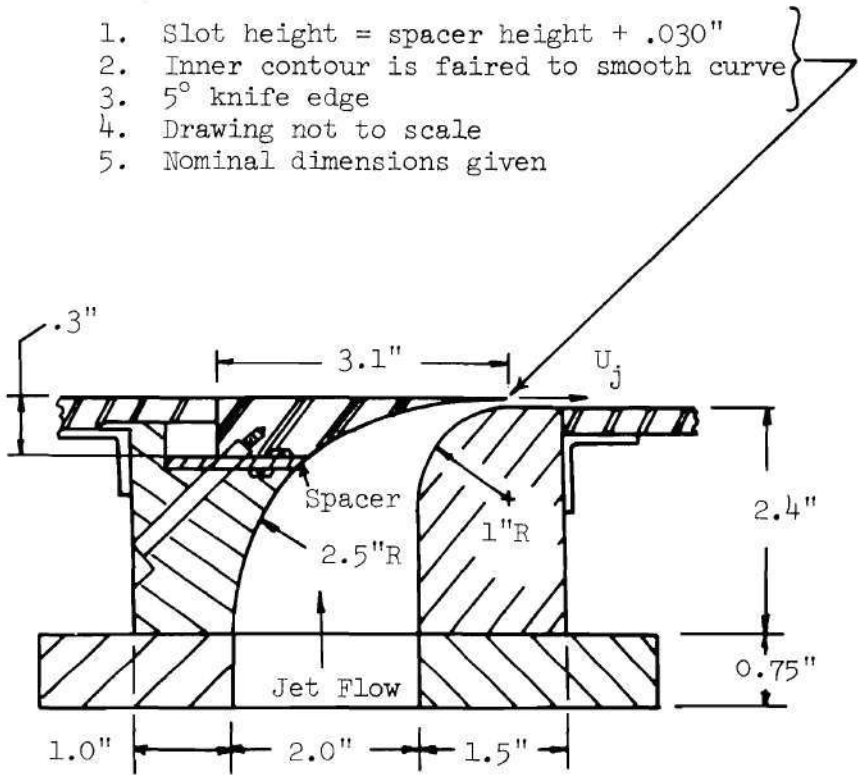

Figure B-1. Jet Nozzle

APPENDIX C

TEST SECTION

Dimensional details of the test section components are given in Figures C-1 and C-2. The test section floor is fabricated from 3/8 inch flat ground aluminum plate. The walls are 3/8 inch clear plexiglas sheet and are 18 inches high to allow for curvature of the ceiling. The removable ceiling is .090 inch perforated mild steel sheet strengthened by external spanwise stringers at 3 inch intervals in the streamwise direction.

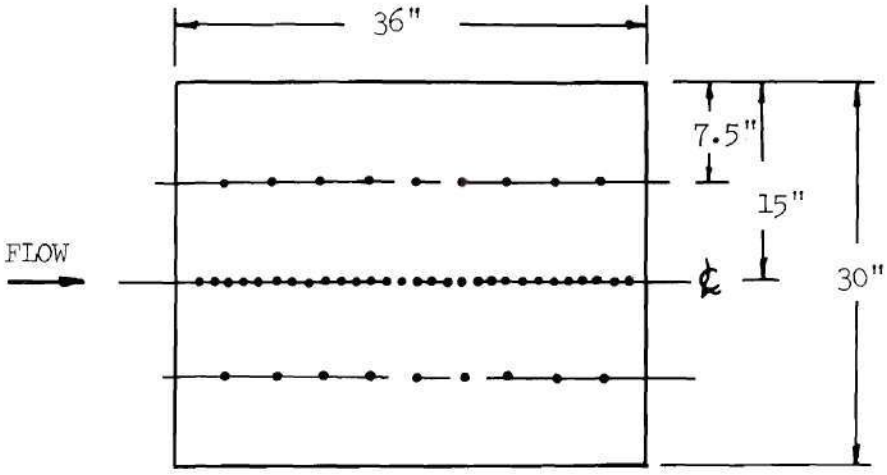

1/16" diameter static pressure taps spaced at 1" intervals on centerline and 3" intervals off-centerline.

Figure C-1. Test Section Floor

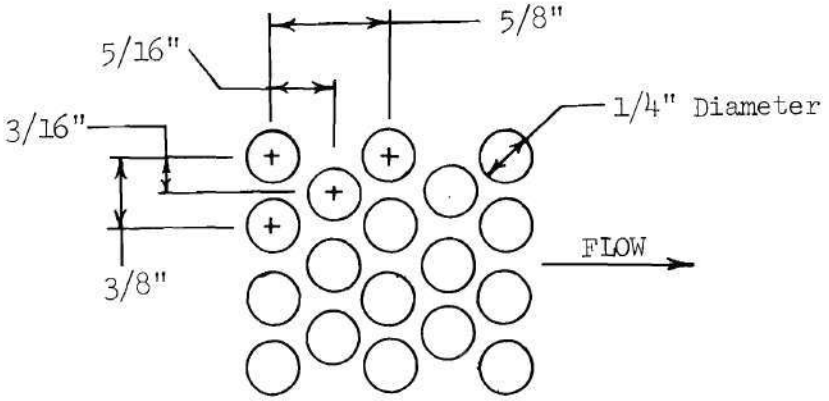

NOTE: $\frac{\text{Open Area}}{\text{Total Area}} = 0.4$

Figure C-2. Perforated Ceiling Bleed Hole Pattern

APPENDIX D

MAIN-STREAM AIR SUPPLY AND PLENUM CHAMBER

Main-stream Blower

The main-stream air is supplied by a single stage centrufugal compressor driven at 3100 RPM by a 60 HP constant speed electric motor. The blower is shown in Figure D-1. The blower performance is given in Figure D-2.

Main-stream Plenum Chamber

The main-stream plenum chamber is shown in Figures D-3 and D-4. The chamber is constructed with 5/8 inch plywood supported internally by a metal frame. The 16 inch diameter cylindrical dead-end baffle employs perforated .090 inch sheet metal (40 per cent open). The box is lined with 2 inch fiberglas padding to reduce the main-stream noise level. A laminated mahogony bellmouth re-accelerates the flow to the 16 inch diameter exhaust duct.

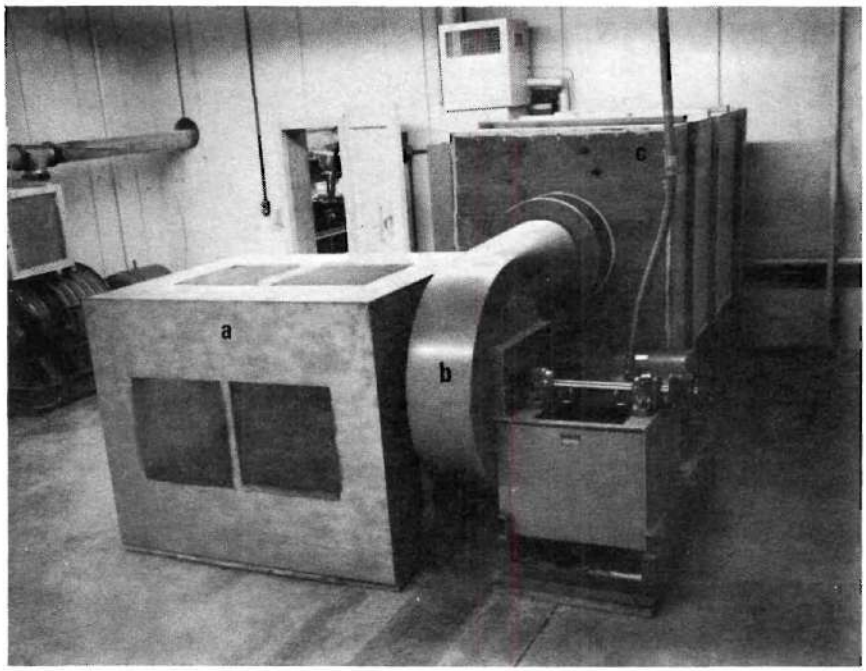

(a) Intake Filter Box
(b) Blower
(c) Plenum Chamber

Figure D-1. Main-stream Air Supply

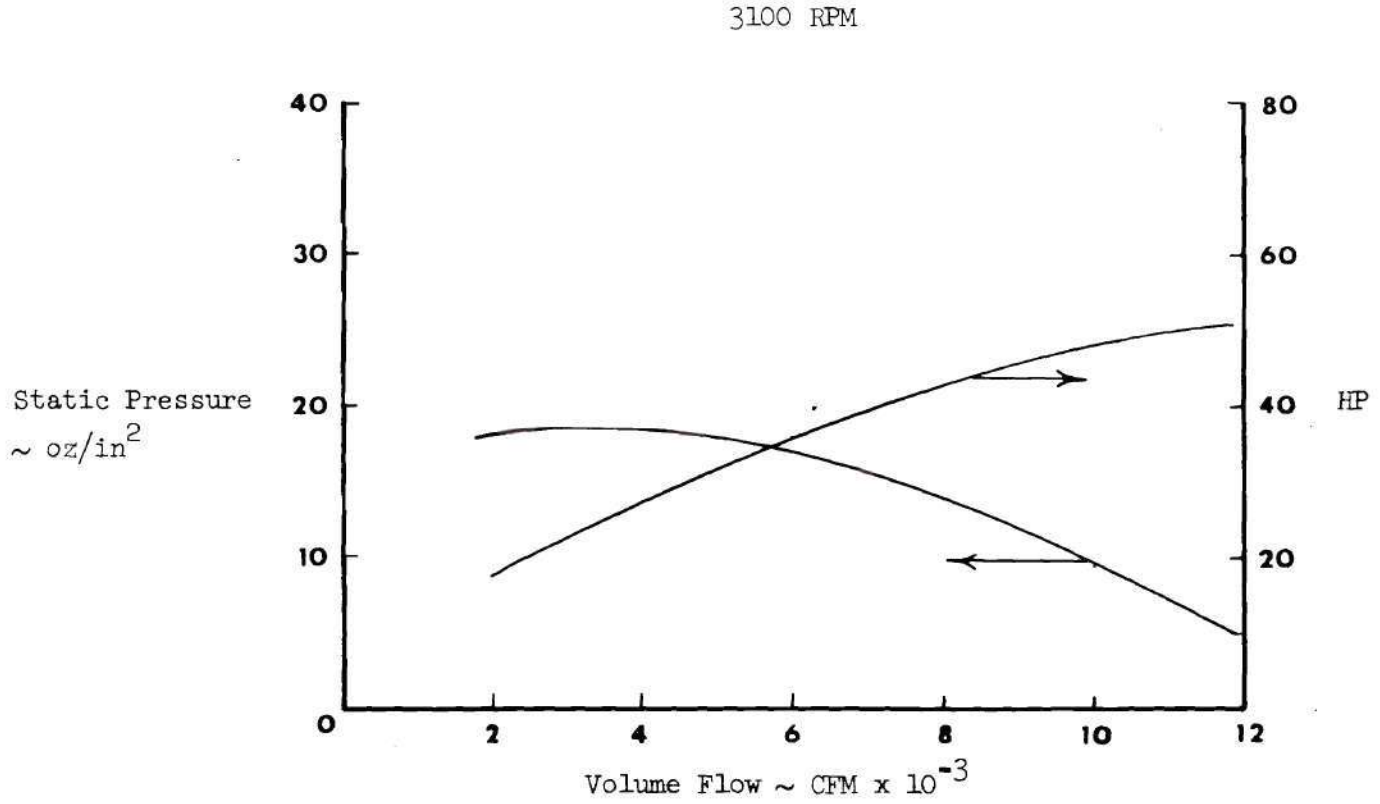

Figure D-2. Mainstream Blower Performance

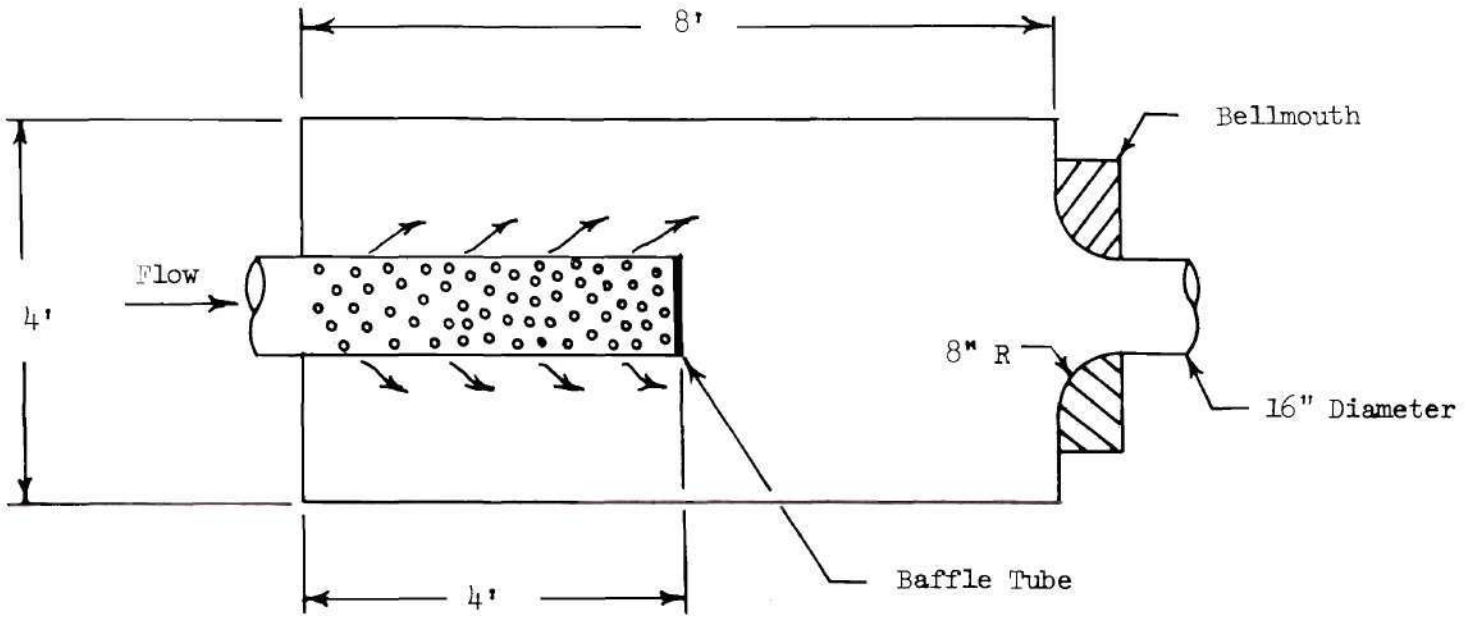

Figure D-3. Main-Stream Plenum Chamber

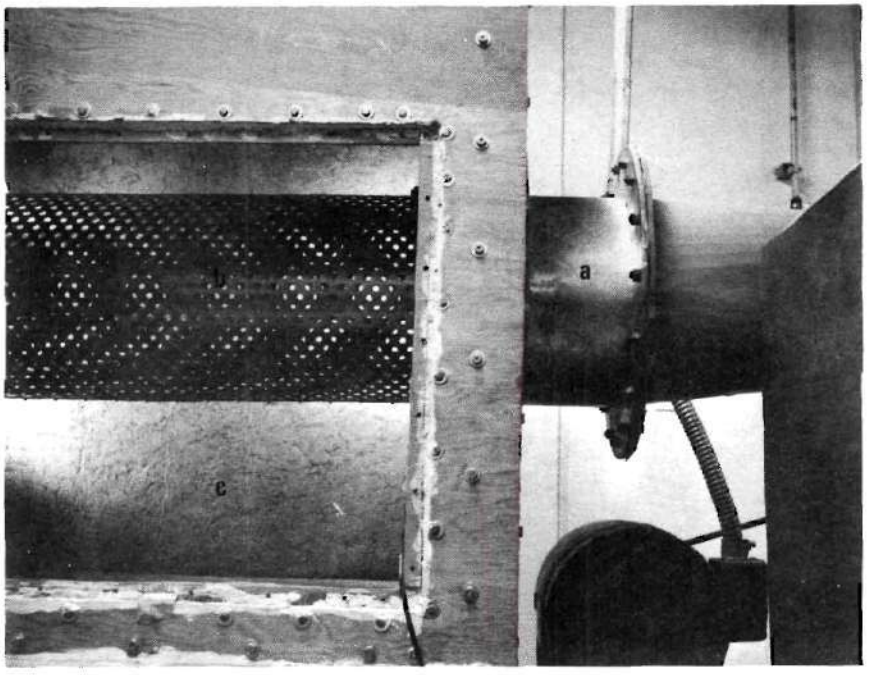

(a) Blower Exhaust
(b) Baffle
(c) Acoustic Lining

Figure D-4. Main-stream Plenum Chamber

APPENDIX E

MAIN-STREAM TRANSITION DUCT WITH SCREENS

The main-stream transition duct is detailed in Figures E-1 and E-2. This sheet metal transition piece carries the flow from a 16 inch diameter duct to a 30 inch wide, 16 inch high rectangular cross section with a 5 degree equivalent total conical diffusion angle. Screen 1 is 24 mesh, 0.0075 inch wire diameter, stainless steel cloth. Screens 2 and 3 are 34 mesh, 0.010 inch wire diameter copper cloth.

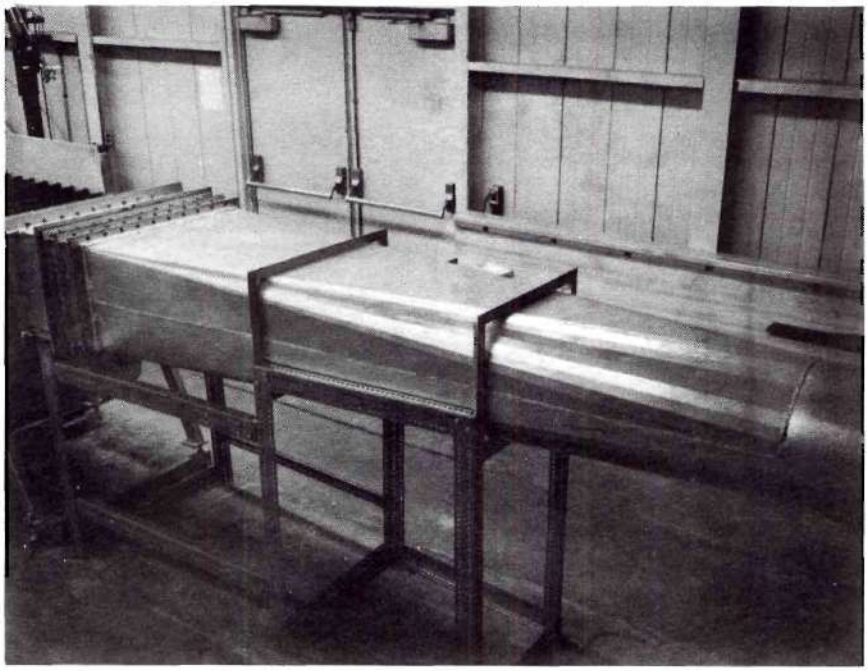

Figure E-1. Main-stream Transition Duct

SIDE VIEW

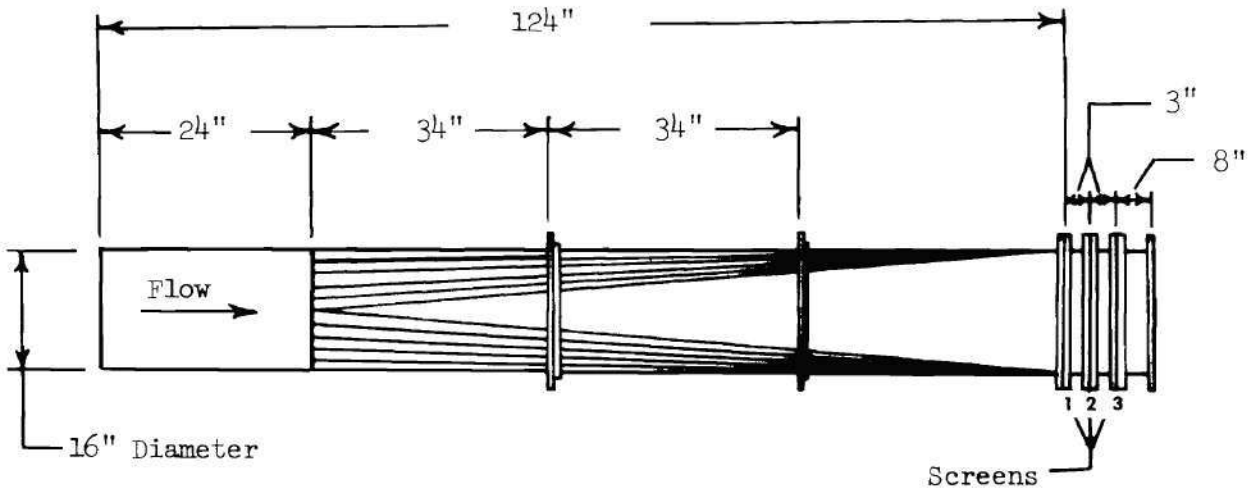

Figure E-2. Mainstream Transition Duct

APPENDIX F

JET AIR SUPPLY AND ORIFICE METER

Jet Compressor

The jet air is supplied by a 5 stage centrifugal compressor driven by a 75 HP constant speed electric motor. The compressor is shown in Figure F-1 and its performance is given in Figure F-2.

Jet Orifice Meter

The jet flow rate may be measured with the 3.814 inch ID orifice plate inserted in the standard six inch pipe. The orifice is preceded by 17 feet of straight duct. Static pressure taps are located in the flanges supporting the plate and a copper-constantan thermocouple probe is located in the flow 30 inches upstream of the orifice.

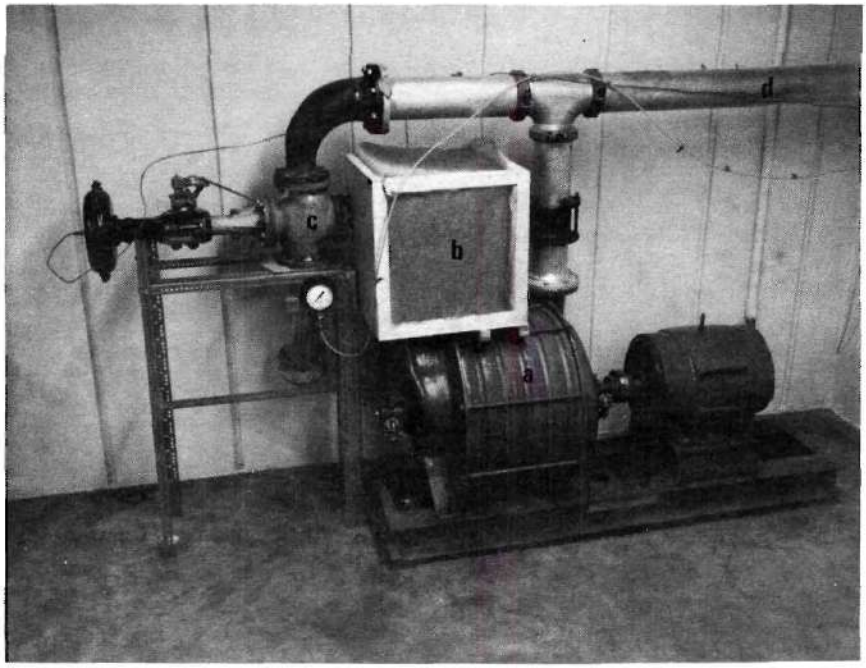

(a) Compressor
(b) Intake Filter Box
(c) Dump Valve
(d) Main Jet Duct

Figure F-1. Jet Compressor and Exhaust Ducts

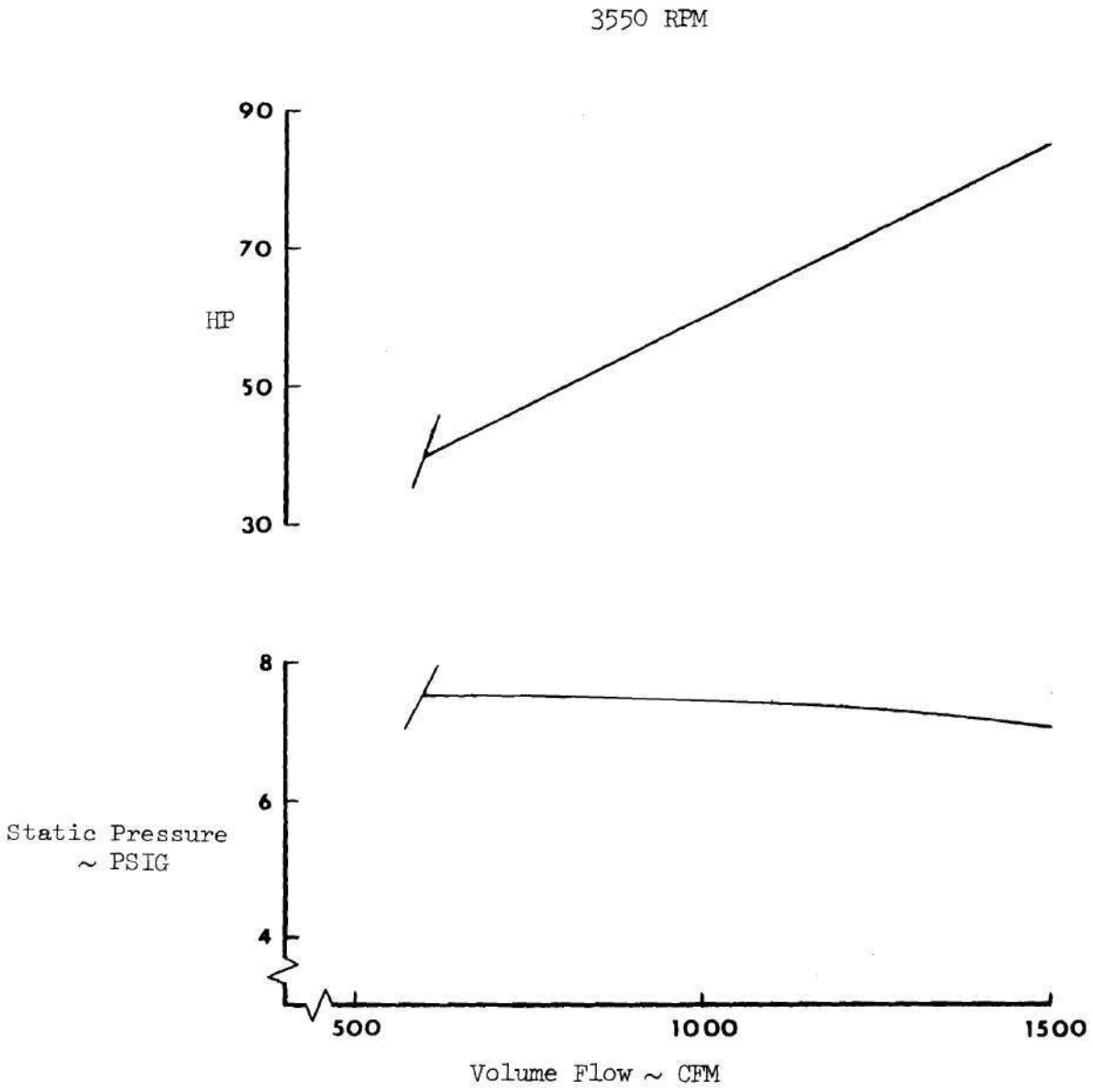

Figure F-2. Compressor Performance

APPENDIX G

JET PLENUM, SCREENS AND NOZZLE ASSEMBLY

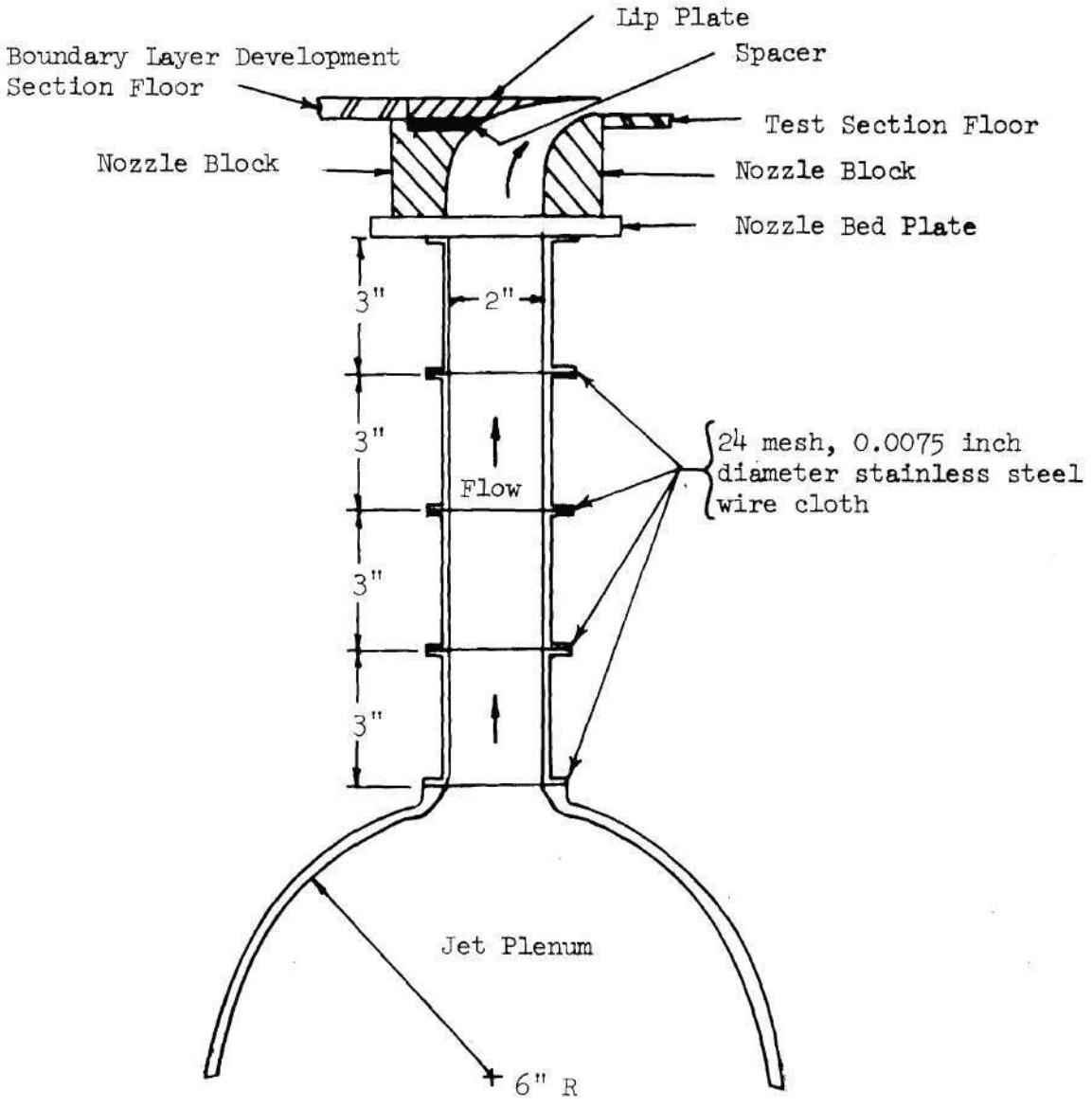

Figure G-1. Jet Plenum, Screens and Nozzle

APPENDIX H

PROBES

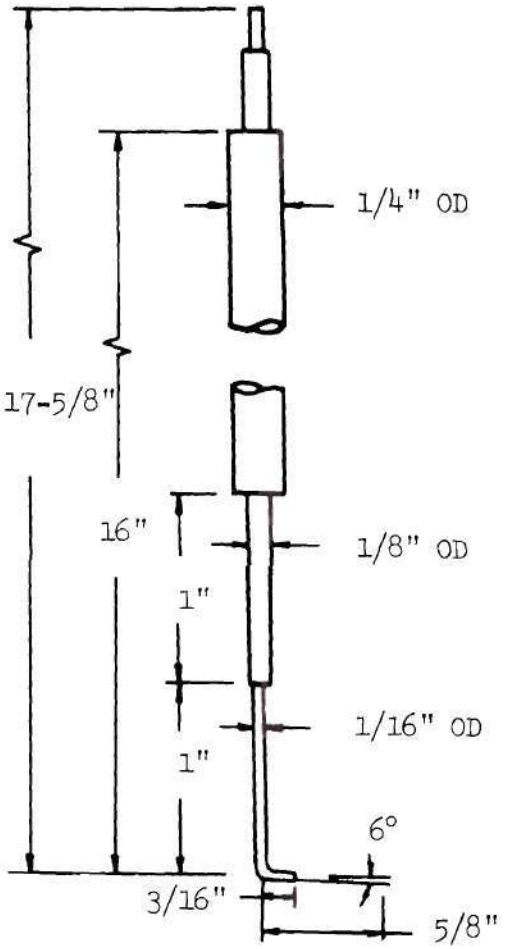

Figure H-1. Total Pressure Probe Detail

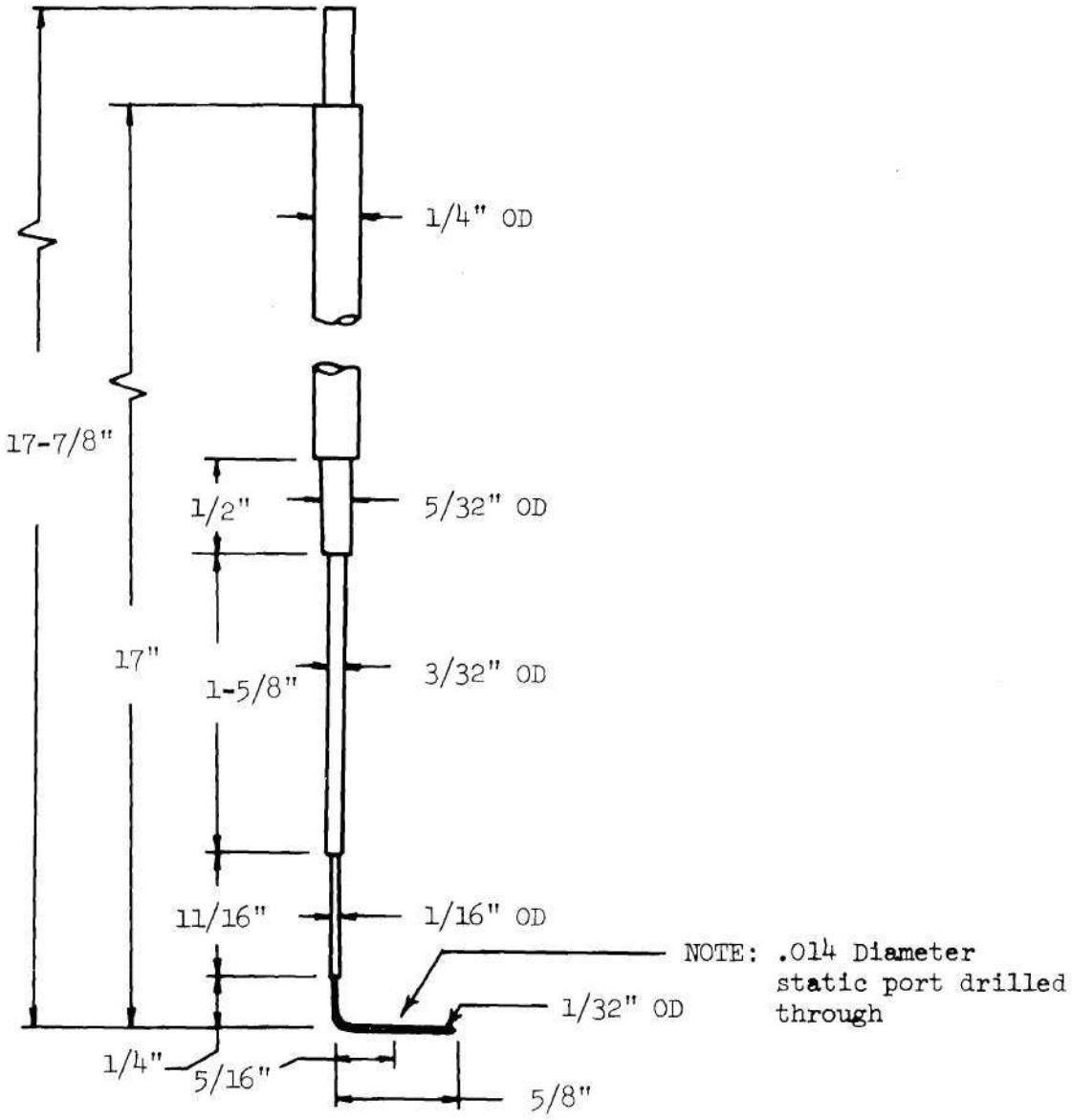

Figure H-2. Static Pressure Probe Detail

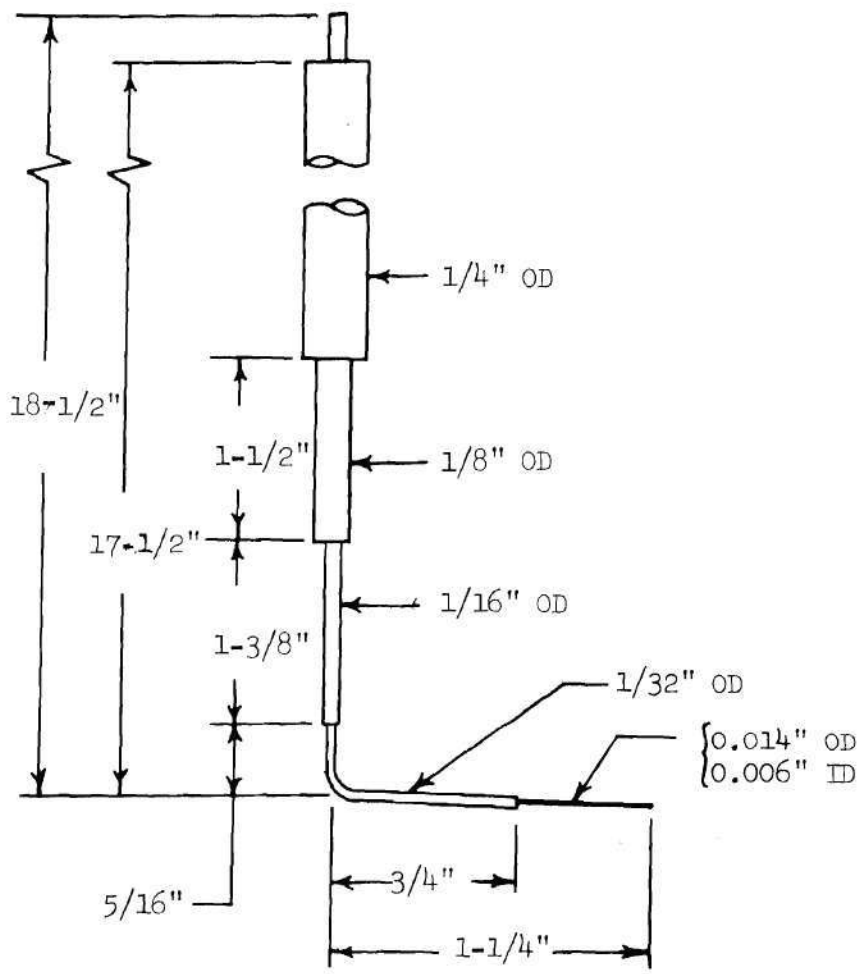

Figure H-3. Preston Probe Detail

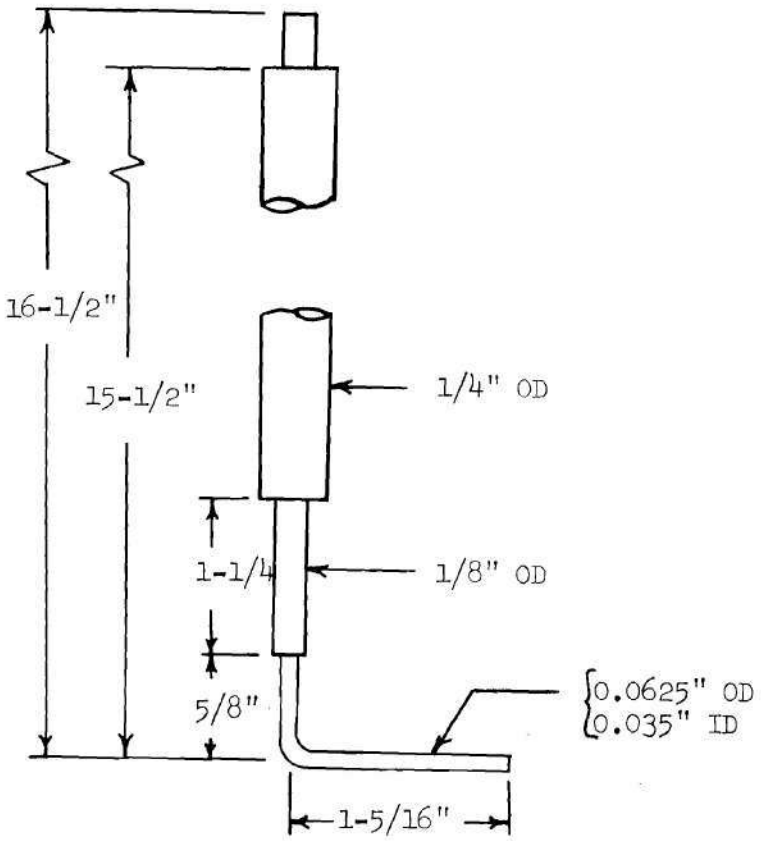

Figure H-4. Preston Probe Detail

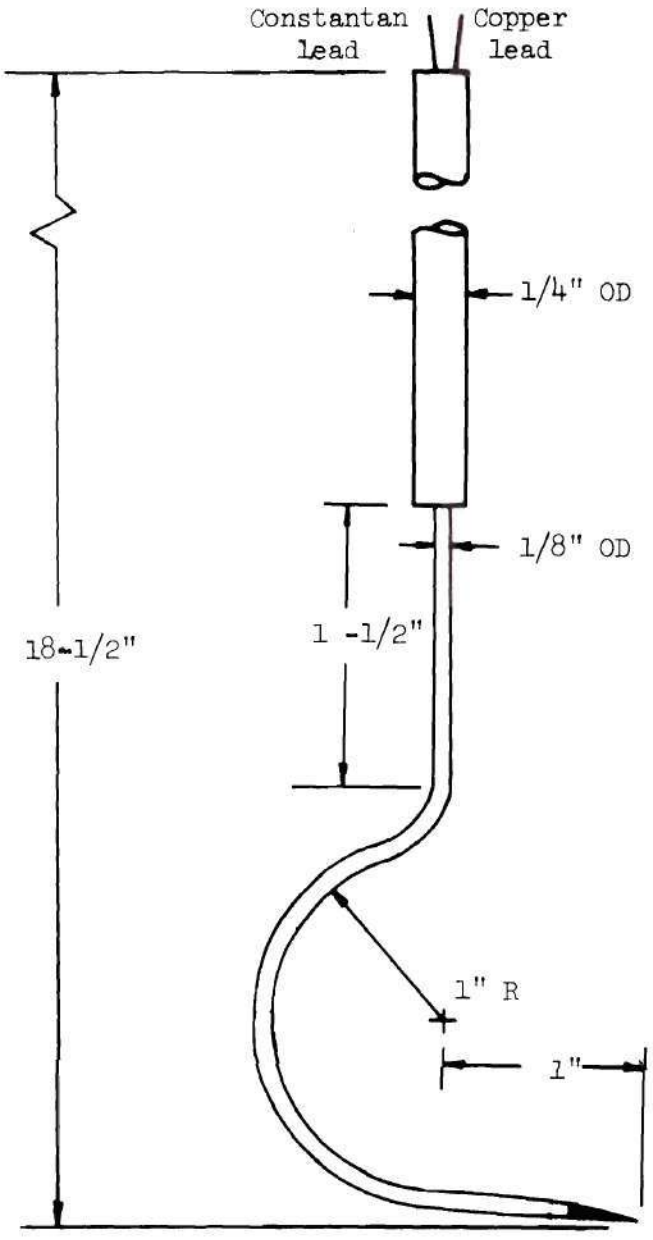

Figure H-5. Thermocouple Probe Detail

APPENDIX I

WALL JET DATA REDUCTION PROGRAM

The present data reduction program is written in Fortran V language for use on the Univac 1108 Computer. The program is divided into six major segments. A brief description of each segment is given in the following paragraphs:

1. Flow Conditions at the Jet Slot: The jet velocity, jet momentum, slot Reynolds number and main-stream velocity at the jet slot are computed from pressure and temperature measurements using the equations of compressible flow. Gas density is evaluated with the perfect gas law and viscosity is determined by using Sutherland's formula [26]. These formulas and equations are used throughout the program for determining flow characteristics.

2. Initial Boundary Layer Characteristics: The initial boundary layer velocity profile is calculated from pressure and temperature data. The addition, the momentum deficit and momentum thickness are evaluated numerically from the velocity and temperature profile measurements using Simpson's Rule for integration.

The boundary layer profile measurements may be divided into several segments with the data in each segment conforming to the requirements for Simpson-rule integration. The incremental height can be selected for each segment so that a reasonable rate of data acquisition is attained. Simpson's rule is then applied to each

segment and the individual segment results are summed to evaluate the total result for the entire profile.

3. Static Pressure Profile: The test section centerline and off-centerline static pressures are evaluated.

4. Wall Jet Velocity Profile: The velocity profile is calculated from pressure and temperature data in a dimensional form as well as in a ratio with a selected reference velocity in the profile.

5. Local Skin Friction: The local skin friction is evaluated using Patel's [22] Preston tube calibration curves for $2.9 \leq \text{LOG}_{10}\left(\frac{\Delta p d^2}{4\rho\nu^2}\right) \leq 6.4$. The local skin friction value is further combined with the flow properties at the jet peak (or other selected reference) to calculate a friction coefficient.

6. Law of the Wall: The local skin friction is combined with near-wall data for the appropriate velocity profile to calculate law of the wall information.

DATA REDUCTION PROGRAM INPUT

Identifier	Description	Units
BL	Initial boundary layer computation option	
CELRA1	Ratio of maximum transducer capacity to full scale voltmeter reading (total pressure)	mm/volt
CELRA2	Ratio of maximum transducer capacity to full scale voltmeter reading (static pressure)	mm/volt
D	Preston tube outside diameter	inches
DELTA	Height to jet peak	inches
DELTAY	Incremental height for Simpson Rule integration	inches
ERATIO	Voltage correction for resistance of damper circuit (= 1.0 if no circuit in line)	
GAMMA	Ratio of specific heats	
H	Lead screw indicator reading	
HBL	Lead screw indicator reading	
HCL	Length from bottom edge to centerline of probe aperture	inches
HSLOT	Height of jet slot	inches
JPTS	Number of data points per given segment of initial boundary layer	
MPOINT	Humber of data points to be calculated for law of the wall	
NCASES	Number of wall jet velocity profiles to be calculated	

Identifier	Description	Units
NPOINT	Number of data points per wall jet velocity profile	
NPTSBL	Number of data points per initial boundary layer profile	
NSEGS	Number of segments in initial boundary layer	
NSETS	Number of complete sets of data to be evaluated	
NTAPS	Number of centerline static pressures to be evaluated	
NTAUS	Number of Preston tube measurements to be evaluated	
PAMB	Ambient pressure	in Hg
PSBL	Static pressure at initial boundary layer location	volts
PSCL	Centerline tap static pressure	volts
PSEXIT	Jet exit plane static pressure	volts
PSL	Off-set tap static pressure (left)	volts
PSR	Off-set tap static pressure (right)	volts
PSWALL	Static pressure at Preston measurement location	volts
PPREST	Preston pressure measurement	volts
PT	Total pressure measurement (velocity profile)	volts
PTBL	Total pressure measurement (boundary layer profile)	volts
PTINF	Total pressure measurement (main stream)	volts
PTMAX	Total pressure measurement (reference)	volts

Identification	Description	Units
PTPLEN	Total pressure measurement (jet plenum)	volts
R	Universal gas constant	$ft^2/sec^2{}^\circ R$
SCALE	Barocel amplification factor	
SCALE0	Barocel amplification factor	
SCALE1	Barocel amplification factor	
SCALE2	Barocel amplification factor	
SCALE3	Barocel amplification factor	
SCALE4	Barocel amplification factor	
SCALE5	Barocel amplification factor	
SCALE6	Barocel amplification factor	
SCA1BL	Barocel amplification factor	
SCA2BL	Barocel amplification factor	
SF	Skin friction compuation option	
SPP	Static pressure profile computation option	
TAP	Velocity profile measurement location indicator	
TAPS	Static pressure tap designation	
TT	Total temperature (velocity profile)	$^\circ F$
TTBL	Total temperature (boundary layer profile)	$^\circ F$
TTINF	Total temperature (main stream)	$^\circ F$
TTMAX	Total temperature (reference)	$^\circ F$
TTPLEN	Total temperature (jet plenum)	$^\circ F$
TTWALL	Total temperature (wall)	$^\circ F$
VP	Velocity profile computation option	

Identifier	Description	Units
WALAW	Law of the wall computation option	
ZERO	Lead screw indicator reading with total pressure probe touching floor	
ZEROBL	Lead screw indicator reading with total pressure probe touching floor	

DATA REDUCTION PROGRAM

```
      DIMENSION Y(50),YBL(100),V(50),VBL(100),Q(50),SUM(50),ARG(50)
      DIMENSION RAT(100)
      NSETS=2
      DO 2000 NSET=1,NSETS
      SUMTOT=0.0
      READ(5,100) R,GAMMA,ERATIO,HSLOT,CELRA1,CELRA2,HCL
      READ(5,229)  NCASES,NSEGS,NPTSBL
      READ(5,236)BL,SPP,VP,SF,WALAW
C
C
C.....CALCULATION OF INITIAL JET VELOCITY BASED ON PLENUM CONDITIONS
C.....AND EXIT STATIC CONDITIONS
C
      READ(5,101) PAMB,PSEXIT,SCALE0,PTPLEN,SCALE1,TTPLEN
      TTPLEN=TTPLEN+459.69
      QJET=.03937*ERATIO*(CELRA1*PTPLEN*SCALE1-CELRA2*PSEXIT*SCALE0)
      PSSLOT=PAMB+CELRA2*ERATIO*PSEXIT*SCALE0*.03937
      PRAT1=(PSSLOT/(PSSLOT+QJET))**((GAMMA-1.)/GAMMA)
      VJET=(((2.*GAMMA*R*TTPLEN)/(GAMMA-1.))*(1.-PRAT1))**.5
C
C
C.....CALCULATION OF SLOT REYNOLDS NUMBER BASED ON STATIC CONDITIONS
C
      TSSLOT=((GAMMA-1.)/(GAMMA*R/32.17))*((GAMMA*R*TTPLEN/32.17)/(GAMMA
     1-1.)-((VJET)**2.)/64.35)
      ANU1=  ((.00227/PSSLOT)*((TSSLOT**2.5)/(TSSLOT+198.6)))/4118.7
      RESLOT=VJET*HSLOT/(12.*ANU1)
C
C
C.....CALCULATION OF JET MOMENTUM
C
      RHOJET=.041187*PSSLOT/TSSLOT
      SLOTMO=(RHOJET*HSLOT*(VJET)**2.)/12.
C
C
C.....CALCULATION OF INITIAL VELOCITY RATIO
C
      READ(5,102) TTINF,PTINF,SCALE2,PSBL,SCA2BL,NTAPS
      TTINF=TTINF+459.69
      QINF=.03937*ERATIO*(CELRA1*PTINF*SCALE2-CELRA2*PSBL*SCA2BL)
      PSABL=PAMB+CELRA2*ERATIO*PSBL*SCA2BL*.03937
      PRAT2=(PSABL/(PSABL+QINF))**((GAMMA-1.)/GAMMA)
      VINF=(((2.*GAMMA*R*TTINF)/(GAMMA-1.))*(1.-PRAT2))**.5
      TSINF=((GAMMA-1.)/(GAMMA*R/32.17))*((GAMMA*R*TTINF/32.17)/(GAMMA-1
     1.)-((VINF)**2.)/64.35)
      RHOINF=.041187*PSABL/TSINF
      VRAT1=VJET/VINF
      WRITE(6,200) VRAT1
```

```
      WRITE(6,201) VJET
      WRITE(6,202) VINF
      WRITE(6,203) VRAT1
      WRITE(6,204) RESLOT
      WRITE(6,223) SLOTMO
      IF(BL-1.)1901,1399,1399
 1399 CONTINUE
C
C
C.....CALCULATION OF MOMENTUM THICKNESS AND MOMENTUM DEFICIT FOR INITIAL
C.....BOUNDARY LAYER
C
      LO=50
      DO 1500 IJ=1,NSEGS
      READ(5,230) JPTS,DELTAY,ZEROBL
      DO 1400 IK=1,JPTS
      READ(5,231) HBL,TTBL,PTBL,SCA1BL
      TTBL=TTBL+459.69
      QBL=.03937*ERATIO*(CELRA1*PTBL*SCA1BL-CELRA2*PSBL*SCA2BL)
      PRATBL=(PSABL/(PSABL+QBL))**((GAMMA-1.)/GAMMA)
      VBL(IK)=(((2.*GAMMA*R*TTBL)/(GAMMA-1.))*(1.-PRATBL))**.5
      YBL(IK)=HBL+HCL-ZEROBL
      LO=LO+1
      VBL(LO)=VBL(IK)
      YBL(LO)=YBL(IK)
      RAT(LO)=VBL(IK)/VINF
      TSBL=((GAMMA-1.)/(GAMMA*R/32.17))*((GAMMA*R*TTBL/32.17)/(GAMMA-1.)
     1-((VBL(IK))**2.)/64.35)
      RHOBL=.041187*PSABL/TSBL
      ARG(IK)=(RHOBL*VBL(IK))*(1.-(VBL(IK)/VINF))
 1400 CONTINUE
      IL=JPTS-2
      SUM(IJ)=0.0
      DO 1300 IM=1,IL,2
      SUM(IJ)=ARG(IM)+4.*ARG(IM+1)+ARG(IM+2)+SUM(IJ)
 1300 CONTINUE
      SUM(IJ)=((DELTAY/3.0)*SUM(IJ))/12.
 1500 CONTINUE
      DO 1200 IN=1,NSEGS
      SUMTOT=SUMTOT+SUM(IN)
 1200 CONTINUE
      THETA=((1./(RHOINF*VINF))*SUMTOT)*12.
      DEFECT=VINF*SUMTOT
      WRITE(6,224)DEFECT
      WRITE(6,225) THETA
      WRITE(6,226)
      WRITE(6,233) VRAT1
      WRITE(6,227)
      NPTSBL=NPTSBL+NSEGS+49
      DO 1900 LO=51,NPTSBL
      WRITE(6,228)YBL(LO),VBL(LO),RAT(LO)
 1900 CONTINUE
 1901 CONTINUE
      IF(SPP-1.)1903,1902,1902
 1902 CONTINUE
C
C
```

```
C.....PRINTOUT OF STATIC PRESSURE PROFILE
C
      WRITE(6,205)
      WRITE(6,234) VRAT1
      WRITE(6,222)PAMB
      WRITE(6,206)
      WRITE(6,221)
      DO 900 J=1,NTAPS
      READ(5,103) TAPS,PSL,PSCL,PSR,SCALE
      CONST=.03937*ERATIO*CELRA2*SCALE
      PSL=CONST*PSL
      PSCL=CONST*PSCL
      PSR=CONST*PSR
      WRITE(6,207)TAPS,PSL,PSCL,PSR
  900 CONTINUE
 1903 CONTINUE
C
C
C.....CALCULATION OF WALL JET VELOCITY PROFILE
C
      DO 1000 I=1,NCASES
      IF(VP-1.)1905,1904,1904
 1904 CONTINUE
      READ(5,104) NPOINT,NTAUS,ZERO
      READ(5,105)PTMAX,SCALE3,TTMAX,PSWALL,SCALE4,TAP
      WRITE(6,208) TAP
      WRITE(6,233) VRAT1
      TTMAX=TTMAX+459.69
      QMAX=.03937*ERATIO*(CELRA1*PTMAX*SCALE3-CELRA2*PSWALL*SCALE4)
      PSLOC=PAMB+.03937*ERATIO*CELRA2*PSWALL*SCALE4
      PRAT3=(PSLOC/(PSLOC+QMAX))**((GAMMA-1.)/GAMMA)
      VMAX=(((2.*GAMMA*R*TTMAX)/(GAMMA-1.))*(1.-PRAT3))**.5
      WRITE(6,209)
      DO 800 K=1,NPOINT
      READ(5,106)H,TT,PT,SCALE5
      TT=TT+459.69
      Q(K)=.03937*ERATIO*(CELRA1*PT*SCALE5-CELRA2*PSWALL*SCALE4)
      PRAT4=(PSLOC/(PSLOC+Q(K)))**((GAMMA-1.)/GAMMA)
      V(K)=(((2.*GAMMA*R*TT)/(GAMMA-1.))*(1.-PRAT4))**.5
      Y(K)=H-ZERO+HCL
      VRAT2=V(K)/VMAX
      WRITE(6,210) Y(K), V(K),VRAT2
  800 CONTINUE
 1905 CONTINUE
      IF(SF-1.)1907,1906,1906
 1906 CONTINUE
C
C
C.....CALCULATION OF SKIN FRICTION
C
      DO 925 NTAU=1,NTAUS
      READ(5,107) PPREST,SCALE6,D,DELTA,TTWALL
      WRITE(6,211) TAP
      WRITE(6,235) D
      WRITE(6,233) VRAT1
      TSMAX=((GAMMA-1.)/(GAMMA*R/32.17))*((GAMMA*R*TTMAX/32.17)/
     1(GAMMA-1.)-((VMAX)**2.)/64.35)
```

```
      ANU2=((.00227/PSLOC)*((TSMAX**2.5)/(TSMAX+198.6)))/4118.7
      REDEL=VMAX*DELTA/(12.*ANU2)
      RELOG=ALOG10(REDEL)
      TTWALL=TTWALL+459.69
      DELTAP=ERATIO*(CELRA1*PPREST*SCALE6-CELRA2*PSWALL*SCALE4)
      ANU3=((.00227/PSLOC)*((TTWALL**2.5)/(TTWALL+198.6)))/4118.7
      RHO=.041187*PSLOC/TTWALL
      A=(.004834*DELTAP*(D)**2.)/(RHO*(ANU3)**2.)
      B=ALOG10(A)
      IF(B-5.6)300,301,301
  300 IF(B-2.9)302,303,303
  302 WRITE(6,212)
  303 YAXIS=.8287-.1381*B+(.1437*(B**2.))-(.0060*(B**3.))
      GO TO 306
  301 IF(6.4-B) 304,305,305
  304 WRITE(6,213)
  305 YAXIS=.875*B-1.375
  306 CONTINUE
      Z=10.**YAXIS
      TAU=(Z*4.*RHO*((ANU3)**2.)*144.)/(D**2.)
      CF=TAU/((.5*.041187*PSLOC/TSMAX)*(VMAX**2.))
      CFLOG=ALOG10(CF)
      WRITE(6,214)
      WRITE(6,215)
      WRITE(6,216) REDEL,RELOG,TAU,CF,CFLOG,DELTA
      IF(WALAW-1.)924,923,923
  923 CONTINUE
C
C
C.....CALCULATION OF LAW OF THE WALL
C
      WRITE(6,217)TAP
      WRITE(6,235) D
      WRITE(6,233) VRAT1
      WRITE(6,218)
      WRITE(6,219)
      READ(5,108)MPOINT
      DO 700 L=1,MPOINT
      UTAU=(TAU/RHO)**.5
      X=(UTAU*Y(L))/(12.*ANU3)
      XLOG=ALOG10(X)
      ZAXIS=V(L)/UTAU
      WRITE(6,220)Y(L),V(L),XLOG,ZAXIS
  700 CONTINUE
  924 CONTINUE
  925 CONTINUE
 1907 CONTINUE
 1000 CONTINUE
 2000 CONTINUE
      WRITE(6,232)
  100 FORMAT(7F10.0)
  101 FORMAT(6F10.0)
  102 FORMAT(5F10.0,I10)
  103 FORMAT(5F10.0)
  104 FORMAT(2I10,F10.0)
  105 FORMAT(6F10.0)
  106 FORMAT(4F10.0)
```

```
107 FORMAT(5F10.0)
108 FORMAT(I10)
200 FORMAT(1H1,10X,62HTEST CONDITIONS FOR WALL JET MEASUREMENTS AT VEL
   1OCITY RATIO = ,F4.2//)
201 FORMAT(15X,23HINITIAL JET VELOCITY = ,1F6.2,8H FT/SEC./)
202 FORMAT(15X,31HINITIAL FREE STREAM VELOCITY = ,1F6.2,8H FT/SEC./)
203 FORMAT(15X,25HINITIAL VELOCITY RATIO = ,1F4.2/)
204 FORMAT(15X,23HSLOT REYNOLDS NUMBER = F6.0/)
205 FORMAT(1H1,28X,23HSTATIC PRESSURE PROFILE//)
206 FORMAT(25X,30HPRESSURE (IN-HG ABOVE AMBIENT)/)
207 FORMAT(21X,F3.0,9X,F6.5,4X,F6.5,4X,F6.5)
208 FORMAT(1H1,25X,28HVELOCITY PROFILE AT STATION ,F3.0/)
209 FORMAT(21X,13HHEIGHT-INCHES,5X,8HV-FT/SEC,5X,6HV/VMAX/)
210 FORMAT(22X,F6.3,11X,F6.2,7X,F6.4)
211 FORMAT(1H1,20X,37HSKIN FRICTION MEASUREMENT AT STATION ,F3.0/)
212 FORMAT(5X,74H*****FOLLOWING POINT FALLS BELOW LOWER LIMIT OF CALIB
   1RATION CURVE FIT*****///)
213 FORMAT(9X,70H*****FOLLOWING POINT EXCEEDS UPPER LIMIT OF CALIBRATI
   1ON CURVE FIT*****///)
214 FORMAT(15X,2HRE,18X,13HSKIN FRICTION,24X,5HDELTA)
215 FORMAT(10X,11H(DELTA MAX),4X,6HLOG RE,4X,12H(LBS/SQ.FT.),7X,2HCF,
   16X,6HLOG CF,3X,8H(INCHES)/)
216 FORMAT(12X,F7.0,7X,F5.3,6X,F7.5,7X,F9.7,2X,F8.5,2X,F5.3)
217 FORMAT(1H1,20X,40HLAW OF THE WALL MEASUREMENTS AT STATION ,
   1F3.0/)
218 FORMAT(50X,5HLOG10)
219 FORMAT(18X,13HHEIGHT-INCHES,2X,15HVELOCITY-FT/SEC,2X,9HUTAU*Y/NU,
   18X,6HU/UTAU/)
220 FORMAT(18X,F10.3,5X,F10.2,5X,F10.4,5X,F10.2/)
221 FORMAT(17X,12HC.L. STATION,5X,4HLEFT, 5X,6HCENTER,5X,5HRIGHT/)
222 FORMAT(18X,19HAMBIENT PRESSURE = ,F5.2,18H INCHES OF MERCURY//)
223 FORMAT(15X,15HJET MOMENTUM = ,F6.4,7H LB/FT./)
224 FORMAT(15X,42HINITIAL BOUNDARY LAYER MOMENTUM DEFICIT = ,F6.4,7H L
   1B/FT./)
225 FORMAT(15X,44HINITIAL BOUNDARY LAYER MOMENTUM THICKNESS = ,F6.4,7H
   1 INCHES)
226 FORMAT(1H1,25X,39HINITIAL BOUNDARY LAYER VELOCITY PROFILE/)
227 FORMAT(19X,13HHEIGHT-INCHES,5X,15HVELOCITY-FT/SEC,7X,6HV/VINF/)
228 FORMAT(23X,F5.3,13X,F6.2,13X,F5.3)
229 FORMAT(3I10)
230 FORMAT(I10,2F10.0)
231 FORMAT(4F10.0)
232 FORMAT(1H1)
233 FORMAT(25X,25HINITIAL VELOCITY RATIO = ,F4.2///)
234 FORMAT(23X,25HINITIAL VELOCITY RATIO = ,F4.2/)
235 FORMAT(25X,4HD = ,F5.4,7H INCHES/)
236 FORMAT(5F10.0)
    END
```

APPENDIX J

EXPERIMENTAL RESULTS FOR SERIES I

Series I Data Summary

Nominal Initial Velocity Ratio ~ ∞

h = 0.056 Inches

Actual Initial Velocity Ratio	x/h	Re_s	U_j ~ ft/sec	T_j ~ °F	U_1 ~ ft/sec	τ_w ~ lb_f/ft^2	c_f^* X 10^3	Velocity Profile Index
∞	193.	5,809	266.55	155.0	84.95	-	-	178
∞	283.	10,916	495.54	167.0	138.76	-	-	178
∞	550.	13,998	625.47	172.0	123.34	0.0829	5.036	179
∞	283.	14,323	641.46	176.0	186.10	0.1958	5.323	179
∞	550.	16,083	720.17	183.0	144.33	0.1112	4.964	180

* Based on Fluid Properties at δ_1

VELOCITY PROFILES

$U_j/U_{e_o} \sim \infty$

Re_s = 5809 x/h = 193

Y ~ In.	U/U_1	T ~ °F
.004	.5487	103.0
.010	.7609	103.0
.020	.8520	103.0
.030	.8958	102.0
.040	.9274	102.0
.050	.9465	102.0
.060	.9644	101.0
.070	.9764	102.0
.080	.9828	101.0
.090	.9937	101.0
.100	.9964	100.0
.120	1.0000	100.0
.140	1.0000	100.0
.160	1.0000	100.0
.180	.9937	99.0
.200	.9865	99.0
.220	.9811	99.0
.240	.9719	99.0
.290	.9385	97.0
.340	.9135	97.0
.390	.8729	96.0
.440	.8411	95.0
.490	.8037	94.0
.540	.7699	94.0
.640	.6879	91.0
.740	.6021	89.0
.840	.5230	87.0
.940	.4384	85.0
1.040	.3638	83.0

$U_j/U_{e_o} \sim \infty$

Re_s = 10916 x/h = 283

Y ~ In.	U/U_1	Y ~ °F
.004	.6209	102.0
.009	.7605	102.0
.014	.8082	102.0
.019	.8350	101.0
.024	.8575	101.5
.029	.8744	101.5
.034	.8880	101.5
.039	.9051	101.5
.044	.9156	101.0
.049	.9286	101.0
.054	.9372	101.0
.059	.9414	101.0
.064	.9498	101.0
.069	.9561	101.0
.074	.9603	101.0
.084	.9726	101.0
.094	.9747	101.0
.104	.9849	101.0
.114	.9864	100.5
.124	.9925	100.5
.134	.9960	100.0
.144	1.0000	100.0
.154	.9980	100.0
.174	.9960	100.0
.194	.9960	100.0
.214	.9940	100.0
.234	.9880	100.0
.254	.9851	99.0
.304	.9647	99.0
.354	.9452	98.0
.404	.9257	97.5
.454	.9014	97.0
.504	.8761	96.0
.554	.8502	95.0
.604	.8214	94.5
.654	.8012	93.5
.704	.7678	92.5
.754	.7414	92.0
.804	.7136	91.0
.854	.6826	91.0
.954	.6274	89.0
1.054	.5643	88.0
1.154	.5047	86.0
1.254	.4467	85.0

VELOCITY PROFILES

$U_j/U_{e_o} \sim \infty$

Re_s = 13998 x/h = 550

Y ~ In.	U/U_1	T ~ °F
.004	.5622	92.5
.010	.7177	92.0
.020	.7859	92.5
.015	.7610	92.5
.025	.8069	92.5
.030	.8243	92.5
.035	.8408	93.0
.040	.8503	92.5
.045	.8630	92.5
.055	.8816	93.0
.065	.9003	93.0
.075	.9114	93.0
.085	.9246	92.5
.095	.9300	92.5
.105	.9381	92.5
.125	.9539	92.5
.145	.9618	92.5
.165	.9772	92.5
.185	.9798	92.5
.205	.9874	92.5
.225	.9929	93.0
.245	.9874	92.5
.265	.9950	92.5
.285	.9920	92.0
.305	1.0000	92.5
.325	.9945	92.0
.345	.9925	92.5
.395	.9941	91.5
.445	.9844	92.0

$U_j/U_{e_o} \sim \infty$

Re_s = 14323 x/h = 283

Y ~ In.	U/U_1	T ~ °F
.004	.6763	106.5
.010	.7779	106.5
.015	.8171	106.5
.020	.8439	106.5
.025	.8622	106.5
.030	.8826	106.5
.035	.8959	106.5
.040	.9123	106.5
.045	.9208	106.5
.050	.9328	106.5
.055	.9399	106.5
.060	.9481	106.5
.065	.9540	106.5
.070	.9598	106.5
.080	.9701	106.5
.090	.9781	106.5
.100	.9848	106.5
.110	.9900	106.0
.120	.9911	106.0
.130	.9956	106.0
.140	1.0000	106.0
.150	.9989	106.0
.160	.9996	105.5
.180	.9969	105.0
.190	.9958	105.0
.210	.9947	105.0
.230	.9916	104.0
.250	.9853	104.5
.270	.9786	104.5
.320	.9588	104.0
.370	.9377	102.5
.470	.8907	101.0
.570	.8374	99.5
.670	.7819	98.0
.770	.7236	96.0
.870	.6639	94.0

VELOCITY PROFILE

$U_j/U_{e_o} \sim \infty$

$Re_s = 16083$

$x/h = 550$

Y ~ In.	U/U_1	T ~ °F
.004	.5882	96.0
.010	.7310	96.0
.015	.7687	96.0
.020	.7923	96.0
.025	.8152	96.0
.030	.8323	96.0
.035	.8455	96.0
.040	.8606	96.0
.045	.8712	96.0
.050	.8824	96.0
.055	.8872	96.0
.060	.8955	96.0
.065	.9036	96.0
.075	.9166	97.0
.085	.9277	96.0
.095	.9375	96.0
.105	.9481	97.0
.115	.9554	96.5
.125	.9612	96.5
.135	.9669	96.5
.145	.9683	96.0
.165	.9740	96.0
.185	.9852	96.0
.205	.9926	96.0
.225	.9945	96.0
.245	.9945	96.0
.265	1.0000	96.0
.285	1.0000	96.0
.305	1.0000	96.0
.355	.9977	95.5
.405	.9926	96.0

Series I Data Summary

Nominal Initial Velocity Ratio ~ ∞

h = 0.155 Inches

Actual Initial Velocity Ratio	x/h	Re_s	U_j ~ ft/sec	T_j ~ °F	U_1 ~ ft/sec	τ_w ~ lb_f/ft^2	C_f^* X 10^3	Velocity Profile Index
∞	43.	19,561	342.19	179.0	204.61	0.2482	5.896	
∞	69.	19,561	342.19	179.0	162.21	0.1530	5.679	182
∞	89.	19,561	342.19	179.0	141.36	0.1171	5.677	
∞	101.	19,561	342.19	179.0	131.32	0.1011	5.642	
∞	121.	19,561	342.19	179.0	119.49	0.0824	5.523	
∞	140.	19,561	342.19	179.0	110.39	0.0693	5.417	
∞	166.	19,561	342.19	179.0	100.09	0.0573	5.424	
∞	179.	19,561	342.19	179.0	96.54	0.0520	5.290	
∞	198.	19,561	342.19	179.0	90.32	0.0462	5.346	182

* Based on Fluid Properties at δ_1

VELOCITY PROFILES

$U_j/U_{e_o} \sim \infty$

Re_s = 19561 x/h = 69

Y ~ In.	U/U_1	T ~ °F
.004	.6282	132.0
.010	.7871	132.0
.015	.8308	132.0
.020	.8566	132.0
.025	.8799	132.0
.030	.8986	132.0
.035	.9112	132.0
.040	.9264	132.0
.045	.9353	132.0
.050	.9473	132.0
.055	.9528	132.0
.060	.9610	131.5
.065	.9670	131.5
.070	.9707	131.5
.075	.9772	131.0
.080	.9787	131.0
.090	.9866	131.0

$U_j/U_{e_o} \sim \infty$

Re_s = 19561 x/h = 198

Y ~ In.	U/U_1	T ~ °F
.004	.5060	114.0
.010	.6980	114.0
.015	.7586	114.0
.020	.7860	114.0
.025	.8100	114.0
.030	.8304	114.0
.035	.8448	113.0
.040	.8560	114.0
.045	.8713	114.0
.050	.8791	114.0
.055	.8851	114.0
.060	.8950	115.0
.065	.9113	115.0
.070	.9113	115.0
.075	.9177	114.0
.080	.9284	114.0
.085	.9301	114.0
.090	.9353	114.0
.095	.9414	115.0
.100	.9457	114.0
.105	.9493	114.0
.110	.9553	115.0
.115	.9569	115.0

Series I Data Summary

Nominal Initial Velocity Ratio ~ ∞

h = 0.155 Inches

Actual Initial Velocity Ratio	x/h	Re_s	U_j ~ ft/sec	T_j ~ °F	U_1 ~ ft/sec	τ_w ~ lb_f/ft^2	C_f^* X 10^3	Velocity Profile Index
∞	43.	31,128	547.23	191.0	337.47	0.6158	5.530	
∞	69.	31,128	547.23	191.0	267.05	0.3829	5.395	184
∞	101.	31,128	547.23	191.0	216.06	0.2503	5.274	
∞	140.	31,128	547.23	191.0	180.99	0.1720	5.120	
∞	160.	31,128	547.23	191.0	169.45	0.1481	4.992	
∞	198.	31,128	547.23	191.0	149.89	0.1158	4.943	184

* Based on Fluid Properties at δ_1

VELOCITY PROFILES

$U_j/U_{e_o} \sim \infty$

Re_s = 31128 x/h = 69

Y ~ In.	U/U_1	T ~ °F
.004	.7003	141.0
.010	.8192	141.0
.015	.8547	141.0
.020	.8817	141.0
.025	.9015	141.0
.030	.9202	141.0
.035	.9337	141.0
.040	.9458	141.0
.045	.9553	141.0
.050	.9642	141.0
.055	.9712	141.0
.060	.9776	141.0
.065	.9833	141.0
.070	.9873	141.0
.075	.9925	141.0
.080	.9965	141.0
.085	.9982	141.0
.090	1.0000	141.0

$U_j/U_{e_o} \sim \infty$

Re_s = 31128 x/h = 198

Y ~ In.	U/U_1	T ~ °F
.004	.5876	119.0
.010	.7262	120.0
.015	.7717	120.0
.020	.7954	120.0
.025	.8197	120.0
.030	.8385	119.0
.035	.8498	120.0
.040	.8630	120.0
.045	.8767	120.0
.050	.8862	119.0
.055	.8969	120.0
.060	.9049	120.0
.065	.9114	119.0
.070	.9192	120.0
.075	.9276	120.0
.080	.9289	120.0
.085	.9384	120.0
.090	.9416	120.0
.095	.9466	120.0
.100	.9498	120.0
.105	.9536	120.0
.115	.9616	121.0
.125	.9659	120.0
.135	.9751	120.0
.145	.9763	120.0
.155	.9861	120.0

Series I Data Summary

Nominal Initial Velocity Ratio ~ ∞

h = 0.155 Inches

Actual Initial Velocity Ratio	x/h	Re_s	U_j ~ ft/sec	T_j ~ °F	U_1 ~ ft/sec	τ_w ~ lb_f/ft^2	C_f^* X 10^3
∞	43.	31,451	546.49	188.0	342.46	0.6131	5.314
∞	69.	31,451	546.49	188.0	266.90	0.3765	5.293
∞	101.	31,451	546.49	188.0	217.08	0.2457	5.143
∞	134.	31,451	546.49	188.0	186.96	0.1811	5.079
∞	166.	31,451	546.49	188.0	166.26	0.1412	4.971
∞	198.	31,451	546.49	188.0	149.77	0.1143	4.940

* Based on Fluid Properties at δ_1

Series I Data Summary

Nominal Initial Velocity Ratio ~ ∞

h = 0.155 Inches

Actual Initial Velocity Ratio	x/h	Re_s	U_j ~ ft/sec	T_j ~ °F	U_1 ~ ft/sec	τ_w ~ lb_f/ft^2	C_f^* X 10^3	Velocity Profile Index
∞	17.5	33,540	598.25	184.0	521.95	-	-	187
∞	69.	33,540	598.25	184.0	274.93	-	-	187
∞	198.	33,540	598.25	184.0	156.96	-	-	188
∞	11.	49,616	785.12	176.0	775.08	-	-	189
∞	69.	49,616	785.12	176.0	338.34	-	-	190
∞	198.	49,616	785.12	176.0	222.82	-	-	191

* Based on Fluid Properties at δ_1

VELOCITY PROFILES

$U_j/U_{e_o} \sim \infty$

$Re_s = 33540$ $x/h = 17.5$

Y ~ In.	U/U_1	T ~ °F
.004	.7958	177.0
.011	.8594	177.5
.016	.8939	177.0
.021	.9251	177.0
.026	.9482	177.0
.031	.9667	177.0
.036	.9772	177.0
.041	.9877	176.0
.046	.9957	175.5
.056	1.0000	174.0
.066	.9957	172.0
.076	.9823	169.0
.086	.9663	166.5
.096	.9443	164.0
.116	.8912	157.0
.136	.8302	152.5
.156	.7748	147.5
.176	.7152	142.5
.196	.6593	138.0
.216	.6011	133.0
.236	.5443	128.5
.256	.4890	124.0
.276	.4387	120.0

$U_j/U_{e_o} \sim \infty$

$Re_s = 33540$ $x/h = 69$

Y ~ In.	U/U_1	T ~ °F
.004	.7884	136.0
.011	.8662	135.5
.016	.8843	135.5
.021	.9066	135.5
.026	.9261	135.5
.031	.9414	135.0
.041	.9634	135.0
.051	.9749	134.5
.061	.9845	134.5
.071	.9919	134.5
.081	.9998	134.0
.101	1.0000	133.0
.121	.9996	132.5
.141	.9918	131.5
.161	.9844	131.0
.181	.9765	130.0
.201	.9690	129.5
.221	.9542	129.0
.241	.9425	128.0
.281	.9149	126.0
.331	.8753	124.5
.381	.8371	122.5
.431	.7935	120.0
.481	.7510	118.5
.531	.7084	116.0
.581	.6669	114.5
.631	.6223	112.0
.681	.5748	110.0
.731	.5310	108.0
.781	.4832	105.5
.831	.4452	104.5

VELOCITY PROFILE

$U_j/U_{e_o} \sim \infty$

$Re_s = 33540$

$x/h = 198$

Y ~ In.	U/U_1	T ~ °F
.004	.6911	109.5
.014	.7862	110.0
.024	.8270	110.0
.034	.8572	110.0
.044	.8839	110.0
.054	.8993	110.0
.064	.9156	110.0
.074	.9305	110.0
.084	.9407	110.0
.094	.9507	110.0
.104	.9551	110.0
.124	.9716	110.0
.144	.9798	109.5
.164	.9862	109.5
.184	.9926	109.5
.204	.9937	109.5
.224	.9968	109.5
.244	1.0000	109.5
.264	.9996	109.0
.324	.9991	108.5
.374	.9928	108.5
.424	.9896	108.5
.474	.9791	107.5
.524	.9690	107.0
.574	.9559	107.0
.624	.9489	106.5
.724	.9216	106.0
.824	.8934	105.5
.924	.8712	104.5
1.024	.8523	103.5
1.124	.8103	103.0
1.224	.7864	102.5
1.324	.7528	101.0
1.424	.7299	100.5
1.524	.6944	100.0
1.624	.6630	99.0
1.724	.6319	98.0
1.824	.5924	97.5

VELOCITY PROFILE

$U_j/U_{e_o} \sim \infty$

$Re_s = 49616$

$x/h = 11$

Y ~ In.	U/U_1	T ~ °F
.004	.7603	173.0
.009	.8327	172.5
.014	.8799	173.0
.019	.9150	173.0
.024	.9473	173.5
.029	.9697	173.0
.034	.9875	173.0
.039	.9957	173.0
.044	1.0000	172.0
.054	.9976	169.0
.064	.9908	165.5
.074	.9771	161.0
.084	.9584	157.0
.094	.9340	151.5
.104	.9040	147.0
.114	.8720	143.0
.124	.8349	139.0
.134	.7942	135.0
.144	.7574	132.0
.154	.7178	128.5
.164	.6770	124.5
.174	.6373	121.5
.184	.5943	118.0
.194	.5563	115.0
.204	.5150	111.5
.214	.4787	109.0
.224	.4417	106.0
.234	.4023	103.0
.244	.3666	101.0
.254	.3329	98.0
.264	.2970	96.0
.274	.2671	94.0
.284	.2354	92.0
.294	.2044	90.0
.304	.1750	87.5
.314	.1491	86.0

VELOCITY PROFILE

$U_j/U_{e_o} \sim \infty$

$Re_s = 49616$

$x/h = 69$

Y ~ In.	U/U_1	T ~ °F
.004	.8167	134.5
.010	.8555	134.5
.015	.8907	135.0
.020	.9095	135.0
.030	.9382	134.5
.040	.9593	134.5
.050	.9765	134.5
.060	.9863	134.0
.070	.9909	133.5
.080	.9988	133.0
.090	.9988	133.0
.100	1.0000	132.5
.110	.9996	132.0
.120	.9979	132.0
.130	.9954	131.0
.140	.9905	131.0
.150	.9867	130.5
.160	.9829	130.0
.170	.9762	130.0
.180	.9686	129.0
.190	.9648	128.5
.200	.9562	128.5
.210	.9506	128.0
.230	.9376	127.0
.250	.9225	126.0
.270	.9073	125.0
.290	.8900	124.0
.310	.8745	123.5
.330	.8585	122.5
.350	.8517	121.0
.370	.8214	120.5
.390	.8064	119.5
.410	.7893	119.0
.430	.7693	118.0
.450	.7511	117.0
.470	.7324	116.0
.490	.7132	115.0
.530	.6785	113.5
.570	.6391	111.5
.610	.6031	110.0
.650	.5690	108.0
.690	.5286	106.5
.710	.5064	105.0
.730	.4909	104.5
.750	.4707	104.0
.770	.4572	103.0
.790	.4365	102.5
.810	.4171	101.5
.830	.4006	100.5
.850	.3810	100.0
.870	.3659	99.5
.890	.3471	98.5
.910	.3320	98.0

VELOCITY PROFILE

$U_j/U_\infty \sim \infty$

$Re_s = 49616$

$x/h = 198$

Y ~ In.	U/U_1	T ~ °F	Y ~ In.	U/U_1	T ~ °F
.004	.7310	111.0	.696	.9204	107.5
.016	.8121	111.0	.736	.9065	107.0
.036	.8731	111.0	.776	.8962	107.0
.056	.9114	111.0	.816	.8837	106.5
.076	.9399	111.0	.856	.8732	106.5
.096	.9562	111.0	.896	.8639	106.0
.116	.9738	111.0	.936	.8473	105.5
.136	.9802	111.0	.976	.8415	105.0
.156	.9869	111.5	1.016	.8285	105.0
.176	.9896	111.0	1.066	.8093	104.5
.196	.9923	110.5	1.116	.7975	104.0
.216	.9969	110.5	1.166	.7858	104.0
.236	.9969	110.5	1.216	.7611	103.0
.256	1.0000	110.5	1.266	.7427	103.0
.276	1.0000	110.5	1.316	.7361	102.5
.296	1.0000	110.5	1.366	.7123	102.0
.316	.9954	110.5	1.416	.6989	101.5
.336	.9949	110.0	1.466	.6832	101.5
.376	.9918	110.0	1.516	.6689	100.5
.416	.9825	110.0	1.566	.6478	100.5
.456	.9737	109.0	1.616	.6355	100.0
.496	.9674	109.0	1.666	.6205	99.5
.536	.9605	108.5	1.716	.6051	99.0
.576	.9493	108.5	1.766	.5868	98.5
.616	.9362	108.5	1.816	.5732	98.0
.656	.9287	107.5	1.916	.5442	97.0

Series I Data Summary

Nominal Initial Velocity Ratio ~ ∞

h = 0.155 Inches

Actual Initial Velocity Ratio	x/h	Re_s	U_j	T_j	U_1	τ_w	$C_f^* \times 10^3$
∞	43.	44,050	718.02	182.0	466.97	1.1624	5.411
∞	69.	44,050	718.02	182.0	368.49	0.6913	5.107
∞	101.	44,050	718.02	182.0	299.99	0.4465	4.916
∞	140.	44,050	718.02	182.0	250.88	0.3083	4.820
∞	166.	44,050	718.02	182.0	227.46	0.2523	4.786
∞	198.	44,050	718.02	182.0	205.68	0.2035	4.704

* Based on Fluid Properties at δ_1

APPENDIX K

EXPERIMENTAL RESULTS FOR SERIES II

SERIES II TYPICAL INITIAL
BOUNDARY LAYER PROFILE

U_{e_o} = 119.34 Ft/Sec

x/h = 0

θ_o = 0.050 Inches

Y ~ In.	U/U_1	T ~ °F
.004	.5440	80.0
.008	.6066	80.0
.013	.6463	80.0
.018	.6672	80.0
.023	.6840	80.5
.033	.7036	80.5
.043	.7258	80.5
.053	.7473	80.5
.063	.7613	80.5
.073	.7796	80.5
.083	.7934	81.0
.093	.8045	81.0
.103	.8132	81.0
.113	.8240	81.0
.123	.8346	81.0
.143	.8554	81.0
.163	.8717	81.0
.183	.8858	81.0
.203	.8996	81.0
.223	.9112	81.0
.273	.9345	81.5
.323	.9587	81.5
.373	.9715	81.5
.423	.9823	81.5
.473	.9894	81.5
.523	.9965	81.5
.573	1.0000	81.5

Series II Data Summary

Nominal Initial Velocity Ratio = 1.50

h = 0.155 Inches

θ_o = 0.050 Inches

Actual Initial Velocity Ratio	x/h	Re_s	U_j ~ ft/sec	T_j ~ °F	U_1 ~ ft/sec	τ_w ~ lb_f/ft^2	C_f^* X 10^3
1.49	30.	10899.	180.65	154.0	156.61	0.1369	5.446
1.49	43.	10899.	180.65	154.0	146.75	0.1206	5.393
1.49	56.	10899.	180.65	154.0	140.31	0.1054	5.115
1.49	69.	10899.	180.65	154.0	135.44	0.0956	4.947
1.49	89.	10899.	180.65	154.0	130.64	0.0845	4.671
1.49	101.	10899.	180.65	154.0	128.81	0.0784	4.441
1.49	121.	10899.	180.65	154.0	126.55	0.0715	4.181
1.49	140.	10899.	180.65	154.0	125.20	0.0678	4.039
1.49	198.	10899.	180.65	154.0	122.84	0.0595	3.680

* Based on Fluid Properties at δ_1

Series II Data Summary (Near-Wall Detail)

Nominal Initial Velocity Ratio = 1.50

h = 0.155 Inches

θ_o = 0.050 Inches

Actual Initial Velocity Ratio	x/h	Re_s	U_j ~ ft/sec	T_j ~ °F	U_1 ~ ft/sec	τ_w^{**} ~ lb_f/ft^2	C_f^* X 10^3	Velocity Profile Index
1.49	101.	10,846	180.84	155.0	128.81	0.0784	-	197
1.49	198.	10,846	180.84	155.0	122.84	0.0595	-	197

* Based on Fluid Properties at δ_1

** Values Determined from Results of Tests Summarized on Page 195.

VELOCITY PROFILES
(Near Wall Detail)

U_j/U_{e_o} = 1.49 x/h = 101

Y ~ In.	U/U_1	T ~ °F
.004	.5545	124.0
.009	.6832	124.0
.014	.7234	124.0
.019	.7514	125.0
.024	.7695	125.0
.029	.7850	125.0
.034	.8044	125.0
.039	.8193	125.0
.044	.8311	125.0
.049	.8446	125.0
.054	.8540	125.0
.059	.8672	125.0
.064	.8766	124.0
.074	.8957	124.0
.084	.9135	124.0
.094	.9293	123.0
.104	.9443	122.5
.114	.9532	122.0
.124	.9649	121.0

U_j/U_{e_o} = 1.49 x/h = 198

Y ~ In.	U/U_1	T ~ °F
.004	.4665	115.0
.009	.5949	115.0
.014	.6368	115.0
.019	.6592	116.0
.024	.6789	116.0
.029	.6920	116.0
.034	.7040	116.0
.039	.7175	116.0
.044	.7275	116.5
.049	.7380	116.0
.059	.7544	116.0
.069	.7717	116.0
.079	.7874	116.0
.089	.8017	116.0
.099	.8147	116.0
.109	.8264	116.0
.119	.8380	116.0
.129	.8484	116.0
.139	.8579	115.0

Series II Data Summary

Nominal Initial Velocity Ratio = 1.75

h = 0.155 Inches

θ_o = 0.050 Inches

Actual Initial Velocity Ratio	x/h	Re_s	U_j ~ ft/sec	T_j ~ °F	U_1 ~ ft/sec	τ_w ~ lb_f/ft^2	C_f^* X 10^3
1.74	40.	12,910	210.98	147.0	178.99	0.1791	5.440
1.74	43.	12,910	210.98	147.0	165.14	0.1535	5.432
1.74	56.	12,910	210.98	147.0	156.75	0.1345	5.251
1.74	69.	12,910	210.98	147.0	150.63	0.1200	5.032
1.74	89.	12,910	210.98	147.0	144.32	0.1051	4.775
1.74	101.	12,910	210.98	147.0	140.87	0.0979	4.654
1.74	121.	12,910	210.98	147.0	137.22	0.0890	4.441
1.74	140.	12,910	210.98	147.0	134.59	0.0831	4,293
1.74	166.	12,910	210.98	147.0	132.30	0.0765	4.071
1.74	198.	12,910	210.98	147.0	129.49	0.0707	3.906

* Based on Fluid Properties at δ_1

Series II Data Summary

Nominal Initial Velocity Ratio = 2.00

h = 0.155 Inches

θ_o = 0.050 Inches

Actual Initial Velocity Ratio	x/h	Re_s	U_j ~ ft/sec	T_j ~ °F	U_1 ~ ft/sec	τ_w ~ lb_f/ft^2	C_f^* X 10^3
1.99	37.	14,649	237.04	143.0	196.27	0.2250	5.611
1.99	69.	14,649	237.04	143.0	166.13	0.1485	5.079
1.99	101.	14,649	237.04	143.0	151.69	0.1210	4.911
1.99	134.	14,649	237.04	143.0	144.03	0.1024	4.578
1.99	166.	14,649	237.04	143.0	139.77	0.0906	4.281
1.99	198.	14,649	237.04	143.0	135.82	0.0828	4.128

* Based on Fluid Properties at δ_1

Series II Data Summary (Near-Wall Detail)

Nominal Initial Velocity Ratio = 2.00

h = 0.155 Inches

θ_o = 0.050 Inches

Actual Initial Velocity Ratio	x/h	Re_s	U_j ~ ft/sec	T_j ~ °F	U_1 ~ ft/sec	τ_w^{**} ~ lb_f/ft^2	C_f^* X 10^3	Velocity Profile Index
2.00	101	14,170	242.16	166.0	152156	0.1210	-	201
2.00	198	14,170	242.16	166.0	136.82	0.0828	-	201

* Based on Fluid Properties at δ_1

** Values Determined from Results of Tests Summarized on Page 199.

VELOCITY PROFILES
(Near Wall Detail)

U_j/U_{e_o} = 2.00 x/h = 101

Y ~ In.	U/U_1	T ~ °F
.004	.6426	130.0
.009	.7322	130.0
.014	.7663	130.0
.019	.7916	130.0
.024	.8139	130.0
.029	.8308	130.0
.034	.8481	130.0
.039	.8636	130.0
.044	.8769	130.0
.049	.8894	130.0
.054	.9010	130.0
.059	.9116	129.0
.064	.9211	129.0
.074	.9379	129.0
.084	.9517	128.0
.094	.9660	128.0
.104	.9765	127.0
.114	.9831	126.5
.124	.9919	126.0

U_j/U_{e_o} = 2.00 x/h = 198

Y ~ In.	U/U_1	T ~ °F
.004	.5312	119.0
.008	.6351	119.5
.013	.6776	120.0
.018	.7054	120.0
.023	.7253	120.0
.028	.7417	120.0
.033	.7550	120.0
.038	.7708	120.0
.043	.7818	120.0
.048	.7953	120.0
.053	.8050	120.0
.058	.8146	120.0
.063	.8242	120.0
.073	.8387	120.0
.083	.8546	120.0
.093	.8710	120.0
.103	.8823	120.0
.113	.8939	119.5
.123	.9064	119.5

Series II Data Summary

Nominal Initial Velocity Ratio = 2.00

h = 0.155 Inches

θ_o = 0.050 Inches

Actual Initial Velocity Ratio	x/h	Re_s	U_j ~ ft/sec	T_j ~ °F	U_j ~ ft/sec	τ_w ~ lb_f/ft^2	C_f^* X 10^3	Velocity Profile Index
2.00	13.	14,833	238.33	145.0	236.02	-	-	203
2.00	26.	14,833	238.33	145.0	214.66	-	-	203
2.00	39.	14,833	238.33	145.0	191.54	-	-	204
2.00	52.	14,833	238.33	145.0	176.65	-	-	204
2.00	65.	14,833	238.33	145.0	166.61	-	-	205
2.00	97.	14,833	238.33	145.0	152.60	-	-	205
2.00	129.	14,833	238.33	145.0	144.27	-	-	206
2.00	161.	14,833	238.33	145.0	138.84	-	-	206
2.00	194.	14,833	238.33	145.0	135.73	-	-	207

* Based on Fluid Properties at T_1

VELOCITY PROFILES

U_j/U_{e_o} = 2.00 x/h = 13

Y ~ In.	U/U_1	T ~ °F
.004	.6036	137.0
.013	.8655	138.5
.023	.9864	140.0
.033	.9994	140.0
.043	1.0000	139.0
.053	.9977	138.0
.063	.9946	136.0
.073	.9868	133.5
.083	.9742	130.5
.093	.9538	127.0
.103	.9365	124.0
.123	.8803	117.0
.143	.8171	111.0
.163	.7510	104.0
.183	.6785	98.0
.203	.6143	92.0
.223	.5534	85.5
.243	.5020	80.0
.263	.4694	74.0
.283	.4491	71.0
.303	.4422	68.5
.323	.4408	67.5
.343	.4443	66.5
.363	.4503	67.0
.383	.4579	67.0
.403	.4633	66.5
.453	.4734	66.5
.503	.4789	66.5
.603	.4928	66.0
.703	.4976	67.0
.803	.5051	66.5
.903	.5053	67.0
1.003	.5066	66.0
1.103	.5057	66.0

U_j/U_{e_o} = 2.00 x/h = 26

Y ~ In.	U/U_1	T ~ °F
.004	.7771	135.0
.018	.9015	134.5
.028	.9476	133.5
.038	.9786	132.0
.048	.9944	130.0
.058	1.0000	128.5
.068	.9962	126.0
.078	.9859	124.0
.088	.9707	122.5
.098	.9546	120.0
.108	.9369	118.0
.118	.9171	116.0
.138	.8770	112.5
.158	.8373	109.0
.178	.7937	105.0
.198	.7505	101.5
.218	.7122	98.0
.238	.6718	94.0
.258	.6344	90.0
.278	.6010	86.5
.298	.5738	82.0
.318	.5524	79.0
.338	.5357	75.0
.358	.5257	73.0
.378	.5200	71.5
.428	.5200	69.5
.478	.5282	68.0
.528	.5341	68.0
.578	.5412	68.5
.628	.5462	69.0
.678	.5491	69.0
.778	.5543	68.0
.878	.5571	68.0
.978	.5580	68.0
1.078	.5585	69.0

VELOCITY PROFILES

U_j/U_{e_o} = 2.00 x/h = 39

Y ~ In.	U/U_1	T ~ °F
.004	.7364	130.0
.013	.8309	129.5
.023	.8933	128.5
.033	.9348	127.0
.043	.9636	126.0
.053	.9801	124.5
.063	.9918	123.0
.073	.9996	122.0
.083	1.0000	120.0
.093	.9961	118.0
.108	.9863	116.5
.118	.9742	115.0
.128	.9643	113.5
.138	.9520	112.0
.188	.8875	105.5
.238	.8139	98.5
.288	.7433	92.0
.338	.6783	84.5
.388	.6313	78.0
.438	.6036	73.0
.488	.5956	70.5
.538	.5981	69.0
.588	.6065	68.5
.638	.6097	68.5
.688	.6143	69.0
.788	.6175	69.0
.888	.6201	68.0
.988	.6236	68.5
1.088	.6243	68.0
1.188	.6233	68.0

U_j/U_{e_o} = 2.00 x/h = 52

Y ~ In.	U/U_1	T ~ °F
.004	.7139	125.0
.013	.7917	124.5
.023	.8632	124.0
.033	.9018	123.0
.043	.9341	122.0
.053	.9599	121.0
.063	.9773	120.0
.073	.9888	118.5
.083	.9960	118.0
.093	.9997	116.5
.103	.9984	115.0
.113	1.0000	114.0
.123	.9941	113.0
.148	.9815	110.0
.198	.9362	105.0
.248	.8869	100.5
.298	.8351	95.5
.348	.7804	90.0
.398	.7352	84.0
.448	.6921	79.0
.498	.6723	75.0
.548	.6590	72.5
.598	.6584	71.5
.698	.6610	70.0
.798	.6680	70.0
.898	.6711	69.5
.998	.6734	69.5
1.098	.6738	70.0
1.198	.6746	69.5
1.298	.6749	70.0

VELOCITY PROFILES

U_j/U_{e_o} = 2.00 x/h = 65

Y ~ In.	U/U_1	T ~ °F
.004	.6925	121.0
.013	.7507	121.0
.033	.8795	120.0
.053	.9382	118.0
.073	.9711	116.0
.093	.9894	114.0
.113	.9990	112.0
.133	1.0000	110.0
.143	.9996	109.5
.153	.9963	109.0
.173	.9862	107.0
.193	.9760	105.0
.213	.9629	103.0
.263	.9251	99.5
.313	.8829	96.0
.363	.8452	92.0
.413	.8022	87.0
.463	.7648	82.5
.513	.7372	78.5
.563	.7194	75.5
.613	.7092	73.0
.663	.7057	71.5
.713	.7032	71.5
.813	.7091	71.0
.913	.7109	70.0
1.013	.7133	70.0
1.113	.7149	70.5
1.213	.7145	70.0
1.313	.7145	70.0

U_j/U_{e_o} = 2.00 x/h = 97

Y ~ In.	U/U_1	T ~ °F
.004	.6828	114.5
.013	.7649	114.0
.033	.8468	113.5
.053	.8995	112.0
.073	.9351	111.0
.093	.9624	110.0
.113	.9801	108.0
.133	.9920	107.5
.153	.9963	106.0
.173	1.0000	104.0
.193	.9980	103.0
.213	.9938	102.0
.263	.9797	98.5
.313	.9585	96.0
.363	.9362	94.0
.413	.9127	91.0
.463	.8848	89.0
.513	.8608	86.5
.563	.8384	83.5
.613	.8202	81.5
.663	.8037	78.5
.713	.7916	76.5
.813	.7788	73.5
.913	.7740	72.5
1.013	.7760	71.5
1.113	.7769	71.0
1.213	.7783	71.0
1.313	.7777	72.0
1.413	.7777	72.0
1.513	.7760	71.5

VELOCITY PROFILES

U_j/U_{e_o} = 2.00 x/h = 129

Y ~ In.	U/U_1	T ~ °F
.004	.6319	109.0
.013	.7228	109.5
.028	.7918	109.0
.048	.8448	108.5
.068	.8885	107.5
.088	.9210	107.0
.108	.9437	105.5
.128	.9627	105.0
.148	.9759	104.0
.168	.9871	102.5
.188	.9949	101.5
.208	.9981	101.0
.228	.9992	99.5
.248	1.0000	99.0
.268	.9967	98.0
.288	.9933	97.0
.308	.9912	96.0
.328	.9866	95.0
.378	.9717	93.5
.428	.9562	91.5
.528	.9208	87.5
.628	.8902	84.0
.728	.8640	80.0
.828	.8426	77.5
.928	.8280	75.0
1.028	.8255	73.5
1.128	.8222	73.0
1.228	.8218	72.5
1.328	.8215	72.0
1.528	.8211	71.5

U_j/U_{e_o} = 2.00 x/h = 161

Y ~ In.	U/U_1	T ~ °F
.004	.6084	106.5
.018	.7218	106.5
.038	.7908	106.0
.088	.8870	104.5
.138	.9426	103.0
.188	.9778	100.5
.238	.9952	99.0
.288	1.0000	97.0
.308	1.0000	96.0
.328	1.0000	95.5
.348	.9965	94.5
.398	.9960	92.5
.448	.9801	91.0
.498	.9668	89.5
.548	.9565	88.5
.648	.9320	85.5
.748	.9103	83.0
.848	.8893	80.0
.948	.8743	77.5
1.048	.8639	75.5
1.148	.8606	75.0
1.248	.8549	73.5
1.348	.8545	73.0
1.548	.8527	72.5
1.748	.8545	73.0

VELOCITY PROFILE

$U_j/U_{e_o} = 2.00$

$x/h = 194$

Y ~ In.	U/U_1	T ~ °F
.004	.5811	103.5
.018	.7017	104.0
.068	.8277	103.5
.118	.8966	102.5
.168	.9412	101.5
.218	.9728	99.5
.268	.9889	97.0
.318	.9972	95.5
.368	1.0000	94.0
.418	.9964	93.0
.468	.9914	90.5
.568	.9748	89.0
.668	.9567	86.0
.768	.9379	84.0
.868	.9218	82.0
.968	.9065	79.5
1.068	.8963	78.0
1.268	.8838	75.5
1.468	.8770	74.5
1.668	.8751	74.0
1.868	.8751	74.0

Series II Data Summary

Nominal Initial Velocity Ratio = 3.0

h = 0.155 Inches

θ_o = 0.050 Inches

Actual Initial Velocity Ratio	x/h	Re_s	$U_j \sim$ ft/sec	$T_j \sim {}^\circ F$	$U_1 \sim$ ft/sec	$\tau_w \sim lb_f/ft^2$	$C_f^* \times 10^3$	Velocity Profile Index
2.96	13.	21,257	351.20	159.0	349.96	-	-	209
2.96	26.	21,257	351.20	159.0	307.96	-	-	209
2.96	39.	21,257	351.20	159.0	271.22	-	-	210
2.96	52.	21,257	351.20	159.0	245.91	-	-	210
2.96	65.	21,257	351.20	159.0	228.62	-	-	211
2.96	97.	21,257	351.20	159.0	201.63	-	-	211
2.96	129.	21,257	351.20	159.0	185.78	-	-	212
2.96	161.	21,257	351.20	159.0	174.76	-	-	212
2.96	194.	21,257	351.20	159.0	166.88	-	-	213

* Based on Fluid Properties at δ_1

VELOCITY PROFILES

U_j/U_{e_o} = 2.96 x/h = 13

Y ~ In.	U/U_1	T ~ °F
.004	.7295	150.0
.009	.9018	151.0
.013	.9516	152.0
.018	.9831	152.5
.023	.9944	153.0
.028	.9983	152.5
.033	.9979	152.0
.038	1.0000	152.0
.043	.9970	151.0
.048	.9962	150.0
.053	.9933	149.0
.058	.9903	148.0
.068	.9775	145.5
.078	.9641	142.5
.088	.9436	139.0
.098	.9210	136.0
.108	.8948	132.0
.128	.8346	126.0
.148	.7652	120.0
.168	.6924	113.5
.188	.6240	107.5
.208	.5536	102.0
.228	.4891	96.0
.248	.4292	90.5
.268	.3771	85.0
.288	.3409	79.5
.308	.3191	76.0
.328	.3090	74.0
.348	.3079	72.5
.368	.3097	72.0
.408	.3154	72.0
.448	.3217	72.0
.488	.3261	72.5
.528	.3285	72.5
.568	.3310	72.5
.608	.3323	73.0
.708	.3363	72.5
.808	.3387	72.5
.908	.3394	73.0
1.008	.3388	73.0

U_j/U_{e_o} = 2.96 x/h = 26

Y ~ In.	U/U_1	T ~ °F
.004	.7809	147.0
.008	.8303	147.0
.013	.8703	147.0
.018	.9049	146.5
.023	.9320	146.0
.028	.9525	145.5
.033	.9691	144.5
.038	.9825	143.5
.043	.9905	143.0
.048	.9953	142.0
.053	1.0000	141.0
.058	.9992	140.0
.063	.9983	139.0
.068	.9975	138.0
.078	.9876	136.0
.088	.9743	133.5
.098	.9586	131.5
.118	.9211	128.0
.138	.8787	124.0
.158	.8386	121.0
.178	.7927	117.0
.198	.7486	114.0
.218	.7095	110.0
.238	.6678	107.0
.258	.6245	103.0
.278	.5844	100.0
.298	.5456	96.0
.318	.5077	92.5
.358	.4449	85.5
.398	.4021	80.0
.438	.3792	75.5
.478	.3730	73.5
.518	.3742	73.0
.568	.3769	73.0
.618	.3783	73.0
.718	.3824	73.0
.818	.3844	73.0
.918	.3850	73.0
1.018	.3857	73.0

VELOCITY PROFILES

U_j/U_{e_o} = 2.96 x/h = 39

Y ~ In.	U/U_1	T ~ °F
.004	.7741	139.5
.008	.8275	139.5
.013	.8721	139.0
.018	.8991	139.0
.023	.9249	138.5
.033	.9575	137.5
.043	.9785	136.0
.053	.9925	134.5
.063	.9981	133.5
.073	1.0000	132.0
.083	.9987	130.5
.093	.9936	129.5
.103	.9859	128.0
.113	.9776	127.0
.123	.9661	125.0
.143	.9431	122.5
.163	.9151	120.0
.183	.8868	118.0
.203	.8581	115.0
.223	.8269	113.0
.273	.7500	107.0
.323	.6753	101.5
.373	.6022	95.0
.423	.5386	90.0
.473	.4859	83.5
.523	.4517	79.0
.573	.4384	76.0
.623	.4332	74.5
.673	.4338	74.0
.723	.4346	74.0
.823	.4353	74.0
.923	.4369	74.0
1.023	.4376	74.0
1.123	.4376	74.0

U_j/U_{e_o} = 2.96 x/h = 52

Y ~ In.	U/U_1	T ~ °F
.004	.7552	133.5
.008	.8030	133.5
.018	.8782	133.0
.028	.9242	132.0
.038	.9513	131.0
.048	.9695	130.0
.058	.9838	129.5
.068	.9922	128.5
.078	.9965	127.5
.088	1.0000	127.0
.098	.9979	126.0
.108	.9957	125.0
.118	.9910	124.0
.128	.9849	123.0
.148	.9714	121.0
.168	.9551	119.0
.188	.9359	117.0
.208	.9164	115.0
.228	.8955	113.5
.278	.8412	109.5
.328	.7835	105.0
.378	.7291	101.0
.428	.6707	96.5
.478	.6177	92.0
.528	.5733	87.0
.578	.5336	83.5
.628	.5060	80.0
.678	.4928	78.0
.728	.4855	76.5
.778	.4819	76.0
.828	.4817	75.5
.878	.4825	75.5
.928	.4844	76.0
1.028	.4827	76.0
1.128	.4825	75.5

VELOCITY PROFILES

U_j/U_{e_o} = 2.96 x/h = 65

Y ~ In.	U/U_1	T ~ °F
.004	.7669	129.5
.008	.8036	129.0
.013	.8425	129.0
.023	.8896	128.5
.033	.9244	128.0
.043	.9494	127.0
.053	.9659	126.0
.063	.9794	125.5
.073	.9881	125.0
.083	.9933	124.0
.093	.9974	123.5
.103	1.0000	123.0
.113	.9991	122.0
.123	.9968	121.0
.133	.9944	120.0
.183	.9688	116.5
.233	.9333	113.0
.283	.8922	110.0
.333	.8494	107.0
.383	.8044	103.5
.433	.7609	100.0
.483	.7157	97.0
.533	.6739	93.5
.583	.6321	90.0
.633	.5975	86.5
.683	.5667	84.0
.733	.5447	81.0
.833	.5265	78.0
.933	.5197	77.0
1.033	.5197	77.0
1.133	.5195	76.5

U_j/U_{e_o} = 2.96 x/h = 97

Y ~ In.	U/U_1	T ~ °F
.004	.7179	121.0
.008	.7652	121.0
.018	.8261	120.5
.028	.8692	120.0
.038	.8999	120.0
.068	.9569	118.5
.088	.9763	118.0
.108	.9891	117.0
.128	.9960	116.0
.148	.9990	115.0
.168	1.0000	114.0
.188	.9972	113.0
.208	.9930	112.5
.228	.9868	112.0
.248	.9801	111.0
.298	.9589	109.0
.348	.9328	106.5
.388	.9087	104.5
.448	.8798	102.5
.498	.8519	100.0
.548	.8259	98.0
.598	.7945	96.0
.648	.7672	94.5
.698	.7384	92.0
.748	.7141	90.0
.848	.6668	87.0
.948	.6247	83.0
1.048	.6021	80.0
1.148	.5934	79.0
1.248	.5898	78.0
1.348	.5885	77.5
1.448	.5862	77.0
1.548	.5865	77.5

VELOCITY PROFILES

U_j/U_{e_o} = 2.96 x/h = 129

Y ~ In.	U/U_1	T ~ °F
.004	.6853	116.5
.013	.7731	116.5
.023	.8196	116.0
.033	.8514	116.0
.043	.8773	115.5
.063	.9198	115.0
.083	.9456	114.0
.103	.9665	113.5
.123	.9799	113.0
.143	.9882	112.0
.163	.9946	111.5
.183	.9982	110.0
.203	1.0000	110.0
.223	.9991	109.0
.243	.9964	108.5
.263	.9933	107.5
.313	.9830	106.0
.363	.9681	104.5
.413	.9534	103.5
.463	.9357	102.0
.563	.8975	99.5
.663	.8554	97.0
.763	.8164	94.0
.863	.7730	91.0
.963	.7363	88.0
1.063	.7018	86.0
1.163	.6786	84.0
1.263	.6544	81.5
1.363	.6469	80.0
1.463	.6418	79.0
1.663	.6357	78.0
1.863	.6357	78.0
2.063	.6357	78.0

U_j/U_{e_o} = 2.96 x/h = 161

Y ~ In.	U/U_1	T ~ °F
.004	.6617	112.5
.018	.7739	112.5
.028	.8138	112.5
.038	.8457	112.5
.078	.9159	112.0
.098	.9398	111.0
.118	.9582	110.5
.138	.9735	110.0
.158	.9830	109.0
.178	.9877	108.5
.198	.9928	108.5
.218	1.0000	108.0
.238	.9996	107.5
.258	.9991	107.0
.278	.9987	106.5
.328	.9944	104.5
.378	.9859	103.5
.428	.9770	102.0
.478	.9606	101.0
.578	.9379	99.0
.678	.9066	97.0
.778	.8747	95.5
.878	.8443	93.5
.978	.8126	91.0
1.078	.7803	89.0
1.178	.7533	87.0
1.278	.7284	84.5
1.378	.7070	83.0
1.478	.6960	82.0
1.678	.6818	80.0
1.878	.6784	78.5
2.078	.6761	78.5
2.278	.6749	78.5
2.478	.6734	78.0

VELOCITY PROFILE

$U_j/U_{e_o} = 2.96$

$x/h = 194$

Y ~ In.	U/U_1	T ~ °F
.004	.6408	110.0
.013	.7194	110.0
.023	.7635	110.0
.043	.8371	110.0
.063	.8759	109.5
.083	.9052	109.5
.103	.9281	109.0
.153	.9616	108.0
.203	.9831	106.5
.253	.9986	105.0
.303	.9977	104.0
.353	1.0000	103.5
.403	.9968	103.0
.453	.9881	102.5
.503	.9751	100.5
.603	.9568	99.0
.703	.9324	97.5
.903	.8850	94.5
1.103	.8317	91.0
1.303	.7854	87.0
1.503	.7447	84.0
1.703	.7264	82.0
1.903	.7127	80.0
2.103	.7061	79.5
2.303	.7033	79.0
2.503	.7020	79.0
2.703	.7017	78.5
2.903	.7017	78.5

Series II Data Summary

Nominal Initial Velocity Ratio = 4.0

h = 0.155 Inches

θ_o = 0.050 Inches

Actual Initial Velocity Ratio	x/h	Re_s	U_j ~ ft/sec	T_j ~ °F	U_1 ~ ft/sec	τ_w ~ lb_f/ft^2	C_f^* X 10^3
3.92	37.	27,331	465.78	171.0	358.57	0.6750	5.157
3.92	69.	27,331	465.78	171.0	285.17	0.4354	5.212
3.92	101.	27,331	465.78	171.0	248.32	0.3157	4.930
3.92	134.	27,331	465.78	171.0	225.49	0.2510	4.719
3.92	166.	27,331	465.78	171.0	211.14	0.2114	4.518
3.92	198.	27,331	465.78	171.0	200.62	0.1848	4.366

* Based on Fluid Properties at δ_1

Series II Data Summary

Nominal Initial Velocity Ratio = 4.0

h = 0.155 Inches

θ_o = 0.050 Inches

Actual Initial Velocity Ratio	x/h	Re_s	U_j ~ ft/sec	T_j ~ °F	U_1 ~ ft/sec	τ_w ~ lb_f/ft^2	C_f^* X 10^3	Velocity Profile Index
3.93	13.	27,556	466.89	175.0	466.40	-	-	216
3.93	26.	27,556	466.89	175.0	402.16	-	-	216
3.93	39.	27,556	466.89	175.0	349.15	-	-	217
3.93	52.	27,556	466.89	175.0	314.36	-	-	217
3.93	65.	27,556	466.89	175.0	288.79	-	-	218
3.93	97.	27,556	466.89	175.0	249.36	-	-	218
3.93	129.	27,556	466.89	175.0	226.25	-	-	219
3.93	161.	27,556	466.89	175.0	212.38	-	-	219
3.93	194.	27,556	466.89	175.0	200.64	-	-	220

* Based on Fluid Properties at δ_1

VELOCITY PROFILES

U_j/U_{e_o} = 3.93 x/h = 13

Y ~ In.	U/U_1	T ~ °F
.004	.7704	167.5
.011	.8548	167.5
.016	.9018	168.0
.021	.9357	168.0
.026	.9624	168.5
.031	.9802	169.5
.041	.9961	170.0
.051	1.0000	169.0
.061	.9969	168.0
.071	.9854	165.5
.081	.9699	162.5
.091	.9489	159.0
.101	.9263	155.5
.111	.8978	151.5
.121	.8657	147.5
.131	.8327	143.5
.151	.7616	136.0
.171	.6878	129.0
.191	.6154	122.0
.211	.5408	115.0
.231	.4719	108.0
.251	.4070	101.0
.271	.3504	94.5
.291	.3032	89.0
.311	.2679	83.5
.331	.2476	80.0
.351	.2395	77.0
.371	.2378	76.0
.391	.2386	75.0
.411	.2414	75.0
.461	.2446	75.0
.511	.2474	75.0
.561	.2506	75.0
.611	.2506	75.0
.711	.2541	75.0
.811	.2546	75.0

U_j/U_{e_o} = 3.93 x/h = 26

Y ~ In.	U/U_1	T ~ °F
.004	.7826	162.5
.008	.8242	162.5
.013	.8712	162.5
.018	.9043	162.0
.023	.9286	161.0
.028	.9491	160.5
.038	.9777	158.5
.048	.9941	156.5
.058	.9985	154.0
.068	1.0000	152.0
.078	.9932	149.5
.088	.9816	147.0
.098	.9670	145.0
.108	.9469	142.5
.118	.9299	140.0
.138	.8888	136.0
.158	.8459	132.0
.178	.8030	128.0
.198	.7580	124.0
.218	.7126	120.0
.238	.6718	116.5
.258	.6259	112.5
.278	.5824	109.0
.298	.5416	105.0
.318	.5031	101.5
.338	.4658	98.0
.358	.4310	94.5
.378	.3983	91.0
.398	.3694	88.0
.418	.3464	85.0
.438	.3264	82.5
.478	.3000	79.0
.518	.2933	77.0
.568	.2905	76.5
.618	.2925	76.0
.718	.2935	76.0
.818	.2940	76.0
.918	.2940	76.0
1.018	.2940	76.0

VELOCITY PROFILES

U_j/U_{e_o} = 3.93 x/h = 39

Y ~ In.	U/U_1	T ~ °F
.004	.7952	153.0
.009	.8490	153.0
.014	.8867	152.5
.019	.9182	152.5
.024	.9390	152.0
.034	.9674	150.5
.044	.9839	149.0
.054	.9939	148.0
.064	.9991	146.5
.074	1.0000	145.0
.084	.9962	143.0
.094	.9911	142.0
.104	.9830	140.0
.114	.9757	139.0
.124	.9658	137.5
.144	.9435	134.5
.164	.9166	132.0
.184	.8887	129.0
.204	.8604	126.5
.224	.8287	124.0
.274	.7556	118.0
.324	.6751	111.0
.374	.6035	105.0
.424	.5312	99.0
.474	.4662	93.0
.524	.4120	87.5
.574	.3729	83.0
.624	.3505	80.0
.674	.3399	78.0
.724	.3387	78.0
.774	.3384	77.0
.824	.3384	77.0

U_j/U_{e_o} = 3.93 x/h = 52

Y ~ In.	U/U_1	T ~ °F
.004	.7826	144.5
.010	.8540	144.0
.015	.8860	144.0
.020	.9100	144.0
.025	.9272	143.5
.030	.9440	143.0
.040	.9683	142.0
.050	.9811	141.0
.060	.9937	140.0
.070	.9982	139.0
.080	1.0000	138.0
.090	.9992	137.0
.100	.9983	136.0
.110	.9949	135.0
.120	.9914	134.0
.130	.9826	133.0
.150	.9680	131.5
.170	.9527	129.5
.190	.9345	127.5
.210	.9157	125.0
.230	.8915	123.5
.270	.8501	120.0
.310	.8069	116.5
.350	.7582	113.0
.390	.7131	109.0
.430	.6681	105.0
.480	.6116	101.0
.530	.5583	97.0
.580	.5075	93.0
.630	.4633	89.0
.680	.4294	85.0
.730	.4030	82.5
.830	.3801	79.5
.930	.3744	78.5
1.030	.3744	78.5
1.130	.3744	78.5

VELOCITY PROFILES

U_j/U_{e_o} = 3.93 x/h = 65

Y ~ In.	U/U_1	T ~ °F
.004	.7575	138.5
.010	.8223	138.5
.015	.8622	138.5
.025	.9136	138.0
.035	.9419	137.5
.045	.9617	136.5
.055	.9743	136.0
.065	.9863	135.0
.075	.9918	134.0
.085	.9977	133.5
.095	1.0000	132.5
.105	.9996	132.0
.115	.9987	131.0
.125	.9979	130.0
.135	.9948	130.0
.155	.9872	128.5
.175	.9765	127.0
.195	.9625	125.5
.215	.9483	124.0
.235	.9340	122.5
.285	.8941	119.0
.335	.8491	115.5
.385	.8058	112.0
.435	.7631	109.0
.485	.7162	105.5
.535	.6708	102.5
.585	.6268	99.5
.635	.5858	96.0
.735	.5066	90.0
.835	.4497	85.0
.935	.4221	81.0
1.035	.4123	79.5
1.135	.4092	79.0
1.235	.4092	79.0
1.335	.4092	79.0

U_j/U_{e_o} = 3.93 x/h = 97

Y ~ In.	U/U_1	T ~ °F
.004	.7161	128.0
.014	.8198	128.0
.024	.8712	128.0
.034	.9052	127.5
.044	.9270	127.0
.054	.9469	126.5
.064	.9598	126.0
.074	.9698	125.5
.084	.9797	125.0
.094	.9874	125.0
.114	.9954	124.0
.134	.9984	123.0
.154	1.0000	122.0
.174	.9979	121.0
.194	.9933	120.0
.214	.9891	119.5
.234	.9806	118.5
.254	.9739	118.0
.304	.9515	116.0
.354	.9274	114.0
.454	.8749	110.0
.554	.8150	106.0
.654	.7545	102.5
.754	.6979	98.5
.854	.6389	94.5
.954	.5852	91.0
1.054	.5429	88.0
1.154	.5093	85.0
1.254	.4888	82.5
1.354	.4755	80.5
1.454	.4711	80.0
1.554	.4711	80.0
1.654	.4711	80.0

VELOCITY PROFILES

U_j/U_{e_o} = 3.93 x/h = 129

Y ~ In.	U/U_1	T ~ °F
.004	.6884	122.0
.016	.8048	122.0
.026	.8460	122.0
.046	.9004	121.5
.066	.9368	121.0
.086	.9602	120.0
.106	.9744	120.0
.126	.9844	119.0
.146	.9932	118.5
.166	.9959	118.0
.186	1.0000	117.5
.206	.9980	117.0
.226	.9957	116.0
.246	.9922	115.5
.266	.9887	115.0
.316	.9786	114.0
.366	.9614	112.0
.416	.9447	111.0
.466	.9262	110.0
.566	.8857	107.0
.666	.8453	104.0
.766	.7999	101.5
.866	.7576	98.5
1.066	.6716	94.0
1.266	.5989	89.0
1.466	.5482	85.0
1.666	.5258	82.0
1.866	.5179	81.0
2.066	.5158	80.5
2.266	.5158	80.5
2.466	.5158	80.5

U_j/U_{e_o} = 3.93 x/h = 161

Y ~ In.	U/U_1	T ~ °F
.004	.6709	118.0
.016	.7753	118.0
.026	.8231	117.5
.036	.8547	118.0
.056	.9000	117.5
.076	.9304	117.5
.096	.9485	117.0
.116	.9608	116.5
.136	.9764	116.0
.156	.9831	115.5
.176	.9914	115.0
.196	.9927	114.5
.216	.9957	114.0
.236	.9987	113.5
.256	1.0000	113.0
.276	.9978	112.5
.326	.9896	111.0
.376	.9823	110.5
.476	.9555	108.0
.576	.9285	106.0
.676	.8967	103.5
.876	.8352	100.0
1.076	.7626	96.0
1.276	.6954	92.0
1.476	.6409	89.0
1.676	.5955	85.0
1.876	.5684	82.5
2.076	.5579	81.0
2.276	.5536	80.5
2.476	.5507	80.5
2.676	.5507	80.5
2.876	.5519	81.0

VELOCITY PROFILE

$U_j/U_{e_o} = 3.93$

$x/h = 194$

Y ~ In.	U/U_1	T ~ °F
.004	.6445	115.0
.022	.7792	114.5
.042	.8488	114.5
.062	.8869	114.5
.082	.9214	114.5
.102	.9418	114.0
.122	.9557	113.5
.142	.9697	113.5
.162	.9749	112.5
.182	.9823	112.0
.202	.9882	112.0
.222	.9960	112.0
.242	.9975	111.5
.262	.9970	111.0
.282	.9985	110.5
.302	1.0000	110.0
.402	.9933	109.0
.502	.9721	107.0
.602	.9546	105.0
.702	.9274	104.0
.902	.8743	101.0
1.102	.8185	98.5
1.302	.7662	95.5
1.502	.7155	92.0
1.702	.6677	89.5
1.902	.6223	86.5
2.102	.6070	84.5
2.302	.5930	83.5
2.502	.5827	82.0
2.702	.5817	82.0
2.902	.5817	82.0

Series II Data Summary

Nominal Initial Velocity Ratio = 6.0

h = 0.155 Inches

θ_o = 0.050 Inches

Actual Initial Velocity Ratio	x/h	Re_s	U_j ~ ft/sec	T_j ~ °F	U_1 ~ ft/sec	τ_w ~ lb_f/ft^2	C_f^* X 10^3
5.70	37.	42,746	670.84	168.0	590.51	1.3941	5.006
5.70	69.	42,746	670.84	168.0	399.38	0.8450	4.950
5.70	101.	42,746	670.84	168.0	341.84	0.6082	4.853
5.70	134.	42,746	670.84	168.0	305.31	0.4682	4.670
5.70	166.	42,746	670.84	168.0	283.17	0.3821	4.426
5.70	198.	42,746	670.84	168.0	264.25	0.3270	4.350

* Based on Fluid Properties at δ_1

Series II Data Summary

Nominal Initial Velocity Ratio = 6.0

h = 0.155 Inches

θ_o = 0.050 Inches

Actual Initial Velocity Ratio	x/h	Re_s	U_j ~ ft/sec	T_j ~ °F	U_1 ~ ft/sec	τ_w ~ lb_f/ft^2	C_f^* X 10^3	Velocity Profile Index
5.78	13.	42,697	675.05	169.0	667.52	-	-	223
5.78	26.	42,697	675.05	169.0	577.12	-	-	223
5.78	39.	42,697	675.05	169.0	500.86	-	-	224
5.78	52.	42,697	675.05	169.0	449.95	-	-	224
5.78	65.	42,697	675.05	169.0	410.67	-	-	225
5.78	97.	42,697	675.05	169.0	348.29	-	-	225
5.78	129.	42,697	675.05	169.0	309.78	-	-	226
5.78	161.	42,697	675.05	169.0	284.02	-	-	226
5.78	194.	42,697	675.05	169.0	267.27	-	-	227

* Based on Fluid Properties at δ_1

VELOCITY PROFILES

U_j/U_{e_o} = 5.78 x/h = 13

Y ~ In.	U/U_1	T ~ °F
.004	.7608	168.5
.009	.8240	169.0
.014	.8700	169.0
.024	.9371	170.0
.034	.9800	169.5
.044	.9971	168.0
.054	1.0000	166.0
.064	.9938	162.0
.074	.9828	159.5
.084	.9656	155.0
.094	.9414	150.0
.104	.9142	146.0
.114	.8861	142.0
.134	.8179	134.0
.154	.7458	127.0
.174	.6752	120.5
.194	.5985	114.0
.214	.5260	108.0
.234	.4575	102.0
.254	.3944	96.5
.274	.3323	91.5
.294	.2798	87.5
.314	.2341	84.5
.334	.1997	82.5
.354	.1807	81.5
.374	.1727	81.5
.394	.1704	81.5
.414	.1714	81.5
.434	.1718	81.5
.454	.1724	81.5
.474	.1737	81.5
.494	.1740	81.5
.514	.1737	81.5

U_j/U_{e_o} = 5.78 x/h = 26

Y ~ In.	U/U_1	T ~ °F
.004	.8034	163.0
.012	.8710	163.0
.017	.9060	163.0
.022	.9296	162.5
.032	.9632	161.5
.042	.9862	160.0
.052	.9974	158.0
.062	1.0000	156.0
.072	.9980	153.5
.082	.9900	151.5
.092	.9774	149.0
.102	.9607	147.0
.112	.9411	144.5
.122	.9214	142.5
.142	.8780	138.0
.162	.8327	134.0
.182	.7873	130.0
.202	.7421	126.0
.222	.6974	122.5
.242	.6529	119.0
.262	.6073	115.0
.282	.5636	111.5
.302	.5221	108.0
.322	.4804	105.0
.342	.4416	101.5
.362	.4031	98.5
.382	.3692	96.0
.402	.3349	93.0
.422	.3045	90.5
.442	.2750	88.0
.462	.2541	86.5
.482	.2354	85.0
.502	.2222	83.5
.522	.2135	83.0
.542	.2077	82.5
.562	.2047	82.0
.582	.2040	82.0
.822	.2031	81.5
.862	.2039	81.5
.902	.2039	81.5

VELOCITY PROFILES

U_j/U_{e_o} = 5.78 x/h = 39

Y ~ In.	U/U_1	T ~ °F
.004	.8338	154.5
.010	.8824	154.5
.020	.9371	154.0
.030	.9695	153.0
.040	.9877	152.0
.050	.9937	151.0
.060	.9983	149.5
.070	1.0000	148.0
.080	.9963	147.0
.090	.9922	145.5
.100	.9851	144.0
.110	.9751	142.5
.130	.9551	140.0
.150	.9282	137.0
.170	.8977	134.5
.210	.8400	129.0
.250	.7760	124.0
.290	.7119	119.0
.330	.6467	115.0
.370	.5824	110.0
.410	.5205	106.0
.450	.4656	101.5
.490	.4084	97.0
.530	.3587	94.0
.570	.3156	90.5
.610	.2826	87.5
.650	.2599	85.0
.690	.2439	83.0
.730	.2385	82.5
.770	.2359	82.5
.810	.2350	82.0
.850	.2354	82.0
.890	.2350	82.0
.930	.2350	82.0

U_j/U_{e_o} = 5.78 x/h = 52

Y ~ In.	U/U_1	T ~ °F
.004	.8083	147.0
.010	.8677	147.0
.015	.8992	147.0
.025	.9406	146.0
.035	.9663	145.5
.045	.9819	144.5
.055	.9915	144.0
.065	.9980	143.0
.075	.9996	142.0
.085	1.0000	141.0
.095	.9967	140.0
.105	.9922	139.0
.115	.9865	138.0
.135	.9725	136.0
.155	.9558	134.0
.175	.9388	132.0
.195	.9189	130.0
.235	.8738	126.0
.275	.8267	122.5
.315	.7800	119.0
.355	.7305	115.5
.395	.6811	112.0
.435	.6323	109.0
.485	.5722	104.5
.535	.5133	101.0
.585	.4604	97.0
.635	.4111	93.5
.685	.3627	90.0
.735	.3261	87.0
.785	.2969	85.0
.835	.2782	82.5
.885	.2686	82.0
.935	.2637	81.0
.985	.2617	80.5
1.035	.2616	80.0
1.085	.2617	80.5
1.135	.2617	80.5

VELOCITY PROFILES

U_j/U_{e_o} = 5.78 x/h = 65

Y ~ In.	U/U_1	T ~ °F
.004	.8001	140.0
.013	.8735	140.0
.023	.9218	139.0
.033	.9504	138.5
.043	.9702	138.0
.063	.9906	137.0
.083	.9994	135.0
.103	1.0000	134.0
.123	.9947	133.0
.143	.9856	131.0
.163	.9743	130.0
.183	.9590	128.0
.203	.9459	127.0
.223	.9302	125.0
.243	.9118	124.0
.293	.8694	120.5
.343	.8226	118.5
.393	.7730	114.0
.443	.7252	110.5
.493	.6742	107.0
.543	.6246	104.5
.593	.5781	101.0
.643	.5311	98.5
.693	.4839	95.5
.743	.4442	93.0
.793	.4052	90.0
.843	.3723	88.0
.893	.3426	85.0
.943	.3192	83.0
.993	.3047	82.0
1.043	.2965	81.0
1.093	.2898	80.5
1.143	.2882	80.0
1.193	.2866	80.0
1.243	.2866	80.0
1.343	.2866	80.0

U_j/U_{e_o} = 5.78 x/h = 97

Y ~ In.	U/U_1	T ~ °F
.004	.7689	128.5
.017	.8609	128.5
.027	.9015	128.0
.037	.9269	128.0
.047	.9468	127.5
.057	.9617	127.0
.077	.9807	126.5
.097	.9925	125.5
.117	.9984	125.0
.137	1.0000	124.5
.157	.9971	123.5
.197	.9875	122.0
.237	.9710	120.0
.277	.9552	119.0
.317	.9320	117.5
.357	.9102	115.5
.457	.8512	112.0
.557	.7876	108.0
.657	.7224	105.0
.757	.6567	101.0
.857	.5950	97.5
.957	.5313	94.0
1.057	.4768	91.0
1.157	.4260	88.0
1.257	.3885	85.5
1.357	.3595	83.0
1.457	.3456	81.5
1.557	.3394	81.0
1.657	.3376	81.0
1.757	.3370	81.0
1.857	.3362	80.5
1.957	.3355	80.0
2.057	.3349	80.0
2.157	.3349	80.0

VELOCITY PROFILES

U_j/U_{e_o} = 5.78 x/h = 129

Y ~ In.	U/U_1	T ~ °F
.004	.7534	122.0
.010	.8047	122.0
.030	.8873	121.5
.050	.9311	121.0
.070	.9589	120.5
.090	.9749	120.0
.110	.9884	120.0
.130	.9960	119.5
.150	.9978	118.5
.170	1.0000	118.0
.190	.9996	117.5
.210	.9996	117.5
.230	.9965	117.0
.250	.9908	116.5
.270	.9850	116.0
.320	.9703	114.5
.370	.9531	113.5
.470	.9141	110.5
.570	.8683	108.5
.670	.8225	105.5
.870	.7268	101.0
.970	.6783	99.0
1.070	.6295	96.0
1.170	.5815	94.0
1.270	.5397	92.0
1.370	.4993	90.0
1.470	.4620	87.0
1.570	.4333	85.5
1.670	.4105	84.0
1.770	.3950	82.5
1.870	.3867	81.5
1.970	.3797	81.0
2.070	.3795	80.5
2.170	.3763	81.0
2.270	.3775	80.5
2.370	.3768	80.5

U_j/U_{e_o} = 5.78 x/h = 161

Y ~ In.	U/U_1	T ~ °F
.004	.7373	117.0
.016	.8158	117.0
.026	.8539	117.0
.046	.9089	116.5
.066	.9399	116.5
.086	.9566	116.0
.106	.9730	116.0
.126	.9822	115.5
.146	.9914	115.0
.166	.9941	114.5
.186	.9969	114.0
.206	1.0000	114.0
.226	.9996	113.5
.246	.9991	113.0
.266	.9991	113.0
.286	.9955	112.5
.386	.9715	110.5
.486	.9441	109.0
.586	.9156	107.0
.686	.8827	105.0
.886	.8020	101.5
1.086	.7305	98.5
1.286	.6566	95.0
1.486	.5806	92.0
1.686	.5174	88.5
1.886	.4667	85.5
2.086	.4346	83.0
2.286	.4188	81.5
2.486	.4126	81.0
2.686	.4125	80.5
2.886	.4117	80.5

VELOCITY PROFILE

$U_j/U_{e_o} = 5.78$

$x/h = 194$

Y ~ In.	U/U_1	T ~ °F
.004	.7162	114.5
.010	.7589	114.0
.030	.8423	114.5
.050	.8895	114.0
.070	.9202	113.5
.090	.9421	113.5
.110	.9591	113.5
.160	.9804	112.5
.210	.9908	112.0
.260	1.0000	111.5
.310	.9970	110.5
.360	.9912	110.0
.410	.9832	109.5
.460	.9730	109.0
.510	.9623	108.0
.610	.9379	107.0
.710	.9102	105.5
.810	.8805	104.0
.910	.8515	103.0
1.010	.8225	101.5
1.110	.7884	100.0
1.210	.7585	98.5
1.310	.7278	97.5
1.410	.6970	96.0
1.510	.6652	95.0
1.610	.6349	93.5
1.710	.6070	92.5
1.910	.5564	90.0
2.110	.5116	87.5
2.310	.4763	85.0
2.510	.4561	83.5
2.710	.4463	82.5
2.910	.4392	82.5
3.110	.4382	82.0
3.310	.4374	82.0
3.510	.4358	82.0
3.710	.4342	82.0
3.910	.4328	82.0

APPENDIX L

EXPERIMENTAL RESULTS FOR SERIES III

SERIES III TYPICAL INITIAL
BOUNDARY LAYER PROFILE

U_{e_o} = 119.21 Ft/Sec

θ_o = 0.206 Inches

x/h = 0

Y ~ In.	U/U_1	T ~ °F
.000	.000	82.0
.004	.331	82.0
.008	.430	82.0
.012	.478	82.5
.016	.503	83.0
.020	.515	83.0
.024	.527	83.0
.034	.549	83.0
.044	.568	83.5
.054	.579	83.5
.064	.589	83.5
.084	.608	84.0
.104	.622	84.0
.124	.635	84.0
.144	.646	84.0
.194	.672	84.0
.244	.694	84.5
.294	.713	84.5
.344	.734	84.5
.394	.743	84.5
.444	.760	85.0
.494	.774	85.0
.544	.783	85.0
.644	.809	85.0
.744	.834	85.0
.844	.856	85.0
.944	.880	85.0
1.044	.902	85.0
1.144	.922	85.0
1.244	.940	85.5
1.344	.957	85.5
1.444	.971	85.5
1.544	.982	85.5
1.644	.991	85.5
1.744	.996	85.5
1.844	1.000	85.5
1.944	1.000	85.5

Series III Data Summary

Nominal Initial Velocity Ratio = 0.0

h = 0.056 Inches

Actual Initial Velocity Ratio	x/h	Re_s	θ_o ~ Inches	U_{e_o} ~ ft/sec	U_e ~ ft/sec	τ_w ~ lb_f/ft^2	C_f^* X 10^3	Velocity Profile Index
0.0 **	125.	0.0	0.220	120.46	119.64	0.0415	2.630	231
0.0 **	554.	0.0	0.220	120.46	117.07	0.0407	2.703	231
0.0	125.	0.0	0.206	119.21	113.74	0.0334	2.339	232
0.0	197.	0.0	0.206	119.21	110.25	0.0299	2.234	232
0.0	286.	0.0	0.206	119.21	104.79	0.0245	2.025	233
0.0	357.	0.0	0.206	119.21	99.74	0.0196	1.780	233
0.0	462.	0.0	0.206	119.21	91.72	0.0123	1.321	234
0.0	554.	0.0	0.206	119.21	85.00	0.0064	0.802	234

* Based on Fluid Properties at δ_e

** Zero Pressure Gradient Test

VELOCITY PROFILES

U_j/U_{e_o} = 0 x/h = 125

Y ~ In.	U/U_e	T ~ °F
.004	.3194	84.5
.008	.4328	84.5
.012	.4866	84.5
.016	.5169	84.5
.026	.5556	84.5
.036	.5824	84.5
.046	.5947	85.0
.056	.6065	85.0
.106	.6570	85.0
.156	.6848	85.0
.206	.7051	85.0
.256	.7188	85.0
.306	.7310	85.0
.356	.7442	85.0
.406	.7619	85.0
.456	.7745	85.0
.506	.7802	85.0
.606	.7996	85.5
.706	.8193	85.5
.806	.8364	85.5
.906	.8553	85.5
1.006	.8737	85.5
1.106	.8927	85.5
1.206	.9094	85.5
1.306	.9267	85.5
1.506	.9530	85.5
1.706	.9750	85.5
1.906	.9902	85.5
2.106	.9973	85.5
2.306	1.0000	85.5
2.506	.9991	85.5

U_j/U_{e_o} = 0 x/h = 554

Y ~ In.	U/U_e	T ~ °F
.004	.3378	84.0
.010	.4861	84.5
.015	.5281	85.0
.020	.5496	85.0
.025	.5663	85.0
.035	.5903	85.0
.045	.6074	85.0
.055	.6255	85.0
.065	.6358	85.0
.085	.6573	85.0
.105	.6768	85.0
.125	.6960	85.5
.145	.7053	85.5
.165	.7131	85.5
.215	.7336	85.5
.265	.7560	85.5
.315	.7670	85.5
.365	.7817	86.0
.465	.7982	86.0
.565	.8154	86.0
.665	.8289	86.0
.765	.8389	86.0
.865	.8554	86.0
1.065	.8778	86.0
1.265	.8987	86.0
1.465	.9190	86.0
1.665	.9394	86.5
1.865	.9579	86.5
2.065	.9714	86.5
2.265	.9837	86.5
2.465	.9912	86.5
2.665	.9958	86.5
2.865	.9995	86.5
3.065	1.0000	87.0
3.265	.9991	87.0

VELOCITY PROFILES

U_j/U_{e_o} = 0 x/h = 125

Y ~ In.	U/U_e	T ~ °F
.004	.2918	85.5
.010	.4440	85.5
.015	.4862	85.5
.020	.5040	85.5
.025	.5287	85.5
.030	.5361	85.5
.040	.5526	86.0
.050	.5700	86.0
.060	.5803	86.0
.070	.5920	86.0
.080	.6035	86.0
.100	.6211	86.0
.120	.6382	86.0
.140	.6444	86.0
.190	.6683	86.0
.240	.6856	86.0
.290	.7054	86.0
.340	.7140	86.5
.440	.7423	86.5
.540	.7670	86.5
.640	.7884	86.5
.740	.8080	86.5
.840	.8319	86.5
.940	.8528	86.5
1.040	.8687	86.5
1.140	.8859	87.0
1.240	.9034	87.0
1.440	.9395	87.0
1.640	.9642	87.0
1.840	.9852	87.0
2.040	.9951	87.0
2.240	.9990	87.0
2.440	1.0000	87.0
2.640	.9990	87.0

U_j/U_{e_o} = 0 x/h = 197

Y ~ In.	U/U_e	T ~ °F
.004	.2793	87.0
.010	.4126	87.0
.015	.4628	87.0
.020	.4892	87.0
.025	.5040	87.0
.035	.5303	87.0
.045	.5478	87.0
.055	.5647	87.0
.065	.5757	87.0
.085	.5936	87.0
.105	.6075	87.0
.125	.6245	87.0
.145	.6361	87.0
.195	.6587	87.0
.245	.6775	87.0
.295	.6912	87.0
.345	.7017	87.0
.395	.7165	87.0
.495	.7380	87.0
.595	.7631	87.0
.695	.7780	87.0
.795	.7991	87.0
.895	.8210	87.0
.995	.8386	87.0
1.095	.8571	87.0
1.195	.8751	87.0
1.295	.8928	87.0
1.395	.9090	87.0
1.595	.9372	87.0
1.795	.9650	87.5
1.995	.9789	87.5
2.195	.9916	87.5
2.395	.9979	87.5
2.595	1.0000	87.5
2.795	.9979	87.5

VELOCITY PROFILES

U_j/U_{e_o} = 0 x/h = 286

Y ~ In.	U/U_e	T ~ °F
.004	.2581	87.0
.010	.3904	87.0
.015	.4353	87.0
.020	.4612	87.0
.025	.4784	87.0
.035	.5020	87.0
.045	.5202	87.0
.055	.5334	87.0
.065	.5462	87.0
.085	.5588	87.0
.105	.5771	87.0
.125	.5930	87.0
.175	.6197	87.0
.225	.6399	87.0
.275	.6612	87.0
.325	.6734	87.0
.425	.6940	87.0
.525	.7170	87.5
.625	.7392	87.5
.725	.7547	87.5
.825	.7729	87.5
.925	.7895	87.5
1.125	.8267	88.0
1.325	.8596	88.0
1.525	.8952	88.0
1.725	.9207	88.0
1.925	.9479	88.0
2.125	.9683	88.0
2.325	.9837	88.0
2.525	.9931	88.0
2.725	1.0000	88.0
2.925	1.0000	88.0

U_j/U_{e_o} = 0 x/h = 357

Y ~ In.	U/U_e	T ~ °F
.004	.2467	85.5
.007	.3227	85.5
.010	.3601	86.0
.015	.4035	86.0
.020	.4250	86.0
.025	.4397	86.0
.035	.4651	86.0
.045	.4812	86.0
.055	.4942	86.0
.075	.5144	86.0
.095	.5314	86.0
.115	.5433	86.0
.135	.5549	86.0
.155	.5662	86.0
.205	.5904	86.0
.255	.6053	86.0
.305	.6239	86.0
.405	.6521	86.5
.505	.6732	86.5
.605	.6992	86.5
.705	.7171	86.5
.805	.7329	86.5
1.005	.7651	86.5
1.205	.8071	86.5
1.405	.8365	86.5
1.605	.8697	87.0
1.805	.8984	87.0
2.005	.9262	87.0
2.205	.9466	87.0
2.405	.9678	87.0
2.605	.9847	87.0
2.805	.9924	87.0
3.005	.9975	87.0
3.205	1.0000	87.0
3.405	.9987	87.0

VELOCITY PROFILES

U_j/U_{e_o} = 0 x/h = 462

Y ~ In.	U/U_e	T ~ °F
.004	.1829	86.5
.007	.2461	86.5
.010	.2805	86.5
.015	.3206	86.5
.020	.3388	86.5
.030	.3645	86.5
.040	.3809	87.0
.060	.4076	87.0
.080	.4257	87.0
.100	.4397	87.0
.150	.4630	87.0
.200	.4914	87.0
.250	.5095	87.0
.350	.5410	87.0
.450	.5682	87.0
.550	.5915	87.0
.650	.6140	87.0
.750	.6357	87.0
.850	.6544	87.0
1.050	.6880	87.0
1.250	.7242	87.0
1.450	.7587	87.0
1.650	.7936	87.0
1.850	.8291	87.5
2.050	.8524	87.5
2.250	.8819	87.5
2.450	.9071	87.5
2.650	.9300	87.5
2.850	.9555	87.5
3.050	.9695	87.5
3.250	.9849	87.5
3.450	.9925	87.5
3.650	.9970	87.5
3.850	1.0000	87.5
4.050	.9985	87.5

U_j/U_{e_o} = 0 x/h = 554

Y ~ In.	U/U_e	T ~ °F
.004	.1027	87.0
.007	.1452	87.0
.010	.1676	87.0
.015	.2217	87.0
.020	.2370	87.0
.025	.2443	87.0
.035	.2650	87.0
.045	.2779	87.0
.065	.2962	87.0
.085	.3191	87.0
.135	.3404	87.0
.185	.3654	87.5
.235	.3887	87.5
.335	.4191	87.5
.435	.4395	87.5
.635	.4923	87.5
.835	.5334	87.5
1.035	.5715	87.5
1.235	.6072	87.5
1.435	.6436	87.5
1.635	.6884	87.5
1.835	.7186	88.0
2.035	.7473	88.0
2.235	.7795	88.0
2.735	.8566	88.0
3.235	.9178	88.0
3.735	.9662	88.0
4.235	.9930	88.0
4.735	1.0000	88.0
5.235	.9965	88.0

Series III Data Summary

Nominal Initial Velocity Ratio = 1.5

h = 0.056 Inches

θ_o = 0.207 Inches

Actual Initial Velocity Ratio	x/h	Re_s	U_j ~ ft/sec	T_j ~ °F	U_1 ~ ft/sec	τ_w ~ lb_f/ft^2	C_f^* X 10^3	Velocity Profile Index
1.52	125.	4,153	179.21	131.	109.35	0.0754	5.917	236
1.52	197.	4,153	179.21	131.	96.31	0.0521	5.221	236
1.52	286.	4,153	179.21	131.	85.50	0.0359	4.542	237
1.51	357.	4,153	178.92	131.	76.59	0.0243	3.784	237
1.51	462.	4,153	178.92	132.	86.69**	0.0129	1.541**	238
1.51	554.	4,153	178.92	132.	78.95**	0.0053	0.759**	238

* Based on Fluid Properties at δ_1

** Based on Measurements at δ_e (Jet Peak not Evident)

VELOCITY PROFILES

U_j/U_{e_o} = 1.52 x/h = 125

Y ~ In.	U/U_1	T ~ °F
.004	.5650	110.0
.007	.7001	110.0
.010	.7637	110.0
.015	.8156	110.0
.020	.8445	109.5
.025	.8703	109.5
.030	.8925	109.0
.035	.9121	109.0
.040	.9277	109.0
.050	.9519	108.5
.060	.9728	107.5
.070	.9847	107.0
.080	.9943	106.5
.090	.9971	106.0
.100	1.0000	105.5
.110	.9991	104.5
.120	.9976	104.0
.140	.9912	103.0
.160	.9770	102.0
.180	.9627	101.0
.200	.9482	100.0
.250	.9116	98.0
.300	.8794	95.5
.350	.8530	93.5
.400	.8340	92.0
.450	.8235	90.0
.500	.8202	89.0
.550	.8202	89.0
.600	.8246	88.0
.650	.8284	88.0
.750	.8437	88.0
.850	.8620	87.5
.950	.8815	87.5
1.150	.9181	87.5
1.350	.9533	87.5
1.550	.9829	87.5
1.750	1.0053	87.5
1.950	1.0210	87.5
2.150	1.0292	87.5
2.350	1.0313	87.5
2.550	1.0303	87.5

U_j/U_{e_o} = 1.52 x/h = 197

Y ~ In.	U/U_1	T ~ °F
.004	.5199	106.0
.007	.6422	106.0
.010	.7034	106.0
.015	.7503	106.0
.020	.7818	106.0
.025	.8032	106.0
.035	.8357	105.5
.045	.8674	105.5
.055	.8895	105.0
.075	.9326	104.5
.095	.9634	104.0
.115	.9843	103.0
.135	.9938	102.5
.155	.9985	101.5
.175	.9995	101.0
.195	1.0000	100.0
.215	.9953	99.5
.265	.9832	98.5
.315	.9704	97.0
.365	.9576	95.5
.415	.9450	94.5
.465	.9353	93.5
.515	.9315	92.5
.565	.9252	92.0
.665	.9224	90.5
.765	.9275	89.5
.865	.9403	89.0
.965	.9530	88.5
1.165	.9855	88.5
1.365	1.0210	88.5
1.565	1.0528	88.5
1.765	1.0823	88.5
1.965	1.1036	88.5
2.165	1.1196	88.5
2.365	1.1269	88.5
2.565	1.1293	88.5
2.765	1.1281	88.5

VELOCITY PROFILES

U_j/U_{e_o} = 1.52 x/h = 286

Y ~ In.	U/U_1	T ~ °F
.004	.4528	103.0
.007	.5623	103.0
.010	.6170	103.0
.015	.6646	103.0
.020	.6988	103.0
.030	.7386	103.0
.040	.7695	103.0
.050	.7925	103.0
.070	.8403	102.5
.090	.8733	102.0
.110	.9015	102.0
.130	.9245	101.5
.180	.9652	100.5
.230	.9880	99.5
.280	.9974	98.0
.330	1.0000	97.0
.380	.9973	96.0
.430	.9951	95.5
.480	.9924	94.5
.530	.9884	94.0
.580	.9862	93.5
.680	.9871	92.5
.780	.9880	91.5
.880	.9946	91.0
.980	1.0024	90.0
1.080	1.0128	90.0
1.280	1.0396	89.5
1.480	1.0667	88.5
1.680	1.0973	88.5
1.880	1.1239	88.5
2.080	1.1529	88.5
2.280	1.1708	88.5
2.480	1.1856	88.5
2.680	1.1944	88.5
2.880	1.1987	88.5
3.080	1.1987	88.5

U_j/U_{e_o} = 1.51 x/h = 357

Y ~ In.	U/U_1	T ~ °F
.004	.3594	97.5
.007	.4614	97.5
.010	.5282	97.5
.015	.5911	97.5
.020	.6202	97.5
.025	.6446	97.5
.035	.6779	97.5
.045	.7065	97.5
.065	.7459	97.5
.085	.7861	97.5
.105	.8105	97.0
.125	.8345	97.0
.175	.8926	96.5
.225	.9349	95.5
.275	.9576	95.0
.325	.9771	94.0
.425	1.0000	92.5
.525	.9991	91.5
.625	1.0004	90.5
.725	1.0085	90.0
.825	1.0119	89.0
.925	1.0157	88.5
1.125	1.0337	87.5
1.325	1.0534	86.5
1.525	1.0751	86.0
1.725	1.1047	86.0
1.925	1.1368	85.5
2.125	1.1666	85.5
2.325	1.1915	85.0
2.525	1.2164	85.0
2.725	1.2339	85.0
2.925	1.2477	85.0
3.125	1.2580	85.0
3.325	1.2597	85.0
3.525	1.2597	85.0

VELOCITY PROFILES

U_j/U_{e_o} = 1.51 x/h = 462

Y ~ In.	U/U_1	T ~ °F
.004	.1942	96.0
.007	.2619	96.0
.010	.3043	96.0
.015	.3464	96.0
.020	.3749	96.0
.025	.3839	96.0
.035	.4056	96.0
.045	.4262	96.0
.065	.4459	96.0
.085	.4720	96.0
.105	.4863	96.0
.155	.5301	96.0
.205	.5584	96.0
.255	.5906	95.0
.355	.6456	94.5
.455	.6810	93.5
.555	.7124	93.0
.655	.7306	92.0
.755	.7392	91.0
.855	.7479	90.5
.955	.7544	90.0
1.155	.7648	89.0
1.355	.7858	88.0
1.555	.7961	87.5
1.755	.8166	87.0
1.955	.8345	86.5
2.455	.8849	86.0
2.955	.9418	86.0
3.455	.9797	85.5
3.955	1.0000	85.5
4.455	1.0000	85.5

U_j/U_{e_o} = 1.51 x/h = 554

Y ~ In.	U/U_1	T ~ °F
.004	.0909	95.0
.007	.1285	95.0
.012	.1817	95.0
.015	.2031	95.0
.020	.2223	95.0
.030	.2403	95.0
.040	.2648	95.0
.050	.2648	95.0
.070	.2872	95.0
.090	.2943	95.0
.140	.3274	95.0
.190	.3517	95.0
.240	.3799	95.0
.290	.4010	95.0
.390	.4540	95.0
.490	.4971	94.5
.590	.5367	94.0
.690	.5698	93.5
.790	.6008	92.5
.890	.6273	92.0
.990	.6465	92.0
1.190	.6799	91.0
1.390	.7029	90.0
1.590	.7226	89.5
1.790	.7362	89.0
1.990	.7546	88.0
2.190	.7807	87.5
2.690	.8258	87.0
3.190	.8777	86.5
3.690	.9266	86.0
4.190	.9692	86.0
4.690	.9939	86.0
5.190	1.0000	86.0
5.690	.9980	86.0

Series III Data Summary

Nominal Initial Velocity Ratio = 2.0

h = 0.056 Inches

θ_o = 0.216 Inches

Actual Initial Velocity Ratio	x/h	Re_s	U_j ~ ft/sec	T_j ~ °F	U_1 ~ ft/sec	τ_w ~ lb_f/ft^2	C_f^* X 10^3	Velocity Profile Index
2.07	125.	5,510	245.39	143.0	139.49	0.1222	5.939	240
2.07	197.	5,510	245.39	143.0	120.08	0.0844	5.480	240
2.07	286.	5,510	245.39	144.0	104.40	0.0577	4.929	241
2.07	357.	5,509	245.78	142.0	95.11	0.0444	4.575	241
2.07	462.	5,509	245.78	144.0	80.65	0.0277	3.957	242
2.07	554.	5,509	245.78	145.0	67.10	0.0151	3.116	242

* Based on Fluid Properties at δ_1

VELOCITY PROFILES

U_j/U_{e_o} = 2.07 x/h = 125

Y ~ In.	U/U_1	T ~ °F
.004	.6497	115.0
.007	.7632	115.0
.010	.8077	115.0
.015	.8478	114.5
.020	.8752	114.0
.025	.8990	114.0
.035	.9357	113.5
.045	.9632	113.0
.055	.9803	112.5
.065	.9916	112.0
.075	.9955	111.0
.095	1.0000	110.0
.115	.9953	108.5
.135	.9815	107.5
.155	.9641	106.5
.175	.9459	105.0
.195	.9258	104.0
.215	.9067	103.0
.235	.8843	102.0
.285	.8319	99.5
.335	.7798	97.0
.385	.7344	94.5
.435	.6968	92.0
.485	.6713	89.5
.535	.6565	88.0
.585	.6497	86.5
.635	.6504	86.0
.735	.6567	85.0
.835	.6695	85.0
.935	.6839	85.0
1.035	.6971	85.0
1.235	.7263	85.0
1.435	.7517	85.0
1.635	.7747	85.0
1.835	.7913	85.0
2.035	.8019	85.0
2.235	.8059	85.0
2.435	.8067	85.0
2.635	.8059	85.0

U_j/U_{e_o} = 2.07 x/h = 197

Y ~ In.	U/U_1	T ~ °F
.004	.5756	110.0
.007	.7035	110.0
.010	.7478	110.0
.015	.7892	109.5
.020	.8188	109.5
.025	.8463	109.5
.030	.8645	109.5
.035	.8809	109.0
.040	.8963	109.0
.050	.9231	108.5
.060	.9426	108.5
.070	.9595	108.0
.080	.9713	107.5
.100	.9876	107.0
.120	.9959	106.0
.140	.9986	105.0
.160	1.0000	104.5
.180	.9946	103.5
.230	.9754	102.5
.280	.9484	100.5
.330	.9235	99.5
.380	.8937	98.0
.430	.8671	96.5
.480	.8397	95.0
.530	.8193	93.5
.580	.8006	92.0
.680	.7710	90.0
.780	.7615	88.0
.880	.7620	87.0
.980	.7708	86.5
1.080	.7807	86.0
1.280	.8050	86.0
1.480	.8329	86.0
1.680	.8578	86.0
1.880	.8790	86.0
2.080	.8929	86.0
2.280	.9017	86.0
2.480	.9046	86.0
2.680	.9065	86.0
2.880	.9036	86.0

VELOCITY PROFILES

U_j/U_{e_o} = 2.07 x/h = 286

Y ~ In.	U/U_1	T ~ °F
.004	.5111	106.0
.007	.6278	106.0
.010	.6849	106.0
.015	.7309	106.0
.020	.7585	106.0
.025	.7835	106.0
.035	.8152	106.0
.045	.8442	106.0
.055	.8664	105.5
.075	.9054	105.0
.095	.9367	105.0
.115	.9603	104.5
.135	.9748	104.0
.155	.9878	103.5
.205	1.0000	102.5
.255	1.0000	101.0
.305	.9919	100.0
.355	.9806	99.5
.405	.9647	98.0
.505	.9322	96.5
.605	.9091	95.0
.705	.8851	93.0
.805	.8665	91.5
.905	.8558	90.0
1.005	.8509	89.0
1.105	.8529	88.0
1.205	.8548	87.0
1.405	.8723	87.0
1.605	.8956	86.5
1.805	.9157	86.0
2.005	.9371	86.0
2.205	.9591	86.0
2.405	.9711	86.0
2.605	.9783	86.0
2.805	.9806	86.0
3.005	.9818	86.0

U_j/U_{e_o} = 2.07 x/h = 357

Y ~ In.	U/U_1	T ~ °F
.004	.5007	102.0
.007	.6011	102.5
.010	.6477	102.5
.015	.6890	102.5
.020	.7179	102.5
.025	.7359	102.5
.035	.7724	102.5
.045	.7983	102.5
.055	.8216	102.5
.065	.8425	102.5
.085	.8779	102.5
.105	.9019	102.0
.125	.9257	102.0
.145	.9454	101.5
.175	.9661	101.0
.205	.9790	100.5
.235	.9903	100.0
.285	1.0000	99.5
.335	.9962	98.5
.385	.9881	97.5
.435	.9789	97.0
.485	.9722	96.0
.585	.9490	95.0
.685	.9310	93.5
.785	.9147	92.5
.885	.9010	91.0
.985	.8906	90.0
1.085	.8870	89.5
1.285	.8874	88.0
1.485	.9008	87.0
1.685	.9128	86.5
1.885	.9367	86.0
2.085	.9560	86.0
2.285	.9750	86.0
2.485	.9935	86.0
2.685	1.0034	86.0
3.185	1.0173	86.0
3.685	1.0131	86.0

VELOCITY PROFILES

U_j/U_{e_o} = 2.07 x/h = 462

Y ~ In.	U/U_1	T ~ °F
.004	.3897	101.5
.007	.5028	101.5
.011	.5812	102.0
.015	.6150	102.0
.020	.6470	102.0
.030	.6774	102.0
.040	.7095	102.0
.050	.7291	102.0
.070	.7721	102.0
.090	.7978	102.0
.110	.8276	102.0
.160	.8837	101.5
.210	.9234	101.0
.260	.9571	100.5
.310	.9775	100.0
.360	.9908	99.0
.410	.9964	98.5
.460	1.0000	98.0
.510	.9996	97.5
.560	.9931	97.0
.660	.9841	96.0
.760	.9690	95.0
.860	.9578	94.0
.960	.9465	93.0
1.060	.9377	92.5
1.160	.9284	91.5
1.260	.9258	91.0
1.360	.9228	90.0
1.560	.9199	89.0
1.760	.9301	88.5
1.960	.9464	88.0
2.160	.9620	87.0
2.660	1.0073	86.5
3.160	1.0454	86.5
3.660	1.0640	86.5
3.960	1.0676	86.5
4.160	1.0658	86.5

U_j/e_o = 2.07 x/h = 554

Y ~ In.	U/U_1	T ~ °F
.004	.2752	101.0
.010	.4317	101.0
.015	.5004	101.0
.020	.5344	101.5
.030	.5766	102.0
.040	.6013	102.0
.050	.6249	101.5
.070	.6611	101.5
.090	.6827	101.5
.110	.7120	101.5
.130	.7400	101.5
.150	.7594	101.5
.170	.7784	101.5
.220	.8255	101.5
.270	.8630	101.0
.320	.8989	100.5
.370	.9302	100.0
.470	.9725	99.5
.570	.9893	98.5
.670	1.0000	97.5
.870	.9929	96.0
1.070	.9711	94.5
1.270	.9553	93.5
1.470	.9419	92.0
1.670	.9411	91.0
1.870	.9402	90.0
2.370	.9628	88.5
2.870	1.0085	88.0
3.370	1.0574	87.5
3.870	1.0937	87.0
4.370	1.1142	87.0
4.870	1.1168	87.0
5.070	1.1193	87.0

Series III Data Summary

Nominal Initial Velocity Ratio = 3.0

h = 0.056 Inches

θ_o = 0.206 Inches

Actual Initial Velocity Ratio	x/h	Re_s	U_j ~ ft/sec	T_j ~ °F	U_1 ~ ft/sec	τ_w ~ lb_f/ft^2	C_f^* X 10^3	Velocity Profile Index
2.92	125.	7,789	347.35	150.0	187.63	0.2169	5.832	244
2.92	197.	7,789	347.35	151.0	157.42	0.1452	5.495	244
2.92	286.	7,789	347.35	152.0	135.33	0.1001	5.106	245
2.92	357.	7,790	347.29	151.0	122.18	0.0773	4.795	245
2.92	462.	7,790	347.29	151.0	105.49	0.0541	4.491	246
2.92	554.	7,790	347.29	152.0	90.25	0.0367	4.159	246

* Based on Fluid Properties at δ_1

VELOCITY PROFILES

U_j/U_{e_o} = 2.92 x/h = 125

Y ~ In.	U/U_1	T ~ °F
.004	.6819	120.0
.007	.7949	119.0
.010	.8337	119.0
.015	.8721	119.0
.020	.8997	118.5
.025	.9227	118.0
.030	.9408	118.0
.035	.9550	118.0
.045	.9762	117.0
.055	.9878	116.0
.065	.9953	115.5
.075	.9982	115.0
.085	1.0000	114.5
.095	.9985	114.0
.105	.9947	113.5
.125	.9788	112.0
.145	.9599	110.0
.165	.9428	109.0
.185	.9195	108.0
.205	.8944	107.0
.225	.8724	106.0
.245	.8456	104.5
.265	.8211	103.5
.315	.7597	101.0
.365	.6961	98.0
.415	.6338	95.5
.465	.5818	92.0
.515	.5402	90.0
.565	.5124	87.5
.615	.4960	86.0
.665	.4890	85.0
.715	.4881	84.5
.765	.4908	84.0
.865	.4994	84.0
.965	.5107	84.0
1.065	.5184	84.0
1.265	.5406	84.0
1.465	.5562	84.0
1.665	.5714	84.0
1.865	.5807	84.0
2.065	.5862	84.0
2.265	.5868	84.0
2.465	.5868	84.0

U_j/U_{e_o} = 2.92 x/h = 197

Y ~ In.	U/U_1	T ~ °F
.004	.6343	113.0
.007	.7420	113.0
.010	.7794	112.5
.015	.8197	113.0
.020	.8505	112.5
.025	.8716	112.0
.030	.8915	112.0
.035	.9085	112.0
.045	.9340	111.5
.055	.9558	111.5
.065	.9701	111.0
.075	.9794	110.5
.095	.9934	110.0
.115	.9993	109.5
.135	1.0000	108.5
.155	.9960	107.5
.175	.9908	107.0
.225	.9642	106.0
.275	.9328	104.0
.325	.9009	102.5
.375	.8626	101.0
.425	.8264	99.5
.475	.7868	98.0
.525	.7535	96.5
.575	.7164	94.5
.625	.6868	93.0
.675	.6571	92.0
.775	.6167	89.0
.875	.5965	87.5
.975	.5931	86.0
1.075	.5980	85.5
1.175	.6064	85.5
1.375	.6254	85.5
1.575	.6422	85.5
1.775	.6571	85.5
1.975	.6678	85.5
2.175	.6739	85.5
2.375	.6761	85.5
2.575	.6761	85.5

VELOCITY PROFILES

U_j/U_{e_o} = 2.92 x/h = 286

Y ~ In.	U/U_1	T ~ °F
.004	.5816	109.0
.007	.6911	109.0
.010	.7324	109.0
.015	.7715	109.0
.020	.7985	108.5
.025	.8197	108.5
.035	.8539	108.5
.045	.8814	108.0
.055	.9038	108.0
.065	.9249	108.0
.075	.9394	108.0
.095	.9652	107.5
.115	.9779	107.0
.135	.9909	107.0
.155	.9957	106.0
.175	1.0000	106.0
.195	.9991	105.0
.245	.9954	104.0
.295	.9817	103.0
.345	.9646	102.5
.395	.9438	101.5
.495	.9013	100.0
.595	.8566	98.0
.695	.8080	96.0
.795	.7649	94.0
.895	.7255	92.5
.995	.6989	90.5
1.095	.6778	89.0
1.195	.6690	88.0
1.295	.6690	88.0
1.495	.6769	86.0
1.695	.6930	86.0
1.895	.7068	86.0
2.095	.7212	86.0
2.295	.7288	86.0
2.495	.7335	86.0
2.695	.7363	86.0
2.895	.7354	86.0

U_j/U_{e_o} = 2.92 x/h = 357

Y ~ In.	U/U_1	T ~ °F
.004	.5642	105.5
.007	.6584	105.0
.010	.7008	105.0
.015	.7396	105.0
.020	.7652	105.0
.025	.7854	105.0
.035	.8202	105.0
.045	.8494	105.0
.055	.8747	105.0
.065	.8931	104.5
.085	.9242	104.0
.105	.9474	104.0
.125	.9665	104.0
.145	.9768	103.5
.195	.9952	102.5
.245	1.0000	102.0
.295	.9956	101.0
.345	.9869	100.0
.445	.9622	99.0
.545	.9273	97.5
.645	.8930	96.0
.745	.8620	95.0
.845	.8233	93.5
.945	.7919	92.5
1.045	.7579	91.0
1.145	.7341	89.5
1.245	.7131	88.0
1.345	.7005	87.0
1.445	.6966	86.5
1.545	.6963	86.0
1.745	.7064	85.0
1.945	.7183	85.0
2.145	.7296	84.5
2.345	.7421	84.5
2.545	.7512	84.5
2.745	.7556	84.5
2.945	.7578	84.5
3.145	.7578	84.5

VELOCITY PROFILES

U_j/U_{e_o} = 2.92 x/h = 462

Y ~ In.	U/U_1	T ~ °F
.004	.4718	103.0
.007	.5887	103.0
.010	.6419	103.0
.015	.6842	103.0
.020	.7159	103.0
.030	.7540	103.0
.040	.7814	103.0
.050	.8064	103.0
.060	.8264	103.0
.080	.8609	103.0
.100	.8902	103.0
.120	.9135	103.0
.140	.9295	102.5
.160	.9456	102.5
.210	.9755	102.0
.260	.9897	102.0
.310	.9958	101.0
.360	1.0000	100.5
.410	.9937	100.0
.460	.9886	99.5
.560	.9689	98.5
.660	.9463	97.5
.760	.9183	96.5
.860	.8908	95.5
.960	.8638	94.5
1.160	.8077	93.0
1.360	.7566	91.0
1.560	.7232	89.5
1.760	.7047	88.0
1.960	.6989	86.5
2.160	.7034	86.0
2.360	.7142	85.5
2.560	.7249	85.0
2.760	.7373	85.0
2.960	.7449	85.0
3.160	.7525	85.0
3.360	.7584	85.0
3.560	.7584	85.0

U_j/U_{e_o} = 2.92 x/h = 554

Y ~ In.	U/U_1	T ~ °F
.004	.4193	102.5
.010	.5847	102.5
.015	.6394	102.5
.020	.6639	102.5
.030	.7035	102.5
.040	.7346	102.5
.050	.7560	102.5
.060	.7747	102.5
.070	.7910	102.5
.080	.8069	102.5
.100	.8341	102.5
.120	.8604	102.5
.140	.8805	102.5
.160	.8984	102.5
.210	.9362	102.0
.260	.9613	102.0
.310	.9805	101.5
.360	.9929	101.0
.460	1.0000	100.0
.560	.9948	99.5
.660	.9795	98.5
.760	.9612	98.0
.860	.9387	97.0
.960	.9128	96.5
1.160	.8674	95.0
1.360	.8140	93.5
1.560	.7698	92.5
1.760	.7249	91.0
1.960	.6912	90.0
2.160	.6699	89.0
2.360	.6647	88.0
2.560	.6664	87.0
2.760	.6707	86.5
3.260	.6976	86.0
3.760	.7129	86.0
4.260	.7280	86.0
4.760	.7301	86.0
5.260	.7216	86.0

APPENDIX M

EXPERIMENTAL RESULTS FOR SERIES IV

SERIES IV TYPICAL INITIAL
BOUNDARY LAYER PROFILE

U_{e_o} = 124.30 Ft/Sec

θ_o = 0.404 Inches

x/h = 0

Y ~ In.	U/U_1	T ~ °F
.000	.000	80.0
.004	.204	80.0
.008	.268	80.0
.012	.304	80.0
.016	.319	80.0
.026	.347	80.0
.036	.363	80.0
.046	.377	80.0
.056	.383	80.5
.076	.396	80.5
.096	.408	81.0
.116	.418	81.0
.136	.428	81.0
.186	.454	81.0
.236	.464	81.0
.286	.482	81.0
.336	.497	81.0
.436	.529	81.0
.536	.552	81.5
.636	.575	81.5
.736	.605	81.5
.836	.634	81.5
.936	.662	81.5
1.036	.685	81.5
1.136	.714	81.5
1.236	.739	81.5
1.336	.770	82.0
1.436	.797	82.0
1.536	.826	82.0
1.636	.850	82.0
1.736	.872	82.0
1.936	.919	82.0
2.136	.958	82.0
2.336	.980	82.0
2.536	.995	82.0
2.736	1.000	82.0
2.936	1.000	82.0

Series IV Data Summary

Nominal Initial Velocity Ratio = 1.0

h = 0.056 Inches

θ_o = 0.402 Inches

Actual Initial Velocity Ratio	x/h	Re_s	U_j ~ ft/sec	T_j ~ °F	U_1 ~ ft/sec	τ_w ~ lb_f/ft^2	c_f^* X 10^3	Velocity Profile Index
1.05	125.	3,118	130.64	120.0	70.91	0.0333	6.145	250
1.05	196.	3,118	130.64	120.0	63.79	0.0226	5.126	250
1.05	287.	3,118	130.64	120.0	110.10**	0.0165	1.241**	251
1.05	357.	3,125	130.53	118.0	106.84	0.0127	1.084**	251
1.05	463.	3,125	130.53	118.0	108.63**	0.0076	0.586**	252

* Based on Fluid Properties at δ_1

** Based on Measurements at δ_e (Jet Peak not Evident)

VELOCITY PROFILES

U_j/U_{e_o} = 1.05 x/h = 125

Y ~ In.	U/U_1	T ~ °F
.004	.4786	99.5
.007	.6293	100.0
.011	.7360	100.0
.016	.7967	99.5
.021	.8252	99.0
.026	.8530	99.0
.031	.8770	99.0
.041	.9090	99.0
.051	.9316	99.0
.061	.9426	99.0
.071	.9586	98.5
.081	.9720	98.5
.091	.9848	98.0
.101	.9874	98.0
.121	1.0000	97.5
.141	.9996	97.0
.161	.9965	96.5
.181	.9935	96.0
.201	.9909	96.0
.251	.9795	95.0
.301	.9574	94.0
.351	.9484	93.0
.401	.9367	92.0
.501	.9359	91.0
.601	.9346	89.5
.701	.9450	89.0
.801	.9681	88.0
.901	.9935	87.5
1.001	1.0213	87.5
1.101	1.0526	87.0
1.301	1.1203	87.0
1.501	1.1905	87.0
1.701	1.2628	87.0
1.901	1.3387	87.0
2.101	1.4165	87.5
2.301	1.4777	87.5
2.501	1.5347	87.5
2.701	1.5850	87.5
2.901	1.6150	87.5
3.101	1.6359	88.0
3.301	1.6482	88.0
3.501	1.6482	88.0

U_j/U_{e_o} = 1.05 x/h = 196

Y ~ In.	U/U_1	T ~ °F
.004	.4470	97.0
.007	.5723	96.5
.010	.6355	96.0
.015	.6977	96.0
.020	.7290	96.0
.025	.7591	96.0
.035	.7960	96.0
.045	.8236	96.0
.055	.8465	96.0
.065	.8578	96.0
.085	.8938	95.5
.105	.9184	95.5
.125	.9419	95.0
.145	.9520	95.0
.165	.9620	95.0
.185	.9714	94.5
.205	.9780	94.5
.225	.9877	94.5
.275	.9936	94.0
.325	1.0000	94.0
.375	.9995	93.5
.425	.9991	93.0
.475	1.0054	93.0
.575	1.0299	92.5
.675	1.0351	91.5
.775	1.0498	91.0
.875	1.0701	90.5
1.075	1.1130	90.0
1.275	1.1671	89.0
1.475	1.2352	89.0
1.675	1.3015	88.5
1.875	1.3719	88.5
2.075	1.4454	88.5
2.275	1.5173	88.5
2.475	1.5780	88.5
2.675	1.6403	88.5
2.875	1.6891	88.5
3.075	1.7276	88.5
3.275	1.7589	89.0
3.475	1.7748	89.0
3.675	1.7836	89.0
3.875	1.7854	89.0
4.075	1.7871	89.0

VELOCITY PROFILES

U_j/U_{e_o} = 1.05 x/h = 287

Y ~ In.	U/U_1	T ~ °F
.004	.1892	95.5
.007	.2436	95.5
.010	.2803	95.0
.020	.3421	95.0
.030	.3634	95.0
.040	.3806	95.0
.050	.3971	95.0
.070	.4153	94.5
.090	.4280	94.5
.110	.4354	94.5
.160	.4639	94.5
.210	.4795	94.0
.260	.4949	94.0
.310	.5076	94.0
.360	.5157	93.5
.460	.5297	93.0
.560	.5397	93.0
.660	.5550	92.5
.760	.5605	92.0
.860	.5661	92.0
.960	.5864	92.0
1.060	.6004	91.5
1.260	.6278	91.0
1.460	.6555	90.5
1.660	.6836	90.0
1.860	.7168	90.0
2.060	.7524	89.5
2.260	.7840	89.5
2.460	.8221	89.5
2.660	.8572	89.5
2.860	.8874	89.5
3.060	.9177	89.5
3.260	.9415	89.5
3.460	.9647	89.5
3.660	.9798	89.5
3.860	.9884	89.5
4.060	.9937	89.5
4.260	.9979	89.5
4.460	1.0000	89.5
4.660	1.0000	89.5

U_j/U_{e_o} = 1.05 x/h = 357

Y ~ In.	U/U_1	T ~ °F
.004	.1775	89.5
.010	.2554	89.5
.015	.2885	89.5
.020	.3037	89.5
.030	.3251	89.5
.040	.3388	90.0
.050	.3519	90.0
.070	.3706	90.0
.090	.3796	90.0
.140	.4054	90.0
.190	.4243	90.0
.240	.4348	90.0
.340	.4597	89.5
.440	.4835	89.5
.540	.5015	89.0
.640	.5126	89.0
.740	.5275	88.5
.840	.5398	88.0
1.040	.5661	88.0
1.240	.5891	87.5
1.440	.6202	87.0
1.640	.6467	87.0
1.840	.6751	86.5
2.040	.7073	86.5
2.240	.7393	86.0
2.440	.7746	86.0
2.640	.8056	86.0
2.840	.8341	86.0
3.040	.8668	86.0
3.240	.8982	86.0
3.440	.9262	86.0
3.640	.9464	86.0
3.840	.9615	86.0
4.040	.9764	86.0
4.240	.9900	86.0
4.440	.9933	86.0
4.640	.9967	86.0
4.840	1.0000	86.0
5.040	1.0000	86.0

VELOCITY PROFILE

$U_j/U_{e_o} = 1.05$

$x/h = 463$

Y ~ In.	U/U_1	T ~ °F
.004	.1043	89.5
.010	.1745	89.5
.020	.2237	89.5
.030	.2378	89.5
.040	.2512	89.5
.060	.2679	89.5
.080	.2760	90.0
.130	.2988	90.0
.180	.3199	90.0
.230	.3299	90.0
.330	.3552	89.5
.430	.3731	89.5
.530	.3873	89.5
.630	.4009	89.0
.830	.4297	89.0
1.030	.4564	88.5
1.230	.4841	88.5
1.430	.5163	88.0
1.630	.5389	88.0
1.830	.5701	88.0
2.030	.5922	87.5
2.230	.6204	87.0
2.430	.6477	87.0
2.630	.6770	87.0
2.830	.7005	87.0
3.030	.7318	86.5
3.230	.7578	86.5
3.430	.7830	86.5
3.630	.8113	86.5
3.830	.8349	86.5
4.330	.8873	86.5
4.830	.9194	86.5
5.330	.9368	86.5
5.830	.9437	86.5
6.330	.9505	86.5
6.830	.9673	86.5
7.330	.9838	86.5
7.830	1.0000	86.5

Series IV Data Summary

Nominal Initial Velocity Ratio = 2.0

h = 0.056 Inches

θ_o = 0.390 Inches

Actual Initial Velocity Ratio	x/h	Re_s	U_j ~ ft/sec	T_j ~ °F	U_1 ~ ft/sec	τ_w ~ lb_f/ft^2	C_f^* X 10^3	Velocity Profile Index
1.97	125.	5,357	235.86	142.0	112.88	0.0854	6.295	254
1.97	196.	5,357	235.86	142.0	89.25	0.0507	5.923	254
1.97	287.	5,357	235.86	142.0	68.99	0.0275	5.356	255
1.96	357.	5,362	235.94	141.0	56.01	0.0174	5.124	255
1.96	463.	5,362	235.94	141.0	41.93	0.0084	4.412	256

* Based on Fluid Properties at δ_1

VELOCITY PROFILES

U_j/U_{e_o} = 1.97 x/h = 125

Y ~ In.	U/U_1	T ~ °F
.004	.6345	113.0
.007	.7554	112.5
.010	.7991	112.0
.015	.8482	112.0
.020	.8771	112.0
.025	.8981	112.0
.035	.9350	111.5
.045	.9542	111.0
.055	.9767	111.0
.065	.9884	110.0
.075	.9947	110.0
.085	.9973	109.5
.095	1.0000	109.0
.105	.9969	109.0
.115	.9929	108.0
.135	.9867	108.0
.155	.9733	107.0
.175	.9565	106.0
.195	.9399	105.5
.245	.8883	104.0
.295	.8408	102.0
.345	.7833	100.5
.395	.7296	98.5
.445	.6813	97.0
.495	.6435	95.0
.545	.6045	94.5
.595	.5671	92.0
.645	.5559	91.0
.695	.5333	90.0
.745	.5328	89.0
.845	.5379	88.0
.945	.5374	87.0
1.045	.5538	87.0
1.145	.5750	87.0
1.345	.6099	86.5
1.545	.6570	86.5
1.745	.6966	86.5
1.945	.7421	86.5
2.145	.7811	86.5
2.345	.8219	86.5
1.545	.8607	86.5
1.745	.8879	86.5
1.945	.9045	86.5
2.145	.9207	86.5
2.345	.9272	86.5
2.545	.9308	87.0
2.745	.9308	87.0

U_j/U_{e_o} = 1.97 x/h = 196

Y ~ In.	U/U_1	T ~ °F
.004	.5204	107.0
.007	.6398	107.0
.010	.7267	107.0
.015	.7876	107.0
.020	.8143	107.0
.025	.8402	107.0
.035	.8818	106.5
.045	.9039	106.5
.055	.9255	106.5
.065	.9409	106.0
.075	.9565	106.0
.095	.9815	105.5
.115	.9960	105.0
.135	.9955	104.5
.155	1.0000	104.0
.205	.9946	103.5
.255	.9739	102.5
.305	.9476	101.5
.355	.9259	100.5
.455	.8648	99.0
.555	.8055	97.5
.655	.7550	96.5
.755	.7138	94.0
.855	.6853	92.5
.955	.6629	91.0
1.055	.6550	90.0
1.155	.6544	89.0
1.355	.6754	88.0
1.555	.7096	87.5
1.755	.7485	87.0
1.955	.7918	87.0
2.155	.8386	87.0
2.255	.8555	87.0
2.655	.9504	87.0
3.055	1.0320	87.0
3.455	1.0770	87.0
3.655	1.0945	87.0
3.855	1.1032	87.0
4.055	1.1075	87.0
4.255	1.1075	87.0

VELOCITY PROFILES

U_j/U_{e_o} = 1.97 x/h = 287

Y ~ In.	U/U_1	T ~ °F
.004	.4192	103.5
.007	.5392	103.0
.010	.6196	103.0
.015	.7025	103.0
.020	.7368	103.0
.025	.7659	103.0
.035	.8043	103.0
.045	.8409	103.0
.055	.8538	103.0
.075	.8884	103.0
.095	.9246	103.0
.115	.9422	103.0
.135	.9591	102.5
.155	.9676	102.5
.175	.9756	102.0
.195	.9839	102.0
.245	1.0000	101.5
.295	.9996	101.0
.345	.9905	100.0
.395	.9738	100.0
.495	.9475	99.0
.595	.9209	98.5
.695	.8840	97.5
.795	.8525	97.0
.895	.8193	96.0
.995	.7986	95.0
1.095	.7738	94.0
1.195	.7555	93.0
1.295	.7441	92.0
1.395	.7402	91.5
1.495	.7398	91.0
1.695	.7535	90.0
1.895	.7909	89.0
2.095	.8105	88.5
2.495	.8860	88.5
2.895	.9802	88.5
3.295	1.0741	89.0
3.695	1.1531	89.0
4.095	1.2210	89.5
4.495	1.2723	89.5
4.895	1.2971	89.5
5.295	1.3027	89.0
5.695	1.3027	89.0
6.295	1.3088	89.0

U_j/U_{e_o} = 1.96 x/h = 357

Y ~ In.	U/U_1	T ~ °F
.004	.4067	98.5
.007	.5145	98.5
.010	.5964	98.5
.015	.6620	98.5
.020	.6988	99.0
.030	.7446	99.0
.040	.7719	99.0
.060	.8237	99.0
.080	.8533	99.0
.130	.9096	99.0
.180	.9408	99.0
.280	1.0000	98.5
.380	.9991	97.5
.480	.9862	97.0
.580	.9732	96.5
.680	.9470	96.0
.780	.9335	95.5
.880	.9063	95.0
.980	.8783	94.5
1.180	.8491	93.5
1.380	.8038	92.5
1.580	.7877	91.5
1.780	.7713	90.5
1.980	.8016	89.5
2.180	.8009	88.5
2.380	.8449	88.0
2.780	.9132	87.0
3.180	1.0014	86.5
3.580	1.0828	86.5
3.980	1.1786	86.0
4.380	1.2771	86.0
4.780	1.3684	86.0
5.180	1.4289	86.0
5.580	1.4706	86.0
5.980	1.4869	86.0
6.380	1.4950	86.0
6.780	1.4950	86.0

VELOCITY PROFILE

$U_j/U_{e_o} = 1.96$

$x/h = 463$

Y ~ In.	U/U_1	T ~ °F
.004	.2973	97.5
.010	.4377	98.0
.020	.5822	98.0
.030	.6427	98.5
.040	.6762	98.5
.060	.7287	98.5
.080	.7585	98.5
.130	.8147	98.5
.180	.8587	98.5
.280	.9248	98.5
.380	.9634	98.0
.480	.9861	98.0
.580	.9931	97.5
.680	1.0000	97.0
.780	1.0000	97.0
.980	.9697	96.5
1.180	.9385	96.0
1.380	.9059	95.0
1.580	.8805	94.0
1.780	.8549	93.5
2.180	.8192	92.5
2.580	.8181	91.0
2.980	.8436	90.0
3.380	.9090	89.0
3.780	.9996	88.5
4.180	1.0892	88.0
4.580	1.1779	87.5
4.980	1.2716	87.0
5.380	1.3849	86.5
5.780	1.4459	86.5
6.180	1.5470	86.5
6.580	1.6549	86.5
6.980	1.7188	86.5
7.380	1.7805	86.5
7.780	1.8165	86.5
7.980	1.8165	86.5

Series IV Data Summary

Nominal Initial Velocity Ratio = 2.0

h = 0.056 Inches

θ_o = 0.392 Inches

Actual Initial Velocity Ratio	x/h	Re_s	U_j ~ ft/sec	T_j ~ °F	U_1 ~ ft/sec	τ_w ~ lb_f/ft^2	C_f^* X 10^3	Velocity Profile Index
2.00	56.	5,245	236.34	148.0	160.67	0.1826	6.865	258
2.00	92.	5,245	236.34	148.0	130.18	0.1163	6.582	258
1.99	125.	5,273	235.44	145.0	111.39	0.0838	6.388	259
2.00	161.	5,245	236.34	148.0	96.90	0.0605	6.116	259
2.00	196.	5,245	236.34	148.0	86.01	0.0478	6.109	260

* Based on Fluid Properties at δ_1

VELOCITY PROFILES

U_j/U_{e_o} = 2.00 x/h = 56

Y ~ In.	U/U_1	T ~ °F
.004	.7399	128.5
.007	.8458	129.0
.010	.8859	129.0
.015	.9255	128.5
.020	.9540	128.5
.025	.9703	128.5
.030	.9843	128.0
.035	.9914	127.0
.040	.9977	127.0
.045	1.0000	126.0
.055	.9980	125.5
.065	.9873	124.0
.075	.9706	123.0
.085	.9536	122.0
.095	.9330	121.0
.115	.8885	118.5
.135	.8463	117.0
.155	.7996	114.5
.175	.7464	112.5
.195	.6981	110.0
.215	.6495	108.5
.235	.6020	106.5
.255	.5516	104.5
.275	.5106	102.5
.295	.4697	101.0
.315	.4389	99.0
.335	.4122	97.0
.355	.3867	96.0
.375	.3691	95.0
.395	.3522	94.0
.415	.3463	93.5
.465	.3386	92.0
.515	.3400	92.0
.565	.3428	91.5
.615	.3512	91.0
.715	.3680	91.5
.815	.3799	91.5
1.015	.4171	91.0
1.215	.4525	91.0
1.415	.4914	91.0
1.615	.5236	91.0
2.015	.5939	91.5
2.415	.6420	91.5
2.815	.6714	91.5
3.015	.6758	91.5
3.215	.6780	91.5
3.415	.6802	91.5
3.615	.6780	91.5

U_j/U_{e_o} = 2.00 x/h = 92

Y ~ In.	U/U_1	T ~ °F
.004	.6934	122.0
.007	.7870	122.0
.010	.8398	122.0
.015	.8813	122.0
.020	.9106	122.0
.025	.9334	121.5
.030	.9482	121.0
.040	.9749	120.5
.050	.9890	120.0
.060	.9957	119.5
.070	1.0000	119.0
.080	.9972	118.5
.100	.9864	117.0
.120	.9663	116.0
.140	.9433	115.0
.160	.9121	114.0
.180	.8825	113.0
.220	.8286	110.5
.260	.7627	108.5
.300	.6973	106.0
.340	.6406	104.0
.380	.5828	102.0
.420	.5407	100.0
.460	.4953	98.0
.500	.4646	97.0
.540	.4421	95.5
.580	.4277	94.5
.620	.4220	93.5
.660	.4253	93.0
.760	.4303	92.0
.860	.4459	92.0
.960	.4557	91.5
1.060	.4768	91.5
1.160	.4955	91.5
1.360	.5366	91.5
1.560	.5694	91.5
1.760	.6116	91.5
1.960	.6546	91.5
2.160	.6916	91.5
2.360	.7236	91.5
2.560	.7572	91.5
2.760	.7778	91.5
3.060	.7979	91.5
3.360	.8064	91.5
3.660	.8095	92.0
3.960	.8095	92.0

VELOCITY PROFILES

U_j/U_{e_o} = 1.99 x/h = 125

Y ~ In.	U/U_1	T ~ °F
.004	.6174	116.0
.007	.7494	116.0
.010	.8033	116.0
.015	.8462	116.0
.020	.8761	116.0
.025	.8975	115.5
.030	.9183	115.0
.040	.9458	115.0
.050	.9655	114.5
.060	.9787	114.5
.070	.9880	114.0
.090	1.0000	113.0
.110	.9996	112.5
.130	.9895	112.0
.150	.9789	111.0
.170	.9588	110.5
.190	.9379	109.5
.240	.8916	108.0
.290	.8388	106.0
.340	.7833	104.5
.390	.7309	103.0
.440	.6764	101.5
.490	.6304	99.5
.540	.5849	98.0
.590	.5531	96.5
.640	.5274	95.0
.690	.5130	94.0
.740	.5005	93.5
.790	.4896	92.5
.840	.4875	92.5
.940	.4975	91.5
1.040	.5096	91.0
1.140	.5274	91.0
1.240	.5503	91.0
1.340	.5669	91.0
1.540	.6035	90.5
1.740	.6526	90.5
1.940	.6982	90.5
2.140	.7326	90.5
2.540	.8164	91.0
2.940	.8746	91.0
3.340	.9023	91.0
3.740	.9125	91.0
4.140	.9125	91.0

U_j/U_{e_o} = 2.00 x/h = 161

Y ~ In.	U/U_1	T ~ °F
.004	.5726	115.0
.007	.7102	115.0
.010	.7735	115.0
.015	.8195	114.5
.020	.8501	114.5
.025	.8748	114.5
.035	.9078	114.0
.045	.9355	114.0
.055	.9531	113.5
.065	.9663	113.5
.075	.9747	113.0
.085	.9876	113.0
.095	.9962	113.0
.105	1.0000	112.5
.125	.9996	112.0
.145	.9991	111.5
.165	.9940	110.5
.205	.9721	110.0
.245	.9449	109.0
.285	.9169	108.0
.325	.8882	107.0
.365	.8537	106.0
.465	.7751	104.0
.565	.6998	101.5
.665	.6407	99.5
.765	.5901	97.5
.865	.5652	95.5
.965	.5547	94.0
1.065	.5544	93.5
1.265	.5802	92.0
1.465	.6145	92.0
1.665	.6575	92.0
1.865	.6936	91.5
2.065	.7448	91.5
2.265	.7823	91.5
2.665	.8717	92.0
3.065	.9437	92.0
2.365	.9777	92.0
2.665	.9984	92.0
2.965	1.0106	92.0
3.265	1.0106	92.0

VELOCITY PROFILE

$U_j/U_{e_o} = 2.00$

x/h = 196

Y ~ In.	U/U_1	T ~ °F
.004	.5369	112.5
.007	.6710	112.5
.010	.7374	112.5
.015	.7911	112.0
.020	.8245	112.0
.030	.8690	112.0
.040	.8994	112.0
.050	.9230	112.0
.060	.9404	112.0
.070	.9513	111.5
.080	.9626	111.5
.100	.9842	111.5
.120	1.0000	110.5
.140	.9996	110.0
.160	.9996	110.0
.200	.9987	109.0
.222	.9816	108.0
.280	.9647	107.5
.380	.9006	106.0
.480	.8383	104.5
.580	.7781	103.0
.680	.7251	101.0
.780	.6790	99.5
.880	.6354	98.0
.980	.6149	96.5
1.080	.5942	95.5
1.180	.5907	94.5
1.380	.6018	93.5
1.580	.6377	92.5
1.780	.6770	92.0
1.980	.7144	92.0
2.180	.7704	92.0
2.380	.8099	92.0
2.680	.8776	92.0
2.980	.9460	92.0
3.280	1.0045	92.0
3.580	1.0450	92.0
3.880	1.0792	92.0
4.180	1.0935	92.0
4.480	1.0982	92.0
4.780	1.0982	92.0

Series IV Data Summary

Nominal Initial Velocity Ratio = 3.0

h = 0.056 Inches

θ_o = 0.386 Inches

Actual Initial Velocity Ratio	x/h	Re_s	$U_j \sim$ ft/sec	$T_j \sim {}^\circ F$	$U_1 \sim$ ft/sec	$\tau_w \sim lb_f/ft^2$	$C_f^* \times 10^3$	Velocity Profile Index
2.99	125.	7,877	357.34	155.	168.27	0.1795	6.062	262
2.99	196.	7,877	357.34	155.	131.77	0.1077	5.882	262
2.99	287.	7,877	357.34	155.	102.88	0.0622	5.534	263
2.98	357.	7,978	355.68	151.	87.19	0.0434	5.306	263

* Based on Fluid Properties at δ_1

VELOCITY PROFILES

U_J/U_{e_o} = 2.99 x/h = 125

Y ~ In.	U/U_1	T ~ °F
.004	.6729	120.0
.007	.7949	120.0
.010	.8366	120.0
.015	.8759	119.5
.020	.9045	119.5
.025	.9257	119.0
.030	.9423	119.0
.040	.9655	118.5
.050	.9810	118.0
.060	.9924	118.0
.070	.9976	117.5
.080	1.0000	117.0
.090	.9996	116.5
.100	.9963	116.0
.120	.9856	115.0
.140	.9676	114.0
.160	.9522	113.0
.180	.9306	112.0
.200	.9075	111.5
.220	.8881	110.5
.270	.8266	108.5
.320	.7605	106.5
.370	.6964	104.5
.420	.6262	102.5
.470	.5670	100.0
.520	.5044	98.0
.570	.4501	96.5
.620	.4055	94.5
.670	.3708	92.5
.720	.3436	91.0
.770	.3271	90.0
.820	.3170	89.0
.870	.3168	88.5
.970	.3195	88.0
1.070	.3347	88.0
1.170	.3425	87.5
1.370	.3691	87.5
1.570	.4007	87.5
1.770	.4331	87.5
1.970	.4603	87.5
2.170	.4860	87.5
2.370	.5158	88.0
2.570	.5338	88.0
2.970	.5657	88.0
3.370	.5775	88.0
3.770	.5798	88.0

U_J/U_{e_o} = 2.99 x/h = 196

Y ~ In.	U/U_1	T ~ °F
.004	.6527	115.5
.007	.7534	114.0
.010	.7921	114.0
.015	.8344	114.0
.020	.8589	114.0
.025	.8822	113.5
.035	.9103	113.5
.045	.9331	114.0
.055	.9521	113.5
.065	.9660	113.0
.075	.9778	113.0
.085	.9843	112.5
.095	.9890	112.5
.105	.9931	112.0
.115	.9977	112.0
.125	1.0000	112.0
.145	.9996	111.5
.165	.9923	111.0
.185	.9872	110.5
.205	.9799	110.0
.255	.9508	109.0
.305	.9159	108.0
.355	.8849	107.0
.405	.8475	106.0
.455	.8113	105.0
.505	.7706	104.0
.555	.7278	103.0
.605	.6889	102.0
.655	.6548	101.0
.755	.5768	98.5
.855	.5054	96.5
.955	.4483	94.5
1.055	.4115	93.0
1.155	.3887	91.5
1.255	.3768	90.5
1.355	.3823	89.5
1.555	.4047	89.5
1.755	.4308	88.5
1.955	.4603	88.0
2.155	.4882	88.0
2.355	.5191	88.5
2.755	.5793	88.5
3.155	.6267	88.5
3.555	.6576	88.5
3.955	.6708	88.5
4.355	.6741	88.5

VELOCITY PROFILES

U_j/U_{e_o} = 2.99 x/h = 287

Y ~ In.	U/U_1	T ~ °F
.004	.6116	110.5
.007	.7028	110.0
.010	.7443	110.0
.015	.7836	110.0
.020	.8071	110.0
.030	.8519	109.5
.040	.8779	109.5
.050	.8990	109.5
.070	.9317	109.5
.090	.9550	109.0
.110	.9706	109.0
.130	.9858	109.0
.150	.9930	108.5
.170	.9963	108.0
.190	1.0000	108.0
.210	1.0000	108.0
.230	.9958	107.5
.250	.9921	107.5
.300	.9841	107.0
.350	.9684	106.5
.400	.9447	106.0
.450	.9240	105.0
.550	.8737	104.0
.650	.8249	103.0
.750	.7733	102.0
.850	.7181	101.0
.950	.6646	101.0
1.050	.6054	99.0
1.150	.5607	98.0
1.250	.5120	96.5
1.350	.4745	96.0
1.450	.4421	95.0
1.550	.4073	94.0
1.750	.3787	92.0
1.950	.3784	91.0
2.150	.3968	90.0
2.350	.4231	89.5
2.750	.4792	89.0
3.150	.5294	89.0
3.550	.5878	89.0
3.950	.6351	89.0
4.350	.6844	89.0
4.750	.7205	89.0
5.150	.7353	89.0
5.550	.7403	89.0

U_j/U_{e_o} = 2.98 x/h = 357

Y ~ In.	U/U_1	T ~ °F
.004	.5111	103.0
.007	.6286	103.0
.010	.6984	103.0
.015	.7482	103.0
.020	.7752	103.0
.030	.8204	103.0
.040	.8389	103.0
.050	.8631	103.0
.070	.9038	103.0
.090	.9318	103.0
.110	.9536	103.0
.130	.9639	102.5
.180	.9849	102.5
.230	1.0000	102.0
.280	1.0000	102.0
.330	.9944	101.5
.380	.9784	101.0
.480	.9511	100.0
.580	.9179	99.5
.680	.8777	99.0
.780	.8356	98.5
.980	.7510	97.0
1.180	.6641	96.0
1.380	.5727	94.0
1.580	.4861	93.0
1.780	.4304	91.5
1.980	.3667	90.5
2.180	.3328	89.5
2.380	.3170	88.5
2.580	.3323	88.0
2.780	.3370	87.0
2.980	.3654	86.5
3.380	.4164	86.0
3.780	.4724	85.5
4.180	.5226	85.5
4.580	.5683	85.5
4.980	.6265	85.0
5.380	.6725	85.0
5.780	.7086	85.0
6.180	.7429	85.0
6.580	.7562	85.0
6.980	.7627	85.0
7.380	.7627	85.0

CITED LITERATURE

1. Glauert, M. B., "The Wall Jet," Journal of Fluid Mechanics, Vol. 1, December 1956.

2. Förthmann, E., "Turbulent Jet Expansion," NACA TM 789, 1936.

3. Bakke, P., "An Experimental Investigation of a Wall Jet," Journal of Fluid Mechanics, Vol. 2, July 1957.

4. Sigalla, A., "Experimental Data on Turbulent Wall Jets," Aircraft Engineering, Vol. 30, May 1958.

5. Sigalla, A., "Measurements of Skin Friction in a Plane Turbulent Wall Jet," Journal of the Royal Aeronautical Society, Vol. 62, December 1958.

6. Schwartz, W. H., and Cosart, W. P., "The Two-Dimensional Turbulent Wall Jet," Journal of Fluid Mechanics, Vol. 10, June 1961.

7. Bradshaw, P., and Gee, M. T., "Turbulent Wall Jets With and Without an External Stream," Aeronautical Research Council Reports and Memoranda, No. 3252, June, 1960.

8. Meyers, G. E., Schauer, J. J., Eustis, R. G., "Plane Turbulent Wall Jet Flow Development and Friction Factor," Journal of Basic Engineering, Transactions of the ASME, Vol. 85, March 1963.

9. George, Albert R., "An Investigation of a Wall Jet in a Free Stream," Department of Aeronautical Engineering, Princeton University, Report 479, September 1959.

10. Seban, R. A., and Back, L. H., "Velocity and Temperature Profiles in a Wall Jet," International Journal of Heat and Mass Transfer, Vol. 3, December 1961.

11. Patel, R. P., and Newman, B. G., "Self Preserving, Two-Dimensional Jets and Wall Jets in a Moving Stream," McGill University Report No. Ae5, September 1961.

12. Eskinazi, S., and Kruka, V., "Mixing of a Turbulent Wall Jet into a Free-Stream," Journal of Engineering Mechanics Division, Proceedings of the ASCE, Vol. 88, April 1962.

13. Verhoff, A., "The Two-Dimensional, Turbulent Wall Jet With and Without an External Free Stream," Princeton University Report No. 626, May 1963.

14. Kruka, V., and Eskinazi, S., "The Wall Jet in a Moving Stream," Syracuse University, Mechanical Engineering Department, Report No. ME937-6309F, August 1963.

15. Erian, F., and Eskinazi, S., "The Wall Jet in a Longitudinal Pressure Gradient," Syracuse University, Mechanical Engineering Department, Report No. ME937-6410F, October 1964.

16. Gartshore, I. S., "Jets and Wall Jets in Uniform Streaming Flow," Mechanical Engineering Research Laboratories, McGill University, Report 64-4, May 1964

17. Harris, G. L., "The Turbulent Wall Jet on Plane and Curved Surfaces Beneath an External Stream," Von Karman Institute for Fluid Dynamics, Technical Note 27, 1965.

18. Kacker, S. C., and Whitelaw, J. H., "Some Properties of the Two-Dimensional, Turbulent Wall Jet in a Moving Stream," Journal of Applied Mechanics, Transactions of the ASME, December 1968.

19. Gartshore, I. S., and Newmann, B. G., "The Turbulent Wall Jet in an Arbitrary Pressure Gradient," The Aeronautical Quarterly, February 1969.

20. Mosher, D. K., "An Experimental Investigation of a Turbulent Jet in a Cross Flow," Georgia Institute of Technology Aerospace Engineering Report No. 70-7, December 1970.

21. Utterback, N. G., and Griffith, T., Jr., "Reliable Submicron Pressure Readings with a Capacitance Manometer," Review of Scientific Instruments, Vol. 37, July 1966.

22. Patel, V. C., "Calibration of the Preston Tube and Limitations on its Use in Pressure Gradients," Journal of Fluid Mechanics, Vol. 23, September 1965.

23. Coles, D. E., and Hirst, E. A., "Computation of Turbulent Boundary Layers," AFOSR-IFP-Stanford Conference, Vol. 2, 1968.

24. Abramovich, G. N., The Theory of Turbulent Jets, MIT Press, Cambridge, Massachusetts, 1963.

25. Patel, R. P., "Self-Preserving, Two-Dimensional Turbulent Jets and Wall Jets in a Moving Stream," McGill University Thesis, April 1962.

26. Ames Research Staff, "Equations, Tables, and Charts for Compressible Flow," NACA Report 1135, 1953.

VITA

Douglas Howard Neale was born in Grosse Pointe, Michigan, on October 1, 1943. He attended elementary schools in Grosse Pointe and in Tampa, Florida. He graduated from H. B. Plant high school in Tampa in June, 1961. In September, 1961, Mr. Neale entered the University of Florida in Gainesville, Florida, and he received the degree of Bachelor of Science in Aerospace Engineering in April, 1966.

During his undergraduate studies Mr. Neale completed an engineering co-op program with Pratt & Whitney Aircraft Company in West Palm Beach, Florida. In addition, he returned to Pratt & Whitney for employment as an Experimental Engineer during the summers of 1966 and 1967.

Mr. Neale entered the Georgia Institute of Technology in September, 1967 and was awarded a NASA fellowship to study under the doctorate program in the Department of Aerospace Engineering. He is a member of Phi Kappa Phi, Tau Beta Pi, Sigma Xi, Phi Eta Sigma and the Delta Sigma Phi social fraternity.

On August 5, 1967 Mr. Neale was married to the former Ingrid Dianne Skow of Coral Gables, Florida.